COLUMN BEHAVIOUR AND DEFLECTION CONTROL IN STEEL FRAMES

JOHN BARRY SALTER B. Sc.

Degree of Doctor of Philosophy

Submitted to the University of Warwick

After Research in the Engineering Department

August 1976

Page

CONTENTS

PREFACE

The investigation reported in this thesis was carried out in the Engineering Department of the University of Warwick under the direction of Dr. D. Anderson and sponsored by a research grant from the Science Research Council; the author wishes to thank this body for its financial support.

The author is eternally grateful to his supervisor, Dr. D. Anderson, not only for his constant advice and valuable suggestions throughout the work, but also for his encouragement and enthusiasm in times of slow progress.

Special thanks is due to, Mr. Ian May, a fellow researcher, for help and valuable criticism throughout the experimental program. Thanks is also due to Mr. Arthur Redhead and his team of laboratory technicians for the assistance in preparing the tests, and to Butler Buildings U.K. for their kind donation of the columns used in the testing.

Professor R.P. Johnson is to be thanked for making available the laboratory facilities, and latterly for continuing the financial support to enable the work to be finalised.

Finally, Mrs. Joan Carrington is to be thanked for her accurate and diligent typing.

DECLARATION

The work reported in this thesis is totally original, except where specific reference to previous work is cited, and has never been previously submitted to any other Academic Institution.

SUMMARY

The work described in this thesis is concerned with the behaviour of steel building frames.

Two computer programs have been developed, based on the formation of stiffness matrices for the frame under analysis, which give ultimate load assessments of uniaxial and biaxial frames respectively. The uniaxial analysis estimates the reduction in stiffness due to specified regions of plasticity forming within the frame. Analysis is then continued until the combined effects of plasticity and elastic frame instability are sufficient to cause collapse of the frame.

The biaxial analysis extends the uniaxial stiffness matrix to allow for the extra minor axis, torsional and warping degrees of freedom which can give rise to out-of-plane buckling failures. In addition, a more general method of calculating reduced flexural and axial stiffnesses due to plasticity is used. The method, based on moment-curvature techniques, is also used to calculate corresponding torsional, warping, and cross product of inertia values. The latter rigidity is then introduced into the overall stiffness matrix to account for the shift in shear centre resulting from non-symmetric formation of plastic regions. Both computer programs are generally found to give good agreement with a variety of previously cited theoretical and experimental analyses.

A series of experimental tests on pin-ended tapered steel

columns have been performed to investigate the ultimate behaviour of these columns as part of a portal frame structure. The columns were subject to a combination of axial load and major axis bending moments, the latter being incremented to cause failure. In general, the columns fail predominantly due to elastic instability rather than excessive plasticity. The tests also serve as a useful check on the validity of the biaxial computer analysis in assessing the ultimate failure loads of the columns.

Finally, a simple linear method of proportioning the members of steel frames to satisfy deflection requirements in an efficient manner is presented. The method, which requires a computer program for a solution, is found to give a design which is usually as good, and sometimes better, than previous optimisation methods based on more rigorous non-linear programming techniques.

NOTATION

A	general term for area of cross-section
$\underline{A}$	rotation transformation matrix
Ae, Ae_{ff}	reduced areas due to plasticity
Aij	element area in the moment-curvature procedure
B =	$E(I_{yz}^2 - I_{zz} \cdot I_{yy})$
b	breadth of a I-section flange or a rectangular section
C	enhancement factor for Wood's design method
c, c_1	cosα and cosβ respectively
c'	tension block width for welded sections
C_{mx}, C_{my}	equivalent moment factors
C_w	warping rigidity
D	total depth of a section
d	half depth of a rectangular section
d_1	depth to neutral axis in an I-section or rectangular section
d_3, d_4	depths of plasticity in an I-section or rectangular section
d_{3i}, d_{4i}	depths of plasticity at iteration 'i'.
E	Young's modulus of elasticity
E_s	secant modulus
F	ratio of axial load to squash load
F_1, F_2	load factors at the current and previous iterations
F_a, F_{bx}, F_{by}	allowable compressive and major and minor axis stresses respectively
Fy	yield stress
{F}	array of force elements
fa, fx, fy	axial and major and minor axis bending stresses

f_{bx}, f_{by}	major and minor axis bending stresses
fo	initial imperfection stress about the minor axis
fs	element residual stress in the moment curvature procedure
G	shear modulus
G_e	effective shear modulus in a partially yielded section
G_s	reduced value of shear modulus in yielded region 'S'
h	distance between flange centroids in an I-section
I	general moment of inertia term
Ic, Ir	column and rafter moments of inertia in a portal frame
Ie_{ff}	reduced moment of inertia due to plasticity
Io	polar moment of inertia
Iyy, Izz	moments of inertia about the two principal axes
Iyz	cross-product of inertia
J	St. Venant torsional constant
$\underline{K}$	overall frame stiffness matrix
k	factor applied to the torsional constant
k_1, k_2	restraint factors for beams with special end conditions
K_c, K_r	cost factors for columns and rafters
k_x,k_y,k_T,k_H	reduction factor's in Young's design method
L, L_i	member length (suffix refers to the member number)
Le	effective member length
$\underline{L}$	external load vector
m	number of joints in a frame or major axis bending moment
M_{ax}	maximum allowable bending moment in Wood's design method
M_{cr}	critical moment for beam buckling

M_{max}	maximum moment present in Wood's design method
M_{PT}	reduced plastic moment in the presence of axial load
M_{px}	fully plastic moment about the x-axis
M_x	torque
M_y, M_z	moments about the y and x axes
M_{y1}, M_{y2}, M_{z1}, M_{z2}	minor and major axis moments at ends 1 and 2 of a member
m	ratio of end moments, or reduction factor for single curvature bending
N	total frame storage requirement
Nx, Ny	major and minor axis stress magnification factors
n	normal boundary direction
$\underline{n}$	geometric matrix
P	member axial load
P_c, P_{crit}	critical loads
P_E	Euler load
P_f	frame failure load
P_u	plastic mechanism load
P'	axial load at a previous iteration
PLAT	plateau length in the steel stress-strain curve
p'	axial stress
Q	heat input to the weld
Q_{y1}, Q_{y1}, Q_{z1}, Q_{z2}	shear forces in the y and z directions at ends 1 and 2 of a member
R, r	radius of curvature
R_x	reduction factor in Wood's design method

r_y	Radius of gyration about the minor axis, y
s, s_1	$\sin\alpha$ and $\sin\beta$ respectively
SH	strain hardening modulus in the steel stress-strain curve
TOL	specific convergence tolerance for plasticity depth or load factor
t_f, t_w	flange and web thicknesses
U	strain energy
u, v, w	displacements in the x, y and z directions respectively
u_1, v_1	co-ordinates of the centroid of a partially yielded I-section
U_{ij}, V_{ij}	major and minor axis element lever arms in the moment-curvature procedure
V	potential energy of the applied loads
W	weight function
x, y, z	co-ordinate axes
y_o	distance of shear centre below the mid-point of an I-section web
$\bar{y}$	distance from the shear centre
Z_x	elastic section modulus
$\underline{Z}$	array of joint displacents
α,β	major and minor axis angles of inclination respectively
α_1, α_2	stress functions in non-homogeneous sections
Δ	axial movement, or crane spread in a portal frame
ε, ε_c	axial strain and net compressive strain in a section
ε_{ij}, σ_{ij}	elemental strain
ε_y, ε_{SH}	yield and strain-hardening strains respectively

θ, ϕ	minor and major axis curvatures in the moment-curvature procedure
θ, ψ	minor and major axis joint rotations
λ	twist per unit length
λ_1, λ_2, λ_2	load factors
ϕ	angle of twist
Φ_1, Φ_2, Φ_3, Φ_4, Φ_5	Livesley's stability functions
πp	potential energy
σ_1, σ_2	stresses at previous and current iterations (load factors F_1 and F_2)
ν	Poisson's ratio
χ	warping displacement

Chapter One Introduction and historical review.

Despite the rapid advances in knowledge brought about by research work in recent years, most designers of steel frames in Great Britain still use traditional elastic methods based on simple beam and column theories. Simple beam design uses idealised end conditions to enable stresses corresponding to the applied loading to be calculated. These values must not exceed certain 'permissible' stresses which are obtained from elastic considerations.

The column design is based on the classical approach of Euler[1] and Lagrange[2] who presented the first mathematical treatments of perfect elastic pin-ended columns subject to compressive axial loads. They showed that bifurcation of equilibrium occurred at certain critical loads. It soon became apparent that if the lowest critical load was taken as the failure load, then the column strength was overestimated. Young[3] recognised that real columns suffer from imperfections and consequently presented the first theoretical analysis which allowed for initial curvature and eccentricity of loading. Perry[4] extended Euler's formula for pin-ended columns to include an undetermined factor for initial curvature. Later experimental tests by Robertson[5] enabled a typical value for this factor to be found. Although he was aware of the presence of residual stresses caused by uneven cooling of the steel section during manufacture, he decided to incorporate this effect into the initial curvature factor. The method of column design specified in the current edition of B.S.449[6] is based on the work of Robertson.

For no-sway frames, the beams are assumed to be simply supported. The eccentricities of beam-column connections (assumed to be 100 mm) result in both axial load and bending moments being applied to the columns. Sections are then chosen so that the maximum stresses in a member do not exceed certain permissible values, the criterion for failure being the attainment of first yield. Practical connections do, however, have some rigidity; hence rotation of the end of a column is partially restrained by adjoining beams and 'effective length' factors are used to determine the permissible stresses for the columns. The method has also been extended for sway frames. The stresses due to vertical loading are calculated as before. To determine the forces and moments due to lateral loading, the frame is rendered statically determinate by assuming points of contraflexure at both the mid-heights of columns and the mid-points of beams. At this stage of design, the joints are assumed to be rigid. Superposition is then used to calculate the total stresses due to the applied loading. The overall design method is essentially an 'empirical package', the success of which depends on the strict following of the procedure to design the whole frame.

Although the concept of design is one of failure at the onset of first yield, an assumption which is generally very conservative, the 100 mm eccentricity used to calculate the bending moments is by no means an upper limit, and only works in practice due to the conservative design of the beams.

A more rational design method can only be developed by identifying the various factors that cause a frame to collapse. The ultimate behaviour of steel frames can broadly be described in terms of two effects, namely plasticity and elastic instability. The former effect is predominant in structures for which deflections are negligible. Failure occurs as a result of the material's inability to resist further increases in stress beyond a certain level. Clearly, a design based on collapse load conditions has a great advantage over designs based on permissible stresses. In the former a definite margin of safety can be automatically entered into the design method, whereas a permissible stress design will result in a load factor against collapse being an unknown quantity varying from frame to frame.

Simple rigid-plastic theory pioneered by Baker[7] et al was based on the conditions at collapse. Plastic 'hinges' were assumed to form at isolated points for which full yielding had developed and further increases in stress due to strain-hardening were not allowed. Failure then occurred when sufficient hinges to cause a mechanism had formed. In general, this 'rigid plastic' method cannot be used in the design of many structures, particularly slender multi-storey sway frames in which the effects of elastic instability are appreciable. In such cases, the actual collapse load may be considerably below the value given by rigid-plastic theory.

As the level of loads acting on an elastic frame is increased from zero, the overall stiffness reduces due to the compressive axial loads. When the frame begins to deflect, the effect of these

compressive axial loads is to give rise to secondary bending moments (the $P - \Delta$ effect). The reduction in stiffness, however, is not proportional to the increase in loading and the relationship between load and deflection is non-linear. As the applied loads on a frame approach a certain level (the elastic critical load), rapid increases in deflection occur for small increases in applied load and the frame can be regarded as being on the point of collapse.

True behaviour of a frame will generally involve both the effects. Wood[8] suggested that the overall stiffness of a frame 'deteriorates' to zero due to the combination of plasticity and elastic instability, and collapse can therefore occur before a complete mechanism of plastic hinges has formed. Hence, when the effects of elastic instability are appreciable, the usual methods of rigid-plastic analysis are invalidated for determining the failure load.

When designing complete frames, attention must also be given to ensure that the individual members do not fail prematurely by lateral, lateral-torsional or local buckling. The design of columns in order to prevent premature failure in a lateral-torsional mode is an important and difficult aspect of the ultimate load design of rigidly jointed frames, and an excessively conservative approach can throw away the gains obtained by moving away from a permissible stress method to one based on conditions at collapse.

A further problem in the design of frames can be caused by the presence of excessive deflections. Economies given by a plastic design approach can lead to less stiff sections which

result in a violation of the deflection requirements at working load.

Recent work in the areas of column design, the determination of deteriorated frame critical loads and the control of deflections will now be reviewed.

1.1 Column design, analysis and tests.

The ultimate load capacity of steel columns can be severely reduced due to the possibility of lateral-torsional buckling. Horne[11] presented the first plastic design method for steel columns which took account of local column instability; this was based on his earlier work on portal frames at Cambridge. He introduced a useful classification scheme for describing the state of the surrounding beam members when examining a particular column. The letters P, E and O are used to represent respectively a plastic (unrestraining) beam, an elastic (restraining) beam and zero end moment (pinned) beam. Thus the designation $P_x P_y$ means plastic beams about both the major (x) and minor (y) axes.

Early Cambridge model tests by Roderick[9] (Ex Ey classification) on both I-sections and rectangular sections demonstrated that first yield considerably underestimated the collapse loads in such situations. Also, the presence of small minor axis beams did not significantly increase the ultimate load. Heyman[10] used a similar rig for his tests on model I-sections with unloaded minor axis restraining beams (Px Ey). He varied the slenderness ratio and major and minor axis end moment ratios and generally found that

torsional instability controlled the ultimate load. The results, at the time were quite remarkable since some columns buckled at loads above the Euler load in spite of a low degree of restraint about the minor axis. The stocky columns (columns with low slenderness ratios) reached the squash load with full plastic moments maintained at lower loads.

Horne's design methods[11,12] cover the two beam classifications Px Py and Px Oy, and as the beams do not therefore restrain the columns, he assumed that failure occurred when the yield stress was reached in an extreme fibre at the mid-height of the column. The first design case (Px Py) also limits the stress to the yield value at each end of the column as moments are applied about both axes and the plastic hinge concept is not applicable to such cases.

The design equation at mid-height takes the form

$$p + Nx\, fx + Ny\, fy \leq f \qquad 1.1$$

where p is the mean axial stress.

Nx and Ny are magnification factors based on the level of axial stress in the column

f is a reduced value of yield stress containing allowances for initial curvature.

Horne introduced the useful simplification that for elastic torsional buckling, there is an 'equivalent' single curvature critical moment. Thus any end moment combination can be reduced to a single case, and this simplification is used to calculate Nx and Ny values.

This method, however runs into difficulties when calculating the design moments to be carried by the column. When considering the worst possible case of single curvature bending, the loads carried by the frame are of the form shown in Fig. 1.1. This 'limited substitute frame', which is obtained by idealising the actual frame to include only adjacent members surrounding the designed member with idealised remote end conditions, is of the form recommended by the Joint Committee[15] for the analysis of internal columns. The beams loaded by the combined dead and live load must possess three plastic hinges to be designed using the rigid-plastic theory. However, the adjacent beams under dead load only must still offer some restraint to the columns, and thus the problem has become one of Ex Ey design rather than Px Py design with the out-of-balance moment at the joint being used to design the column. As a result, the method has been criticised since the reduced stiffness of the column due to its compressive axial load should have been used to calculate the column moments. Horne argues, however, that the stiffness of the column will reduce under axial load and thus the resulting redistribution of bending moment reduces the amount taken by the column.

As a result of the design criterion (Eqn. 1.1), any end moment combination approaching single curvature was not allowed, whatever the slenderness ratio. This was severely criticised due to the fact that in stocky columns, instability is usually not a problem, and even in single curvature bending, some yielding can take place at mid-height without detriment. Horne thus modified his later charts

which appeared in a British Constructional Steelwork Association Publication (B.C.S.A. No. 23[13]) to allow for end moment combinations approaching single curvature in stocky columns by adding a limiting slenderness curve to the charts; columns with slenderness values below this curve were thus assumed not to be affected by instability.

A further problem arises in the case of Px Oy beams when a plastic hinge is permitted at the column end. The method of design would be perfectly acceptable if there were an infinite number of column sections available. However, difficulties can be encountered due to the finite number of sections available. For instance, if for a particular section and loading combination, the maximum permissible slenderness ratio was just unsuitable, the next chart would be used to obtain a satisfactory design, resulting in a larger section. Unfortunately, a larger plastic moment is now assumed at one end of the column, and the corresponding allowable slenderness ratio may still be unsuitable. The process thus becomes one of 'chasing ones tail', and it may be necessary to revert to the elastic column method, thus resulting in a conservative design.

Attempts were made at about the same time to suggest design methods for columns with differing beam conditions to those examined by Horne. Many of the problems associated with column design at this time were due to attempts to determine the maximum column moment in terms of magnification of one of the end moments. This magnification factor is indeterminate at the Euler load, since for single curvature bending, the end moments become zero.

In 1957, Wood[14] was able to avoid this problem by the use of nomograms which enabled this magnification factor to be found for

all values of axial load. However, designers appeared to be unwilling to use these charts, probably due to their complex nature. A new simpler method of presentation was thus introduced several years later and included in the Joint Committee's[15] design recommendations. The factor was based on the elastic critical load rather than the Euler load. This has the effect of automatically bringing the 'effective length' into the solution which naturally would prove to be popular with designers accustomed to B.S.449. The effective length, L_e, is then defined as:-

$$L_e/L = \sqrt{P_E/P_{crit}} \qquad 1.2$$

The critical load, P_{crit}, is itself dependent on the beam to column stiffnesses and corresponding charts were given in the design document (JCR2)[15] for the recommended 'limited substitute frame'. Furthermore, it was found that although the end moments and the ratio of maximum moment to end moment tend to change rapidly as the axial load is increased, their product (the maximum moment) is a smooth function for all load values. The designer could thus obtain the end moments at zero axial load and find a corresponding magnification factor (m) under increasing axial load to account for instability effects, without using stability functions.

The design criterion was stress based and had the following form:

$$f_a + f_x + mf_y + f_{ic} \leq F_y \qquad 1.3$$

where f_a axial stress

f_x, f_y major and minor axis bending stresses respectively

f_{ic} initial curvature stress

F_y yield stress

The Joint Committee had previously decided that the $P_x E_y$ classification of design would offer the most economy. Sway was not allowed due to the detrimental effects of overall frame instability. Although initial stresses are relatively unimportant when considering restrained columns, the term 'f_{ic}' was introduced principally as an additional safeguard to prevent design up to the squash load in the absence of major and minor axis moments. The overall method is one of partial plastic design which allows unspecified amounts of plasticity in double curvature, a decision which was proved to be correct by tests. Torsional instability safeguards were also introduced by limiting both the slenderness ratio and depth/flange ratio in order to keep the torsional stresses small. Two full scale tests using mild[16] and high yield[17] steel were subsequently undertaken at the Building Research Station to test the viability of the Committee's proposals. The tests however were rather disappointing since the column design proved to be rather conservative. Up to this time, all design methods had been based on a limiting stress philosophy. Wood, however, in an earlier paper had indicated that the correct criterion for collapse was one of 'vanishing stiffness'. Consequently two design methods, obviating the use of limiting stresses, were later presented based on considerable theoretical and experimental evidence.

The first method[18] was applicable for sway braced I-section columns with the $P_x E_y$ beam classification, which as Horne[7] had pointed out would generally offer the most economy in design.

The collapse load, P_c, of the column is assumed to be given by:

$$P_c = R_x C P_E \qquad 1.4$$

where R_x is a reduction factor based on assessment of the deterioration of the minor axis stiffness due to major axis bending moments and axial load.

P_E is the Euler load

C is an enhancement factor dependent on beam restraint and is an exact value read from charts based on the reduced Euler load, $R_x P_E$.

Gent and Milner[19] had previously tested model I-section columns with both major and minor axis beam restraints subject to single curvature bending and axial load. They demonstrated that one of the primary factors controlling the load capacity of the column was the elastic critical load of one flange. If this critical load is above the squash load, then the squash load would be reached. Otherwise failure would occur at the elastic critical load.

Wood, therefore used this concept to limit the maximum allowable bending moment so as to ensure that only one flange could ever become fully plastic.

The allowable moment is then given by:-

$$M_{ax} = 1.08\, Z_x\, F_y (1 - F) \qquad 1.5$$

where Z_x = elastic section modulus

F_y = yield stress

F = ratio of axial load to squash load.

The overall intuitive reduction factor, R_x, takes the form:

$$R_x = \left(1 - \frac{M_{max}}{M_{ax}} (0.4 - 0.2\, m)\right) (1 - F^2) \qquad 1.6$$

where M_{max} = maximum moment in the column

m = ratio of end moments.

The first main bracketed term distinguishes linearly between single and double curvature (in the absence of axial load, R_x is 0.4 or 0.8 respectively) and reverts to unity if the maximum moment is zero. The second term , $1 - F^2$, prevents the squash load being reached and also reflects the small effect of axial load on stiffnesses at low loads.

The collapse load, however, is found not to be very sensitive to the intuitive value of R_x. If too high a value of R_x had been assumed, then too high a value of F is forecasted. This is partially compensated by a greater reduction in the '$1 - F^2$' term. Also the R_x term gives rise to a smaller value of C, and hence the product, CR_x, tends to equalise. Wood also gives values of R_x based on previous experimental results for the intuitively more difficult problem of columns subject to predominant minor axis bending. For such cases, an assessment of the maximum spread of plasticity that can be permitted cannot be uniquely defined.

His method however ignores the effect of minor axis beam

loads on column stability in the case of predominant major axis bending. A series of tests by Stringer[20] on slender restrained columns under doublecurvature bending indicated both significant torsional behaviour and also significant reduction in ultimate load with minor axis beam loading. Hutchings[21], therefore, tested a range of columns with differing torsional rigidities and a range of both minor axis beam stiffness and minor axis beam loads. To simplify the study, he considered only single curvature bending. He demonstrated that for low loads ($P/P_{crit} < 0.5$), minor axis beam loads have little effect on the ultimate load; however for higher loads the effect became significant. Hutchings therefore concluded that Wood's method is applicable to columns with small minor axis beam loading. Generally Wood's method gives a lighter overall design than previous stress based methods.

Young[22] has also presented an intuitive design method for isolated columns subject to biaxially applied end moments (P_x P_y classification). He assumes that the detrimental effects of axial load and major and minor axis moments, giving rise to possible lateral or lateral torsional buckling, may be independently assessed to obtain multiplying factors (< 1) which are then combined to obtain a reduced allowable major axis moment below the full plastic value.

The major axis moment capacity of the column (M_x) is then given by:

$$M_x = K_x K_T K_y K_H M_{px} \qquad 1.7$$

where K_x is a buckling parameter if major axis moment and axial load are considered only

K_y is a buckling parameter for minor axis moments and axial load only

K_T is a lateral torsional buckling parameter based on major axis moment capacity due to the presence of axial load and minor axis moments.

The buckling parameters (K_x, K_y and K_T) are based on several analytical studies performed by Young. Previous investigations to obtain the reduction in carrying capacity of a column under uniaxial bending[23,24] (equivalent to K_x) have necessitated separate charts for different ratios of end moments. Young, however, by incorporating the slenderness ratio and axial load into one parameter was able to present the reduction values on a single chart. He also suggested the use of a "stocky" column concept for columns with low slenderness ratios. These columns are designed so that a full plastic hinge occurs at one end without the need to consider instability effects (the K values are unity). The method is essentially an extension of Horne's[12] P_x O_y method to allow biaxial plasticity to occur at the ends of the column.

These two methods of Wood and Young are probably the most advanced methods available for the design of columns in steel frames. Any design method, however, is dependent on a considerable amount of previously obtained analytical and experimental results. A summary of recent British work in these fields will now be given.

Much of the recent analytical work on steel columns in Britain

has aimed at extending the previously obtained elastic theories to include plasticity effects. Milner[25] was the first researcher to examine the effect of beam restraint on biaxially loaded columns. He segmented the column into small elements and iteratively obtained a deflected shape assuming end moments alone were acting. Further equilibrium shapes were then obtained under increasing axial loads. The deflected shape was assumed to be unaffected by the calculated twist deformations. However a separate torsional analysis was used to determine new values of twist and corresponding forces which were then included in a subsequent incremental analysis.

Milner used this method to independently assess the effect of strain hardening, strain reversal and torsion on the ultimate load. He concluded that unloading was relatively unimportant except possibly when columns were acted on by heavy moments from stiff restraint beams.

Taylor[26] has analysed and tested continuous steel columns under biaxial bending. His theoretical analysis examined two independent perpendicular two-dimensional frames about the major and minor axes. Twist was not included in the analysis since he assumed that torsional deformations were small in continuous columns. Hence, the only link between major and minor axis moments was through the biaxial stiffness properties and the sharing of the axial load. The column was segmented into a number of 'elements' and a stiffness matrix set up using stability functions. 'Recursive relationships' connecting stiffness properties in adjoining segments of the column were used to avoid excessively

large stiffness matrices. The analysis, however, neglected residual stresses and initial imperfections.

Taylor tested to failure model 2 bay, 3 storey frames in which he varied the minor axis restraint and distribution of beam loads whilst keeping the stiffness ratio of beam to column in the major axis constant. He could thus investigate the effect of minor axis restraint and minor axis beam load on the failure mode, which usually involved lateral-torsional buckling of the columns. He concluded that the minor axis restraint beams would significantly increase the ultimate load, whilst large minor axis beam loads would cause large reductions in the collapse load.

Hutchings[21] has used a discrete element model in his analysis of restrained columns. His principal assumption is that discrete elements of infinite flexural and torsional stiffness connected by flexural-torsional springs at nodal points can be used to describe the behaviour of a continuous member. Each element deforms axially whilst the flexural and torsional deformations are assumed to be concentrated at these nodes. His analysis essentially extends Taylor's method to include torsional effects. Values for end slopes, shear, torque and warping displacement are initially guessed corresponding to the applied loading and are later improved upon using a second order correction process. In order to reduce the number of variables, warping is assumed to be either fully restrained or unrestrained at the end of the member. The method however did not appear to show particularly good agreement with his corresponding experimental studies.

1.2 Overseas steel column investigations.

North American specifications for the design of steel building frames provide for column design through the use of interaction equations. In this procedure, the axial force and bending moment on the member are matched against its axial strength and flexural capacity. Approximate equations have been developed to ensure that the member possesses both adequate strength and has a sufficient factor of safety against failure through elastic instability. In using these equations, a distinction is made between sway and no-sway modes by using the concept of effective length; for braced members, the effective length is always less than the actual length, whilst in unbraced frames the effective length is greater than the actual length.

The basic Euler curve using the tangent modulus concept was modified by the Column Research Council[27] (CRC) in formulating their inelastic column strength curve for members under axial load only. This modification involved assuming an arbitary residual stress pattern to give a smooth transition from the Euler curve for elastic buckling to the curve representing inelastic buckling. The curve gave critical values of axial stress for various effective slenderness ratios.

The American Institute of Steel Construction (A.I.S.C.) design proposals[28] use this critical value in their method for members under combined bending and axial load. The early interaction form took the following form:

$$\frac{f_a}{F_a} + \frac{f_x . C_{mx}}{F_{bx}} + \frac{f_y . C_{my}}{F_{by}} \leq 1 \qquad 1.8$$

where f_a is the axial stress

F_a is the allowable compressive axial stress

f_x, f_y are flexural bending stresses

F_{bx}, F_{by} are allowable bending stresses based on consideration of lateral and lateral-torsional buckling in the absence of axial load.

C_{mx}, C_{my} are equivalent uniform moment factors.

In 1961, this formula was modified by introducing magnification factors into the two bending terms to allow for the secondary bending effects due to axial load. However, at this time, no theoretical analysis of combined bending and axial load had been performed, and the formula was thus based on separate investigations of uniaxial buckling effects. The above interaction equation is essentially a stability check on the member under design. Separate strength checks were also used, again in the form of interaction formulae to prevent the squash load or the fully plastic moment being reached.

Recent American analytical work on elastic-plastic columns has focused attention on the isolated pin-ended column subject to eccentric axial load about both axes (P_x P_y). Researchers have realised that exact numerical solutions of the governing differential equations are generally not possible and consequently analyses have used specific approximations to obtain a solution. Birnstiel

and Michalos[29] presented the first analysis of the problem using numerical integration. Initial values of curvatures were assumed at the ends of the column and corresponding values of "internal" forces were obtained at various points along the column length. The "external" and "internal" forces would not, in general, agree due to incorrect initial assumptions, and a numerical correction procedure was used to improve these initial guesses. This analysis was continued until satisfactory convergence was obtained, and thus by successive increases in load, a load-deflection curve could be obtained. However, the process required a large number of successive manual trials and corrections and hence considerable effort to obtain a solution. The method was however fully computerised a few years later[30]. At the same time, a series of tests[31] on rolled and welded sections was performed to obtain the post buckling deflected shape as well as the ultimate load for biaxially loaded columns. Some of the sections tested were previously stress relieved so as to minimise the effects of residual stresses and thus give better correlation with theory. The ends of the column were restrained against twisting and warping, and the maximum twist at the ultimate load was found to be small. It was concluded that bending about the minor axis governed the ultimate load capacity. Generally agreement between theory and experiment was found to be good.

Sharma and Gaylord[32] later presented a simpler method of analysis for the biaxially loaded pin ended column. They assumed the deflected shape to be part of a sine wave and established

equilibrium conditions at only one point (midheight). They found that warping stresses were small, and thus examined the effect of neglecting twist. This resulted in an overestimate of the ultimate load of between 1 - 8% compared to the analysis including twist. Syal and Sharma[33] have generalised the problem to include columns with unequal end eccentricities, and assume a power series approximation for the deflected shape. Equilibrium was again established at only one point. However due to unequal end eccentricities, the section examined was the one at which first yield occurred. The shift of the shear centre with increasing plasticity was however ignored. Good agreement with Birnstiel's testswas obtained.

Santathadaporn and Chen[34] performed an incremental method of analysis by setting up a tangent stiffness matrix connecting the rate of change of forces to the rate of change of displacements at mid-height. Load-deflection curves were generated by incrementing curvatures and consequently post buckling effects could be examined. The analysis dealt with both proportional and non-proportional loading and was used to examine the effect of beam restraint on column strength.

Chen and Atsuta[35] used an approximate elastic analysis to identify the section at which first yield occurred. They introduced "averaged interaction relationships" (between yield and full plasticity) which made allowances for the reduction in column stiffness. The ultimate load of the column could then be obtained from Chen's interaction curves, which gave a failure surface for

various combinations of axial load and bending moments.

A recent method of analysis by Vinnekota[36] determined the load deflection behaviour of biaxially loaded columns with symmetrical or unsymmetrical end restraints. The governing differential equations of bending were solved iteratively using finite difference approximations. The stiffness properties were based on the remaining elastic core, whilst the effects of plasticity were introduced as "pseudo" lateral loads in the governing differential equations.

1.3 Overall frame instability

The review so far has been principally concerned with the analysis and design of individual columns. To design such members it is necessary to determine the distributions of bending moments and axial forces in the frame. For sway structures these distributions are affected by the instability effects in the frame. These effects must also be considered to determine the failure load of the frame as a whole. These aims can most easily be achieved by using a computer program which performs an 'elastic-plastic' stability analysis to determine the actual behaviour of the frame up to collapse. The method, essentially, is to obtain a stiffness matrix for the whole frame by use of the well known slope-deflection equations. Frame instability effects and allowance for plasticity are introduced in subsequent analyses under increasing loads.

An elastic-plastic analysis program for frames has been presented by Jennings and Majid[37]. A complete stiffness matrix

for the frame was formed, and as loading progressed, extra rows and columns were introduced into the matrix to allow for the formation of plastic hinges. An analysis was performed at working load, and the load factor at which first yield occurred was estimated, and subsequently converged onto by the use of stability functions. These stability functions reflect the reduction in stiffness of a member under compressive axial loads. A plastic hinge is then inserted into the frame, at the point at which yield has occurred, by placing an additional row and column in the overall stiffness matrix to correspond to the hinge rotation. A linear extrapolation procedure is then used to calculate the load factor at which the next hinge will form, based on the current information. This stage was a refinement of Livesley's[38] earlier method in which the load factor was incremented by a predetermined amount. At load levels approaching failure, two or more hinges may form between load increments and inclusion of these at the same time may alter the mode of collapse.

The process of inserting hinges one by one into the stiffness matrix is continued until collapse occurs (indicated by the determinant of the overall stiffness matrix becoming zero). The method, however, ignores strain-hardening, residual stresses and the reduction of the 'full plastic moment' due to axial load. Also as a result of using the full stiffness matrix, restrictions on computer storage space limit the method to only fairly small frames.

Majid and Anderson[39] utilised the symmetric properties of

the stiffness matrix to reduce storage space requirements. The matrix used had an irregular banded form, dependent on the frame geometry, and required only the storage of stiffness terms between the joint in consideration and the lowest numbered joint connected to it for each row in the overall matrix. The method also allowed for the reduction of the full plastic moment due to axial load. As a result of the great storage savings in the stiffness matrix, large frames could be analysed.

Other methods[40,41] for the analysis of frames have included strain-hardening effects. Davies[40] has shown that the presence of strain-hardening can result in a theoretical increase of 30% in the failure load, a fact confirmed by experiment. Chin[41] considers the effects of overall frame instability, including instability due to partially plastic regions, as well as strain-hardening. However, this analysis neglects the reduction in the moment capacity of a section due to axial load and this renders it unsuitable for frames under significant axial loads. It also requires considerable computer time in comparison to other methods[39,40].

Merchant has proposed an intuitive formula to calculate the failure load of a frame in which both elastic instability and plasticity effects are present.

The formula has the following form:

$$\frac{1}{P_f} = \frac{1}{P_{crit}} + \frac{1}{P_u} \qquad (1.9)$$

where P_f is the frame failure load

P_{crit} is the elastic critical load

P_u is the plastic mechanism collapse load.

A similar formula has been recommended by research workers at Lehigh University[42] for the design of frames up to three stores high.

$$P_f = 3.4\ P_{crit}/(1 + 3 \cdot P_{crit}/P_u) \qquad (1.10)$$

Although the correct plastic collapse mechanism can usually be found quite easily, the elastic critical load is usually more difficult to obtain, and thus limited the use of these simple equations. Wood[43], however, has recently introduced a desk method using stiffness distribution techniques to enable designers to calculate the elastic critical load of sway frames by using a modified limited substitute frame (called a Grinter frame). A suitable estimation of the collapse load could then be found by substitution of this value into Merchant's formula.

1.4 Deflection control in frames.

Practical methods for the design of building frames should ensure that the resulting structure has both adequate strength and stiffness. Despite this, a considerable amount of attention has been paid to unbraced rigidly-jointed steel frames subject only to strength requirements. Livesley[44] and Palmer[45] both go to considerable trouble to obtain a minimum weight rigid-plastic design by mathematical programming techniques. Majid and Anderson[46] and Holmes and Sinclair-Jones[47] have produced economical

elastic-plastic frame designs without having to resort to complex mathematical programming techniques. Majid and Anderson used repeated elastic-plastic analyses to obtain a solution, whilst Holmes and Sinclair-Jones used sub-frame analyses suitable for hand design. Whilst the above methods produced light structures, there was no guarantee that deflection limitations would be satisfied. For this reason, several recently proposed methods have enabled deflection constraints to be included in the design procedure. The various members of the frame are apportioned so as to satisfy the deflection constraints in the most efficient manner.

Majid and Elliott[48] give two methods for limiting deflections in frames using true non-linear programming techniques. The first method was limited to portal frames whilst their second, more general method, was effectively limited due to the excessive computer time and storage space it required. Horne and Morris[49] again use true non-linear programming techniques to limit deflections in rectangular frames. They assume points of contraflexure at various points in the frame to render the frame statically determinate, and then solve the optimisation procedure using piecewise linearisation and the simplex method.

Majid and Anderson[51,52] use the matrix flexibility method coupled with piecewise linearisation to optimise the deflection constraint. Although these methods are not restricted to any particular shaped frame, the analysis is limited to fairly small frames due to the excessive amount of computer time and storage

space required for a solution.

Most of these above methods[48,49,51] neglect the increase in deflections resulting from the reduction in frame stiffness due to compressive axial loads. Their use is thus limited to frames for which this effect is small. Moy[53], however, makes allowance for this effect in producing a feasible design for regular rectangular frames under deflection constraints. Deflections are calculated by assuming non-linear elastic behaviour together with points of contraflexure in the frame. The control of deflections in the frame is achieved by examining the effect of increasing the beam sections only and assessing their corresponding influence on the deflections.

1.5 Tapered sections.

The use of tapered sections in steel buildings can often result in weight savings for many structural and loading situations. Particular regions of high stress within a member require a larger section than adjacent regions of lower stress, and thus economies can be achieved by varying the section within a member.

A recent elastic design method[54] for members which have web-depth taper only has been proposed, based on the modification of the A.I.S.C. interaction formulae. For prismatic members with relatively small axial load, this equation has the form:

$$\frac{f_a}{F_{a\,O}} + \frac{f_b}{F_{b\,L}} \leq 1 \qquad (1.11)$$

where F_a and F_b are the allowable axial and bending stresses obtained from lateral and torsional buckling considerations suffices O and L refer to the smaller and larger end of a column respectively in the case of a tapering member.

This formula is extended to tapering members by introducing modifying length factors into the values of F_a and F_b, which are dependent on the angle of taper of the section. Thus in analysing the effects of axial and bending stresses, the member is assumed to be prismatic and modifying length factors based on the section properties at the top and bottom of the member are introduced into the solution. These factors are obtained by solving the basic differential equations of flexure and torsion using variable stiffness properties. The corresponding buckling loads are obtained, and compared with the known results for prismatic members. Curve fitting techniques are then used to give analytical expressions for the modifying length factors in terms of the tapering angle.

Two series of tests have been reported at Columbia University[55] and New York University[56] which investigated respectively the elastic and inelastic stability of tapering I-beams. The New York research team simulated cantilevered gable roof beams of different pitches loaded vertically at the free end. This produced a member under high bending stress and low axial stress. The results for all the beams showed a similar trend with overall failure occurring due to local buckling. Prior to this, however, lateral buckling had usually commenced giving a rapid increase in lateral deflections

at mid-span. Comparison of the design method with these results showed it to be very conservative. There were two main reasons for this. Firstly, only partial buckling resistance was assumed (the larger stress value of St. Venant torsion or warping resistance) in deriving the allowable bending stress, F_b. Secondly, simply supported end conditions were assumed, and hence no allowance for partial end restraint was made. A finite element analysis method was subsequently developed[57] to enable less conservative allowable stress values to be used.

1.6 Scope for the present work.

A. Elastic-plastic analysis for biaxially loaded columns.

Most previous work on biaxially loaded steel columns has been concerned with investigating the ultimate load behaviour of either pin-ended columns or columns with idealised end restraints. Several methods of complete elastic-plastic frame analysis are also available, but these analyses can generally deal only with loading in one plane (a combination of axial load and major axis bending moment).

The aim of the present work is to extend the previous ideas used in these uniaxial frame analyses to the biaxial loading case. This involves linking the separate behaviour of a member in both the major and minor axis planes through the torsion equation, and estimating the reduction in stiffness due to biaxial plasticity. Chapters 3 and 4 of this thesis develop general analyses for the elastic and plastic behaviour of biaxial frames of limited size.

B. Tapered column tests.

The necessity for economy in design has resulted in the adoption of tapered sections in many structural situations. Very little experimental data, however, is available on the ultimate behaviour of such sections. In America, two series of tests have been performed on tapered beams, whilst no work has so far been reported on tapered columns. In Chapter 5, therefore, a series of ultimate load tests on a series of pin-ended tapered columns subject to major axis bending moment and axial load are described.

C. Optimisation of deflection constraints in frames.

Economical designs of frames for strength will generally be achieved using ultimate load theories. However, in many situations, deflection limitations under the applied loading will be violated, thus invalidating the original design. Subsequent modification of the design by arbitarily increasing the section sizes to satisfy these deflection requirements may result in an uneconomical design. In recent years, several methods of design have been suggested which will satisfy the deflection controls in an efficient manner. True optimisation requires complex non-linear programming techniques; however, these methods are found to require large amounts of computer time and storage space.

The aim of the present work is to present a rapid method of design to satisfy deflection limitations. The non-linear programming method of optimisation is reduced to a linear programming technique by separately investigating the effect of small increases in each

section size in limiting deflections in the frame. This method is set out in Chapter 6 of this thesis.

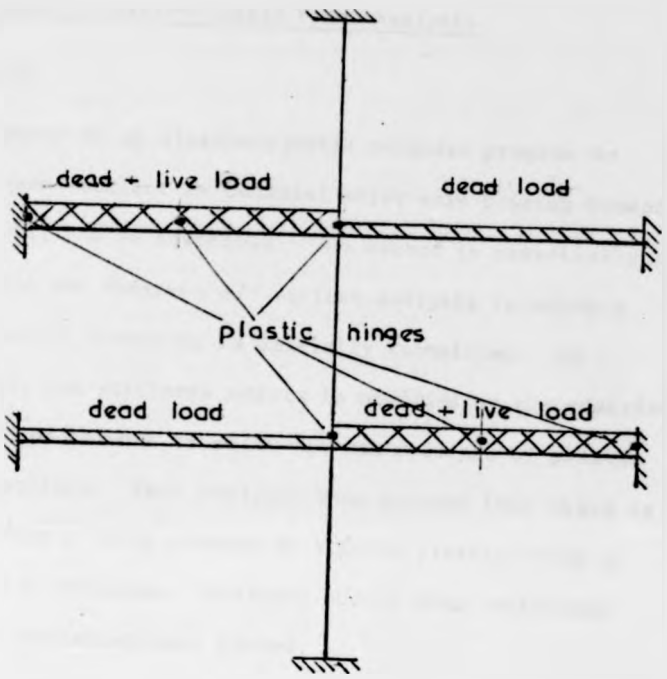

Fig. 1.1 limited substitute frame

Chapter 2. Uniaxial Elastic-Plastic Frame Analysis

2.1 Introduction.

The development of an elastic-plastic computer program to analyse plane frames subject to uniaxial major axis bending moment and axial load will now be described. The method is essentially an extension of Majid and Anderson's[39] earlier analysis in which a matrix for the entire structure is initially formulated. As loading increases, the stiffness matrix is modified by the addition of suitable rows and columns to allow for the presence of plastic hinges in the structure. This analysis thus assumes that there is a sudden change from a fully elastic to a fully plastic state at various points in a structure. Collapse occurs when sufficient hinges to cause a mechanism have formed.

The method to be described herein uses the same basic elastic stiffness matrix as Majid and Anderson; however the development of plasticity is allowed for in a more progressive manner. Reduced values of axial and flexural stiffnesses are calculated corresponding to specific regions of plasticity forming in a member. Consequently extra rows and columns in the stiffness matrix representing plastic hinge rotations are not required. The analysis proceeds by estimating load levels for which these specified amounts of plasticity will form and the stiffness matrix is suitably modified. The method, as before, is iterative and continues until the 'deterioration of stiffness' due to the combination of plasticity and elastic instability effects render the determinant of the stiffness matrix non-positive. Collapse is then assumed to have occurred.

2.2 Assembly of the overall stiffness matrix.

The frame is initially segmented into small members connected together by suitably numbered joints. The unknown joint displacements of a structure, $\underline{Z}$, can be determined by an inverse matrix transformation of the form

$$\underline{Z} = \underline{K}^{-1}\underline{L} \qquad 2.1$$

where $\underline{L}$ is the externally applied load vector

$\underline{K}$ is the overall stiffness matrix of the structure.

Fig. 2.1 gives the stiffness matrix, $\underline{K}$, for an individual member with respect to an overall system of co-ordinates, where

$$\begin{aligned} a &= (EA\cos^2\alpha + 12\,EI\Phi_5 \sin^2\alpha/L^2)/L; \\ b &= (EA - 12EI\Phi_5/L^2)\cdot\sin\alpha\cos\alpha/L; \\ c &= 6\,EI\Phi_2\cos\alpha/L^2; \\ d &= 6\,EI\Phi_2\sin\alpha/L^2; \\ e &= (EA\sin^2\alpha + 12\,EI\Phi_5\cos^2\alpha/L^2)/L; \\ f &= 4\,EI\Phi_3/L; \\ g &= 2\,EI\Phi_4/L; \end{aligned} \qquad 2.2$$

and α, E, A, I, L are respectively the angle of inclination, Young's modulus, area, second moment of area and length of the member.

The Φ values are the usual Livesley stability functions[58], and account for the reduction in the member's stiffness due to compressive axial loads. The contribution of other members to obtain the overall stiffness matrix is of a similar form to the above.

The stiffness matrix is assembled joint by joint by considering the contributions of each member connected to that joint. If more than one member meet at a particular joint, the stiffness values are combined. However non-zero stiffness will only occur in the matrix for a particular member at locations corresponding to the joints that are connected by that member. Thus by reference to Fig. 2.2 (where the ringed numbers represent frame members and the unringed

numbers represent joints) the formation of the stiffness contributions at Joint 5 will be described. There are three members (3, 5 and 8) and three joints (3, 6 and 7) connected to Joint 5. Hence submatrices K_{53}, K_{56} and K_{57} are the stiffness contributions of members 3, 8 and 5 respectively. Similarly, the leading diagonal submatrix contains the summation of three sets of stiffness values for these three members. However, there is no member connecting Joint 4 to Joint 5. Consequently submatrix K_{54} (shown unshaded) is a null matrix.

Thus the overall stiffness matrix of a frame contains many zero elements, the positioning of which will depend on the joint connection list. Also, the overall stiffness matrix will be symmetrical about its leading diagonal. This follows directly from Maxwell's reciprocal theorem.

An efficient storage scheme for the stiffness matrix must eliminate as many zeros as possible, as well as being capable of dealing with a wide range of frame geometries. The method used by Majid and Anderson was based on the compact elimination technique of Jennings[59]. The symmetric nature of the matrix was utilised by storing only elements on, and to one side of, the leading diagonal. The method used an irregular band width, with the zero elements beyond the end of the band being neither stored nor operated on.

The storage required by the overall stiffness matrix is then obtained as follows: if i is the lowest numbered joint that is connected to a given joint j ($j > i$) then $9 \cdot (j - i)$ locations are required by the K_{jk} submatrices (K is from i to $j - 1$). Since only elements to one side of the leading diagonal are stored, a further 6 locations are needed for the submatrix K_{jj}.

The total storage required by the matrix is then

$$N = 6M + \sum_{j=1}^{m} 9(j - i) \qquad 2.3$$

where M is the number of joints.

A further $3 \cdot M$ locations are also needed to store the address locations of the leading diagonal terms. If a restraint occurs at a particular joint due to direction or rotation fixity, then the corresponding row (and column) is removed from the overall-matrix and the above storage requirement is reduced.

2.3 Non-linear elastic analysis

The input data specifies the frame geometry, loading and section and material properties. Allowance is made for the possibility of part of this loading remaining fixed as loading increases by specifying the applied load in two parts; the first part varies linearly as the load factor is increased whilst the second part remains constant. The overall stiffness matrix is then assembled joint by joint by introducing the corresponding stiffness values of the various members after specification of the position and direction of any joint restraints. By reference to Fig. 2.2, Joints 1 and 2 will be omitted from the matrix as these positions are fully fixed. If, however, these joints had been pinned, then an extra row and column would have been required for each position corresponding to the joint rotation. The joint numbering scheme adopted for this example ensures that only three null submatrices (at Joints 5, 7 and 9) appear in the overall matrix, thus reducing the storage requirements as well as the computer time required to

solve the stiffness equations. Once the stiffness matrix is constructed at a given load level, Eqn. 2.1 is performed using the compact elimination process and the resulting deflections are calculated. The member forces are then evaluated by back substitution. For the first analysis, Livesley's 'ϕ' functions are set to unity. This analysis is thus a linear elastic one with no modification of the stiffnesses of the frame due to compressive axial loads. The calculated axial loads are then used for an improved solution of the stiffness matrix, by calculating new 'ϕ' values. Iteration continues until for each member $|P/P' - 1|$ is less than a stipulated tolerance, where P is the axial load in a member for the current analysis and P' is the axial load in a member from the previous analysis. Convergence at this load level is now assumed to have occurred.

2.4 Plasticity effects due to axial load and major axis bending moment.

Once the yield stress is reached in a particular member in either tension or compression, the effective stiffness of the member will be reduced due to the subsequent development of plasticity. The two states of plasticity for a rectangular section are shown in Fig. 2.3. The first state called 'primary plasticity' occurs due to the combination of axial stress with bending stress resulting in the yield stress being reached on one side of the cross-section only. The second state called "secondary plasticity" occurs if the bending stress predominates, and causes yielding on both sides of the cross-section.

The derivation of the reduced stiffness values for a rectangular and I-section will now be given. These values will then be used in the previously described non-linear stiffness matrix to obtain an overall elastic-plastic frame analysis.

2.4.1 Primary plasticity for a rectangular section.

Assuming that the combination of axial load, P, and bending moment M is sufficient to cause the yield stress to be reached in the top fibres of the section, the resultant static forces and moments are calculated about the centre line of the section.

For Zone 1, (Fig. 2.3), the force and bending moment are given by:-

$$P_1 = Fy\ b\ d_3 \qquad 2.4a$$

$$M_1 = Fy\ b\ d_3\ (d - d_3/2) \qquad 2.4b$$

Similarly for Zones 2 and 3, the forces and moments can be obtained by substituting for the stress, σ, in terms of d, d_1, d_3 and F_y.

Hence:-

$$P_2 = Fy\ b(d_1 - d_3)/2 \qquad 2.4c$$

$$M_2 = Fy\ b(d_1 - d_3)(3d - d_1 - 2\ d_3)/6 \qquad 2.4d$$

$$P_3 = -b(2d - d_1)^2.\ Fy/(2\cdot(d_1 - d_3)) \qquad 2.4e$$

$$M_3 = Fy\cdot b\cdot(2d - d_1)^2\ (d + d_1)/\ (6\cdot(d_1 - d_3)) \qquad 2.4f$$

addition of the components of P and M from Eqns. 2.4 will enable internal and external forces to be equated.

Hence $P = F_y \cdot b \cdot (d_1 + d_3 - (2d - d_1)^2 / (d_1 - d_3)) / 2$ 2.5a

$M = F_y \cdot b \cdot (4d^3 - 3d\, d_3^2 + d_3^3) / (6 \cdot (d_1 - d_3))$ 2.5b

The net compressive strain at the centre line, ε_c, is given by

$$\varepsilon_c = Fy \cdot (d_1 - d) / (E \cdot (d_1 - d_3)) \quad 2.6$$

Hence for a member of length, L,

Axial movement, $\Delta = Fy \cdot (d_1 - d) \cdot L / (E \cdot (d_1 - d_3))$ 2.7

Substituting for Fy in Eqn. 2.5a gives

$$P = E \cdot b \cdot (2d\, d_1 - 2d^2 - d_3^2 / 2) / (d_1 - d) \cdot \Delta / L \quad 2.8$$

Considering bending only, for plane sections remaining plane, the bending strain, $\varepsilon_b = Y/R$.

Hence $Fy = E \cdot (d_1 - d_3) / R$ 2.9

Substituting this value in Eqn. 2.5b gives

$$M = E \cdot b \cdot (4d^3 - 3d\, d_3^2 + d_3^3) / (6 \cdot R) \quad 2.10$$

For elastic behaviour

$$P = EA\, \Delta / L \quad 2.11a$$

$$M = EI / R \quad 2.11b$$

Comparison of Eqns. 2.11 with Eqns. 2.8 and 2.10 gives

$$A_{eff} = b \cdot (2d\, d_1 - 2d^2 - d_3^2/2) / (d_1 - d) \quad 2.12a$$

$$I_{eff} = b \cdot (4d^3 - 3d\, d_3^2 + d_3^3) / 6 \quad 2.12b$$

where I_{eff} and A_{eff} are respectively the effective inertia and area of the partially plastic cross-section.

2.4.2 Secondary plasticity for a rectangular section.

Similar effective inertias and areas can be obtained for the secondary plastic stress state of Fig. 2.3(b).

By summation of the various stress blocks, the effective area and inertia can be shown to be:-

$$A_{eff} = b(2d - d_3 - d_4) \qquad 2.13a$$

$$I_{eff} = b\cdot(2d-d_3-d_4)\cdot(2d^2+d\cdot(d_3+d_4) + d_3.d_4-d_3^2-d_4^2)/6 \qquad 2.13b$$

Chen[60] has presented some approximate analytical formulae for the moment curvature properties of rectangular sections. The above values for both the primary and secondary plasticity cases are in good agreement with Chen's values.

2.4.3 Reduced stiffness values for steel I-sections.

The same basic method can be used to calculate effective section properties for I-section shapes. The section is idealised into three rectangles, and equilibrium of axial force and bending moment enable the reduced stiffness values to be obtained. There are, however, several more cases to consider for each plasticity state (primary and secondary) corresponding to the plasticity either occurring in one, or both, flanges only or developing into the web also (see Fig. 2.4).

The reduced axial and flexural stiffnesses are summarised in Table 2.1.

2.5 Overall elastic-plastic method of analysis

Fundamentally, an elastic-plastic analysis consists of tracing the non-linear load-deflection history of a frame up to collapse.

Initially a linear elastic analysis is performed by setting all the 'ϕ' functions of Eqn. 2.2 to unity. At this stage, it is assumed that the applied loads are such that instability effects are small and thus a separate analysis with modified 'ϕ' values is not needed. If the bending moments at the joints connecting member j are BM1 and BM2, with BM1 acting at the first end of the member and BM2 acting at the second end, according to the frame geometry then the average bending moment in member j, BMj, is given by:-

$$BMj = (BM2 - BM1)/2 \qquad 2.14$$

This value is assumed to create tension on the upper side of the member when positive (the upper side is on the left hand side of the member when viewing from the first end to the other end of the member). The average bending moment is assumed to act uniformly over member j when assessing its reduction in stiffness due to plasticity. Each member is now considered in turn and a linear extrapolation procedure is used to estimate the load factor at which first yield occurs. Two values will be obtained for each member corresponding to the combination of axial load and bending moment at the two extreme fibres.

With reference to Fig. 2.5, the estimated load factor for first yield, λ_E, can be assessed by setting σ_1 and F1 to zero, and F2 to unity.

The load factor for first yield is given by

$$\lambda_E = F_y/\sigma_2 \qquad 2.15$$

This procedure is repeated twice for each member until the smallest value of λ_E is found for the entire frame. Values of axial load corresponding to this load factor are estimated and a new stiffness analysis is performed at this load level. For this analysis, the values of the stability functions, 'ϕ', are obtained from the estimated axial load values and are thus not necessarily unity. By solving the stiffness matrix, new values of axial load are obtained and are then compared with the assumed values. If these values do not agree within a certain tolerance, a better estimate of this first yield load factor can be obtained by using the new values of axial load. This iteration procedure is repeated until at a particular assumed load factor, the estimated and actual values of axial load are in agreement.

Once yielding commenced in a member, further increases in stress result in a spread of plasticity across the section and a reduction in stiffness. A check on the extent of plasticity can be made by consideration of the equilibrium equations.

For instance, if a rectangular section has developed primary plasticity, combination of Eqns. 2.5a and 2.5b to eliminate d_1 will give the following:-

$$Ad_3^3 + Bd_3^2 + Cd_3 + D = 0 \qquad 2.16a$$

where

$$A = -F_y \cdot b \qquad 2.16b$$

$$B = 3.M.\ F_y \cdot b/(P - 2 \cdot F_y\ b.d.) + 3\ F_y \cdot b \cdot d \qquad 2.16c$$

$$C = 6 \cdot M \cdot P/(P - 2 \cdot F_y \cdot b \cdot d) - 6\ M \qquad 2.16d$$

$$D = -12 \cdot M \cdot F_y \cdot b/(P - 2 \cdot F_y \cdot b \cdot d) - 4d^3 \cdot F_y \cdot b \qquad 2.16e$$

It can be readily seen that these coefficients (A, B, C and D) contain only the section properties, yield stress, axial load and bending moment in a member. Thus by solving the above equation to obtain the smallest positive root gives the depth of plasticity corresponding to any combination of axial load and bending moment.

Similarly, a polynomial equation can be obtained for the secondary plastic rectangular section by combining Eqns. 2.13a and 2.13b

$$d_4^2 + d_4(P/(F_y \cdot b) - 2d) + 3M/(F_y \cdot b) - 2d^2 - P \cdot d/(F_y \cdot b) + \left(P/(F_y \cdot b)\right)^2 = 0 \qquad 2.17a$$

This quadratic equation is solved to find the lowest positive value of d_4. The corresponding depth of plasticity at the other side of the member, d_3, is given by

$$d_3 = d_4 + P/(F_y \cdot b) \qquad 2.17b$$

The load factor corresponding to a specific depth of plasticity developing in a member is now estimated using a linear extrapolation procedure. Successive applications of this process enable improved values to be obtained.

By reference to Fig. 2.5, the estimated load factor for which a certain depth of plasticity, X, is reached in primary plasticity is given by:-

$$\lambda_p = \frac{(F2 - F1).\ \chi + F1.d_{32} - F2.d_{31}}{d_{32} - d_{31}} \qquad 2.18a$$

where F2 and F1 are the load factors at the current and previous iterations d_{32} and d_{31} are the corresponding plasticity depths obtained for instance from Eqn. 2.16.

Similarly, if the member is in the secondary plastic state, another load factor corresponding to a certain depth of plasticity, Y, developing at the other extreme fibre is given by

$$\lambda_p = \frac{(F2 - F1)\cdot Y + F1\cdot d_{42} - F2\cdot d_{41}}{d_{42} - d_{41}} \qquad 2.18b$$

where d_{41}, d_{42} are the depths of plasticity at the other extreme fibre for the current and previous load factors respectively.

Also, if plasticity has not commenced in a member, the estimated load factor for which the member will yield is given by:-

$$\lambda_E = \frac{(F2 - F1)\cdot F_y + F1\cdot \sigma_2 - F2\cdot \sigma_1}{\sigma_2 - \sigma_1} \qquad 2.18c$$

where σ_2 and σ_1 are the stresses at the current and previous iterations respectively.

The expressions of Eqns. 2.16, 2.17 and 2.18 give actual depths of plasticity corresponding to certain applied loadings and also estimates of load factors for which predetermined depths of plasticity will form. These equations are now used to modify the overall stiffness matrix to allow for this growth in plasticity. Initially, a small percentage of the overall depth, TOL, is specified as an input parameter. Each time a particular member reaches an integer multiple of this value, its stiffness is suitably reduced. Hence, the modification of stiffnesses is done in a step-wise rather than in continuous fashion. This

feature of the analysis will now be described in detail.

2.6 Modification of stiffnesses.

Two values of λ are calculated for each member corresponding to each extreme fibre using Eqns. 2.18. The lowest load factor is thus found for which a stiffness analysis is performed. Once the tolerance on axial load is not exceeded, a check on the plasticity depths of each member is made using Eqns. 2.16 and 2.17. If plasticity has already occurred in the member for which the lowest load factor was obtained, its stiffness is modified as follows; assuming this member's stiffness has not previously been altered, the depth of plasticity used for modifying I and A is given by:-

$$d_3 = 1{\cdot}5 \cdot TOL \qquad 2.19$$

where TOL is the specified depth of plasticity converged onto. This value is then substituted into the reduced stiffness equations (e.g. Eqns. 2.12a and 2.12b). However stiffness values are only altered for one particular member at any one convergence (the member for which the specified depth of plasticity has been reached). Consequently members with depths of plasticity between zero and 'TOL' will retain their full stiffnesses. The subsequent convergence values of plasticity are 2 × TOL, 3 × TOL etc. It is therefore thought to be a better approximation to initially overestimate the reduction in stiffnesses once the depth, 'TOL' has been reached. Hence the corresponding depth of plasticity to be substituted into the reduced stiffness expressions at the next convergence (2 × TOL) is given by

$$d_3 = 2{\cdot}5 \cdot TOL \qquad 2.20$$

The process is thus one of estimating load factors corresponding to specific regions of plasticity and modifying the stiffness values accordingly. Analysis continues until the determinant of the stiffness matrix becomes negative due to the combined effects of plasticity and frame instability. Collapse is then assumed to have occurred.

If unloading occurs in a member, then its extent of plasticity reduces, and thus the effective stiffness will begin to increase. The analysis allows for this by enabling the member to retrace its original stress-strain curve and thus recover some of its original stiffness (see Fig. 2.6).

A flow diagram for the computer analysis is given in Fig. 2.7. The accuracy of the analysis depends largely on the length of the members specified initially as input data. Clearly, the assumption of Eqn. 2.14 becomes more exact the smaller the member length. It is necessary, therefore, to ensure that expected areas of high stress contain the majority of the members of the frame.

2.7 Examples using the analysis.

1. Rectangular Section.

Baker et al[7] give details of several experimental tests performed on model rectangular section columns with end beam restraint. The example used here is of a column initially bent into single curvature by end restraining beams and subsequently loaded to collapse by increasing the axial load. Details of the frame and beam loadings are given in Fig. 2.8.

The corresponding computer analysis was performed by splitting the frame into 47 members and performing an initial elastic analysis with the full beam loading applied together with a small axial load of 1 ton. Subsequent analyses are performed in the manner previously described. The axial load is incremented by tracing the formation of plasticity in the column. Corresponding plots of axial load versus mid height major axis deflection and axial load versus bending moment are given in Figs. 2.9 and 2.10.

The analysis continues until considerable unloading occurs at the ends of the column at an axial load of 6.65 tons. Collapse is then assumed to have occurred, and this value compares well with the experimental collapse load of 6.67 tons. The plot of axial load versus bending moment at the end and mid-height of the column also gives good agreement with the experimental curve. Progressive increase of the axial load relaxes the end moment, until at some value of axial load, this moment changes sign. Collapse occurs soon afterwards, due to the loss of restraint previously offered by the end beams.

At first sight, it would appear that agreement for the mid-height deflections between the experimental and computer analyses is not good. However, Gent and Milner[19] have shown that the OA part of the curve in Fig. 2.9 is governed solely by the column stiffness whilst the subsequent part of the curve, ABC, is governed by the beam stiffness. The computer analysis gives good agreement with the second part of the curve (ABC), whilst giving poor agreement with the first part (OA). This is thought to be due

to the difficulty of modelling the effect of the heavy end block forming the connection between the beam and column in the computer analysis. The ultimate behaviour appears to be predominantly dependent on the beam stiffness, due to the relaxing of the end moments, and this is demonstrated by the excellent ultimate load agreement between the experimental and theoretical analyses.

Two different values of incremental plasticity depths (TOL) of 0.0375 ins. and 0.075 ins. have been used in the analysis. These two analyses give almost identical results, with the smaller plasticity value requiring considerably more computer time. At high values of axial load, extensive regions of plasticity begin to spread within the structure. Consequently, incrementing for each specified region of plasticity in any member elements results in a very small increase in the frame load factor, and hence a considerable number of iterations to obtain a state of collapse. The amount of computer time required for a solution using the above values of TOL (0.0375 ins. and 0.075 ins.) are respectively 35 mins. and 18½ mins. using an ICL 4130 series computer.

2. I-shaped section.

The second example is based on a rolled steel joist tested experimentally by Ajmani[61]. The column analysed is a 5" × 3" × 9 lb RSJ which is laterally restrained at various points along its length and has pinned end conditions. The loading path used is one of fixed axial load (6 tons) and subsequently increasing the major axis bending moment at one end until collapse occurs. The other end has zero moment throughout, corresponding to the $\beta = 0$ case.

The corresponding computer analysis splits the column into 24 elements, each 3 ins. in length. The lateral supports are modelled by assuming full restraint at the corresponding joint locations. The initial analysis applies full axial load together with a small amount of bending moment (10 t-in).

Subsequent iteration indicates that yielding commences at $M/M_p = 0.75$. Plasticity then develops over the top part of the column and moment-rotation agreement is excellent between theoretical and experimental analyses until $M/M_p = 0.85$ (Fig. 2.11). At this point, the two analyses commence to diverge with the computer analysis predicting larger end rotations than were actually observed. The computer analysis continues until failure occurs at $M/M_p = 0.95$. However the corresponding experimental failure load is much higher ($M/M_p = 1.31$). The large discrepancy between these two values is thought to be partially attributable to strain hardening, which is not allowed for in the analysis. Davies[40] has shown that the effect of strain hardening can considerably increase the failure load of a structure. He demonstrated that for a particular pitched roof portal structure, strain hardening alone was responsible for a 33.4% increase in the theoretical failure load. Clearly, this difference is of the same order as the discrepancy between experimental and theoretical failure loads in the present example. Indeed, the ultimate moment of the present analysis compares well with the reduced fully plastic moment under axial load. As a result of instability effects, the maximum column moment shifts away from the top end of the column to about the quarter point adjacent

to the column head. Thus according to the rigid plastic theory a mechanism forms when the reduced plastic moment is reached at this point due to the presence of three 'hinges' (two real, one plastic) and collapse occurs. The corresponding value of M/M_p is 0.98.

Case	Effective areas and Inertias due to plasticity - see Fig. 2 : 4
a	$A=\frac{4\,b\omega\,(d-d_f)(d_1-d)+4b_f d_f(d_1-d)-b_f d_3^2}{2(d_1-d)}$
	$I=\frac{b_f(12d^2d_f-12d\,d_f^2-3dd_3^2+d_3^3+4d_f^3)/6-b\omega(12d^2d_f-12dd_f^2-4d^3+4d_f^3)/6}{}$;
b	$A=2b_f d_f+2b\omega(d-d_f)+\frac{b_f(d_f^2-2d_3 d_f)-b\omega(d_3-d_f)^2}{2(d_1-d)}$
	$I=\frac{(b_f-b\omega)(12d^2d_f-9d_f^2d+3d_3d_f^2-6dd_3d_f+2d_f^3)/6-b\omega(3dd_3^2-d_3^3-4d^3)/6}{}$;
c	$A=\frac{(b_f(2d_f(d_1-d_3)-(2d-d_3)^2/2)+b\omega(2(d_f-d)(d_3-d_1)))}{(d_1-d)}$
	$I=b_f(12d\,d_f(d_1-d_3)-6d_f^2(d_1-d_3)+3dd_3^2-d_3^3-4d^3)/6$
d	$A=\frac{b_f(2d_f(d_1-d_3)-(2d-d_3)^2/2)+b\omega(2(d_f-d)(d_3-d_1))}{(d_1-d)}$
	$I=b_f(12dd_f(d_1-d_3)-6d_f^2(d_1-d_3)+3dd_3^2-d_3^3+4d^3-6dd_1^2+2d_1^3)/6$
e	$A=\frac{2(b_f-b\omega).d_f(d_1-d)+b_f(d_4^2-d_3^2)/2-2b\omega(d_1-d)(d_f+d)}{(d_1-d)}$
	$I=((b_f-b\omega)(12dd_f(d-d_f)+4d_f^3)+b_f(d_3^3+d_4^3-3d(d_3^2+d_4^2)+4d^3b\omega)/$
f	$A=(b_f(d_4-d_f)^2+b\omega(4dd_1-4d^2-d_3^2-d_f^2+2d_f d_4))/2(d_1-d))$;
	$I=\frac{((b_f-b\omega)(12d^2d_f-6ddd_3d_f-9dd_f^2+3d_3d_f^2+2d_f^3)+b_f(d_4^3-3dd_4^2)+b\omega(3dd_3^2-d_3^3-4d^3))/6}{}$
g	$A=2b\omega(d_1-d_3)$
	$I=\frac{(d_1-d_3)(b\omega(3d(d_3+d_4)-d_3^2-d_4^2-4d^2-2d_1^2+4dd_1-d_1d_3-2dd_4+d_1d_4)+6b_f d_f(2d-d_f))/6}{}$;
h	$A=(2b_f(d_f-2d+d_1)+2b\omega(d-d_f))\cdot(d_1-d_3)/(d_1-d)$;
	$I=b_f(d_1-d_3)(d_f(2d-d_f)+(d-d_1)(d_1-d_3))$

Table 2:1 Reduced stiffness values for I-section shapes

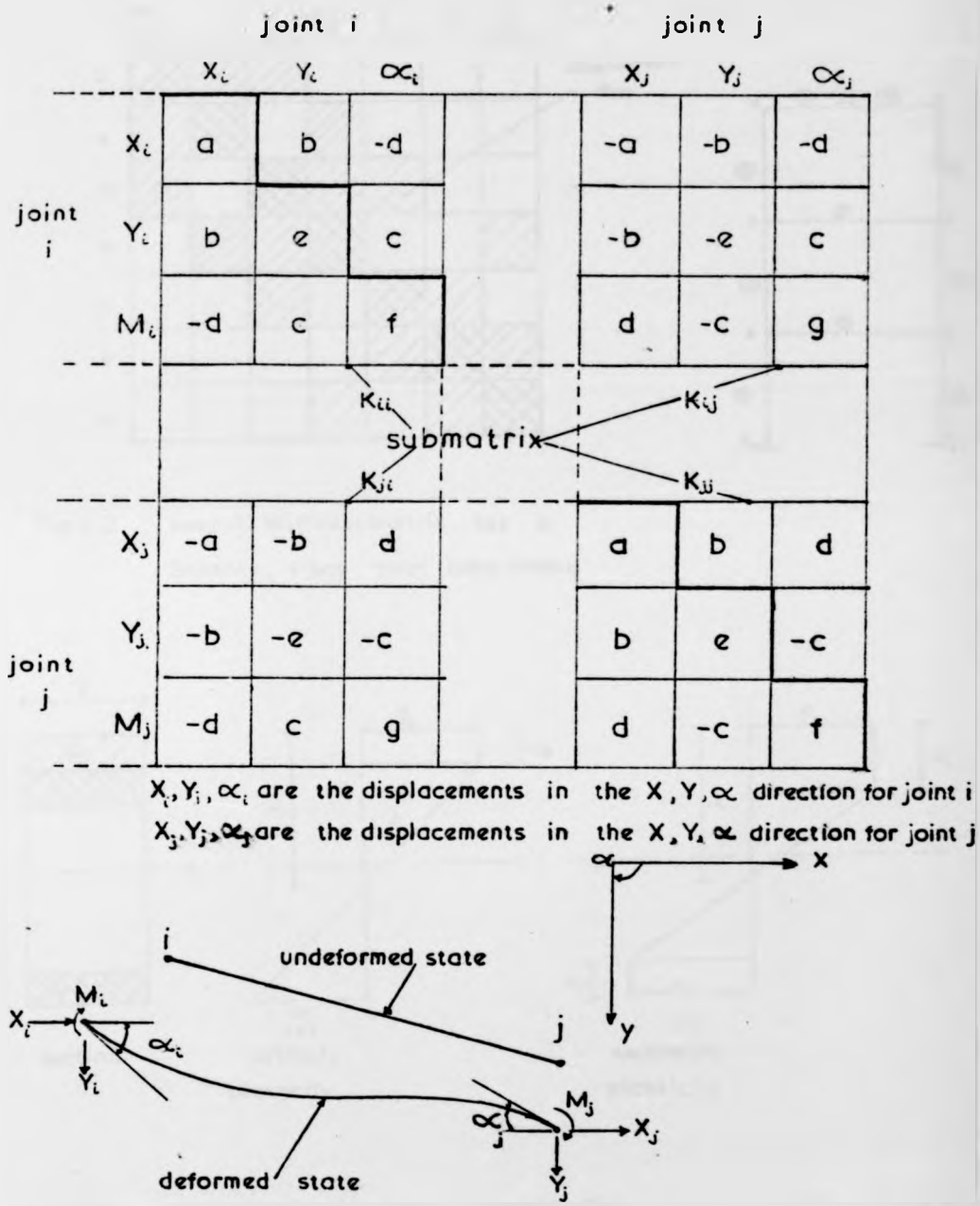

Fig.2-1 contribution of an individual member to the overall stiffness matrix

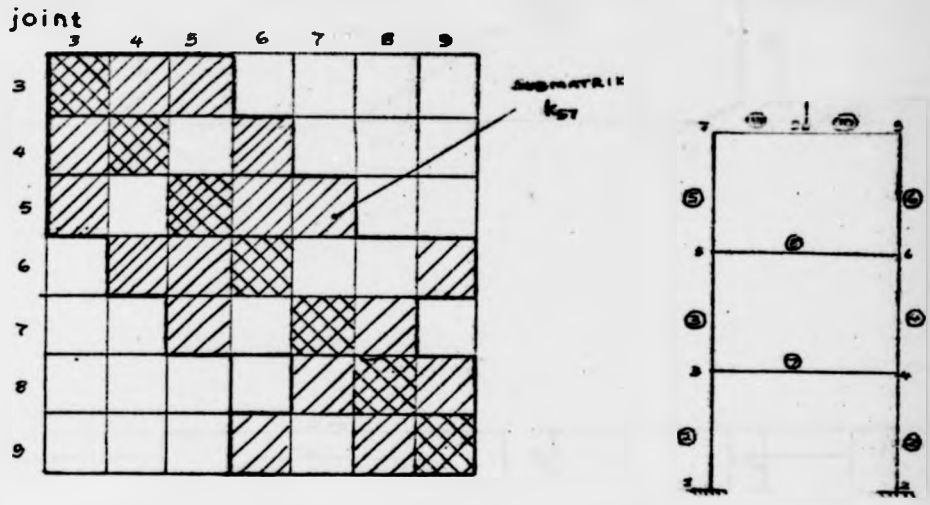

Fig 2.2 overall stiffness matrix for a 3-storey, 1-bay fixed base frame

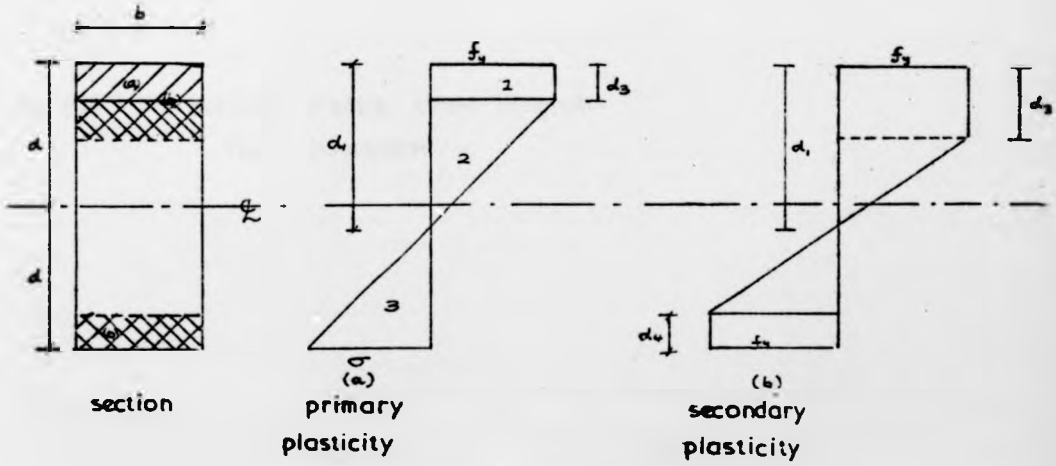

Fig 2.3 partially plastic stress diagrams for rectangular sections

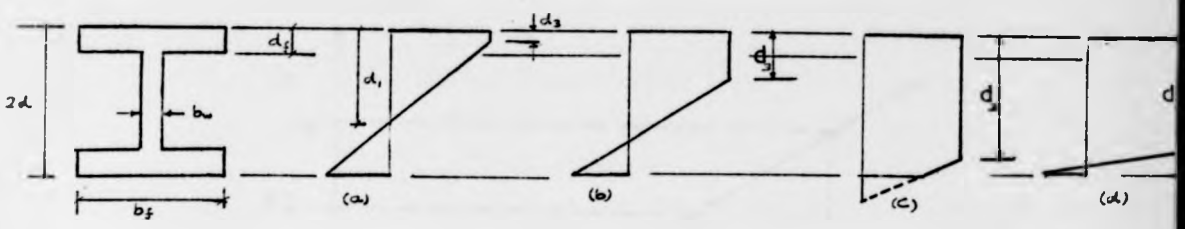

primary
plasticity

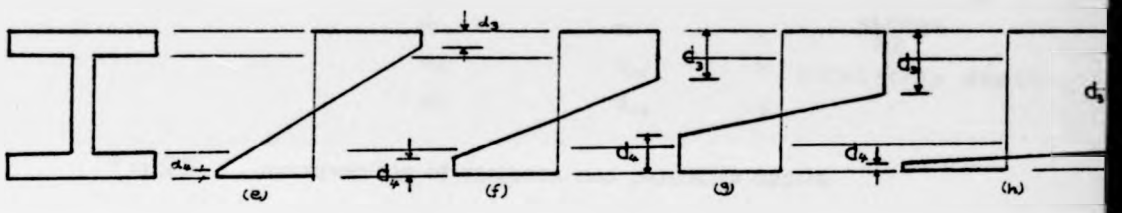

Secondary
plasticity

Fig 2·4 partially plastic stress diagrams for I-sections

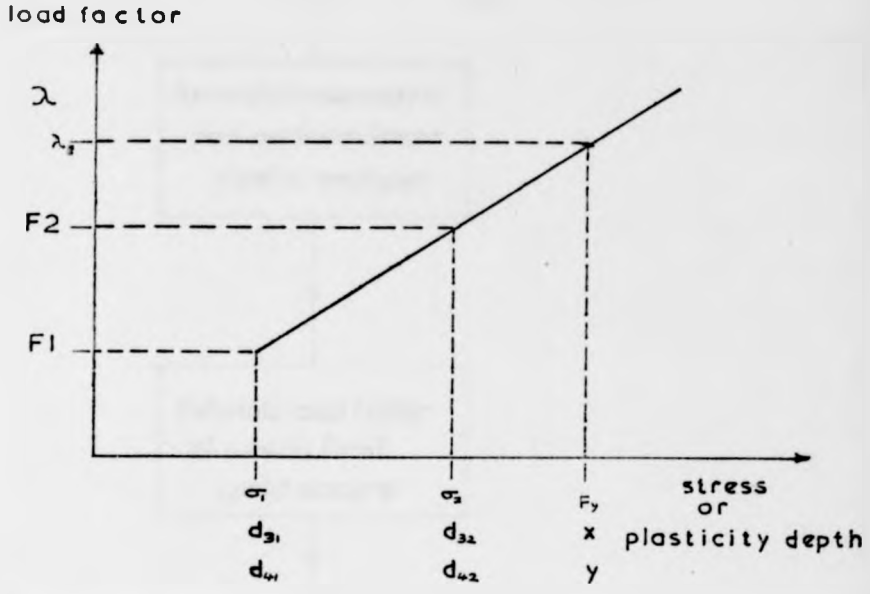

Fig. 2.5 extrapolation of stresses and plasticity depths

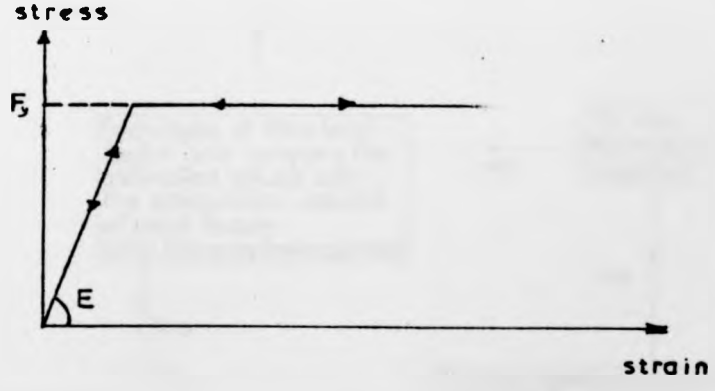

Fig. 2.6 assumed stress-strain relationship

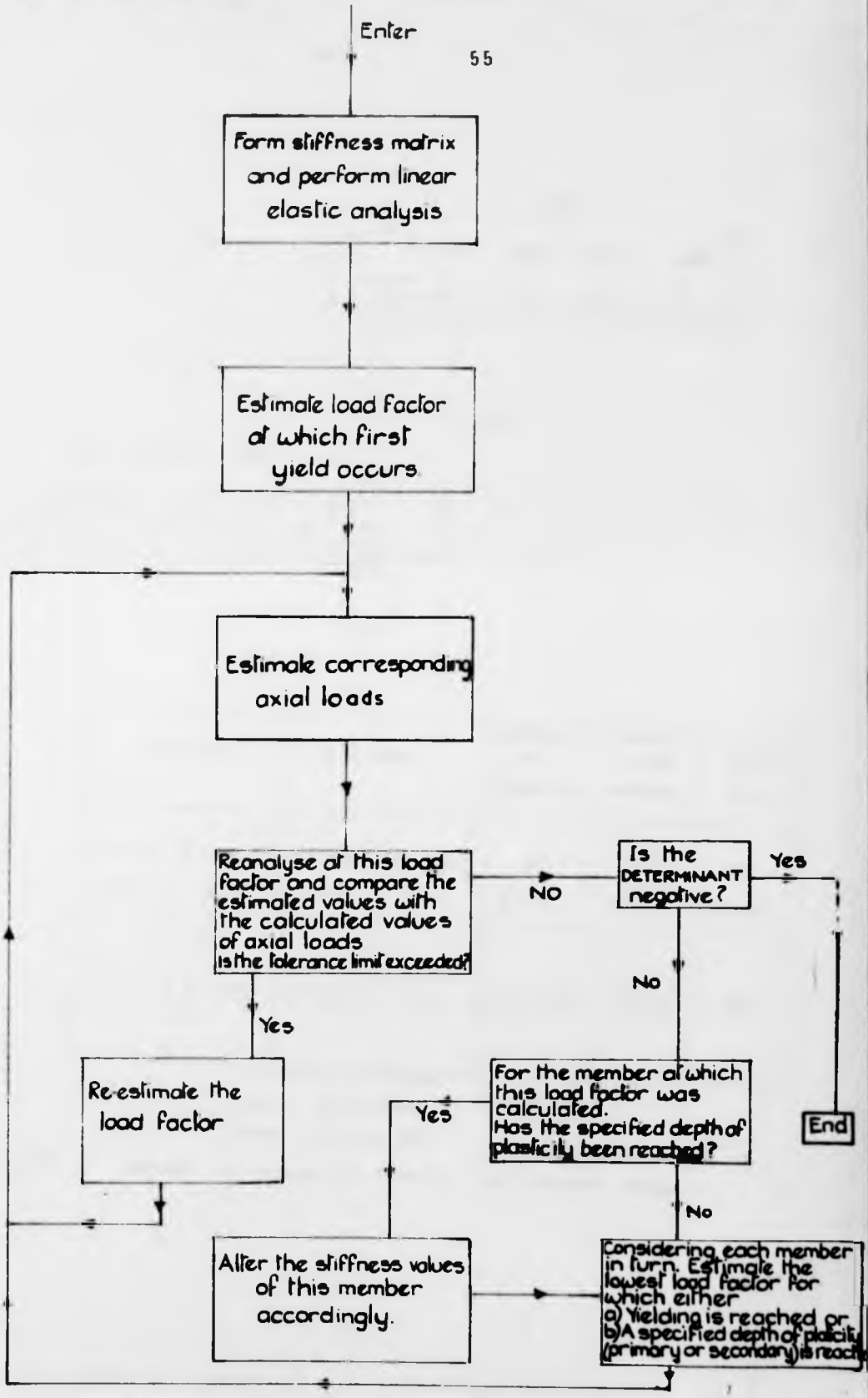

Fig 2:7 Flow Diagram of the Elastic - Plastic Computer Analysis

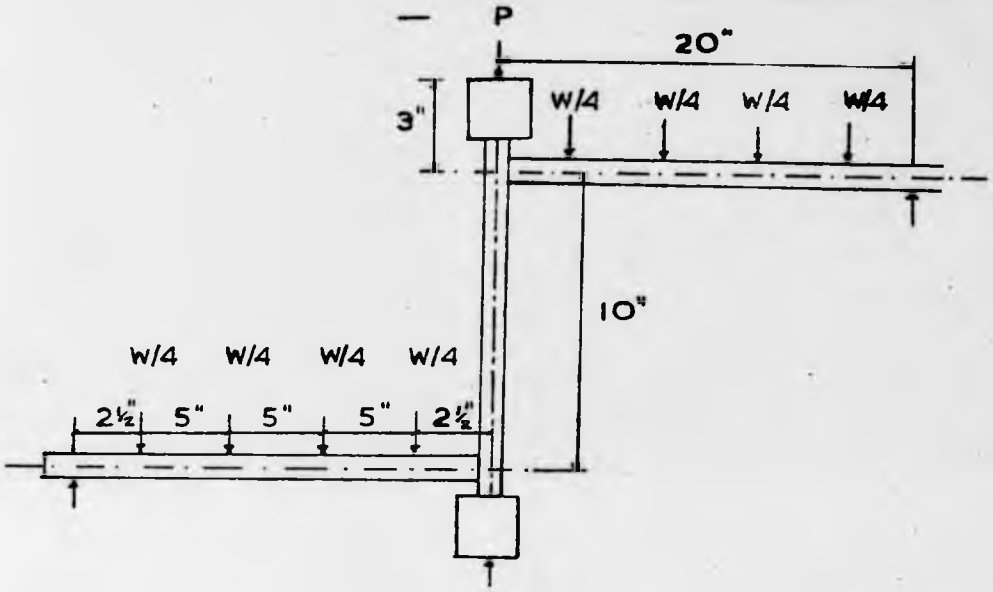

BEAMS		COLUMN		modulus of elasticity	lower yield stress	total beam load
depth [ins]	breadth [ins]	depth [ins]	breadth [ins]	E [t/in²]	[t/in²]	W [tons]
1.25	0.75	0375	1.25	13000	20.3	1.99

1 t/in² = 15.44 N/mm²
1 in = 25.40 mm
1 ton = 9.964 kN

Fig.2.8 details of frame and loading for horne's analysis

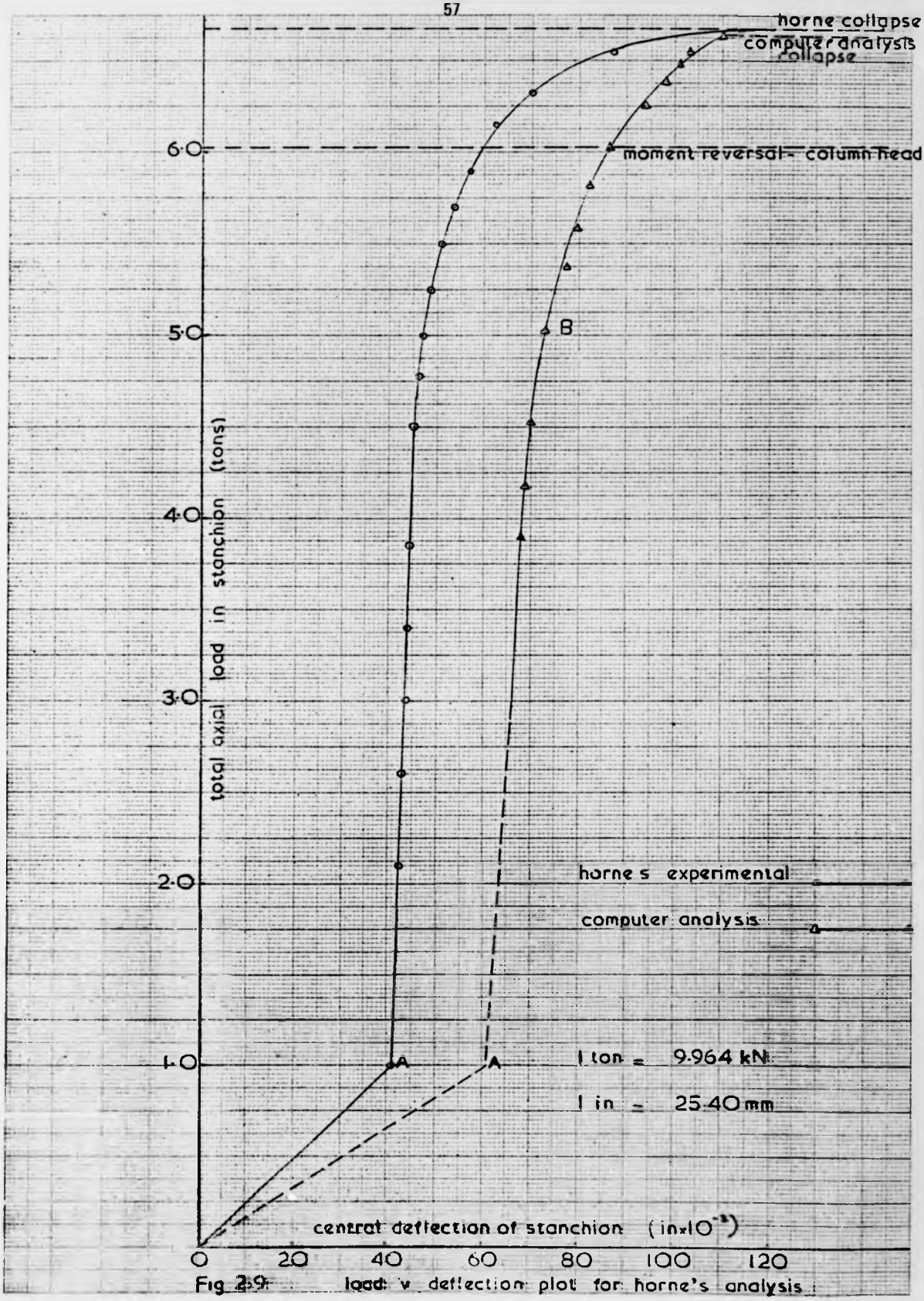

Fig 2.9 load v deflection plot for horne's analysis

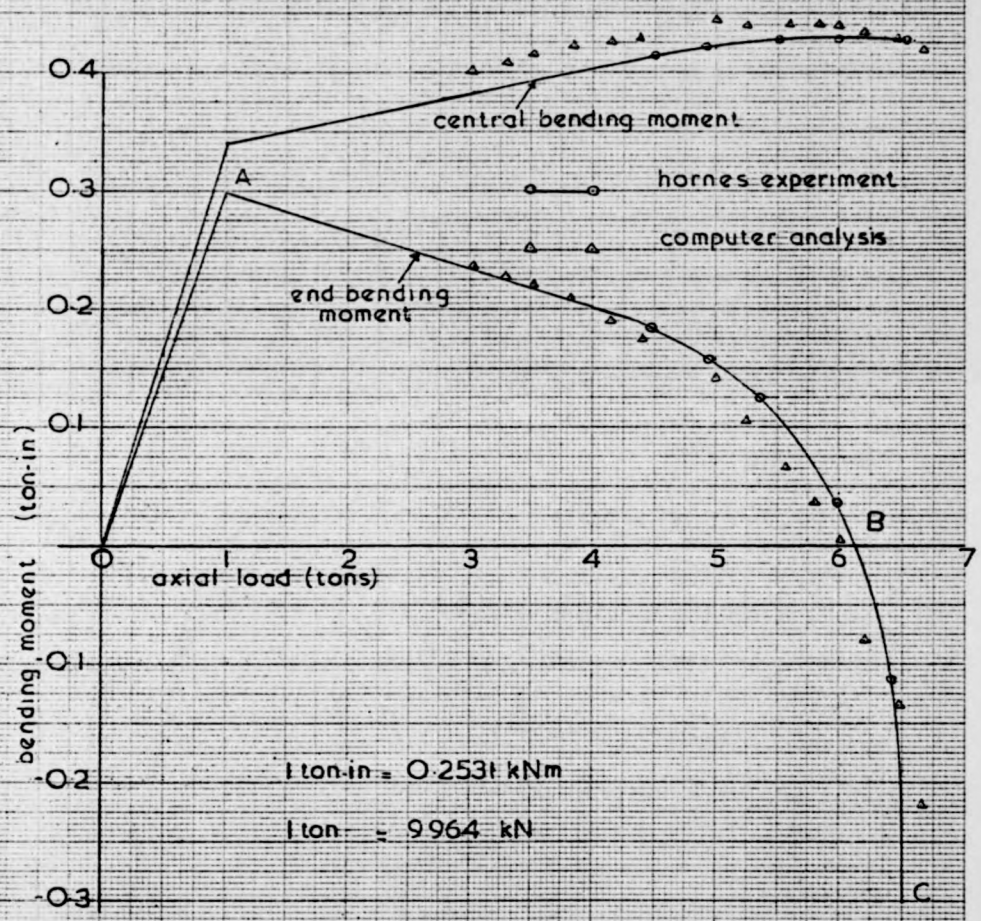

Fig 2·10 bending moment v axial load plot for horne's analysis

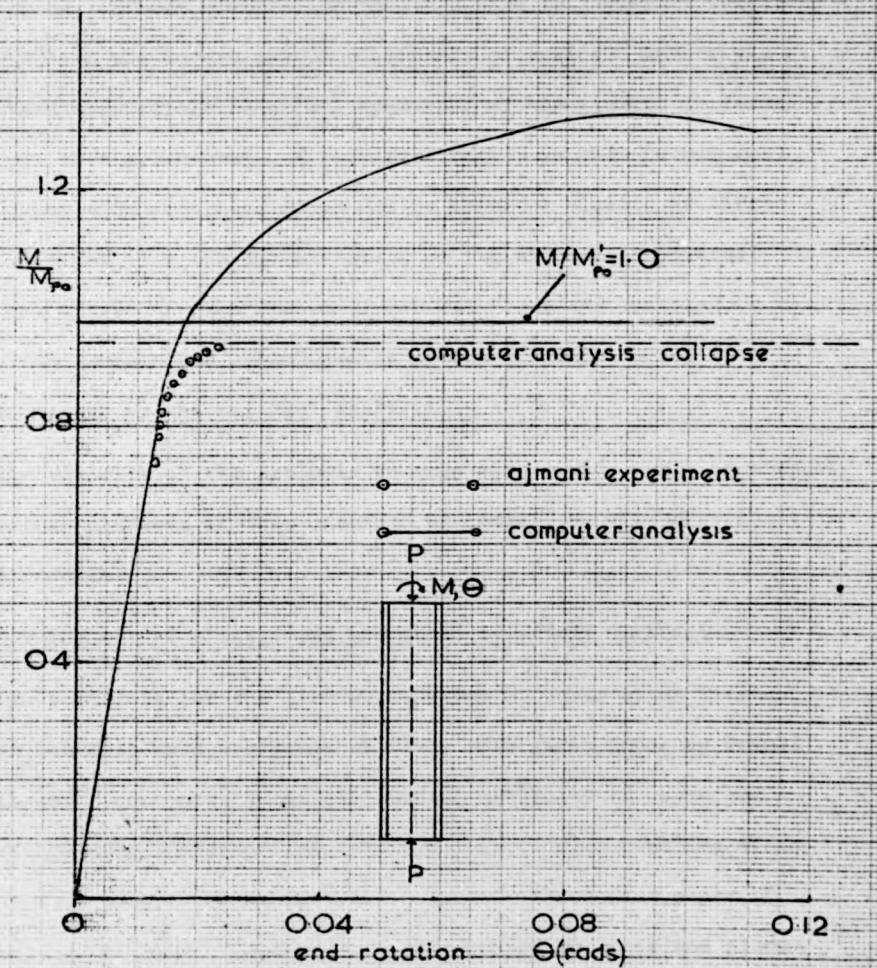

Fig. 2·11 load-rotation curve for ajmani's column C_{23} ($\beta = 0$)

Chapter 3. Elastic biaxial analysis of steel frames.

3.1 Introduction

A method which allows for elastic instability effects in steel frames loaded about the major axis only has previously been described in Chapter 2. Consideration of problems associated with space frameworks and biaxial loading of planar frames necessitate the extension of this analysis to cope with torsional and lateral-torsional instability. Finite element concepts are used to formulate relationships between the forces and displacements of a single member via simplified assumptions as to the behaviour of the element in terms of stress or displacement. A stiffness matrix is then formed for each member which contains terms due to both the elastic stiffness properties and also the forces acting on the member. An overall stiffness matrix is then assembled for the frame and operated on to obtain the deflections corresponding to the applied loading in a similar manner to the uniaxial analysis.

The validity of the analysis to cope with a wide range of elastic instability problems is then examined by comparison with previously quoted results.

3.2 Development of elastic and geometric stiffness matrices.

Two solutions for the lateral buckling of beams using finite element concepts were published in 1970. The first paper by Powell and Klinger[62] concentrated on the lateral stability of beams and ignored any axial deformations that may occur during buckling since these values tend to be quite small. However the second paper by Barsoum and Gallagher[63] generalised the problem to space and planar

frames by the inclusion of the axial deformation terms. In such frames, co-ordinate transformation techniques are usually used to specify the geometry of each member relative to some arbitary global axes, and in such cases these axial deformations should be included to allow for axial-flexural deformations. The method of Barsoum and Gallagher is summarised below.

The classical procedure for determining the buckling load of beams has been to solve the governing equations of Timoshenko.[64] However due to the complex form of the equations, only particular cases of loading and support conditions could be attempted. A finite element approach, however, enables solutions to be obtained for a wide range of loading and end restraint conditions. Furthermore, the extension to include non-prismatic and inelastic members as well as a variety of cross-sectional shapes is usually fairly straightforward.

The subject element is shown in Fig. 3.1. The rectangular co-ordinate system is chosen so that x and y coincide with the principal axes of the cross-section before buckling and x coincides with the centroidal axis C_1 C_2 before buckling. Let v, w denote the displacements of the centroidal axis in the y and z directions respectively; ϕ is the angle of twist and u is the axial displacement.

The following assumptions are then made:-

1. u, v, w and ϕ are assumed to be small such that their products are negligible.

2. The shear deformations of the middle surface are zero.
3. The cross-section is not deformed in its plane i.e. no distortion.
4. The axial load passes through the centroidal axis.

The angular displacements, θ, and ψ about the minor and major axis respectively are then defined by:-

$$\theta = \frac{dv}{dx} \quad , \qquad \psi = \frac{dw}{dx} \tag{3.1a}$$

The element in Fig. 3.1 is acted upon by an axial force P, end forces and end moments Q_{y_1}, Q_{y_2}, Q_{z_1}, Q_{z_2}, M_{y_1}, M_{y_2}, M_{z_1}, M_{z_2} act along axes parallel to the principal axes through the shear centre, and a torque M_x along an axis through the shear centre.

The warping displacement, χ, is defined as:

$$\chi = -\frac{d\phi}{dx} \tag{3.1b}$$

The potential energy of the system, πp, is given by:

$$\pi p = U - V \tag{3.2}$$

where U is the strain energy and V is the potential of the applied loads. Bleich[65] has shown that the strain energy can be expressed as

$$U = \frac{1}{2}\int_L (EI_{zz}v''^2 + EI_{yy}w''^2 + EC_w\phi''^2 + GJ\phi'^2 + EA\,u'^2)dx \tag{3.3}$$

where prime denotes d/dx ; E is Young's modulus, G is the shear modulus; I_{yy}, I_{zz} are the second moments of area about principal axes y, z; J is the St. Venant torsion constant, A is the area and C_w is the warping rigidity.

The potential of the applied load consists of two parts; the first part, V_1, is the product of the applied loads and their corresponding displacements

$$V_1 = P(u_1 - u_2) + Q_{y1} v_1 + Q_{y2} v_2 + Q_{z1} w_1 + Q_{z2} w_2 + M_{y1} \psi_1 + M_{y2} \psi_2 + M_{z1} \theta_1 + M_{z2} \theta_2 + M_x(\phi_1 - \phi_2) \qquad 3.4$$

The second part of V is the potential energy due to flexural and torsional action.

$$V = \sum_{i=2}^{7} V_i$$

where V_i are the separate contributions of the different forces. Corresponding values of these potential energy terms have been obtained by Barsoum and Gallagher.

Their values are:

$$V_2 = \tfrac{1}{2} \int_L P\left(v^{1^2} + w^{1^2} + I_o/A \cdot \phi^{1^2}\right) dx \qquad 3.6$$

$$V_3 = -\tfrac{1}{2} Q_{y1} \int_L w^{11} \cdot \phi \cdot x \, dx - \tfrac{1}{2} Q_{y2} \int_L w^{11} \phi \, (1-x) dx \qquad 3.7$$

$$V_4 = -\tfrac{1}{2} Q_{z1} \int_L v^{11} \phi x \, dx - \tfrac{1}{2} Q_{z2} \int_L v^{11} \phi \, (1-x) dx \qquad 3.8$$

$$V_5 = -\tfrac{1}{2} M_{y1} \int_L v^{11} \phi \, dx + \tfrac{1}{2} M_{y2} \int_L v^{11} \phi \, dx \qquad 3.9$$

$$V_6 = -\tfrac{1}{2} M_{z1} \int_L w^{11} \phi \, dx + \tfrac{1}{2} M_{z2} \int_L w^{11} \phi \, dx \qquad 3.10$$

$$V_7 = -\tfrac{1}{2} M_x \int_L (v^1 w^{11} - w^1 v^{11}) \, dx \qquad 3.11$$

Transformation of Eqn. 3.2 into the form of stiffness expressions requires the selection of a displacement function to describe the behaviour of the element. These functions are dependent on the

co-ordinate x, and are chosen to be exact solutions of axial and flexural displacements.

The required functions are given by:-

$$u = (1 - x/L)\, u_1 + x/L \cdot u_2 = [f_u]\ \{u\} \qquad 3.12a$$

$$v = f_1 v_1 + f_2 v_2 + f_3 \theta_1 + f_4 \theta_2 = [f_v]\ \{{}^{v}_{\theta}\} \qquad 3.12b$$

$$w = f_1 w_1 + f_2 w_2 + f_3 \psi_1 + f_4 \psi_2 = [f_w]\ \{{}^{w}_{\psi}\} \qquad 3.12c$$

$$\phi = f_1 \phi_1 + f_2 \phi_2 + f_3 \chi_1 + f_4 \chi_2 = [f_\phi]\ \{{}^{\phi}_{\chi}\} \qquad 3.12d$$

where $f_1 = 1 + 2\cdot(x/L)^3 - 3\cdot(x/L)^2$ 3.13a

$f_2 = 3\cdot(x/L)^2 - 2\cdot(x/L)^3$ 3.13b

$f_3 = - x\cdot(x/L - 1)^2$ 3.13c

$f_4 = - x\left((x/L)^2 - x/L\right)$ 3.13d

and $\theta_1 = -\left(\frac{dv}{dx}\right)_1$; $\theta_2 = -\left(\frac{dv}{dx}\right)_2$; $\psi_1 = -\left(\frac{dw}{dx}\right)_1$ 3.14a

$$\psi_2 = -\left(\frac{dw}{dx}\right)_2 \ ; \ \chi_1 = -\left(\frac{d\phi}{\phi\chi}\right)_1 \ ; \ \chi_2 = -\left(\frac{d\phi}{dx}\right)_2 \qquad 3.14b$$

Combination of Eqns. 3.2 - 3.14 gives the following value for the potential energy, πp.

$$\pi p = \frac{[u]}{2}\left(\int_L \{f_u^{\,1}\}[f_u^{\,1}]\ EA\ dx\right)\{u\} + \frac{[w,\psi]}{2}\left(\int \{f_w^{\,11}\}\ [f_w^{\,11}] EI_{yy} dx\right)\{{}^{w}_{\psi}\}$$

$$+ \frac{[v,\theta]}{2}\left(\int_L \{f_v^{\,11}\}\ [f_v^{\,11}]\ EI_{zz}\ dx\right)\{{}^{v}_{\theta}\} + \frac{[\phi,\chi]}{2}\left(\int_L \left(\{f_\phi^{11}\}[f_\phi^{11}]\ EC_w\right.\right.$$

$$\left.\left. + \{f_\phi^{\,1}\}\ [f_\phi^{\,1}]\ GJ\right)\ dx\right)\{{}^{\phi}_{\chi}\} - \frac{[w,\psi]}{2}\left(P\cdot\int_L \{f_v^{\,1}\}\ [f_v^{\,1}]\ dx\right)\{{}^{w}_{\psi}\}$$

$$- \frac{[v,\theta]}{2}\left(P\int_L \{f_w^{\,1}\}\ [f_w^{\,1}]\ dx\right)\{{}^{v}_{\theta}\} - \frac{[\phi,\chi]}{2}\ P\cdot\int_L \frac{I_o}{A}\cdot\{f_\phi^{\,1}\}[f_\phi^{\,1}]dx\ \{{}^{\phi}_{\chi}\}$$

$$+ [w,\psi]\cdot\left(\tfrac{1}{2}\ Q_{y_1}\int_L \{f_w^{11}\}\ [f_\phi]\ x\ dx + \tfrac{1}{2}\ Q_{y_2}\int_L \{f_w^{11}\}[f_\phi](L-x)dx\right)\{{}^{\phi}_{\chi}\}$$

$$+ [w,\psi] \cdot (\tfrac{1}{2}(M_{z1} - M_{z2}) \cdot \int_L \{f_w^{11}\} \cdot [f_\phi]\, dx)\, \{{}^{\phi}_{\chi}\} +$$

$$[v,\theta] \cdot (\tfrac{1}{2} Q_z \int_L \{f_v^{11}\}\, [f_\phi] x\, dx + \tfrac{1}{2} Q_{z2} \cdot \int_L \{fv^{11}\}[f_\phi](L-x)dx)\, \{{}^{\phi}_{\chi}\}$$

$$+ [v,\theta] \cdot (\tfrac{1}{2}(M_{y1} - M_{y2}) \cdot \int_L \{fv^{11}\} \cdot [f_\phi] dx \cdot \{{}^{\phi}_{\chi}\} +$$

$$[v,\theta] \cdot \Big(M_x/2 \cdot \int_L (\{f_v{}^{1}\}\, [fw^{11}] - \{fw^{1}\, [fv^{11}]\}) dx\, \{{}^{w}_{\psi}\} - [u]\{Fx\}$$

$$- [v,\theta]\, \{{}^{Q_y}_{M_z}\} - [w,\psi] \cdot \{{}^{Q_z}_{M_y}\} - [\phi]\, \{M_x\} \qquad 3.15$$

Terms like $\int_L \{fw^{11}\}[fw^{11}]\, EI_{yy}\, dx$ can be evaluated by substituting in this expression the displacement values from Eqns. 3.12 and 3.13, and integrating over the length L. A 4×4 submatrix in w_1, w_2, ψ_1 and ψ_2 will result, which forms part of the overall matrix. Similar submatrices for all the other displacement terms can be obtained by further integrations.

The overall stiffness matrix, which connects the externally applied forces and moments to their corresponding displacements, can conveniently be split into two distinct parts. The first part, $\underline{k}$, (the stiffness matrix) contains terms which depend only on the section properties (i.e. axial, flexural, torsional and warping stiffnesses) of the particular section in question. This matrix is thus a measure of the material's ability to withstand the applied loading. The second part, $\underline{n}$, (the geometric matrix) contains terms depending only on the internal forces (i.e. axial force, shear forces, bending moments and torque acting at the ends of a member). This geometric matrix accounts for the secondary effects caused by these internal forces, giving rise to buckling of the member.

Eqn. 3.15 can thus be written:

$$\pi p = [\, u,\ v,\ \theta,\ w,\ \psi,\ \phi,\ \chi\,] \cdot [\underline{k}]\ \{u,\ v,\ \theta,\ w,\ \psi,\ \phi,\ \chi\}^{-1} +$$

$$[\, u,v,\theta,w,\psi,\phi,\chi\,]\ [\underline{n}]\ \{u,v,\theta,w,\psi,\phi,\chi\}^{-1} - [u,v,\theta,w,\psi,\phi,\chi]\{F\} \qquad 3.16$$

The first term of the above equation (containing $\underline{k}$) is the strain energy U, the second term (containing $\underline{n}$) is the potential, V, of the applied load and the third part is the potential of the applied loads in the prebuckling state.

For stable equilibrium, using the principle of minimum potential energy.

$$\delta\pi p = 0 \qquad 3.17$$

Applying this to Eqn. 3.16, gives:

$$\{F\} = [\underline{k}] + [\underline{n}]\ \{\Delta\} \qquad 3.18$$

where $\{F\}$ is a vector of forces acting at the ends of the element.

$\{\Delta\}$ are the corresponding displacements.

Combining the stiffness and geometric matrices gives:

$$\{F\} = [\underline{K}]\ \{\Delta\} \qquad 3.19$$

where $\underline{K}$ is the combined stiffness and geometric matrix for the element. This matrix is given in Fig. 3.3 corresponding to the loading and deformations of Fig. 3.1.

3.3 Extension of the analysis to include unsymmetrical bending.

The previous discussion concentrated on deriving stiffness expressions for a beam when the loading was applied about principal axes. This analysis is now extended to consider the more general case of unsymmetrical bending where the loading is applied through any arbitary axes. The method is thus suitable for the elastic analysis of unsymmetrical sections.

The analysis will also enable allowance to be made for the unsymmetrical formation of plasticity under biaxial bending in a member which is initially symmetrically loaded in its elastic state. When a section is loaded biaxially so that plasticity develops, the orientation and position of its principal axes will change due to the reduction in effective stiffness brought about by the development of plastic regions.

Allowance for unsymmetrical bending can be made by altering the previous stiffness analysis in one of two ways.

Either: 1. By calculating the orientation of the new principal axes with respect to the elastic principal axes and then modifying the original stiffness matrix by using rotation transformations.

Or: 2. By basing the stiffness matrix on the original axes. The usual assumption for bending about the principal axes that $\int yzdA = 0$ does not now hold. Hence more general governing bending equations must be used and the stiffness matrix altered accordingly.

It was decided to retain the original elastic axes as a basis for the formation of the stiffness matrix and hence 'method 2' above was used. A slope deflection method is used to calculate the extra terms for inclusion in the stiffness matrix of Fig. 3.3.

3.4 Derivation of the stiffness coefficients for unsymmetrical bending.

The governing differential equations for unsymmetrical bending[65] are:

$$EI_{yy}\, z'' - EI_{yz}\, y'' = - M_y \qquad 3.20$$

$$EI_{zz} y'' - EI_{yz}\, z'' = - M_z \qquad 3.21$$

where prime denotes differentation with respect to x, and the definitions of the end forces and displacements are given in Fig. 3.1.

By manipulating the above equations, in terms of one differential variable, they become:

$$By'' = M_y\, I_{yz} + M_z\, I_{yy} \qquad 3.22$$

$$Bz'' = M_y\, I_{zz} + M_z\, I_{yz} \qquad 3.23$$

where $$B = E(I_{yz}^2 - I_{zz} \cdot I_{yy}) \qquad 3.24$$

By taking moments at an arbitary point along the member length:

$$M_z = M_{z1} + Q_{y1} \cdot x \qquad 3.25$$

$$M_y = M_{y1} - Q_{z1} \cdot x \qquad 3.26$$

Substitution into Eqn. 3.22 gives:

$$By'' = M_{y1}\, I_{yz} + Q_{z1} \times I_{yz} + M_{z1}\, I_{yy} + Q_{y1} \times I_{yy} \qquad 3.27$$

By integrating the equation with respect to x, and introducing the end rotations, the following expression is obtained:

$$B(\theta_2 - \theta_1) = L\cdot(M_{y1}\cdot I_{yz} + M_{z1}\cdot I_{yy}) + L^2/2\cdot(Q_{z1}\cdot I_{yz} + Q_{y1}\cdot I_{yy}) \quad 3.28$$

Integrating again and applying the end conditions:

$$B(v_2 - v_1) = = L^2/2\cdot(M_{y1}\cdot I_{yz} + M_{z1} I_{yy}) + L^3/6\cdot(Q_{z1}\cdot I_{yz} + Q_{y1}\cdot I_{yy}) + B\theta_1 L \quad 3.29$$

Similarly, by substitution of Eqns. 3.25 and 3.26 into Eqn. 3.23 and performing two integrations gives:

$$B(\phi_2-\phi_1) = L\cdot(M_{y1}\cdot I_{zz} + M_{z1} I_{yz}) + L^2/2\cdot(Q_{z1}\cdot I_{zz} + Q_{y1}\cdot I_{yz}) \quad 3.30$$

$$B(w_2- w_1) = L^2/2\ (M_{y1}\ I_{zz} + M_{z1} I_{yz}) + L^3/6\ \ (Q_{z1}\ I_{zz} + Q_{y1}\ I_{yz}) + B\phi_1 L \quad 3.31$$

Combination of Eqns. 3.28 - 3.31 enables each force Q_{y1}, Q_{z1}, M_{y1}, M_{z1} to be expressed in terms of the stiffness values and displacements.

Hence:

$$M_{z1} = \frac{2E}{L}\cdot\left(I_{zz}\left(\theta_2 + 2\theta_1 - \frac{3(v_2-v_1)}{L}\right) - I_{yz}\left(\phi_2+2\phi_1 - \frac{3(w_2- w_1)}{L}\right)\right) \quad 3.32$$

$$M_{y1} = \frac{2E}{L}\left(I_{yy}\left(\phi_2 +2\phi_1 - \frac{3(w_2- w_1)}{L}\right) - I_{yz}\left(\theta_2+2\theta_1 - \frac{3(v_2- v_1)}{L}\right)\right) \quad 3.33$$

$$Q_{y1} = \frac{-6E}{L^2}\left(I_{zz}\left(\theta_2+\theta_1 - \frac{2(v_2- v_1)}{L}\right) - I_{yz}\left(\phi_2+\phi_1-\frac{2(w_2- w_1)}{L}\right)\right) \quad 3.34$$

$$Q_{z1} = \frac{-6E}{L^2}\left(I_{yy}\left(\phi_2+\phi_1- \frac{2(w_2- w_1)}{L}\right) - I_{yz}\left(\theta_2+ \theta_1- \frac{2(v_2- v_1)}{L}\right)\right) \quad 3.35$$

Taking moments about End 2 gives:

$$M_{y2} + M_{y1} + Q_{z1}\cdot L = 0 \quad 3.36$$

$$M_{z2} + M_{z1} + Q_{y1}\cdot L = 0 \quad 3.37$$

Combination of Eqns. 3.36 and 3.37 with Eqns. 3.32 and 3.33 enable values of M_{z2} and M_{y2} to be found. Corresponding values of the shear forces Q_{y2} and Q_{z2} can also be obtained. These values are:

$$M_{z2} = \frac{2E}{L}\left(I_{zz}\left(2\theta_2+\theta_1-3\frac{(v_2-v_1)}{L}\right) - I_{yz}\left(2\phi_2+\phi_1 - 3\frac{(w_2-w_1)}{L}\right)\right) \qquad 3.38$$

$$M_{y2} = \frac{2E}{L}\left(I_{yy}\left(2\phi_2 + \phi_1 - 3\frac{(w_2-w_1)}{L}\right) - I_{yz}\left(2\theta_2+\theta_1 - 3\frac{(v_2-v_1)}{L}\right)\right) \qquad 3.39$$

$$Q_{y2} = -Q_{y1} \qquad 3.40$$

$$Q_{z2} = -Q_{z1} \qquad 3.41$$

The matrix of Fig. 3.3 is therefore modified by alteration of the following values:

$$B4 = -12EI_{yz}/L^3 \qquad 3.42a$$

$$D4 = -4EI_{yz}/L \qquad 3.42b$$

$$Q4 = 6EI_{yz}/L^2 + M_x/L \qquad 3.42c$$

$$Q5 = 6EI_{yz}/L^2 - M_x/L \qquad 3.42d$$

$$Q6 = -2EI_{yz}/L - M_x/2 \qquad 3.42e$$

$$Q7 = -2EI_{yz}/L + M_x/2 \qquad 3.42f$$

This matrix thus corresponds to a beam loaded biaxially through non-principal axes. The extension of this matrix to include members of any orientation will now be described.

3.5 Transformation of displacements.

In order to analyse plane frames of arbitary geometries and to relate the internal actions of the members, a rotation matrix[66] with respect to some global system of axes must be used. In the case of a plane frame, rotation about one axis only is required. Hence, in Chapter 2, the angle α was used to represent the inclination of any member to the overall axes. The extension to space frames necessitates a further rotation about a perpendicular set of axes. Thus in the present case, a member is assumed to have a rotation of α in the XZ plane (rotation about the Y axis) and a rotation of β in the XY plane (rotation about the Z axis) of Fig. 3.1. The corresponding sign convention for these rotations is given in Fig. 3.2. This second rotation, β, changes the method from a plane frame analysis to a space frame analysis and thus enables initial curvature about the minor axis to be dealt with easily by means of a suitable deflected shape.

Any member orientation can thus be specified with respect to some arbitary set of rectangular coordinate axes. The overall axes assumed here correspond to the beam element of Fig. 3.1. Hence the rotation matrix for such a member must revert to the unit matrix when $\alpha = \beta = 0$.

This rotation matrix is given by:-

$$\underline{a} = \begin{bmatrix} cc_1 & cs_1 & 0 & s & 0 & 0 & 0 \\ -s_1 & c_1 & 0 & 0 & 0 & 0 & 0 \\ 0 & 0 & c & 0 & ss_1 & sc_1 & 0 \\ sc_1 & -ss_1 & 0 & c & 0 & 0 & 0 \\ 0 & 0 & 0 & 0 & c_1 & -s_1 & 0 \\ 0 & 0 & -s & 0 & cs_1 & cc_1 & 0 \\ 0 & 0 & 0 & 0 & 0 & 0 & 1 \end{bmatrix} \begin{matrix} u_1 \\ v_1 \\ \theta_1 \\ w_1 \\ \psi_1 \\ \phi_1 \\ \chi_1 \end{matrix} \qquad 3.43$$

where c, c_1 are $\cos\alpha$ and $\cos\beta$ respectively; s, s_1 are $\sin\alpha$ and $\sin\beta$ respectively.

The above matrix refers to the transfer of displacements at end 1 of the member to the overall coordinate system or:-

$$\underline{X} = \underline{a}\,\underline{Z} \qquad 3.44$$

where $\underline{X}$ represents the member system of axes and $\underline{Z}$ the overall system of axes.

The corresponding rotation matrix, $\underline{A}$, for the member is given by:-

$$\underline{A} = \begin{bmatrix} \underline{a} & \underline{0} \\ \underline{0} & \underline{a} \end{bmatrix} \begin{matrix} \underline{X}_1 \\ \underline{X}_2 \end{matrix} \qquad 3.45$$

$\underline{A}$ is a 14×14 element matrix corresponding to the seven degrees of freedom at each joint. The $\underline{0}$ values in Eqn. 3.45 are null matrices of degree 7×7.

The above rotation matrix takes no account of any transformation of the warping displacement, χ. It will however be seen later that when any two members of differing orientation to the overall system of axes meet at a joint, it is assumed that there is full warping restraint.

Hence the modification of χ in the above matrix is not required.

The overall stiffness matrix of the frame is then obtained in the following way. The relationships between forces and displacements expressed in both local and global co-ordinates are as follows.[66]

$$\underline{F} = K\underline{X} \qquad 3.46$$

$$\underline{X} = \underline{A}\underline{Z} \qquad 3.47$$

$$L'\underline{Z} = \underline{F}'\underline{X} \qquad 3.48$$

where $\underline{F}$ is a vector of member forces

$\underline{X}$ is a vector of joint displacements expressed in local co-ordinates

$\underline{K}$ is the overall stiffness matrix

$\underline{A}$ is the transformation matrix from local to global co-ordinates

$\underline{Z}$ is a vector of displacements with respect to the global system

$\underline{L}$ is a vector of applied loads.

Prime denotes the transpose of the vector.

From Eqns. 3.46 and 3.47,

$$\underline{F} = K\,\underline{A}\,\underline{Z} \qquad 3.49$$

also from Eqns. 3.47 and 3.48

$$\underline{L}^1 = \underline{F}^1\,\underline{A} \qquad 3.50$$

By using matrix algebra, this gives

$$\underline{L} = \underline{A}^1\,\underline{F} \qquad 3.51$$

Combining Eqn. 3.49 and Eqn. 3.51 gives

$$\underline{L} = \underline{A}^1\,\underline{K}\,\underline{A}\,\underline{Z} \qquad 3.52$$

This equation thus connects the applied loads to the displacements in terms of the overall co-ordinate system.

Matrix $\underline{A}^1 \underline{K} \underline{A}$ is the overall stiffness matrix, and is given for the single member of Figs. 3.1 and 3.2 in Fig. 3.4.

3.6 Formation and solution of the overall stiffness matrix.

The stiffness matrix of Fig. 3.4 is now of a similar form to Fig. 2.1 for the uniaxial bending case with seven, rather than three, degrees of freedom at each joint. The matrix is also symmetrical about the leading diagonal and thus can be formulated using the irregular bandwidth technique and solved using the compact elimination process.[59] The need for an efficient joint numbering scheme now becomes even more necessary due to the large increase in storage space required by the extra degrees of freedom.

The storage requirement for a frame is given by:-

$$N = 28M + \sum_{j=1}^{m} 49 \cdot (j - i) \qquad 3.53$$

where M = number of joints

i is the lowest numbered joint that is connected to a given joint j (j > i).

The first term (28M) in the above expression is the amount of storage required by the 7×7 submatrices which lie on the leading diagonal. The second term gives the storage requirements of the off diagonal submatrices. A further $7 \cdot M$ locations are also needed to specify the address locations of the leading diagonal terms. If a restraint appears at a joint due to direction, rotation or warping fixity, then the corresponding row (and column)

is removed from the overall matrix.

By reference to Fig. 2.2, a comparison between the storage requirements of the uniaxial and biaxial cases can be made. No provision is made for rotation transformation of the warping displacement in the latter case. This means that joints such as 3, 4, 5, 6, 7 and 9 in Fig. 2.2 are assumed to be fully restrained against warping. This assumption is thought to be reasonable since the additional stiffness given by the joint connection will normally prevent any differential movement of the flanges of an I-section. The corresponding storage requirements including the address locations of the leading diagonal for the 3-storey, 1-bay frame are 162 and 599 respectively for the uniaxial and biaxial cases.

3.7 Non-linear elastic analysis procedure.

The required initial data is specified and an initial linear elastic analysis is performed by setting all the force and moment terms of the overall stiffness matrix to zero. The matrix is then solved using Gaussian elimination to calculate the internal forces corresponding to the applied loading. These internal forces are then substituted into the matrix for the previously zero geometric terms and the matrix is re-solved. Iteration is then continued until agreement between two consecutive sets of displacements obtained from the stiffness analysis are within a certain tolerance of each other. In the uniaxial method of Chapter 2, this tolerance test was performed solely on axial loads rather than displacements since the axial load is responsible for the lateral

instability effects. However when considering the biaxial case, instability will depend on the combined effects of forces and moments giving rise to the various flexural and flexural-torsional buckling modes. Application of a tolerance test to all the displacements ensures that an accurate assessment of instability effects due to a particular load level is made. Once convergence on deflections is obtained, the load factor is increased, and a linear extrapolation procedure is used to estimate the geometric terms to be used in the new overall stiffness matrix, based on the previous values. The process of analysis and reanalysis is again performed until the tolerance test on deflections is satisfied. The applied loading is again increased, and the process is continued until the determinant of the stiffness matrix becomes zero or negative. If necessary, the applied loading can now be reduced to a value halfway between the last convergence and the present collapse value. In this way, a more accurate assessment of the failure load is obtained. A flow diagram for the procedure is given in Fig. 3.5.

3.8 Use of the program to examine various elastic buckling problems.

Several examples which test the validity of the computer analysis in dealing with both frame and member elastic buckling will now be given. The examples cover various types of both beam and column buckling with various end restraint conditions and also some experimental results on continuous beams and portal frames.

3.8.1 Column buckling.

1) Pin-ended column.

For a perfectly straight pin-ended column, the elastic critical load is given by the well-known Euler buckling equation:

$$P_e = \pi^2 EI/L^2 \qquad 3.54$$

where P_e = Euler load; E = Young's modulus; I = second moment of area about the minor axis; L = column length.

If the column has initial single curvature about the minor axis, then the central deflection, y, is given by:

$$y = y_o / (P_e/P - 1) \qquad 3.55$$

where y_o is the initial central deflection and P is the axial load. The corresponding computer model had the following properties:-

E = 1000; I_y = 0.167; L = 10; assuming these values are part of a consistent set of units.

The column was split into 10 elements each of unit length, and an initial axial load of one unit was applied to the column.

From Eqn. 3.54, the Euler load, P_e = 16.45.

An initial deflected shape about the minor axis can be obtained by applying a constant single curvature moment about the minor axis. The load vector for inclusion in the analysis is thus specified in two parts. The first part contains the axial load and increases linearly as the load factor increases, the second part containing the minor axis moments is independent of this load factor. By applying a small unit moment about the minor axis, M_y', the initial central deflection was

$$y_o = 0.072$$

at a value of P close to the Euler load of 16.25 units, the central deflection is given by (Eqn. 3.55)

$$y_o = 0.072/ (16.45/16.25 - 1) = 5.870$$

The bending moment at the centre of the column, M_{yc}, is given by

$$M_{yc} = M_y + P \cdot y = 1 + 16.25 \times 5.87 = 96.39$$

The corresponding computer analysis gave values for y_o and M_{yc} as 5.900 and 97.00 respectively. The determinant of the stiffness matrix becomes negative at a load factor of 16.5, corresponding to an axial load of 16.5 units. A load factor increment of 0.1 had been used and thus the column had buckled at an axial load value of between 16.4 and 16.5. Further analyses, could have been performed as previously described by reducing the load increment and reanalysing. However agreement was thought to be excellent, particularly since only a small number of member elements had been used, and thus the extension to a greater number of elements was not attempted.

2) Restrained Columns.

The elastic critical load of a column which has full restraint against both translation and rotation at its ends is given by:

$$P_c = 4\pi^2 EI/L^2 \qquad 3.56$$

The same problem as for the pin-ended case has been attempted by setting $E = 250$ and thus the expected failure load is as above.

The computer analysis again indicated that the determinant of the stiffness matrix becomes negative at an axial load of 16.5. Increments of 0.1 for the axial load have again been used at values approaching the critical value.

3) Pure Torsional buckling of columns under axial load.

Pure torsional buckling is represented here by an axially loaded uniform section member constrained with respect to lateral displacements at its ends but free to rotate about its longitudinal axis.

The governing differential equation is:

$$EC_w \phi^{1111} + (PI_o/A - GJ)\phi^{11} = 0 \qquad 3.57$$

where prime denotes differentiation with respect to the longitudinal axis, x.

The boundary conditions are $\phi = 0$ at $x = 0$ and $x = L$

The exact solution is:

$$P_c = \frac{A}{I_o} (\pi^2 EC_w/L^2 + GJ) \qquad 3.58$$

Since the critical load is a function of several section properties of a member, a specific choice is used for these parameters in the finite element approximations. Consequently in the computer analysis, the values of E, G and L have arbitarily been set to 1000, 250 and 100 respectively whilst the section properties correspond to a 152 × 152 × 30 UC. The column is again split into 10 equal length elements and the non-linear analysis is performed under increasing axial load. Agreement between Eqn. 3.58 and the computer analysis is good. The computer solution gives a critical load of 550, compared to a value of 542 obtained from Eqn. 3.58.

4) Torsional buckling of pin-ended columns under unequal uniaxial end-moments.

Horne[13] has introduced the concept of 'equivalent uniform moment',

enabling columns acted on by a variety of unequal end moments to be treated as a single case under single curvature bending with respect to torsional instability. He gives charts relating the ratio of end moments, β, to a reduction factor which when multiplied by the larger end moment gives the corresponding single curvature moment. A check on the validity of the present analysis to deal with torsional instability under different combinations of end moments can be made by comparing this analysis with Horne's charts.

In order to test the validity of the computer analysis, it is necessary to consider an isolated pin-ended column under a series of different end moment ratios covering the range between single and double curvature bending. This reduction factor, m, is found to be dependent on the warping rigidity of the section. Hence a wide range of sections should be used to study the effects of this warping rigidity respectively.

The corresponding computer analysis is performed on a 203 × 203 × 46 UC of length 3 m and split into 20 elements of equal length. The buckling moment is then found for various ratios of end moments; each value of moment is then compared with the value obtained from the single curvature analysis.

The reduction coefficient, m, is given by

$$m = M_o/M_\beta \qquad 3.59$$

where M_o is the torsional buckling moment for single curvature bending

M_β is the buckling moment for an arbitary ratio of end moments.

For each value of end moment ratio, two values of buckling moment can be obtained by artificially setting the warping rigidity to zero and a very high value respectively (corresponding to a large universal column section, 356 × 406 × 634) in the overall stiffness matrix and performing two separate analyses.

The corresponding $m - \beta$ charts of Horne are compared with the present analysis in Fig. 3.6. Agreement between the two sets of values is found to be excellent.

3.8.2 Beam buckling

1. Lateral buckling of an I-section beam under single curvature bending moment.

The solutions of the governing differential equations for lateral buckling of beams with simple support conditions have been given by Timoshenko[64]. The equation for the critical moment, M_{cr}, is

$$M_{cr} = \frac{\pi}{L}\sqrt{EI_{yy} \cdot GJ \cdot (1 + \pi^2 EC_w/(GJL^2))} \qquad 3.60$$

An I-section with a total depth of 500 mm, flange breadth = 250 mm, flange and web thickness = 25 mm and a length of 7.5 m is used in the analysis. The beam is split into ten elements of equal length and the resulting buckling moment of 1100 kN gives exact agreement with Eqn. 3.60.

2. Lateral buckling of beams with varying end support conditions.

The extension of the governing differential equations to cover various end conditions is very difficult and so far has not been attempted by previous researchers. Nethercot[67], however, has proposed the introduction of two factors into Eqn. 3.60 which take

account of the additional end restraint. The critical moment, M_{cr}, now becomes

$$M_{cr} = \frac{k_1 \pi}{L} \sqrt{EI_{yy} \cdot GJ \cdot (1 + k_2 \pi^2 \, EC_w/(G \cdot J \cdot L^2))} \qquad 3.61$$

where k_1 and k_2 are the restraint factors, and revert to unity for simple end supports.

In order to obtain the factors k_1 and k_2 using the analysis program, it was necessary to treat the problem in two stages. Initially, an analysis is performed under the required support conditions by setting the warping rigidity, C_w, to zero in the overall stiffness matrix. When the determinant of the stiffness matrix becomes zero, k_1 can be found corresponding to this buckling moment by substitution into Eqn. 3.61. A second analysis is then performed to calculate a new buckling moment for the warping rigidity set to its correct value. A corresponding value of k_2 can thus be obtained by substituting the value of k_1 in Eqn. 3.61.

Values of k_1 and k_2 for various end conditions are given in Table 3.1. Using the above method, any small error in k will be magnified when obtaining the value k_2. The buckling moments obtained from the analysis correspond to a particular load level at which the determinant of the stiffness matrix is zero or negative. A more accurate value could be obtained if necessary by reducing the increment in load factor which is added to the full load factor at each convergence. However, agreement between the present analysis and Nethercot's values is thought to be excellent.

3.8.3 Experimental elastic buckling.

(i) Trahair[68] has presented some experimental and theoretical analyses for the elastic buckling of continuous beams. The tests were performed on a series of high strength aluminium beams of two spans which were loaded at the mid point of each span. The loading was applied to the top flange of the beam and various buckling modes were found for different ratios of span loading. As the load on one span of a continuous beam is increased from zero, the critical load of the other span increases due to changes in the major axis bending moment distribution, until a certain critical value is reached for which there is no load interaction between the two spans. This point corresponds to the situation where neither span offers any lateral buckling restraint to its neighbour. The section properties of the section and the corresponding interaction diagram of buckling are given in Fig. 3.7.

The effect of applying the load at a point away from the shear centre is to cause an extra term to appear in the overall stiffness matrix. As the beam rotates, the applied load vector will change due to the offset load causing additional twisting about the longitudinal axis. The stiffness matrix of Fig. 3.3 is thus altered by adding an extra moment term to the leading diagonal of the matrix.

Thus if a load, P_i, is applied at joint 'i', a distance $\bar{y}_i$ from the shear centre, the term E2 of submatrix K_{ii} corresponding to the twist term ϕ_i is given by

$$E2 = 1{\cdot}2\ GJ/L_i + 12\ EC_w/L_i^3 + P_i\bar{y}_i \qquad 3.62$$

A comparison between the experimental results of Trahair and the buckling values using the present analysis is given in Fig. 3.7. Each span is split into ten members of equal length and the applied loading (initially set at a fraction of the expected failure load) is specified in two parts, corresponding to either a fixed ratio between P_1 and P_2 or a fixed value of P_1 (i.e. P_1 remaining constant as the load factor is increased). Trahair found that his theoretical analysis consistently underestimated the experimental buckling loads by about 4%; a fact he attributed to additional restraint given by the supports. However the present analysis does not show a similar trend and gives better agreement with the experimental values.

(ii) Vacharajittiphan and Trahair[69] have extended the previous elastic buckling solution to cover simple rigid jointed fixed base I-section portal frames with vertical point loads on the columns and at the centre of the adjoining beam. In such a frame (see Fig. 3.8), the columns buckle out of plane when there is zero beam load. However, if the beam only is loaded, flexural-torsional buckling occurs. Thus in the general case of both beam and column loading, buckling is an interaction between these two cases. Corresponding small scale portal frame tests were performed on high strength I-sections which were of similar cross-section to the previous continuous beams. The section properties and frame details are given in Fig. 3.8 together with the interaction plot of column versus beam loads. For low-wide portal frames, the beam critical load was found to be fairly constant for a large range of column

loads. However, for high-narrow profile portal frames, the beam critical load significantly reduced after the application of only small column loads. In such frames, the stiffness of the columns is appreciably reduced due to the effects of compressive axial forces and hence the restraint at the beam-column intersection becomes less effective.

The present computer analysis has examined the low-wide portal frame and the results are compared in Fig. 3.8. The applied loading was again displaced from the shear and thus modifications using Eqn. 3.62 were used at the beam-column joints and at the mid-point of the beam. Generally, agreement between the two sets of results is good. Vacharajittiphan and Trahair found that the maximum discrepancy between his own theoretical studies and the experimental results was 6%. The present analysis gives values which are generally within 3% of the empirical curve.

3.9 Conclusions.

The present computer analysis has been used to obtain elastic buckling loads for a wide range of beam, column and simple portal frames with various loadings and end restraints. In all cases, agreement between the present analysis and previously cited results is found to be excellent. This demonstrates the validity of the method in dealing with various types of elastic lateral and lateral-torsional buckling modes.

End condition	Nethercot		Computer Analysis	
	k_1	k_2	k_1	k_2
simply supported both ends	1.0	1.0	1.0	1.0
warping fixed each end	1.09	4.38	1.08	4.42
complete fixity each end	2.00	4.00	2.00	4.00
one end s/s other end fixed	1.434	2.00	1.430	2.03

Table 3.1 restraint parameters for beams

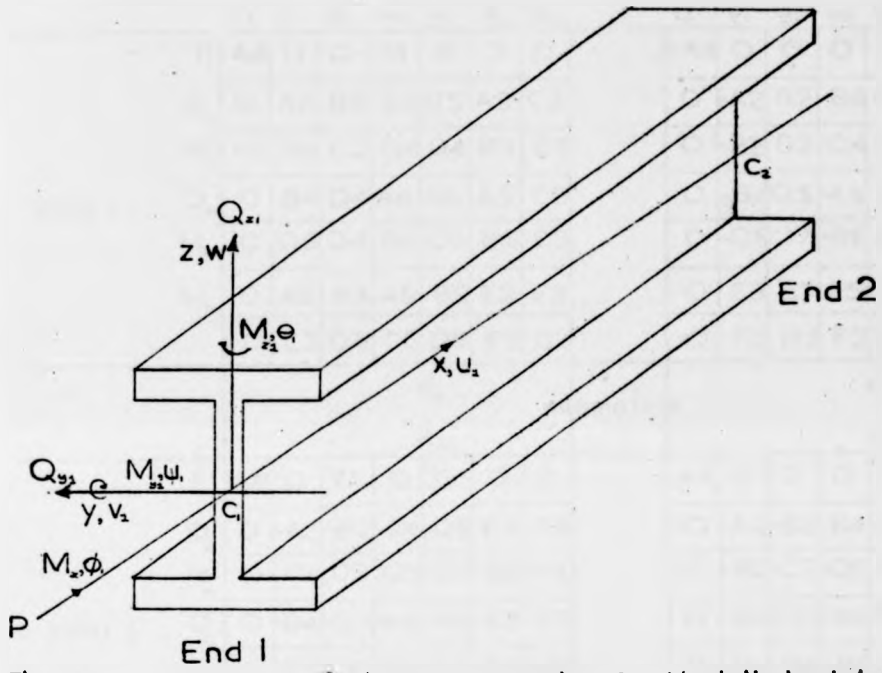

Fig. 3.1 force and displacement notation for biaxially loaded member

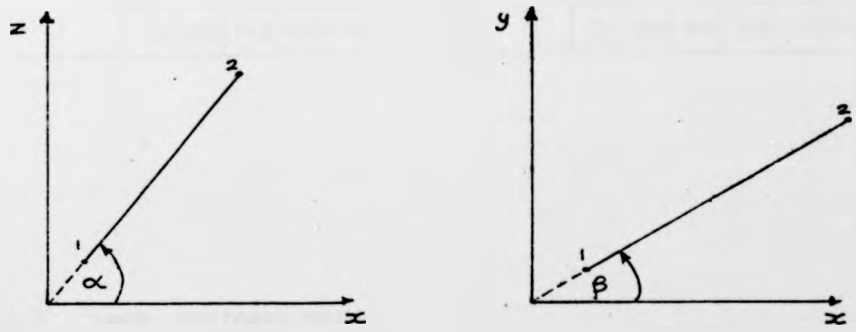

Fig 3.2 sign convention for rotations α and β

		u_i	v_i	θ_i	ω_i	ψ_i	ϕ_i	χ_i		u_j	v_j	θ_j	ω_j	ψ_j	ϕ_j	χ_j
joint i	P_i	A4	O	O	O	O	O	O		-A4	O	O	O	O	O	O
	Q_{zi}	O	A2	B2	B4	Q5	A3	C3		O	-A2	B2	-B4	Q4	I3	M3
	M_{xi}	O	B2	C2	Q4	D4	B3	D3		O	-B2	D2	-Q4	Q6	J3	N3
	Q_{xi}	O	B4	Q4	A6	B6	A5	C5		O	-B4	Q5	-A6	B6	I5	M5
	M_{yi}	O	Q5	D4	B6	C6	B5	D5		O	-Q5	Q7	-B6	D6	J5	N5
	M_{zi}	O	A3	B3	A5	B5	E2	F2		O	E3	G3	E5	G5	H2	I2
		O	C3	D3	C5	D5	F2	G2		O	F3	H3	F5	H5	-I2	J2
		K_{ii}							submatrix	K_{ij}						
		K_{ji}								K_{jj}						
joint j	P_j	-A4	O	O	O	O	O	O		A4	O	O	O	O	O	O
	Q_{zj}	O	-A2	-B2	-B4	-Q5	E3	F3		O	A2	-B2	B4	-Q4	K3	Ø3
	M_{xj}	O	B2	D2	Q5	Q7	G3	H3		O	-B2	C2	-Q5	D4	L3	P3
	Q_{xj}	O	-B4	-Q4	-A6	-B6	E5	F5		O	B4	-Q5	A6	-B6	K5	Ø5
	M_{yj}	O	Q4	Q6	B6	D6	G5	H5		O	-Q4	D4	-B6	C6	L5	P5
	M_{zj}	O	I3	J3	I5	J5	H2	-I2		O	K3	L3	K5	L5	E2	-F2
		O	M3	N3	M5	N5	I2	J2		O	Ø3	P3	Ø5	P5	-F2	G2

Fig.3.3 beam stiffness matrix

$A4 = EA/L$; $A2 = 12EI_z/L^3 + 1{\cdot}2P/L$; $B2 = -6EI_z/L^2 + P/10$;

$C2 = 4EI_z/L - 2PL/15$; $D2 = 2EI_z/L + PL/30$; $E2 = 1{\cdot}2GJ/L + 12EC_w/L^3$
$-1{\cdot}2\,P(A-L)$; $F2 = -GJ/10 - 6EC_w/L^2 + P(L-A)/10$;

$G2 = 2GJL/15 + 4EC_w/L - 2P(L-A)/15$;

$H2 = -1{\cdot}2GJ/L - 12EC_w/L^3 + 1{\cdot}2\,P(L-A)/L$;

$I2 = -GJ/10 - 6EC_w/L^2 + P(L-A)/10$;

$J2 = -GJL/30 + 2EC_w/L + P(L-A)/30$;

$A6 = 12EI_y/L^3 - 1{\cdot}2\,P/L$; $B6 = -6EI_y/L + P/10$;

$C6 = 4EI_y/L - 2PL/15$; $D6 = 2EI_y/L + PL/30$;

$A3 = -0{\cdot}6\,(M_{y1} - M_{y2})/L - 0{\cdot}05Q_{z1} - 0{\cdot}55Q_{z2}$

$B3 = 0{\cdot}55\,(M_{y1} - M_{y2}) + 0{\cdot}1Q_{z1}L + 0{\cdot}45Q_{z2}L$

$C3 = 0{\cdot}05\,(M_{y1} - M_{y2}) + 0{\cdot}05Q_{z2}L$

$D3 = -(M_{y1} - M_{y2})L/15 - Q_{z1}L^2/60 - 0{\cdot}05Q_{z2}L^2$

$E3 = 0{\cdot}6\,(M_{y1} - M_{y2})/L + 0{\cdot}05Q_{z1} + 0{\cdot}55Q_{z2}$

$F3 = -0{\cdot}05\,(M_{y1} - M_{y2}) - 0{\cdot}05Q_{z1}L$

$G3 = 0{\cdot}05\,(M_{y1} - M_{y2}) - 0{\cdot}05Q_{z1}L + 0{\cdot}1Q_{z2}L$

$H3 = (M_{y1} - M_{y2})L/60 + Q_{z1}L^2/60$

$I3 = 0{\cdot}6\,(M_{y1} - M_{y2})/L + 0{\cdot}55Q_{z1} + 0{\cdot}05Q_{z2}$

$J3 = -0{\cdot}05\,(M_{y1} - M_{y2}) - 0{\cdot}1Q_{z1}L + 0{\cdot}05Q_{z2}L$

$K3 = -0{\cdot}6\,(M_{y1} - M_{y2})/L - 0{\cdot}55Q_{z1} - 0{\cdot}05Q_{z2}$

$L3 = -0{\cdot}55\,(M_{y1} - M_{y2}) - 0{\cdot}45Q_{z1}L - 0{\cdot}1Q_{z2}L$

$M3 = 0{\cdot}05\,(M_{y1} - M_{y2}) + 0{\cdot}05Q_{z1}L$

$N3 = (M_{y1} - M_{y2})L/60 + Q_{z2}L^2/60$

$\emptyset 3 = -0{\cdot}05\,(M_{y1} - M_{y2}) - 0{\cdot}05Q_{z2}L$

$P3 = -(M_{y1} - M_{y2})L/15 - 0{\cdot}05Q_{z1}L^2 - Q_{z2}L^2/60$

A5, B5 ..... P5 are given by replacing M_{y1}, M_{y2}, Q_{z1}, Q_{z2} by respectively M_{z1}, M_{z2}, Q_{y1}, Q_{y2} in A3, B3..... P3 above

$B4 = D4 = 0$

$Q5 = -M_x/L$

$Q4 = M_x/L$

$Q6 = -M_x/2$

$Q7 = M_x/2$

Fig.3.3 (cont.)

	u_i	v_i	θ_i	ω_i	ψ_i	ϕ_i	x_i		u_j	v_j	θ_j	ω_j	ψ_j	ϕ_j	x_j
	A7														
	B7	C7													
	D7	E7	F7												
joint i	G7	H7	I7	J7					symmetric						
	K7	L7	M7	N7	Ø7										
	P7	Q7	R7	S7	T7	U7									
	V7	W7	X7	Y7	Z7	A8	B8								
	-A7	-B7	C8	-G7	D8	E8	F8		A7						
	-B7	-C7	G8	-H7	H8	I8	J8		B7	C7					
	K8	L8	M8	N8	Ø8	P8	Q8		R8	S8	T8				
joint j	-G7	-H7	U8	-J7	V8	W8	X8		G7	H7	Y8	J7			
	Z8	A9	B9	C9	D9	E9	F9		G9	H9	I9	J9	K9		
	L9	M9	N9	Ø9	P9	Q9	R9		S9	T9	U9	V9	W9	X9	
	Y9	Z9	A10	B10	C10	D10	E10		F10	G10	H10	I10	J10	K10	B8

Fig.3-4 overall member stiffness matrix

$A7 = A4c_1^2c^2 + A2s_1^2 + 2B4s_1s_1c_1 + A6s_1^2c_1^2$

$B7 = A4c_1sc^2 + A6s_1cs^2 - A2c_1s_1 + B4s(s_1^2 - c_1^2)$

$C7 = A4s_1^2c^2 + A2c_1^2 - 2B4s_1sc_1 + A6s_1^2c_1^2$

$D7 = A3s_1s + A5s_1^2c_1 - B2s_1c - Q4c_1cs$

$E7 = B2c_1c - Q4s_1cs - A3c_1s + A5s_1s^2$

$F7 = C2c^2 - 2B3sc + E2s^2$

$G7 = (A4-A6)c_1cs - B4s_1c$

$H7 = (A4-A6)s_1cs + B4c_1c$

$I7 = Q4c^2 - A5cs$; $J7 = A4s^2 + A6c^2$

$K7 = -B2s_1^2s - Q4s_1c_1s^2 - Q5c_1s_1 - B6c_1^2s - A3s_1^2c - A5s_1c_1c$

$L7 = B2c_1ss - Q4s_1^2s + Q5c_1^2 - B6c_1ss + A3c_1sc - A5s_1^2c$

$M7 = C2s_1cs - B3s_1s^2 + D4c_1c - B5c_1s - E2s_1cs$

$N7 = Q4s_1cs + B6c_1c + A5s_1c^2$

$\emptyset 7 = 2D4c_1ss + 2B5c_1sc + 2B3s_1^2cs + C2s_1^2s^2 + C6c_1^2 + E2s_1^2c^2$

$P7 = (B6-B2)c_1ss + Q5s_1^2 - Q4c_1^2s^2 - A3c_1sc - A5c_1^2cs$

$R7 = (C2-E2)c_1cs + B3c_1(c^2-s^2) + B5s_1s - D4sc$

$S7 = Q4c_1cs - B6sc + A5c_1c^2$

$T7 = D4s(c_1^2-s_1^2) + B5c(c_1^2-s_1^2) + 2B3c_1s_1cs + C2c_1ss^2 - C6c_1s_1 + E2c_1s_1c^2$

$U7 = 2B3c_1^2cs - 2B5c_1sc - 2D4c_1ss + C2c_1^2s^2 + C6s_1^2 + E2c_1^2c^2$

$V7 = -C3s_1 - C5c_1s$; $W7 = C3c_1 - C5s_1s$

$X7 = D3c - F2s$; $Y7 = C5c$

$Z7 = D3s_1s + D5c_1 + F2sc$

$A8 = D3c_1s - D5s_1 + F2c_1c$; $B8 = G2$

$C8 = B2s_1c + E3s_1s + Q4c_1cs + E5c_1s^2$

$D8 = B2s_1^2s + Q5s_1c_1 - E3s_1^2c + Q4c_1s_1s^2 + B6c_1^2s - E5c_1s_1cs$

$E8 = B2c_1ss - Q5s_1^2 - E3c_1sc + Q4c_1^2s^2 - B6c_1ss - E5c_1^2cs$

$F8 = -F3s_1 - F5c_1s$

$G8 = E5s_1s^2 + Q4s_1cs - E3c_1s - B2c_1c$

$H8 = B6c_1ss + Q4s_1^2s^2 - B2c_1ss - Q5c_1^2 + E3c_1sc - E5s_1^2cs$

$I8 = -B2c_1^2s + Q5c_1s_1 + E3c_1^2c + Q4c_1s_1s^2 - B6s_1^2s - E5c_1s_1cs$

$J8 = F3c_1 - F5s_1s$

$K8 = I3s_1s + I5c_1s^2 - B2s_1c - Q5c_1cs$

$L8 = B2c_1c - Q5s_1cs - I3c_1s + I5s_1s^2$

$M8 = D2c^2 - G3cs - J3cs + H2s^2$

$N8 = Q5c^2 - I5cs$

$\emptyset 8 = (D2-H2)s_1cs + Q7c_1c + G3s_1c^2 - J3ss^2 - J5c_1s$

$P8 = (D2-H2)c_1cs - Q7s_1c + G3c_1c^2 - J3c_1s^2 + J5s_1s$

$Q8 = H3c + I2s$

$R8 = B2s_1c + Q5c_1cs + K3s_1s + K5c_1s^2$

$Q7 = B2c_1^2s - Q4c_1s_1s^2 - Q5c_1s_1 + B6s_1^2s + A3c_1^2c - A5c_1s_1c$

Fig. 3-4 (cont.)

$S8 = -B2c_1c + Q5s_1cs - K3c_1s + K5s_1s^2$

$T8 = C2c^2 + E2s^2 - 2L3sc$

$U8 = -Q4c^2 - E5cs$

$V8 = E5s_1c^2 - B6c_1c - Q4s_1cs$

$W8 = E5c_1c^2 + B6s_1c - Q4c_1cs$

$X8 = F5c$; $Y8 = -Q5c^2 - K5cs$

$Z8 = -B2s_1s - Q5c_1s_1s^2 - Q4s_1c_1 - B6c_1s^2 - I3s_1^2c - I5c_1s_1cs$

$A9 = (B2 - B6)c_1s_1s - Q5s_1^2s^2 + Q4c_1^2 + I3c_1s_1c - I5s_1^2cs$

$B9 = (D2 - H2)s_1cs - G3s_1s^2 + Q6c_1c - G5c_1c + J3s_1c^2$

$C9 = Q5s_1cs + B6c_1c + I5s_1c^2$

$D9 = (Q7 + Q6)c_1s_1s + (G5 + J5)c_1s_1c + D2s_1^2s^2 + (G3 + J3)s_1^2sc + D6c_1^2 + H2s_1^2c^2$

$E9 = (G3 + J3)c_1s_1cs + (D2s^2 + H2c^2)c_1s_1 + (Q6s + G5c)c_1^2 - (J5c + Q7s)s_1^2 - D6c_1s_1$

$F9 = H3s_1s + H5c_1 - I2s_1c$

$G9 = (B2s - K3c)s_1^2 + (Q5s^2 + Q4)c_1s_1 + B6c_1^2s - K5c_1s_1cs$

$H9 = (B6 - B2)c_1s_1s + Q5s_1^2s^2 - Q4c_1^2 + K3c_1s_1c - K5s_1^2cs$

$I9 = (C2 - E2)s_1cs + L3s_1(c^2 - s^2) + D4c_1c - L5c_1s$

$J9 = K5s_1c^2 - B6c_1c - Q5s_1cs$

$K9 = 2D4c_1ss + 2L5c_1s_1c + 2L3s_1^2cs + C2s_1^2s^2 + C6c_1^2 + E2s_1^2c^2$

$L9 = (B6 - B2)c_1s_1s - Q5c_1^2s^2 + Q4s_1^2 - I3c_1s_1c - I5c_1^2cs$

$M9 = (B2s + I3c)c_1^2 - (Q5s^2 + Q4)c_1s_1 + B6s_1^2s - I5c_1s_1cs$

$N9 = (D2 - H2)c_1cs - G3c_1s^2 - Q6s_1c + G5s_1s + J3c_1c^2$

$\emptyset 9 = Q5c_1cs - B6s_1c + I5c_1c^2$

$P9 = (G3 + J3)c_1s_1cs + (Q7s + J5c)c_1^2 - (Q6s + G5c)s_1^2 + (D2s^2 - D6)c_1s_1 + H2c_1s_1c$

$Q9 = (G3 + J3)c_1^2cs - (Q7 + Q6)c_1s_1s - (J5 + G5)c_1s_1c + (D2s^2 + H2c^2)c_1^2 + D6s_1^2$

$R9 = H3c_1s - H5s_1 - I2c_1c$

$S9 = (B2 - B6)c_1s_1s + Q5c_1^2s^2 - K3c_1s_1c - Q4s_1^2 - K5c_1^2cs$

$T9 = (Q5s^2 + Q4)c_1s_1 - B2c_1^2s - B6s_1^2s + K3c_1^2c - K5c_1s_1cs$

$U9 = (C2 - E2)c_1cs + L3c_1(c^2 - s^2) - D4s_1c + L5s_1s$

$V9 = B6s_1c + K5c_1c^2 - Q5c_1cs$

$W9 = 2L3c_1s_1cs + D4s(c^2 - s^2) + L5c(c_1^2 - s_1^2) + (E2c^2 + C2s^2 - C6)c_1s_1$

$X9 = 2L3c_1^2cs - 2D4c_1ss - 2L5c_1s_1c + E2c_1^2c^2 + C2c_1^2s^2 + C6s_1^2$

$Y9 = -M3s_1 - M5c_1s$; $Z9 = M3c_1 - M5s_1s$

$A10 = N3c - I2s$; $B10 = M5c$

$C10 = N3ss + N5c_1 + I2s_1c$; $D10 = N3c_1s - N5s_1 + I2c_1c$

$E10 = J2$; $F10 = -\emptyset 3s_1 - \emptyset 5c_1s$

$G10 = \emptyset 3c_1 - \emptyset 5s_1s$; $H10 = P3c + F2s$

$I10 = \emptyset 5c$; $J10 = P3s_1s + P5c_1 - F2s_1c$

$K10 = P3c_1s - P5s_1 - F2c_1c$;

$c = \cos\alpha$; $s = \sin\alpha$; $c_1 = \cos\beta$; $s_1 = \sin\beta$

Fig. 3-4 (cont.)

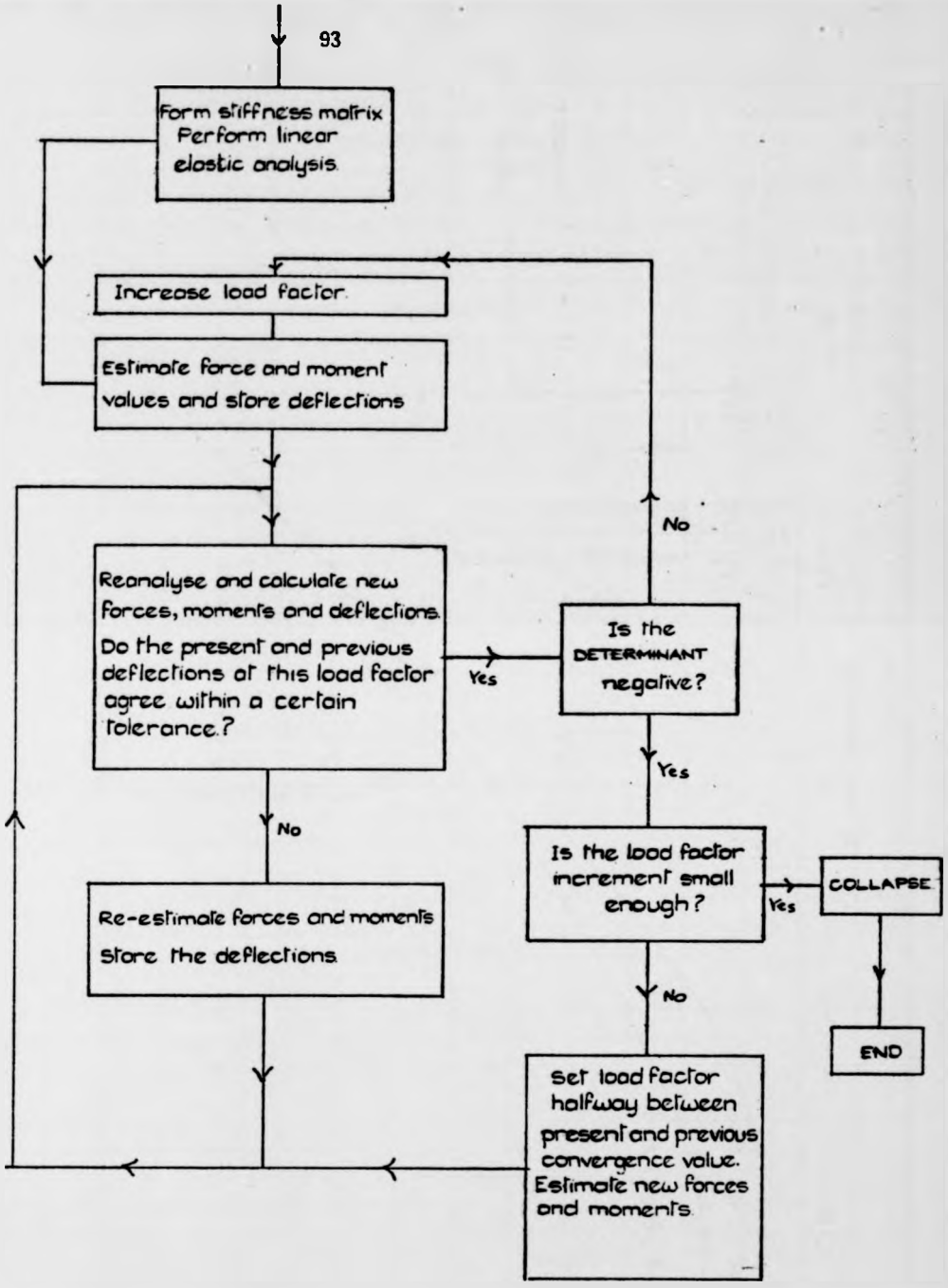

Fig. 3:5 Flow diagram for non-linear elastic program

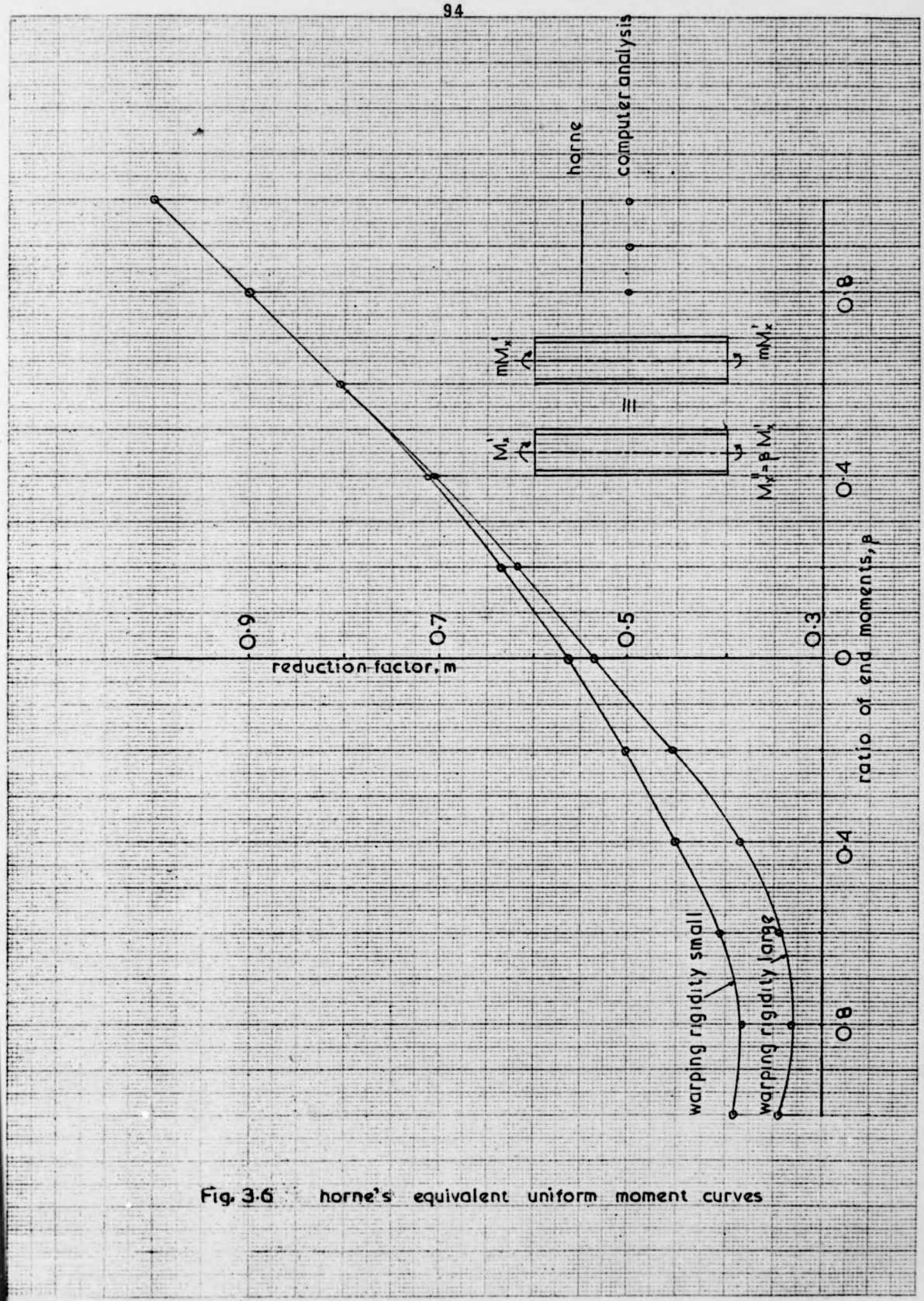

Fig. 3.6 horne's equivalent uniform moment curves

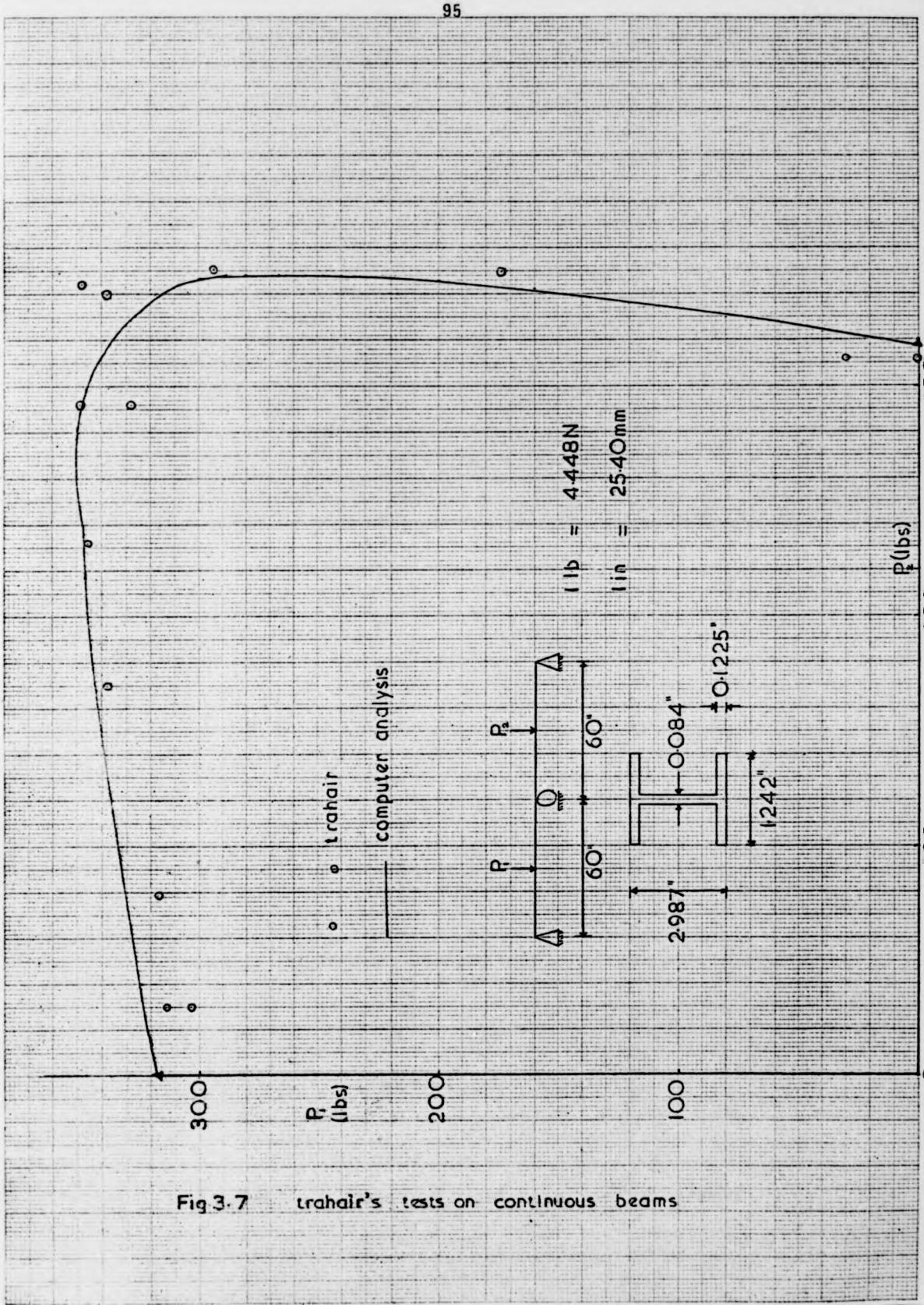

Fig 3.7 trahair's tests on continuous beams

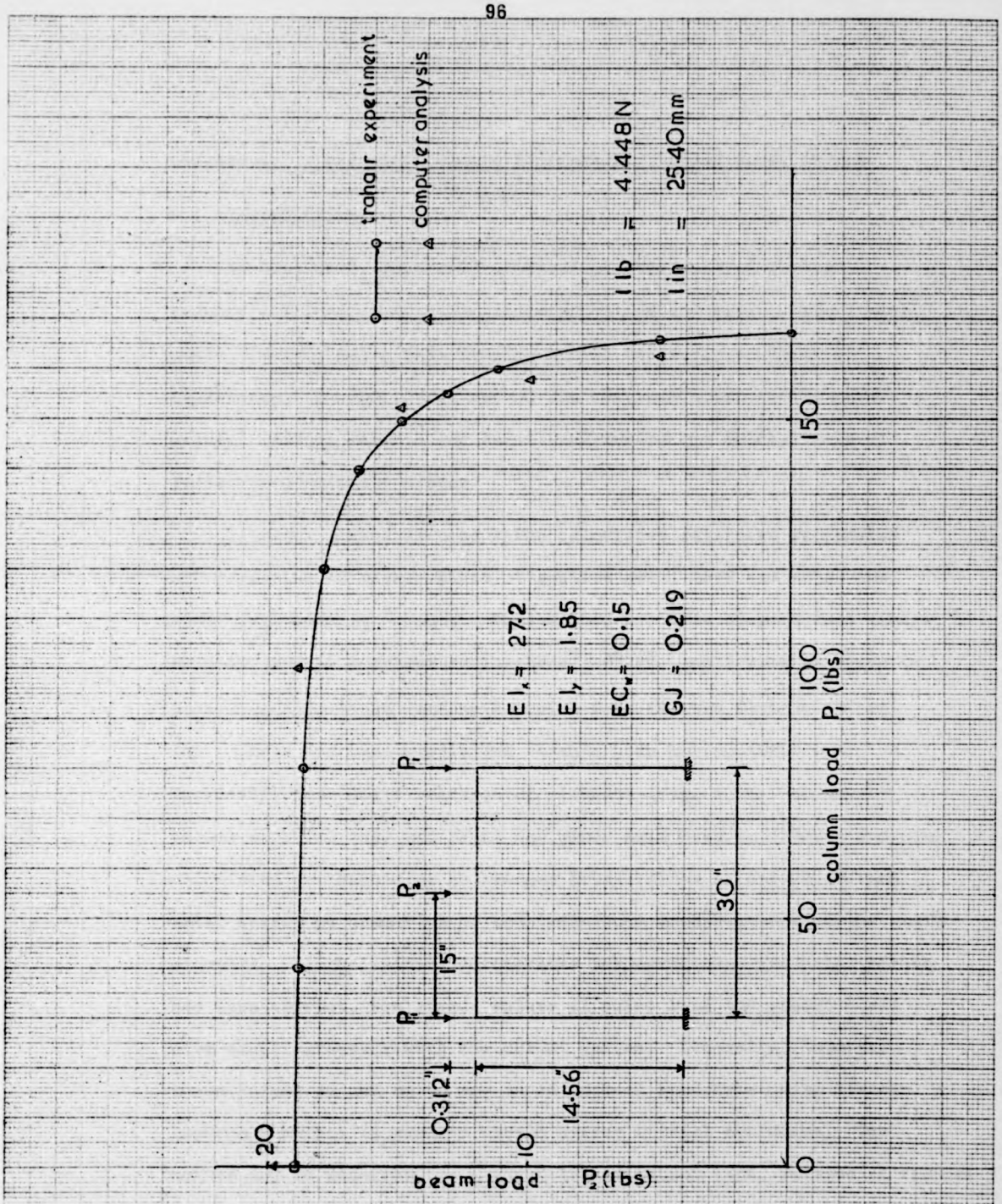

Fig. 3.8 tests on rigid base portal frames

Chapter 4. Plasticity effects in biaxially loaded steel frames.

4.1 Introduction.

In Chapter 2, algebraic expressions were derived giving reduced stiffness values for rectangular and I-shaped sections under axial load and major axis bending moment for various stages of plasticity. However, this method has not been attempted to cover biaxial bending moments and axial load due to the multiplicity of different plasticity states.

A direct method is used which calculates stiffness properties corresponding to given values of applied axial load and major and minor axis bending moments. This method has been adopted in a similar form by several previous researchers[21,29,30]. An I-section shape is idealised into three rectangles which form the two flanges and the web. These are then subdivided further both horizontally and vertically into small rectangular elements (Fig. 4.1). Estimated values of axial load and major and minor axis bending moments are then calculated corresponding to assumed trial values of curvatures and axial strain by summation of the individual contributions of the small elements. If the initial assumptions for curvatures and axial strain had been correct, the summed values of axial load and moment would give exact agreement with the actual values. Generally, however, these values do not agree and an adjustment procedure using Newton-Raphson's method is used to obtain better initial estimates. The method may be described as a quasi-linearisation type, because it reduces a set of non-linear terms in a Taylor series about an assumed solution, retaining only the linear terms. This method is continued

until satisfactory agreement between the two sets of axial force and moments is obtained.

The general nature of the method gives it the following advantages over the method for uniaxial bending:

1. Any shape of cross-section can be specified.
2. Any stress-strain relationship can be used, including combinations of two or more different materials.
3. Various arbitary residual stress patterns can be used.
4. Knowledge of the extent of the plasticity zones within a section enables reduced values of torsional, warping and cross-product of inertia rigidities as well as the usual second moments of area about the principal axes to be calculated.

Once these reduced values of flexural and torsional stiffnesses have been obtained, an elastic-plastic frame analysis is performed by suitably modifying the stiffness matrix of Fig. 3.4.

4.2 Derivation of moment-curvature properties for steel I-sections.

The following assumptions are made in deriving the moment-curvature properties.

1. The cross section is split into small elements (see Fig. 4.1). Across each element, the strain is assumed to remain constant, and to correspond to the value at the centroid of the element. It is further assumed that the section properties and forces and moments in a section can be obtained by summation of the individual contributions of the small elements.

These assumptions obviously become more exact as more elements are used in the cross-section. Practical values of these subdivisions, however, must strike a balance between giving sufficiently accurate results whilst not using excessive computer time or computer storage space.

2. A plane distribution of strain is used, and the effect of warping stresses on yielding is ignored. Culver[70] has shown that for warping unrestrained elastic columns under biaxial bending, these warping stresses constitute approximately 10% of the total normal stresses at the critical load. The corresponding value for restrained warping is 2%. This assumption will therefore indicate that yielding occurs at larger stresses than in reality. In practice, beam-column connections will offer some restraint against warping and an overestimate of the yield stress of about 5% would be expected. The elastic effects of warping however have been included as an extra degree of freedom in the elastic stiffness matrix.

3. The stress-strain relationship of the material is idealised as being trilinear, consisting of elastic, plastic and strain-hardening regions (Fig. 4.2). An upper limiting value of stress is not specified in the strain-hardening region, and it is further assumed that the behaviour is similar in both tension and compression.

This stress-strain behaviour is found to be fairly typical of structural steels and the idealisation to three distinct regions of linear behaviour is therefore justified.

4. A suitable pattern of residual stresses satisfying internal equilibrium is used, which is assumed not to vary across the flange and web thicknesses. Experimental results given by Young[71] have shown that the residual stresses vary only slightly across the thickness, until this thickness reaches 40 mm, or so (a 'thick' section). At values of thickness greater than this, far more severe values of residual stresses are encountered and result in significant stress variations across the flange thickness.

5. It is assumed that yield is produced by the sum of the normal stresses only acting on a section. Hence the shear stresses are assumed not to affect the yield point. Similar assumptions have been made by Galambos[72] and Trahair[73] in their examination of inelastic buckling of beams and by Hutchings[21] and Fukomoto and Galambos[74] in their analyses of inelastic columns. Their studies indicate that this assumption is reasonable.

6. Elastic unloading from the plastic or strain hardening region is not considered. Milner[25] and Baker et al[7] have indicated that unloading will generally result in an increase in collapse load, thus making this assumption conservative. Indeed, Milner suggested that unloading was unimportant except when a column was subject to very large initial moments from stiff restraining beams.

4.2.1 Moment-thrust curvature relationships.

The section is split into small elements (Fig. 4.1). Values of major and minor axis curvature (ϕ and θ) and axial strain (ε) are assumed. As a first approximation, these can be obtained from

the elastic equations.

$$\phi = M_y/(EI_{yy}) \qquad 4.1a$$

$$\theta = M_z/(EI_{zz}) \qquad 4.1b$$

$$\epsilon = P/(EA) \qquad 4.1c$$

The corresponding strain on element ij, ϵ_{ij}, is given by -

$$\epsilon_{ij} = \epsilon + \phi \cdot U_{ij} + \theta \cdot V_{ij} + f_s/E \qquad 4.2$$

where U_{ij} and V_{ij} are the lever arms about the major and minor axes respectively taken from the mid-point of the element.

f_s is the average residual stress acting at the centre of the element. Typical residual stress patterns have been given by Galambos[72] for American rolled sections and by Young[65] for British rolled and welded sections.

A corresponding stress, σ_{ij}, is found from Fig. 4.2. By summation of all the elements in the cross-section, values of axial load and major and minor axis bending moments are obtained. Hence:

$$P_1 = \Sigma \sigma_{ij} A_{ij} \qquad 4.3a$$

$$M_{y1} = \Sigma \sigma_{ij} A_{ij} U_{ij} \qquad 4.3b$$

$$M_{z1} = \Sigma \sigma_{ij} A_{ij} V_{ij} \qquad 4.3c$$

where A_{ij} is the area of the element, and summation is taken over all the elements.

The values P_1, M_{y1}, M_{z1} obtained from Eqn. 4.3 will in general not be in agreement with the actual values P_a, M_{ya} and M_{za}. A Newton-Raphson procedure is thus used to give better re-estimates of ϵ, ϕ and θ.

The non-linear relationships connecting the axial force and moments with curvatures and strains can be expressed as

$$P = f_1 (\varepsilon, \phi, \theta) \qquad 4.4a$$

$$M_y = f_2 (\varepsilon, \phi, \theta) \qquad 4.4b$$

$$M_z = f_3 (\varepsilon, \phi, \theta) \qquad 4.4c$$

By expanding Eqn. 4.4 in a Taylor series about the assumed values of Eqn. 4.3 and retaining only linear terms.

$$P_a = P_1 + \frac{\partial P}{\partial \varepsilon}\cdot\delta\varepsilon + \frac{\partial P}{\partial \phi}\cdot\delta\phi + \frac{\partial P}{\partial \theta}\cdot\delta\theta \qquad 4.5a$$

$$M_{ya} = M_{y1} + \frac{\partial M_y}{\partial \varepsilon}\cdot\delta\varepsilon + \frac{\partial M_y}{\partial \phi}\cdot\delta\phi + \frac{\partial M_y}{\partial \theta}\cdot\delta\theta \qquad 4.5b$$

$$M_{za} = M_{z1} + \frac{\partial M_z}{\partial \varepsilon}\cdot\delta\varepsilon + \frac{\partial M_z}{\partial \phi}\cdot\delta\phi + \frac{\partial M_z}{\partial \theta}\cdot\delta\theta \qquad 4.5c$$

By incrementing ε, ϕ and θ successively by small amounts $\Delta\varepsilon$, $\Delta\phi$ and $\Delta\theta$ respectively further values of P_i, M_{yi} and M_{zi} $(i = 2, 3, 4)$ are obtained.

Thus the differential coefficients of Eqn. 4.5 are given by

$$\frac{\partial P}{\partial \varepsilon} = \frac{P_2 - P_1}{\Delta\varepsilon}\ ; \quad \frac{\partial P}{\partial \phi} = \frac{P_3 - P_1}{\Delta\phi}\ ; \quad \frac{\partial P}{\partial \theta} = \frac{P_4 - P_1}{\Delta\theta}\ ;$$

$$\frac{\partial M_z}{\partial \varepsilon} = \frac{M_{y2} - M_{y1}}{\Delta\varepsilon}\ ; \quad \frac{\partial M_y}{\partial \phi} = \frac{M_{y3} - M_{y1}}{\Delta\phi}\ ; \quad \frac{\partial M_y}{\partial \theta} = \frac{M_{y4} - M_{y1}}{\Delta\theta}\ ; \qquad 4.6$$

$$\frac{\partial M_z}{\partial \varepsilon} = \frac{M_{z2} - M_{z1}}{\Delta\varepsilon}\ ; \quad \frac{\partial M_z}{\partial \phi} = \frac{M_{z3} - M_{z1}}{\Delta\phi}\ ; \quad \frac{\partial M_z}{\partial \theta} = \frac{M_{z4} - M_{z1}}{\Delta\theta}\ ;$$

Suffix 2 refers to incrementing ε to $\varepsilon + \Delta\varepsilon$ and repeating Eqns. 4.2 and 4.3 with ϕ and θ retaining their original values. Suffices 3 and 4 refer to a similar procedure on ϕ and θ respectively.

The non-linear equations of Eqn. 4.4 have thus been reduced

to a set of linear simultaneous equations with umknowns $\delta\varepsilon$, $\delta\phi$ and $\delta\theta$.

Solution of these equations gives the new values of axial strain and curvature.

These are

$$\varepsilon_1 = \varepsilon + \delta\varepsilon \qquad 4.7a$$

$$\phi_1 = \phi + \delta\phi \qquad 4.7b$$

$$\theta_1 = \theta + \delta\theta \qquad 4.7c$$

These values are now used to obtain new values of P, M_{y1} and M_{z1} in Eqn. 4.3. If these values do still not agree with P_a, M_{ya} and M_{za}, the Newton-Raphson procedure is repeated until satisfactory convergence is achieved.

If one, or more, of the forces P_a, M_{ya} and M_{za} is zero, the process is much reduced. For instance, if M_{za} is zero, then the value of θ is zero and only two increments (on ε and ϕ) are required. Hence the last terms of Eqns. 4.5a and 4.5b and the whole of Eqn. 4.5c are omitted, and values of $\delta\varepsilon$ and $\delta\phi$ are obtained from Eqns. 4.5a and 4.5b.

The moment curvature procedure can be explained in geometrical terms by reference to Fig. 4.3. Here it is assumed that the axial load and minor axis moment are zero for simplicity. The value of M_a is known from the stiffness analysis and convergence onto ϕ_a is required. An assumed value of curvature, ϕ_1, is introduced and Eqn. 4.3 will give point A on the curve, and thus a corresponding moment M_1. The Newton-Raphson procedure, by adopting a small change in ϕ_1, ($A\phi_1$ in Eqn. 4.6) will predict

an increase of $\delta\phi_1$ to ϕ_2. Geometrically, this is the construction of the tangent to the curve at A which intersects the M_a line (FG) at B. If a very small change in ϕ_1 ($\Delta\phi_1$) had been adopted convergence problems can occur due to round off errors in the computer analysis. The resultant value of moment could be exactly equal to M_1, and the Newton-Raphson procedure would thus try to construct a tangent which is horizontal to the ϕ axis and which would never intersect the $M - \phi$ curve. To prevent this occurring, the curvature is always incremented by a fixed amount of the assumed value ϕ_1. In the present analysis, a value of $\phi_1/50$ is used as the increment and has been found to be satisfactory. The incrementing procedure is now repeated until the value of moment obtained from Eqn. 4.3 is within a certain specified tolerance of the actual moment, M_a. If too tight a tolerance has been adopted here, excessive computer time would be required, without improving the accuracy of the solution. A value of 1% has been used in the analysis, and convergence generally occurs within three cycles of the Newton-Raphson procedure.

A further convergence problem can occur by specifying too few elements in the web of a member subject predominantly to major axis bending moment together with a small amount of axial load. Each element is assumed to have a uniform stress acting over it, and is given by the value at its centroid. In such a case, the section may be strained such that each element has a value of stress at the yield value (± Fy) in Fig. 4.2. By applying Eqn. 4.3, this will give a zero value for P. Increasing the number of elements in the

an increase of $\delta\phi_1$ to ϕ_2. Geometrically, this is the construction of the tangent to the curve at A which intersects the M_a line (FG) at B. If a very small change in ϕ_1 ($\Delta\phi_1$) had been adopted convergence problems can occur due to round off errors in the computer analysis. The resultant value of moment could be exactly equal to M_1, and the Newton-Raphson procedure would thus try to construct a tangent which is horizontal to the ϕ axis and which would never intersect the $M - \phi$ curve. To prevent this occurring, the curvature is always incremented by a fixed amount of the assumed value ϕ_1. In the present analysis, a value of $\phi_1/50$ is used as the increment and has been found to be satisfactory. The incrementing procedure is now repeated until the value of moment obtained from Eqn. 4.3 is within a certain specified tolerance of the actual moment, M_a. If too tight a tolerance has been adopted here, excessive computer time would be required, without improving the accuracy of the solution. A value of 1% has been used in the analysis, and convergence generally occurs within three cycles of the Newton-Raphson procedure.

A further convergence problem can occur by specifying too few elements in the web of a member subject predominantly to major axis bending moment together with a small amount of axial load. Each element is assumed to have a uniform stress acting over it, and is given by the value at its centroid. In such a case, the section may be strained such that each element has a value of stress at the yield value ($\pm$ Fy) in Fig. 4.2. By applying Eqn. 4.3, this will give a zero value for P. Increasing the number of elements in the

web, however, will ensure that the elements closest to the elastic centroid are no longer yielded and hence that the summed value of P is no longer zero. A suitable subdivision of the web is 8 elements in the z-direction and 4 elements in the y-direction of Fig. 4.1.

Santathadaporn and Chen[75] using the Galambos[72] pattern of residual stresses have given minor axis moment-curvature curves for an 8" × 8" × 31 lb/ft steel section with various non-dimensionalised values of axial load and major axis bending moment. These curves are plotted in Fig. 4.4 together with the results using the Newton-Raphson method. This analysis uses the tolerances and web subdivision previously given together with 8 elements in the y-direction and 4 elements in the z-direction for the flanges. The average value of residual stress using Galambos's residual stress pattern is found for each element and is assumed to act uniformly over it. Agreement between the two curves is found to be excellent.

4.3 Calculation of the St. Venant torsional rigidity of partially yielded I-sections.

Early investigations into inelastic flexural-torsional buckling of rectangular beams under uniform moment were made by Neal[76]. He showed that according to the incremental theory of plasticity, the shear modulus of the yielded material remained constant and thus concluded that the torsional rigidity should stay at its elastic value. His subsequent experimental tests on annealed rectangular beams appeared to confirm this. Haaijer[77], however, found that the shear modulus of the yielded material of strain

hardened plates decreased rapidly with small shear strains. Massey[78] also found that the torsional rigidity of an I-beam reduced to about 40% of the fully elastic value when the flanges became fully plastic. He concluded that the shear modulus in the yielded region was approximately given by

$$\frac{G_s}{G} = \frac{2}{1 + \frac{SH}{4(1 + \nu)}} \qquad 4.8$$

where G_s is the reduced shear modulus

G is the elastic shear modulus

SH is the strain hardening modulus (Fig. 4.2)

ν is Poisson's ratio.

This value was in reasonable agreement with Haaijer's experiments, and was assumed to remain constant during further straining. Any partially yielded section, therefore, can be thought of as being effectively composed of two different materials, and the torsional rigidity can be determined by forming and solving the equations which govern the St. Venant torsion of such sections. Using this direct approach, Ely and Zienkiewicz[79] presented a numerical solution, whilst a more recent analytical solution is due to Booker and Kitipornchai[80,81]. The latter method results in simple algebraic expressions for the case of a rectangular cross-section composed of two parallel layers each a different material. The method of Booker and Kitipornchai is extended here to give simple expressions for the torsional rigidity of I-sections in which the yielded region does not form a parallel layer. The validity of these expressions can

be examined using the method of Ely and Zienkiewicz.

The equations governing St. Venant torsion can be written in terms of Prandtl's stress function, α for the composite section of Fig. 4.5.

$$\frac{\partial^2 \alpha_1}{\partial x^2} + \frac{\partial^2 \alpha_1}{\partial y^2} = -2 G_1 \lambda \qquad 4.9a$$

$$\frac{\partial^2 \alpha_2}{\partial x^2} + \frac{\partial^2 \alpha_2}{\partial y^2} = -2 G_2 \lambda \qquad 4.9b$$

where α is the stress function

λ is the twist per unit length of the member

Suffices 1 and 2 refer to the different materials of the two layers. Along the internal boundary, C_2, the shear stresses normal to the boundary must be the same in each region. Hence

$$\alpha_1 = \alpha_2 \qquad 4.10$$

Also on the external boundary, the lateral surface of the member is assumed to be free from external forces

$$\alpha = 0 \qquad 4.11$$

The axial displacement on C_2 must also be the same in each region giving

$$\frac{1}{G_1} \cdot \frac{\partial \alpha_1}{\partial n} = \frac{1}{G_2} \frac{\partial \alpha_2}{\partial n} \qquad 4.12$$

n being the direction of the normal to C_2

The torque acting on the cross-section, T, is given by:

$$T = \iint \alpha \, dx \, dy \qquad 4.13$$

The torsional rigidity, GJ, can then be found from:

$$GJ = T/\lambda \qquad 4.14$$

Standard finite difference techniques are used to solve Eqns. 4.9 - 4.12 and give the corresponding variation of the stress function over the section. A volume integration using Eqn. 4.13 will give the required torsional rigidity.

However, this numerical approach is not suitable for the determination of GJ in computer analyses of beam-column as it requires the solution of a large set of simultaneous equations and correspondingly large amounts of machine time and storage space.

Booker and Kitipornchai[80,81] have given simple analytical expressions for the effective shear modulus of a rectangular section composed of two layers (see Fig. 4.6). The boundary between the two layers is taken as parallel to the sides of length d.

Then for $d/b \gg 1$, the effective shear modulus, G_e, is given by

$$G_e = 4(G_2 (1 - \beta)^3 + G_1\beta^3) - \frac{3(G_2 (1 - \beta)^2 - G_1 \beta^2)^2}{(G_2 (1 -\beta) + G_1 \beta)} \quad 4.15$$

This expression holds exactly for $d/b = \infty$.

For $d/b \ll 1$, the effective shear modulus is given approximately by

$$G_e = G_2 + \beta (G_1 - G_2) \quad 4.16$$

This expression is exact for $d/b = 0$.

The effective torsional rigidity can be obtained by multiplying the usual torsion constant, J, by the effective shear modulus obtained from Eqn. 4.15 or Eqn. 4.16.

If region 2 represents the elastic part and region 1 is the yielded region, then G_2 will be the elastic shear modulus and G_1

will be given by Eqn. 4.8. When steel beam-columns are subjected to biaxial bending, the yielded regions will not necessarily extend across the full depth or width of a flange or web. For example, Fig. 4.7 shows part of a rectangular flange in which the yielded region lies above the inclined boundary AB. In such cases, the boundary does not follow the pattern assumed by Booker and Kitipornchai. However it will be shown that the expressions of Eqns. 4.15 and 4.16 can still be used to determine the effective shear modulus of a partially yielded rectangular flange or web element with reasonable accuracy. The yielded portion of the cross-section can be obtained from the previously described moment-curvature procedure. Hence when the flange of Fig. 4.7 is split into the rectangular elements shown, the boundary between the elastic and inelastic regions being along CDEFH.

The lack of fit between the continuous and the stepped boundaries can be reduced to any desired degree of accuracy by increasing the number of elements used in the cross-section. In order to investigate the application of Eqns. 4.15 and 4.16 to such situations, the two yield patterns shown in Fig. 4.8 are considered. For convenience the rectangular cross-section being studied will be referred to as a flange. However the same procedures can be applied to webs also.

4.3.1 Application of Booker and Kitipornchai's formulae.

For the simpler pattern of Fig. 4.8a, the region ABCD is first considered in isolation from the remainder of the flange. In order to apply the correct expressions to this region (Eqn. 4.15 or 4.16), it is necessary to consider the breadth/ depth for ABCD. The minimum value of βb will be the width of one element from the cross-section

and is thus governed by the pattern of elements adopted in the moment-curvature analysis since an element is assumed to be fully yielded when the average stress on it is at the yield value. Unless the total stress at any point is due predominantly to minor axis curvature, the number of elements across the breadth of a flange can be small. As the flange breadth/thickness ratio for I-sections is large (usually > 10), elements will tend to have high width/depth ratios and βb will always be greater than d. If however, it is found desirable to use many elements across the breadth of the flange, then the minimum value of βb could be less than d. However, as b/d is usually greater than 10, the plastic region of width βb will, in such cases, be small in relation to the entire flange which could be assumed to be still completely elastic without undue error.

It is therefore concluded that $d < \beta b$ and Eqn. 4.15 can be used to obtain the effective shear modulus, G' for ABCD. This calculation ignores the connection between ABCD and the remainder of the flange. To obtain a value of the effective shear modulus, G_e, for the entire flange, Eqn. 4.16 is now applied

$$G_e = G_2 + \beta(G' - G_2) \qquad 4.17$$

The torsional rigidity is thus obtained by multiplying the above equation by the usual torsion constant, and a factor k which is dependent on the ratio b/d[80].

$$GJ = G_e k\ bd^3 \qquad 4.18$$

This procedure has been followed for the case where $b = 10$, $d = 1$, $G_1 = 0.1$ and $G_2 = 1.0$; various values of α and β

give the results for GJ shown in the third column of Table 4.1.

For the yield pattern in Fig. 4.8b, Eqn. 4.15 is applied to regions ABCD and BFHC to obtain effective shear moduli G^1 and G^{11} respectively. The entire flange can now be regarded as a three-layered section and Eqn. 4.16 may be extended to give

$$G_e = (1 - \beta - \gamma)\, G_2 + \beta G^1 + \gamma G^{11} \qquad 4.19$$

with $b = 10$, $d = 1$, $G_1 = 0.1$, $G_2 = 1.0$ and $\delta = 0.2$, the resulting values of GJ corresponding to various values of α, β and γ are given in the fourth column of Table 4.2.

4.3.2 The finite difference method.

To apply the methods of Eqns. 4.9 - 4.14 to cover the partially yielded cross-section, an imaginary square mesh of length a is used (Fig. 4.9). At each mesh point within the region ABCD, the finite difference form of Eqn. 4.9a is set up, using Eqn. 4.11 to satisfy the conditions on the external boundary. A similar procedure is adopted in the region with modulus G_2.

The treatment of intermediate points along the internal boundaries BD and CD, such as mesh points 5 and 7 is also straightfoward; however the procedure for point 5 will be outlined in view of the difficulties described below that arise at the corner point 8. On the internal boundary, Eqns. 4.9a and 4.9b both apply. Considering just Eqn. 4.9a, the finite difference approximation for $\partial^2\alpha^1/\partial x^2$ at point 5 is $(\alpha_{61} - 2\alpha_{51} + \alpha_{41})/a^2$ where α_{i1} is the value of the stress function at point i in region 1. However, point 6 is within the region governed by the

stress function α_{i2}, and thus α_{61} is an imaginary value which must be expressed in terms of real values of α_{i1} and α_{i2}. This can be achieved by applying Eqn. 4.12 to point 5, which gives

$$\frac{\alpha_{61} - \alpha_{41}}{G_1} = \frac{\alpha_{62} - \alpha_{42}}{G_2} \qquad 4.20$$

A further imaginary value, α_{42}, is introduced by Eqn. 4.20 but this can be eliminated by applying Eqn. 4.9b to point 5, and noting that $\alpha_{51} = \alpha_{52}$.

Ely and Zienkiewicz[79] only examined cross-sections in which the internal boundary, C_2, (Fig. 4.5) was continuous, whereas in the problem assuming a stepped boundary, discontinuities occur at "corner" points, such as 8 in Fig. 4.9. This creates difficulties in applying the compatibility condition (Eqn. 4.12) and the stress condition (Eqn. 4.11) since they both require the specification of a direction which is normal to the internal boundary. To overcome this problem, it is assumed that in the region of a corner mesh point, the vertical and horizontal internal boundaries are connected by a circular boundary of very small radius. At such a point, the normal to the boundary can therefore be regarded as inclined at an angle of 45° to the x-axis (Fig. 4.9) and Eqn. 4.12 gives

$$\frac{\alpha_{121} - \alpha_{41}}{G_1} = \frac{\alpha_{122} - \alpha_{42}}{G_2} \qquad 4.21$$

However, if Eqn. 4.9a is formulated in the x-y system of axes at the corner point, the resulting imaginary values α_{91} and α_{111} cannot

be expressed in terms of other real variables by this boundary condition. Eqns. 4.9a and 4.9b are therefore transformed into the co-ordinate system, $X^1 - Y^1$, of Fig. 4.9. It can be shown that the form of these equations remains unchanged with X^1 and Y^1 replacing X and Y. Application of the finite difference expressions for $\partial^2\alpha/(\partial x^1)^2$ and $\partial^2\alpha/(\partial y^1)^2$ now introduces imaginary values α_{121}, α_{101}, α_{61} and α_{42}. Thus four equations are needed to eliminate these values. These are Eqn. 4.21, Eqn. 4.9b in the $X^1 - Y^1$ system and Eqn. 4.12 applied at points 5 and 7.

The finite difference equations were formulated for a unit rotation, λ, and the corresponding simultaneous equations were solved using a banded matrix routine. The value of GJ was then found using volume integration of the stress function and applying Eqns. 4.13 and 4.14. The results obtained for the two yield patterns of Fig. 4.6 are shown in Tables 4.1 and 4.2 using both 5×50 and 10×100 meshes. In the final column of each table, the differences between the finite difference results (using the 10×100 mesh) and the values given by the combination of Eqns. 4.15 and 4.16 are expressed as percentages of the former.

4.3.3 Discussion of results.

The results given for the two mesh sizes are found to be in very close agreement, and it is therefore concluded that the results for the 10×100 mesh are close approximations to the true values. When comparison is made in both tables between the results for the 10×100 mesh and those given by Eqns. 4.15 and 4.16, it is seen that in general there is good agreement. The varying differences

between the two sets of figures are due to the assumptions which have been made in the derivation of these equations (Eqns. 4.15 and 4.16).

Consider the use of Eqn. 4.15 to determine the effective shear modulus of region ABCD in Fig. 4.8a. For this equation to hold exactly, the ratio $\beta b/d$ should be infinite. For the flange considered herein, this value varies from 2 to 8, and thus as β increases, decreasing errors between the two sets of values would be expected. However, this is not the case for the results of Table 4.1, and the reason can be found by considering Eqn. 4.16. This expression used to calculate the effective shear modulus of the complete flange from the values of G^1 and G_2, and holds exactly when $d/b = 0$. For the fixed value of d/b (0·1) used herein, Fig. 4 of Ref. 80 shows that the error introduced by Eqn. 4.16 increases with β up to a value of $\beta = 0.9$ approximately. This characteristic is shown by the results of Table 4.1. The tendency for the errors due to Eqn. 4.16 to control the results is assisted by the fact that when β is small, the effects of errors in the value of G^1 due to Eqn. 4.15 will exercise a small influence only on the effective shear modulus for the complete flange. Booker and Kitipornchai also show that the errors due to the application of Eqn. 4.16 increase with the ratio G_2/G^1. This characteristic is also shown in Table 4.1; as the ratio α increases, G^1 falls relative to G_2 due to the increasing amount of material with the lower modulus G_1 contributing to the value of G^1, and it can be seen that for a fixed value of β_1, the difference in the

results given by the two methods increases with α. Finally, it is interesting to note that the greatest error arises in the case of $\alpha = 1$ when the flange is a simple two layered section and G is obtained by the application of Eqn. 4.16 only. The assumptions made in the derivation of Eqns. 4.15 and 4.16 can also be used to explain the varying differences between the values in Table 4.2 for the yield pattern of Fig. 4.8b.

In assessing the accuracy of Eqns. 4.15 and 4.16 for use in determining the effective torsional rigidity, it should be noted that the values of Table 4.1 and 4.2 are for one rectangular component of an I-section, such as a flange or a web. In many cases, only one such rectangular component will be partially yielded, and therefore the error in the reduced value of GJ for the entire cross-section will usually be considerably less than the values given in the tables.

4.4 Derivation of reduced flexural and warping rigidities and the cross-product of inertia.

The extent of plasticity within a partially yielded cross-section for a particular combination of axial load and bending moments can be found by using the moment-curvature procedure of Eqns. 4.1 - 4.7. This partially yielded section can then be used to estimate the reduced rigidity terms to be used in the stiffness analysis.

Previous researchers have made differing assumptions in order to calculate these reduced values. Several assumed that the warping and torsional rigidities are based on the elastic core of

the cross-section, and thus the yielded regions have zero rigidity. This so called tangent modulus approach uses the instantaneous value of Young's modulus (zero in the plastic range) and is suitable for analyses which attempt to calculate the bifurcation point for lateral stability.

A more progressive allowance for the reduction in rigidity has been used by Hutchings[21]. He analysed restrained columns under increasing loads and used the secant modulus to obtain torsional and warping rigidities. As the material becomes strained in the plastic region, the secant approach assumes that the effective steel modulus progressively reduces, and is given by the ratio of the actual stress to the strain.

Most grades of steel, however, exhibit quite marked strain hardening behaviour at relatively low strains. The tangent modulus approach of assuming zero rigidity in such will thus underestimate the rigidity of a section. A secant approach has therefore been used in the present analysis to calculate the partially plastic flexural and warping rigidities and cross-product of inertia. The main justification for this assumption is given by the method of analysis used; the total load (rather than a small increment) being applied for each iteration of the computer analysis.

4.4.1 Calculation of reduced flexural rigidities and cross-product of inertia using a secant modulus approach.

In order to calculate these reduced rigidity terms, the co-ordinates of the centroid of the transformed section[82] must be initially estimated.

With reference to Fig. 4.10, if element dA is fully yielded, a distance p from the neutral axis, then assuming plane sections remain plane, the strain is given by:

$$\epsilon = p/r \qquad 4.22$$

where r is the radius of curvature.

On element dA, assuming the secant modulus is E_s (Fig. 4.11), the stress σ is :

$$\sigma = E_s\ p/r \qquad 4.23$$

assuming that the element is subject to pure bending moments only, the resultant direct load on any section must be zero

$$\int_A \sigma dA = 0 \qquad 4.24$$

substituting for σ from Eqn. 4.23, gives:

$$\int_A E_s\ p/r\ \ dA = 0 \qquad 4.25a$$

For an element of a given material subject to given bending moment this equation becomes

$$\int_A E_s\ p\ dA = 0 \qquad 4.25b$$

The modular ratio m, is given by: $m = E/E_s$ 4.26a

The effective area, $d\ A_e$, of the element is similarly defined as

$$d\ A_e = dA/m = E_s\ dA/E \qquad 4.26b$$

Substituting for E_s into Eqn. 4.25b

$$\int_{Ae} E \cdot p \cdot d\ A_e = 0 \qquad 4.27a$$

Since E is constant

$$\int_{Ae} p\ d\ A_e = 0 \qquad 4.27b$$

Thus the neutral axis passes through the centroid of the transformed cross-section.

The moment curvature procedure gives values of major and minor axis curvatures and axial strain corresponding to particular combinations of bending moments and axial load. These convergent values of curvatures and axial strain are then used to obtain values of strain, ε_{ij}, acting on each individual element by use of Eqn. 4.2. By reference to Fig. 4.11, the secant modulus is obtained from the following:

$$\text{For } |\varepsilon_{ij}| < \varepsilon_y , \quad E_s = E \tag{4.28a}$$

$$\varepsilon_y < |\varepsilon_{ij}| < \varepsilon_{SH} \quad E_s = \frac{\varepsilon_y}{|\varepsilon_{ij}|} \cdot E \tag{4.28b}$$

$$|\varepsilon_{ij}| > \varepsilon_{SH} \quad E_s = \frac{\varepsilon_y}{|\varepsilon_{ij}|} \cdot E + \frac{E}{SH} \cdot \left(1 - \frac{\varepsilon_{SH}}{|\varepsilon_{ij}|}\right) \tag{4.28c}$$

where E_s is the secant modulus.

ε_y, ε_{SH} are the yield and strain hardening strains respectively. If u_1 and v_1 are the co-ordinates of the centroid of the transformed area,

$$u_1 = \Sigma E_s A_{ij} U_{ij}/EA \tag{4.29a}$$

$$v_1 = \Sigma E_s A_{ij} V_{ij}/EA \tag{4.29b}$$

The summation being taken over all the elements, A being the area of the complete transformed section and A_{ij} is the area of element ij.

When $E_s = E$ for all the elements, u_1 and v_1 will be zero. After locating the co-ordinates of the centroid of the transformed

area, the reduced second moments of area and cross-product of inertia are given by:

$$I_{yy} = \int \frac{E_s \cdot z^2 \, dA}{E} \qquad 4.30a$$

$$I_{zz} = \int \frac{E_s \cdot y^2 dA}{E} \qquad 4.30b$$

$$I_{yz} = \int \frac{E_s \cdot y \cdot z \cdot dA}{E} \qquad 4.30c$$

These equations are converted from an integral type to a standard form suitable for summation using the segmented section of Fig. 4.1. Eqns. 4.30a - 4.30c thus become:

$$I_{yy} = \Sigma \, E_s \, A_{ij} (U_{ij} - u_1)^2 / E \qquad 4.30d$$

$$I_{zz} = \Sigma \, E_s \, A_{ij} (V_{ij} - v_1)^2 / E \qquad 4.30e$$

$$I_{yz} = \Sigma \, E_s \, A_{ij} \, (U_{ij} - u_1)(V_{ij} - v_1) / E \qquad 4.30f$$

The polar moment of inertia, I_o, is given by the sum of Eqns. 4.30d and 4.30 e.

$$I_o = I_{yy} + I_{zz} \qquad 4.30g$$

4.4.2 Calculation of the reduced warping rigidity.

Any partially yielded steel section subject to non-uniform torsion will warp and twist about a longitudinal axis, the position of which varies with respect to the resulting geometric centroid of the cross-section along the length of the beam. In the general case, this variation will depend on three factors.

1. The amount of yielding due to the applied moments and axial load.
2. Secondary yielding due to warping and torsional stresses.

3. Elastic unloading in the cross-section.

Birnstiel and Michalos[29] examined the effects of these stresses using an incremental method of analysis. The section they studied was a 12WF79 column loaded in simple curvature about both axes by an eccentric axial load, split into four element lengths.

They assumed that the rotation of each element occurred about an average centre of twist, which was obtained from the condition that the resulting warping strains due to yielding do not produce any net axial load or bending moments about any axis in the cross-section. For the section investigated, they found that the corresponding shifts of the centre of twist at the ultimate load were respectively 3% and 7½% of the total depth in the y and z directions of Fig. 4.1.

An approximation to the above is to assume that the shift of the shear centre in the 'y' direction is zero in order to calculate the warping rigidity. This assumption will be conservative, since the warping rigidity will rapidly tend to zero as the centre of twist moves towards a flange-web junction.

Consequently, in order to calculate the reduced warping rigidity, due to partial plasticity, it is assumed that the centre of twist moves only in the 'z' direction of Fig. 4.1. For this purpose, therefore, the section is effectively monosymmetric.

Anderson and Trahair[83] have shown that the distance, y_o, of the shear centre below the midpoint of the web is given by

$$\frac{y_o}{h} = \frac{(EI_z)_{BF}}{(EI_z)_{TF} + (EI_z)_{BF}} - 0.5 \qquad 4.31$$

where h is the distance between flange centroids.

$$(EI_z)_{BF} = \Sigma E_s V_{ij}^2 A_{ij} \qquad 4.32a$$

$$(EI_z)_{TF} = \Sigma E_s U_{ij}^2 A_{ij} \qquad 4.32b$$

where the summation is taken over the bottom flange only for Eqn. 4.32a and over the top flange only for Eqn. 4.32b.

The warping rigidity (EC_w) during buckling varies with the flexural rigidity and the variation in y_o due to yielding.

For monosymmetric sections it is given by

$$EC_w = \frac{(EI_{zz})_R h^2}{4} (1 - 4 y_o^2/h^2) \qquad 4.33$$

where $(EI_{zz})_R$ is the reduced value of minor axis rigidity obtained from Eqn. 4.30e.

4.5 Summary of the procedure to calculate the reduced rigidities.

1. Values of curvature and axial strain are obtained corresponding to the particular combinations of axial load and bending moments acting on the section by use of the Newton-Raphson procedure.
2. Any elements in the cross-section which have yielded are identified and given the reduced shear modulus value of Eqn. 4.8. The reduced torsional rigidity is then obtained by use of Eqns. 4.15 and 4.16.
3. A value of secant modulus is given to the yielded regions using Eqns. 4.28. The new centroid of the transformed area is found from Eqns. 4.29. The reduced major, and minor axis rigidities, cross-product of inertia and polar moment of inertia are obtained from Eqns. 4.30d - 4.30g. The warping rigidity is then given by Eqns. 3.31 - 3.33.

4. The onset of unsymmetrical yielding causes the principal axes of the cross-section to change. The analysis for unsymmetrical bending developed in Chapter 3 is thus used, which includes the non-zero cross-product of inertia terms.

4.6 Overall elastic-plastic analysis procedure.

The elastic-plastic method of analysis which combines the overall stiffness matrix of Chapter 3 together with the moment curvature procedure of the present chapter will now be described. The analysis procedure is shown in the flow diagram of Fig. 4.12. It begins by carrying out a linear elastic analysis of the frame at working load. From the results, a prediction is made of the load factor, λ_E, at which first yield will occur in the frame. It should be noted that it is assumed that a member begins yielding when the maximum stress at the mid-point of a member's length reaches the yield stress. Thus, regions of the frame in which high stresses are expected will normally be split into elements of smaller length than the regions which will remain elastic. The axial loads and bending moments at λ_E are estimated by multiplying the values at working load by the load factor. An analysis is then made at this load level, the change in the frame stiffness due to the estimated forces now being considered. Further cycles of prediction and analysis follow.

If λ_2 and λ_1 are the predicted load factors at two successive iterations (λ_2 being the most recent prediction) and if the corresponding maximum stresses at the midpoint of the most highly stressed member are σ_2 and σ_1, then the predicted load factor for the next iteration is given by:

$$\lambda_E = \lambda_1 + (\lambda_2 - \lambda_1) \cdot F_y/(\sigma_2 - \sigma_1) \qquad 4.34$$

where F_y is the yield stress of the member.

If the axial loads obtained by analysis at λ_2 and λ_1 are P_2 and P_1 respectively, then an estimate of the axial load, P, at λ_E is:

$$P = (\lambda_E - \lambda_1) \cdot P_2 - (\lambda_E - \lambda_2) \cdot P_1) / (\lambda_2 - \lambda_1) \qquad 4.35$$

Similar predictions are used to estimate the other forces used in the stiffness analysis (bending moments and shears) at load factor λ_E.

The iteration procedure is terminated when the values of λ_E and λ_2 are within a small tolerance of each other. The condition used in the program for convergence is:-

$$1 - (\lambda_2/\lambda_1) \leq 0.005 \qquad 4.36$$

Once first yield has been reached, the load factor is incremented by an amount $\Delta\lambda$ and the axial loads in the members corresponding to this new load factor are calculated by Eqn. 4.34. In this case, λ_E corresponds to the incremented load factor, λ_2 to the load factor at first yield and λ_1 is taken as working load. The frame is now analysed at the incremented load level, the stiffness of the frame corresponding to the axial loads just estimated. As the frame is now beyond first yield, the stiffness of the frame must be adjusted to account for the non-elastic regions. The moment-curvature routine is therefore entered with the moments and axial loads just calculated and the corresponding effective rigidities of the members determined.

Further cycles of analysis follow at constant load level, each analysis using the axial loads and effective rigidities just calculated. The iteration procedure is terminated when all the deflections obtained from two successive analyses are within a small tolerance. The condition used has a similar form to Eqn. 4.36, the tolerance used being 0.05.

The load factor is successively incremented, analyses being obtained at each load level. The facility exists in the program to reduce the increments of load factor as the expected collapse load is approached, the increments being specified by the user. Collapse of the frame occurs when the determinant of the stiffness matrix becomes non-positive.

4.7 Examples using the program.

Several examples of columns and complete frames for which load-deflection plots and ultimate loads have been obtained by previous research workers will now be given. The accuracy of the present elastic-plastic computer program in predicting frame and member behaviour will be examined with respect to the various assumptions used in forming the analysis. The wide variety of examples examined is an indication of the versatility of the method. A summary of the failure loads of the various columns and frames analysed is given in Table 4.3, together with the main assumptions made in the present computer analysis.

1. Uniaxial pin-ended column.

Van-Kuren and Galambos[84] have tested experimentally a large series of pin-ended columns subject to various combinations of axial load and major axis bending moment. The column analysed herein is designated T13 and has a loading path of fixed axial load ($P/P_y = 0.12$) whilst the bending moment is increased to collapse. The column is effectively constrained to cause failure about the major axis due to the development of excessive plasticity, with the bending moment applied at one end only.

The corresponding moment versus end-rotation curve is given in Fig. 4.13. It can be seen from the curve that strain hardening appears to influence the ultimate load since the collapse failure moment is greater than the fully plastic value even in the presence of axial load. Although Van Kuren and Galambos do not give values for the stress-strain properties of the steel, typical values of PLAT = 10 and SH = 50 (see Fig. 4.2) have been used in the analysis.

The column is split into 20 elements of equal length, and two separate analyses with and without residual stresses have been performed. The residual stress pattern used is the one suggested by Galambos[72] after many tests on American hot-rolled sections. The computer analyses give failure moments of 1140 Kip-in (with residual stresses) and 1249 kip-in (without residual stresses). These values are in good agreement with the experimental failure moment of 1258 kip-in. It appears from Fig. 4.13 that greater strain hardening behaviour was present in the actual tested column

than was actually allowed for in the analysis. At values of $M/M_p = 0.95$ and above, the end-rotation predicted by the computer analysis begin to increase at a faster rate than the experimental curve.

2. Uniaxial column curvature curves.

Chen and Atsuta[60] have presented column curvature curves for both I-section and rectangular pin-ended columns. They solve the governing differential equations for major axis bending by assuming approximate moment-curvature relationships in the three regions of elasticity, primary plasticity and secondary plasticity. The columns analysed here are subject to eccentric axial load which causes unequal major axis bending moments at each end. The members again fail due to excessive plasticity, the extent of plasticity at failure (either primary or secondary) being dependent on the ratio of end-moments.

Axial stress versus maximum non-dimensionalised curvature curves together with loading and parameter details are given in Figs. 4.14 and 4.15. For the I-section member, two values of α(1 and 10) have been plotted. The former case gives rise to failure when primary plasticity only has developed, whilst the second case has developed secondary plasticity also at collapse.

In the present computer analysis, each column is split into 20 elements. The maximum curvature will occur near to end A, and thus element lengths of 12 ins. have been used in this expected region of high curvature, with larger values elsewhere. The maximum curvature values are obtained at various axial load levels

for the most highly stressed member element from the moment-curvature procedure. The curvature values are then non-dimensionalised with respect to the yield curvature. The moment-curvature procedure has been specifically written for use with I-section shapes in the present analysis. However it can be simply adapted to study rectangular sections by setting the areas and lever arms of the sections of the flanges to zero. A corresponding axial stress versus maximum curvature curve for a rectangular section is given in Fig. 4.14. Out of plane behaviour has been prevented in all these analyses by restraining the minor axis, torsional and warping displacements at each joint. The sections are also assumed to be free from residual stresses and initial imperfections. Agreement between the corresponding curves of Chen and the present analysis is found to be excellent.

3. Laterally restrained columns under uniaxially applied bending moment.

Ajmani[61] has tested a series of pin-ended columns subject to major axis bending moment and axial load. The columns are laterally restrained on one flange at various positions along its length to compensate for the effects of sheeting rails in framed buildings. Two columns are analysed herein, with lateral restraints being included in the stiffness matrix at the corresponding restraint points.

The first column analysed is subject to moment at one end only and has been investigated previously using the uniaxial analysis of Chapter 2, where no allowance was made for the beneficial effects

of strain hardening. End moment-rotation curves for the experimental test and the two analyses are given in Fig. 4.16. In the present analysis, the column has been split into 24 elements of equal length. The effect of including strain hardening in the analysis (PLAT = 11, SH = 56 in Fig. 4.2) is to increase the failure moment ratio, M/M_p, from 0.94 in the analysis method of Chapter 2 to 1.09 in the present analysis. This value, however, is still somewhat below the experimental failure load of 1.30. This experimental failure moment ratio is approximately 37% above the rigid plastic failure load. It is thought that this large increase in failure load is probably not solely attributable to strain hardening effects. In practice, it is usually very difficult to reproduce perfect pin-ended conditions. For instance, the loading yoke used by Ajmani probably provided additional restraint to the column at its ends, and hence would have enhanced the failure load. Harstead[30] has shown theoretically that the effect of restraining warping at the ends of a pin-ended column subject to single curvature bending about both axes is to increase the ultimate load by 12% compared to the unrestrained case. Hence it is anticipated that the experimental results should give higher ultimate loads than the theoretical values.Moment-rotation agreement between the curves is found to be good up to the onset of failure in the theoretical analysis.

The second example analysed is a column bent in double curvature. The column is again split into 24 elements and analysed separately with and without residual stresses. The analysis neglecting residual stresses gives excellent ultimate load agreement with the experimental

value. However the corresponding moment-rotation curves do not show the same agreement. The experimental curves showed a marked deviation from linearity at relatively small values of moment ratio ($M/M_p = 0.4$) for which yielding would not be expected. Consequently a second analysis which included the effects of residual stresses was performed. The effect of these stresses is to cause early yielding, and thus to reduce the ultimate load. The pattern of residual stresses adopted in the analysis is the one proposed by Young, and the corresponding moment-rotation curves are plotted in Fig. 4.17. The curve for this analysis gives better moment-rotation agreement with the experimental curve. However the failure moment is now reduced by about 7%.

4. Uniaxial frame analysis neglecting strain hardening.

The previous examples have been concerned with individual members loaded with axial load and various combinations of major axis end bending moments such that failure occurred in the plane of loading. The program is now used to predict the ultimate behaviour of a plane frame constrained from any out-of-plane movement.

Wood[8] with the aid of a differential analyser presented a theoretical analysis of a four-storey, single bay frame loaded to collapse (see Fig. 4.18). The frame was loaded by both vertical and horizontal point loads, and was designed to demonstrate the effects of instability on the value of the collapse load. The stanchions were designed by Wood to fail ultimately at a load factor of 2.00 (based on consideration of torsional instability), the ideal plastic

mechanism occurring at a load factor of 2.15.

Wood's analysis showed that first yield occurred at a load factor, λ, of 1.51 at the centre of the third storey beam. This hardly altered the rotational stiffness of the frame, and thus Wood continued using elastic analysis up to a load factor of 1.70. Beyond this stage however, considerable yielding had occurred elsewhere in the structure, and allowance for partially plastic zones was subsequently made in the analysis. At a load factor of 1.90, deflections began to increase rapidly and collapse was assumed to have occurred. Hence the combined effects of partial plasticity and frame instability cause a reduction in the ideal plastic collapse load. At collapse, only four complete hinges had formed out of a possible ten. At this load factor also, no elastic unloading or strain hardening had occurred.

For the computer analysis, the frame is split into 56 members, and in the vicinity of fully plastic or partially plastic regions, member lengths of 3 ins. are used. The estimated first yield load factor is 1.56, which is slightly higher than Wood's value of 1.51. This is probably due to finding the average value of stress in a member based on the values of axial loading at its two ends. Strain hardening has been neglected in the analysis by arbitarily setting the length of the plateau region (PLAT of Fig. 4.2) to a value of 1000. The load factor is subsequently increased in increments to a value of 1.90 at which stage the determinant of the stiffness matrix becomes negative and collapse is thus assumed to have occurred.

Load-deflection plots for each storey and the bending moments

in the frame at a load factor of 1.90 are given in Figs. 4.19 and 4.18. The values of deflections given by the present analysis are generally greater than the corresponding values given by Wood once significant yielding is present in the frame. This is probably due to the idealisation of the section into three rectangles based on its average dimensions for inclusion in the moment-curvature procedure. This assumption generally underestimates the stiffness of the section by about 1%. Consequently the deflections given by the present analysis would be expected to be greater than Wood's values. Indeed, this discrepancy would be expected to increase from the bottom storey to the top storey since yielded zones in the lower part of the structure will be overestimated and give correspondingly higher deflections elsewhere. Generally, however, agreement between the two sets of results is thought to be good.

5. Uniaxial analysis of a portal frame including strain-hardening effects.

Charlton[85] has tested a series of pitched roof portals subject to vertical loading (Fig. 4.20). Two frames, designated 10X and 10Y were tested side-by-side connected together by suitable purlins and sheeting rails. The example is a test of the present method's ability to deal with plane frames which exhibit considerable strain-hardening behaviour.

The frame and loading details are given in Fig. 4.20 together with the load-deflection curve of the apex. The maximum total load applied to each frame was 10.75 tons at which stage the loading platforms grounded. The resulting collapse mode was symmetrical, with six plastic hinges forming at the points shown in Fig. 4.20.

In the absence of strain-hardening, elastic-plastic failure was predicted at a load of 7.8 tons, with only three plastic hinges in the structure. Strain hardening is therefore responsible for a theoretical increase of 33.4% in the failure load. Davies[40] has subsequently analysed this frame allowing for strain-hardening, and giving a theoretical failure load of 10.4 tons for each frame.

The present analysis segments the frame into 24 small members. At the expected hinge positions, small member lengths of 3 ins. have been used to obtain accurate assessments of reduced stiffnesses once yielding has commenced. The length of the plateau region (PLAT of Fig. 4.2) used by Davies was 5.2. However, he does not give details of the gradient of the stress-strain curve in the strain hardening region (defined by SH in Fig. 4.2). Ajmani[61] in a later series of tests on a similar section found this coefficient from coupon tests to be approximately 56. This value of SH has therefore been assumed in the present analysis. The load-deflection plot for the computer analysis is given in Fig. 4.20 also. The collapse load of 10.44 tons compares well with both Davies' theoretical results and the experimental failure load of 10.75 tons.

It should be noted however that no allowance for residual stresses or initial imperfections has been made in this analysis.

6. Biaxial bending of an unrestrained pin-ended column.

Harstead, Birnstiel and Leu[30] have presented theoretical analyses for pin-ended columns loaded with eccentric axial load which causes single curvature bending about both axes. They use this analysis to investigate the effects of warping restraint and residual stresses

on the ultimate load of the section, assuming that the section is free of initial imperfections, and possesses an elastic-perfectly-plastic stress-strain relationship. Gent[86] has subsequently analysed one of Birnstiel's columns using his more general column analysis which allowed for elastic end restraint. The column, designated No. 4 by Birnstiel was free of residual stress and restrained from warping at its ends, and has been analysed also using the present computer analysis.

The column is split into 22 elements of equal length (10 ins.) and is analysed under various values of axial load. Corresponding plots of mid-height, major and minor axis displacements and twist for the three analyses are given in Fig. 4.21.

Gent's failure load of 164 kips is about 7% above Birnstiel's value of 153 kips. The major difference between these two analyses occurs in the approximations used for the torsion parameter calculations. However, better agreement was obtained between the twist values than for the bending displacements. Gent therefore concluded that the difference between the two computations was probably attributable to the sensitive nature of the analyses when plasticity developed in the member.

The present analysis gives an ultimate load value of 160.5 kips, which lies in between the failure loads of Birnstiel and Gent. It is thought that the present analysis predicts a higher failure load than Birnstiel due to the neglect of the warping stresses on yielding. This assumption will mean that the load at which first yield occurs is underestimated and hence the subsequent spread of plasticity will be underestimated also. At collapse, the analysis indicates that

yielding has spread from the centre of the column to within 20 ins. from each end.

7. Biaxial analysis of a restrained column.

The final problem examined here is one of a series of tests by Hutchings[21] on columns with restraining beams about the minor axis. The example studied is subject to single curvature bending about both axes and axial load. The minor axis moment is supplied by connecting the beams together by a turnbuckle and predeflecting them to simulate the imposed loading. The column is effectively restrained at its ends about the minor axis and although major axis beams are present, they are only used to supply a moment about that axis.

The load path used by Hutchings was to initially apply the full beam moment, and then to increase the axial load to collapse. This situation represents columns in multi-storey frames for which the predominant loading will be due to axial load carried down from other floors, rather than from the adjacent beams. Details of the frame and its loading are given in Fig. 4.22 together with the experimental and theoretical plots of the mid-height displacements. At low values of axial load ($P < 80$ kips), agreement between the present analysis and the experimental results is good. However, at a value of axial load of approximately 90 kips, the present analysis predicts a sudden increase in deflections, indicating imminent collapse.

The experimental failure mode is however much more progressive, with the effectiveness of this elastic restraint becoming less and less as the deflections begin to increase until failure occurs at an axial load of 99.1 kips.

The computer analysis has specifically been formulated to analyse complete frames and it has thus been found to be difficult to correctly model the effects of the turnbuckle in providing elastic restraint. The minor axis beams are assumed to be simply supported at their remote ends in the present analysis. As a result, a sudden rather than a progressive collapse mode is obtained, indicating that restraint is no longer being provided by the minor axis beam. The column thus reverts to a pin-ended column under biaxial bending.

4.8 Design of a single-storey portal frame.

A further use of the present computer analysis has been to make allowance for the beneficial effects of strain hardening in single-bay portal frames designed plastically. A suggested design procedure for such frames will now be described.

Structures must usually satisfy not only strength, but also deflection requirements and B.S.449[5] gives permissible values for the horizontal movement at the head of a column and the vertical deflection of the rafters in a portal frame. In practice, frames which are designed to strength requirements by plastic theory are usually assumed to satisfy the deflection requirements of B.S.449, providing the structure does not carry overhead travelling cranes. If such cranes are carried, it is important to limit the horizontal spread of the building at the level at which the longitudinal crane girders are supported by the portal frame. For the frame shown in Fig. 4.23, for example, the change in the distance BF is to be constrained. The spread may be controlled by the provision of a

tie between the eaves at C and E. In such tied portal frames, the design is usually governed by strength requirements.

If a tie is not provided, then the column and rafter sections must be stiff enough to control the spread of the frame at BF, and this requirement may control the design. In such cases it is usual practice for the designer to select suitable section sizes by analysing a trial design and then increasing or reducing the sections as required. Providing the ratio of the moment of inertia of the rafter to that of the column remains constant, a satisfactory design is obtained without further analysis. Generally, this trial analysis will be performed using one of the many programs available for the linear elastic analysis of plane frames. However, such programs give no guidance to the designer on the selection of sections for the trial design if the deflection constraint is to be satisfied in an economical manner.

The use of the present computer analysis together with an optimisation procedure to limit deflections in designing single-bay portal frames will now be described. If has been found convenient in the program to first of all design the portal frame to satisfy the deflection constraint, and then to consider strength requirements.

4.8.1 Design to limiting deflections.

The optimum design of portal frames to satisfy deflections has previously been given by Anderson in a paper by Anderson and Salter[87]. A summary of this design procedure will now be given. Expressions for the bending moments in untied single-bay portal frames are given in standard reference books such as 'The Steel

Designers Manual'[89]. By use of the slope-deflection equations, the horizontal movement of point B (see Fig. 4.23) with respect to the column base can be obtained in terms of the section properties and dimensions of the frame.

For instance, for a fixed base frame under vertical loading only

$$\Delta_{AB} = \frac{k\,a^2\,d\,(p.\ell - n.e) + a^2 \cdot d\,(p\phi^2 - ng)}{18Ek^2I_1 + 6E \cdot i \cdot k \cdot I_1 + 6\,E \cdot j \cdot I_1} \qquad 4.37$$

where $k = I_2 h / I_1 s$, $d = wL^2/16$, $p = 1 - b/h$, $\ell = 16 + 15\phi$

$n = 2 + b/h$, $e = 8 + 15\phi$, $g = \phi(6 - \phi)$, $i = 4 + 4m + 4m^2 + 4\phi^2 + 2\phi q$,

$j = 4(\phi^2 + m\phi^2 + m^2\phi^2) - \phi^2 q^2$, $m = 1 + \phi$, $q = 1 + 2m$, $\phi = f/h$.

In deriving these expressions, it is assumed that the horizontal forces, H, at B and F which result from surging of the crane are equal, and do not cause a change in span length, and can therefore be ignored. Wind loading, acting alone, can either increase or decrease the span at the crane girders, depending on the relative magnitudes of the forces acting on the windward column and the rafters to the force on the leeward column. The usual effect will be to decrease the span, in opposition to the increase due to the downward dead and imposed loadings on the rafters. Frames so far designed show that the critical deflection to control is the spread of the span under the vertical roof loading and crane loading. Hence if this deflection is satisfied, then any decrease of the span under vertical dead and full wind loading will be within the specified limit, and thus deflections due to the wind loading are not included in the design procedure.

To simplify the algebra in Eqn. 4.37, it was further assumed that the load carried by the crane is at mid-span, resulting in M_B and M_F being equal. Several frames were analysed with the load in this position, and also close to either column, showing that the change in span at the level BF is independent of the position of the crane load.

Similar expressions can be obtained for a pinned base frame. Due to symmetry, the spread of the span L at the level BF, Δ, is given by

$$\Delta = -2\Delta_{AB} \qquad 4.38$$

For a given permissible value of Δ, and a chosen value of I_2/I_1, the required value of I_1, and thus I_2 can be obtained from Eqns. 4.37 and 4.38.

By assuming that the weight per unit length of a member is proportional to the moment of inertia, the weight of the frame, W, can be expressed as

$$W = 2h\ I_1 + 2s\ I_2 \qquad 4.39$$

A design satisfying Eqn. 4.37 can then be determined by assuming a value for I_2/I_1. By using a whole series of these ratios, a minimum weight design corresponding to the optimum ratio I_2/I_1 can be found to satisfy Eqn. 4.39.

Corresponding real sections corresponding to the calculated values I_2 and I_1 are then selected, and this design is then taken as a lower bound for the next part of the design stage (design to strength requirements).

In the case of a tied portal frame (for which deflection constraints are not usually critical), a nominal initial design will normally be used as a lower bound solution. A flow diagram for the procedure is given in Fig. 4.24.

4.8.2 Redesign of the frame to satisfy strength requirements.

The designer will specify the required load factors that the frame must sustain under the various load cases. The frame is now analysed under vertical roof loading and crane forces and moments, excluding surge forces, using the elastic-plastic analysis programs which includes allowance for strain hardening. This load combination is usually the critical loading case for portal frames. Since when surge forces exists, the permissible load factor is reduced.

Let the required load factor for collapse be λ_p and the actual collapse load factor λ_F. If λ_F is less than λ_p, it is assumed that all those member that contain non-elastic regions are underdesigned. Let the fully plastic moment of a member in the weak design be M^1_p. The required plastic moment M_p is then given by:

$$M_p = M^1_p \lambda_p/\lambda_F \qquad 4.40$$

Sections with plastic moments at least equal to the required values are not selected. However, those members that remain elastic at collapse are now increased, as it is assumed that they are not contributing to the premature collapse of the frame.

In a similar manner, if λ_F is greater than λ_p the required plastic moment capacities for all members are obtained using Eqn. 4.40.

In this case, an elastic member will be contributing to the excess strength of the frame and its section should therefore be reduced. Sections are not, however, reduced below those required to satisfy deflection requirements. In addition to withstanding a specified degree of overload, the frame should also remain elastic at working load. If some members violate this condition, then the analysis is terminated at working load and the members concerned are redesigned, using Eqn. 4.40, with $\lambda_p = 1$ and λ_F is the load factor at which the member being redesigned first yielded.

When sections are being reduced during redesign of the frame, the bending moments and axial forces at working load are examined to ensure that sections which would yield before working load are not selected. The redesigned frame is now analysed. The iterative procedure of analysis and redesign to strength requirements continues until the redesign procedure shows that none of the sections comprising a safe design can be changed to the next smallest in the section tables. This design is now analysed under other loading cases specified by the designer. If the frame was found to be weak under one of these loading cases, further cycles of analysis and redesign under this load case would follow.

In order to reduce analysis time using the elastic-plastic program, all out of plane behaviour (minor axis displacements, twist and warping) is restrained. Hence the columns are not designed against lateral-torsional instability. It is assumed therefore that a designer would have initially used a method such as Horne's[13] to check for this possible failure mode.

4.8.3 Portal frame examples.

1. Tied Portal Frame.

The dimensions, material properties and loading of the frame are as in Fig. 4.23, with the distributed loading on the rafters being treated as a series of equivalent point loads along each rafter.

For the elastic–plastic analysis, the frame is segmented into 38 unequal element lengths with 16 elements in the columns and 20 elements in the rafters, the final two elements representing the crane members. Near the expected regions of high stress under the imposed loading, element lengths of 200 mm have been used. In addition, a tie of yield stress 350 N/mm^2 is connected between points C and E (Fig. 4.23).

As a result, a deflection check on the frame is not required and the frame is designed solely to satisfy strength requirements. An initial design is made using simple plastic theory under vertical roof loads and neglecting strain hardening.

i) Tie design. Tie force at working load = 164.8 kN.

With reference to B.C.S.A. Publication[89] No. 28.

Area required for the tie = $\frac{1.75 \times 164{\cdot}8}{0.35}$ = 825 mm^2

Hence a 76 × 51 R.S.J. Grade 50 Section is used (Area = 849 mm^2).

ii) Rafter and stanchion design.

Assuming the depth of column section = 250 mm, the clear span = 17.75 m

Plastic moment required (M_p) = $\frac{7.5 \times 17{\cdot}75^2}{64}$ = 36.9 kNm (For a unit load factor)

Hence the plastic modulus of the section = $\frac{36900 \times 10^{-3} \times 1.75}{0.25}$ = 258 cm^3

Hence a 254 × 102 × 22 U.B. is used (Plastic modulus = 261·5 cm^3)

A summary of the subsequent design procedure is given in Table 4.4. In the first stage of the analysis, yielding commenced at a load factor below unity and consequently λ_p is set to 1 in Eqn. 4.40 and the members are redesigned. In subsequent analyses, the frame is unyielded at a load factor of 1.0 and hence redesign is based on the collapse load factor. For all these analyses, the effects of strain hardening are included, and the loading consists of the vertical crane loads together with the vertical roof loading.

The final design obtained for the frame is given in Row 3 of Table 4.4. The frame collapses at a load factor of 1.87, and redesign to a load factor of 1.75 results in the same discrete sections being picked.

2. Pinned Base Portal Frame.

The loading, material properties and dimensions of the frame are again given in Fig. 4.23, with the frame being segmented in the same way as Example 1 for the elastic-plastic analysis and the permissible spread of the span at BF being set to 18 mm.

The optimum design to satisfy the deflection constraint was I_1 = 981.8 × 10^6 mm^4 and I_2 = 471·5 × 10^6 mm^4. In the corresponding discrete section design a 686 × 254 × 125 U.B. (I = 1177 × 10^6 mm^4) was adopted for the columns. The rafter used was a 457 × 191 × 74 U.B. (I = 333·24 × 10^6 mm^4).

The discrete section design was now subjected to elastic-plastic analysis under vertical roof and downward vertical crane loads. The frame collapsed at a load factor of 2.0, approximately, which is greater than the required value of 1.75. First yield had occurred in the rafter at E at a load factor of 1.56. At collapse, the rafter at E had yielded throughout its depth, and strain hardening had occurred. A similar region was present two-thirds of the way along rafter CD.

As the frame had safely carried the above load case, it was now analysed under

(i) vertical roof load, and vertical and horizontal crane forces

(ii) vertical roof, vertical crane loads and typical wind loading

For both these load cases, the load factor at collapse exceeded the usual required values of 1.59 and 1.4.

The above frame was also designed by rigid-plastic theory, it being assumed that the rafters and stanchions have the same section. The resulting design used a 610 × 229 × 113 U.B. The frame weight, W, was 4.15 tonnes, compared with a weight of 3.66 tonnes for the design given by the program.

3. Fixed base portal frame.

The dimensions and loading of the frame were as given for the previous examples, with the permissible spread of the span at BF being set to 36 mm.

The optimum design to satisfy the deflection constraint was $I_1 = 281\ 24 \times 10^6 mm^4$ and $I_2 = 137{\cdot}8 \times 10^6\ mm^4$. In the corresponding discrete section design, a 457 × 191 × 67 U.B. ($I = 293{\cdot}37 \times 10^6\ mm^4$) was adopted for the columns. The rafter used was a 406 × 140 × 39 U.B. ($I = 124{\cdot}08 \times 10^6\ mm^4$).

When subjected to the elastic-plastic analysis under vertical roof and vertical crane loads, the rafter yielded at E (Fig. 4.23) at a load factor of 0.89. Using Eqn. 4.40, the rafter was redesigned to be a 406 × 140 × 46 U.B. The following elastic-plastic analysis showed that the strengthened design collapsed at a load factor above the required value of 1.75. At collapse (see Fig. 4.23), partial plastic hinges had occurred at point B (in the column beneath the crane bracket), point E (in the rafter) and point G (the base of the column). In addition, yielding had commenced into the rafters at the apex of the column (C).

As no reduction in section was possible, the design under this loading case was complete. Further analyses under the loading cases (i) and (ii) as for the pinned base frame showed that this design was adequate. Using the standard methods of design, and assuming a uniform section throughout, a design using a 457 × 152 × 60 U.B. was adopted, the frame weight being 2.2 tonnes. The design given by the present program weighed 2.07 tonnes.

α (1)	β (2)	eqs 4.15 and 4.16 (3)	finite difference mesh 5×50 (4)	finite difference mesh 10×100 (5)	$\frac{\lvert(3)-(5)\rvert}{(5)}$ % (6)
0.2	0.2	2.8342	2.7341	2.8372	0.1
	0.4	2.5684	2.4531	2.5527	0.6
	0.6	2.3036	2.1721	2.2681	1.6
	0.8	2.0368	1.8915	1.9838	2.7
	1.0	1.7710	1.6924	1.7769	0.3
0.4	0.2	2.6876	2.5825	2.6812	0.2
	0.4	2.2753	2.1487	2.2403	1.6
	0.6	1.8629	1.7150	1.7993	3.5
	0.8	1.4505	1.2817	1.3587	6.8
	1.0	1.0382	0.9758	1.0411	0.3
0.6	0.2	2.6301	2.5182	2.6116	0.7
	0.4	2.1601	2.0276	2.1102	2.4
	0.6	1.6903	1.5368	1.6086	5.1
	0.8	1.2202	1.0466	1.1074	10.2
	1.0	0.7505	0.6937	0.7404	1.4
0.8	0.2	2.6229	2.5061	2.5951	1.1
	0.4	2.1459	2.0131	2.0877	2.8
	0.6	1.6689	1.5194	1.5796	5.7
	0.8	1.1916	1.0264	1.0720	11.2
	1.0	0.7149	0.6638	0.6922	3.3
1.0	0.2	2.5480	2.4257	2.5115	1.5
	0.4	1.9840	1.8498	1.9175	3.5
	0.6	1.4260	1.2738	1.3235	7.7
	0.8	0.8680	0.6981	0.7302	18.9
	1.0	0.3100	0.2984	0.3088	0.4

$b = 10$ $d = 1$

$G_2 = 10$ $G_1 = 0.1$

Table 4.1 effective torsional rigidities for yield pattern of Fig. 4.8(a)

α (1)	β (2)	γ (3)	eqns 4.15 and 4.16 (4)	finite difference mesh 5×50 (5)	finite difference mesh 10×100 (6)	$\frac{(4)-(6)}{(6)}$ % (7)
0.4	0.2	0.2	2.3925	2.3271	2.4528	2.5
		0.4	2.1267	2.0461	2.1682	1.9
		0.6	1.8607	1.7655	1.8839	1.2
		0.8	1.5951	1.5664	1.6770	5.0
	0.4	0.2	1.9507	1.8933	2.0119	3.0
		0.4	1.6849	1.6127	1.7276	2.5
		0.6	1.4191	1.4136	1.5207	6.7
	0.6	0.2	1.5088	1.4599	1.5711	4.0
		0.4	1.2430	1.2606	1.3642	8.9
	0.8	0.2	1.0672	1.1080	1.2078	11.6
0.6	0.2	0.2	2.3643	2.2732	2.3937	1.2
		0.4	2.0986	1.9923	2.1091	0.5
		0.6	1.8328	1.7116	1.8336	0.0
		0.8	1.5700	1.4680	1.6179	3.0
	0.4	0.2	1.8943	1.7828	1.8928	0.1
		0.4	1.6285	1.5022	1.6084	1.2
		0.6	1.3627	1.3031	1.4015	2.8
	0.6	0.2	1.4245	1.2923	1.3913	2.4
		0.4	1.1587	1.1107	1.1844	2.2
	0.8	0.2	0.9546	0.8834	0.9674	1.3
0.8	0.2	0.2	2.3572	2.2634	2.3764	0.8
		0.4	2.0914	1.9824	2.0919	0.0
		0.6	1.8256	1.7018	1.8075	1.0
		0.8	1.5598	1.5077	1.6006	2.5

$b=10$ $d=1$
$G_2=10$ $G_1=0.4$

Table 4.2 effective torsional rigidities for yield pattern of Fig. 4.8(b)

α (1)	β (2)	γ (3)	eqns 4·15 and 4·16 (4)	finite difference mesh 5×50 (5)	finite difference mesh 10×100 (6)	$\frac{\lvert(4)-(6)\rvert}{(6)}$ % (7)
0·8	0·4	0·2	1·8802	1·7708	1·8701	0·5
		0·4	1·6144	1·4901	1·5858	1·8
		0·6	1·3486	1·2910	1·3789	2·2
	0·6	0·2	1·4032	1·2774	1·3622	3·0
		0·4	1·1374	1·0783	1·1575	1·7
	0·8	0·2	0·9261	0·8656	0·9318	0·6
1·0	0·2	0·2	2·2761	2·1786	2·2748	0·1
		0·4	2·0104	1·8977	1·9903	1·0
		0·6	1·7445	1·6170	1·7059	2·3
		0·8	1·4788	1·4179	1·4990	1·3
	0·4	0·2	1·7182	1·6028	1·6810	2·2
		0·4	1·4524	1·3221	1·3967	4·0
		0·6	1·1866	1·1230	1·1898	0·3
	0·6	0·2	1·1602	1·0271	1·0872	6·7
		0·4	0·8944	0·8280	0·8803	1·6
	0·8	0·6	0·6022	0·5331	0·5710	5·5

$b=10$ $d=1$

$G_2=10$ $G_1=0·1$

Table 4·2 (cont.) effective torsional rigidities for yield pattern of Fig. 4·8(b)

Table 4.3 comparison of biaxial computer analysis with previous experimental and theoretical results

analysis	ref.	number of column/frame	nature of analysis	present computer analysis				type of load increased to cause failure	failure load	
				number of elements	strain hardening?	residual stress?	initial imperfection?		original analysis	present analysis
Van Kuren and Galambos	84	T13 $\beta = 0$	experimental	20	✓	x	x	end moment M_o(kip-in)	1258	1249
			experimental	20	✓	✓	x	end moment M_o(kip-in)	1258	1140
Chen		L/r=160; e/r=1	theoretical	20	x	x	x	ratio of axial	0.210	0.212
Chen and Atsuta	60	14WF246 $\alpha=1$	theoretical	20	x	x	x	load to squash	0.430	0.430
		$\alpha=10$	theoretical	20	x	x	x	load, P	0.120	@ 0.125
Ajmani	61	C_{23} $\beta = 0$	experimental	24	✓	x	x	ratio of end	1.30	1.09
		C_{44} $\beta = -1$	experimental	24	✓	x	x	moment to fully	0.90	0.90
		C_{44} $\beta = -1$	experimental	24	✓	✓	x	plastic moment	0.90	0.83
Harstead, Birnstiel	30	problem 4 - $\beta = 1$	theoretical	22	x	x	x	axial	153.0	160.5
Gent	86	about both axes	theoretical	22	x	x	x	load (kips)	164.0	160.5
Charlton	85	pitched roof	experimental	24	✓	x	x	total beam	10.75	10.44
Davies	40	portal 10X, 10Y	theoretical	24	✓	x	x	loading (tons)	10.40	10.44
Wood	8	4-storey, 1-bay frame	theoretical	56	x	x	x	load factor	1.90	1.90
Hutchings	21	restrained column B2	experimental	32	✓	✓	x	axial load (kips)	99.6	90.0

collapse load factor	stanchion			rafter			tie	
	first yield load factor	present plastic modulus	new plastic modulus	first yield load factor	present plastic modulus	new plastic modulus	present area	new area
		cm^3	cm^3		cm^3	cm^3	mm^2	mm^2
1	0·467	258 → (261·5)	561 → (651·8)	0·67	258 → (261·5)	366 → (406·9)	825 → (849)	849 → (849)
1·4		651·8 → (886·3)	815 → (886·3)		406·9 → (537·9)	508 → (537·9)	849 → (1230)	895 → (1230)
1·87		886·3 →	831 → (886·3)		537·9 →	505 → (537·9)	1230 →	890 → (1230)

bracketed values — discrete sections used in analysis
other values — estimated plastic moduli and area

Table 4·4 design of tied portal frame

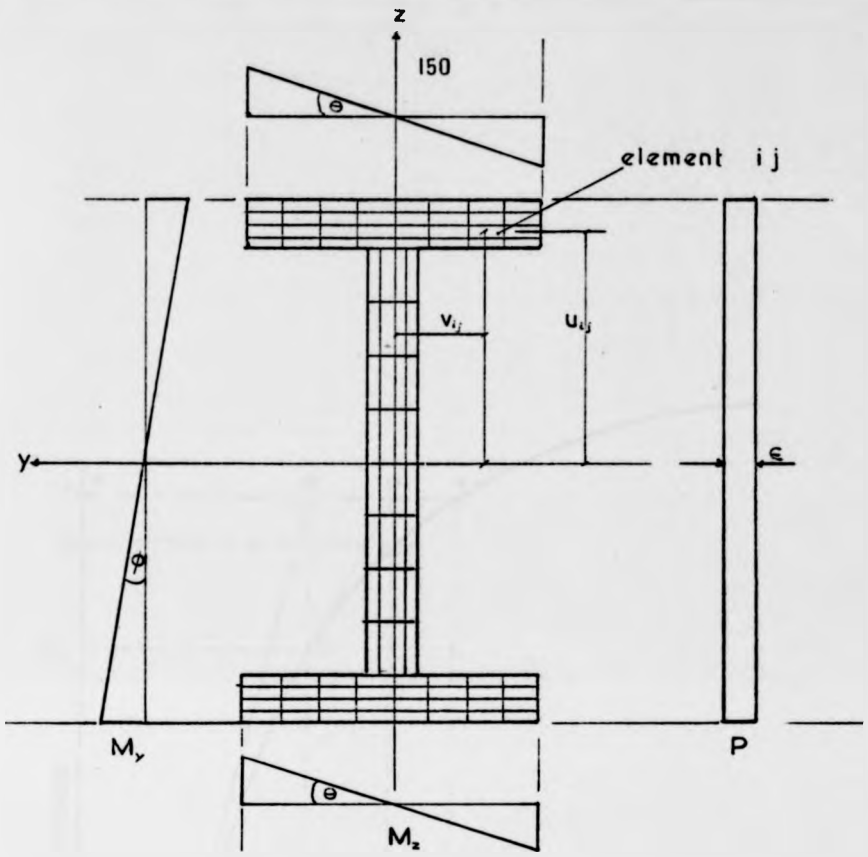

Fig 4.1 subdivision of the I-section into elements with assumed curvature and axial strain distributions

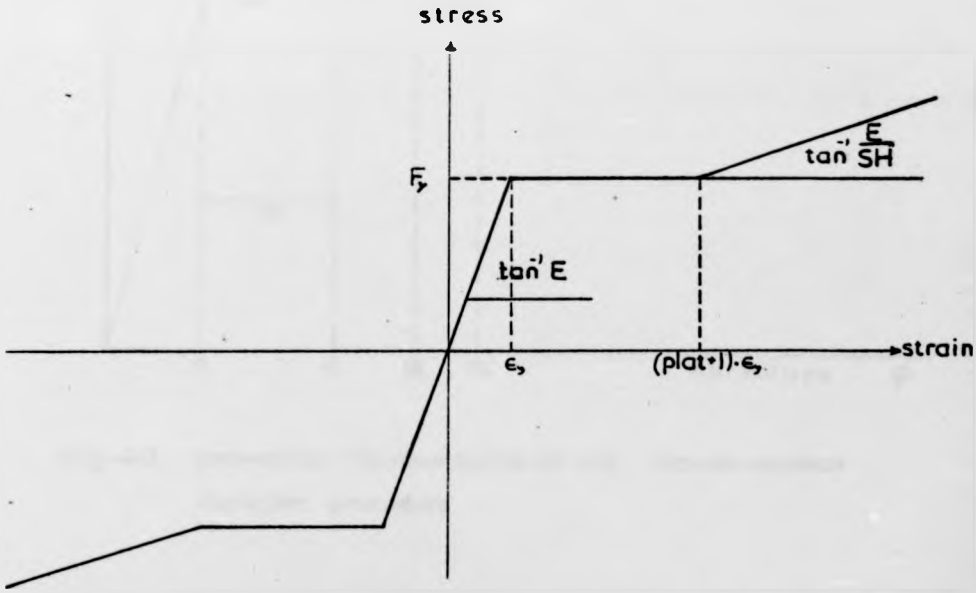

Fig. 4.2 assumed stress-strain relationship including strain hardening

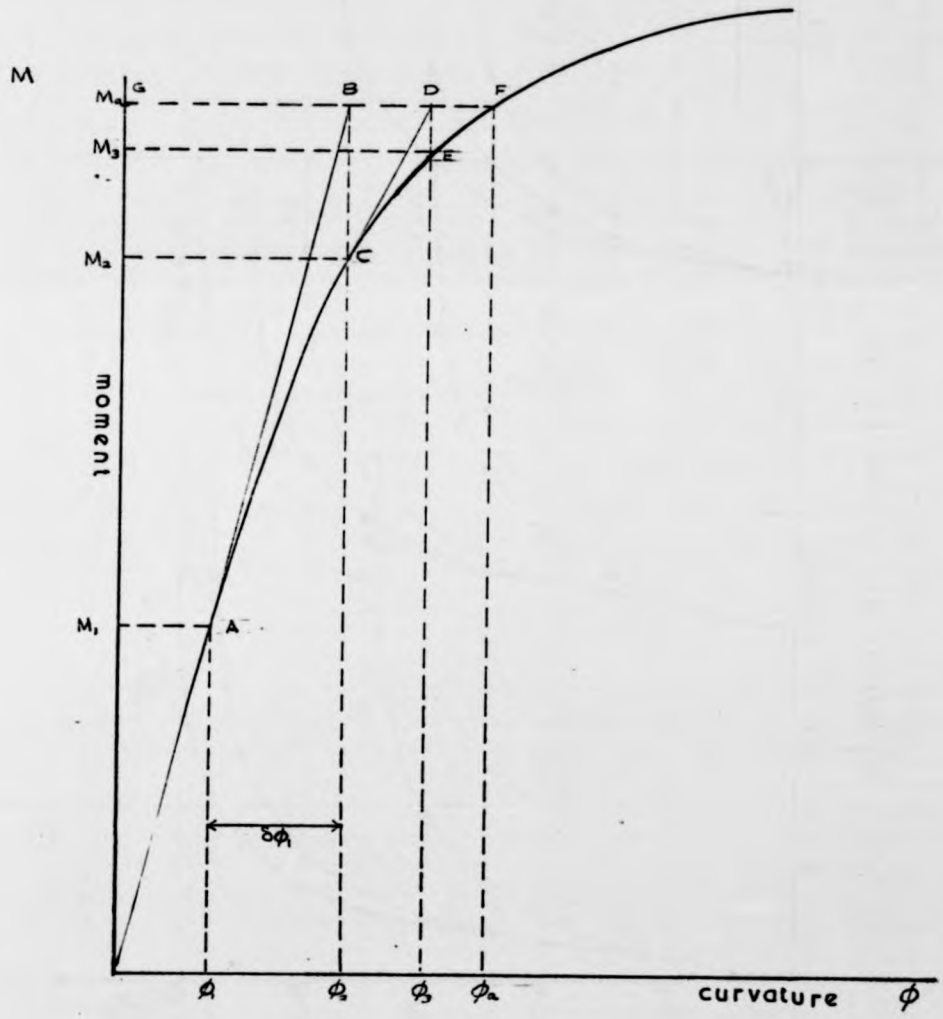

Fig·4·3 geometrical representation of the newton-raphson iteration procedure

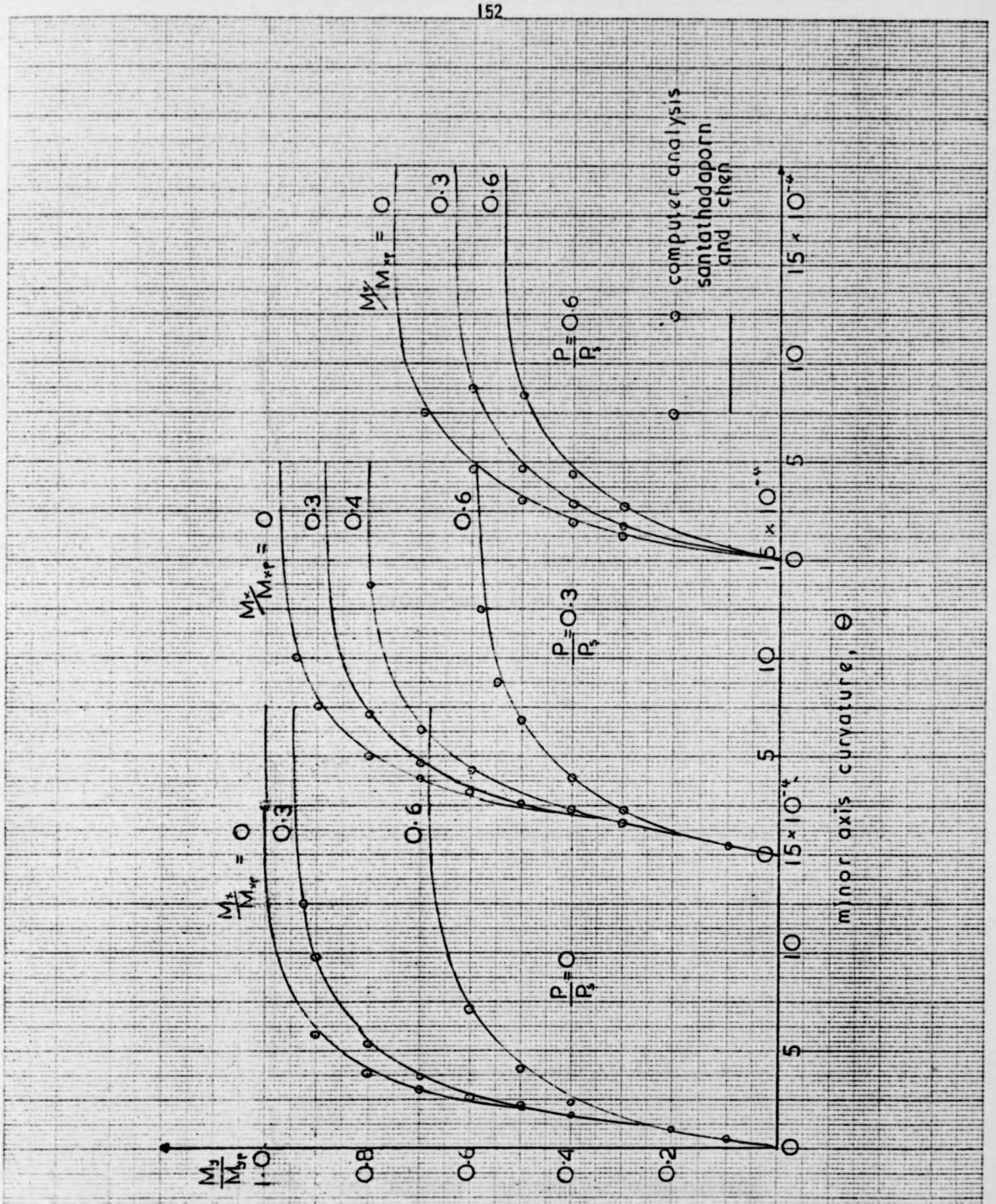

Fig. 4.4 moment- curvature curves

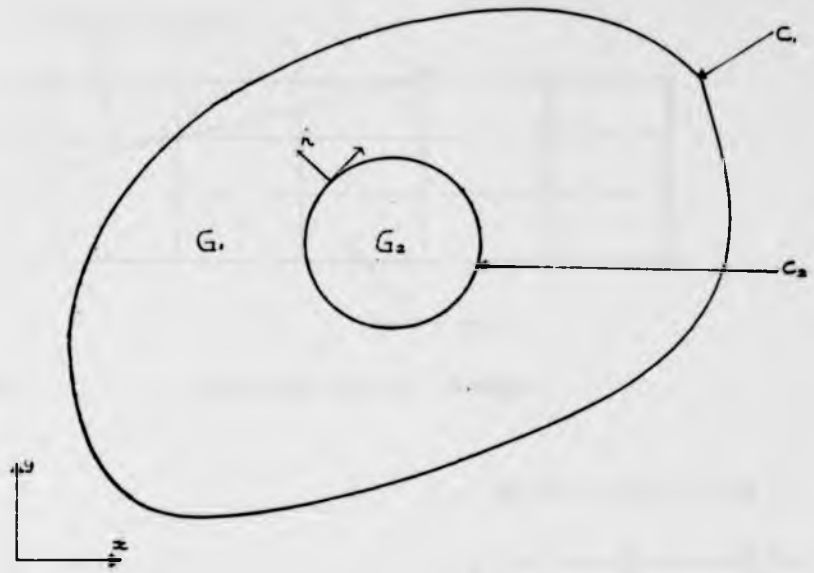

Fig.4.5 cross-section of a composite bar

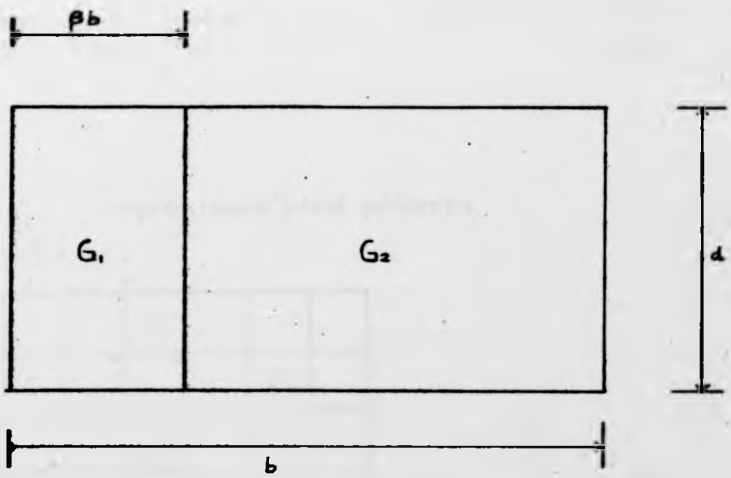

Fig. 4.6 two-layered rectangular cross-section

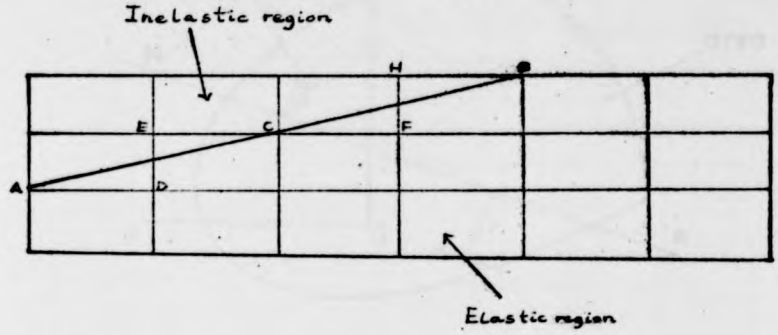

Fig. 4.7 partially yielded flange

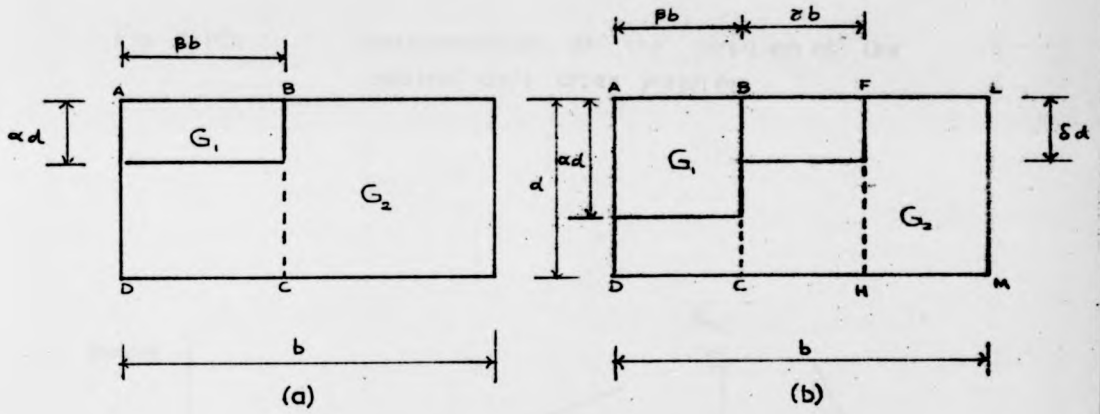

Fig. 4.8 approximate yield patterns

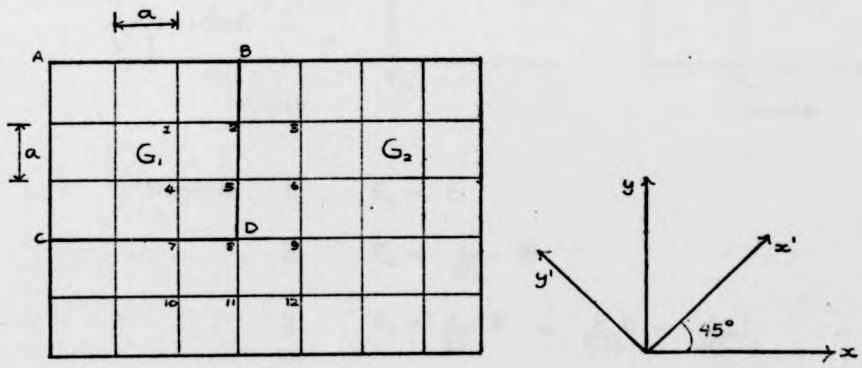

Fig 4.9 finite difference mesh

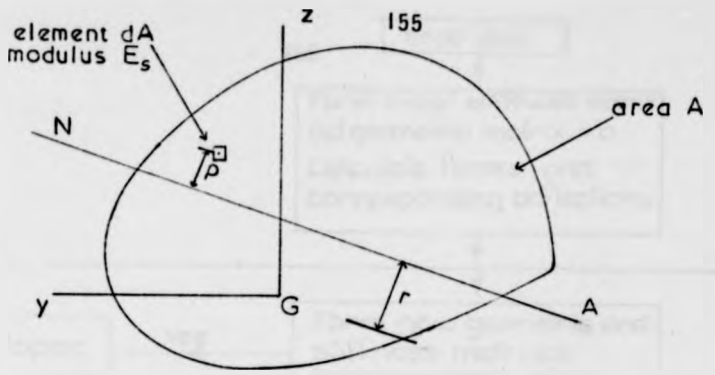

Fig. 4.10 determination of the position of the neutral axis after yielding

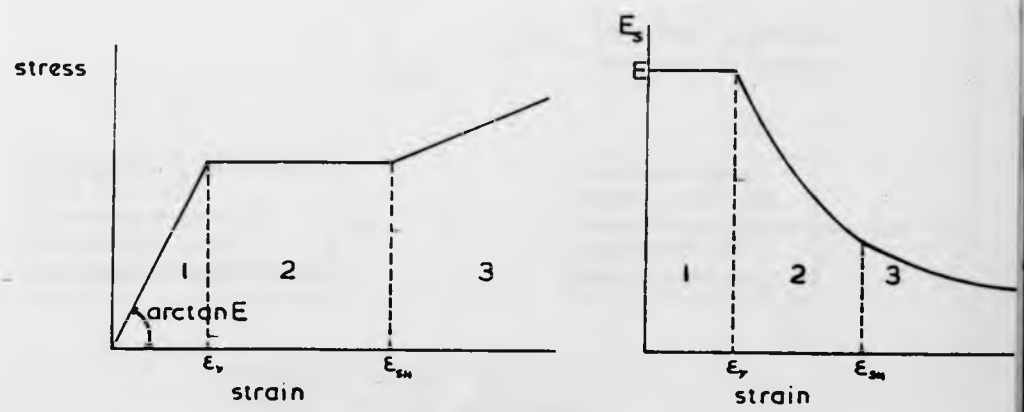

Region 1 $E_s = E$

2 $E_s = \frac{\varepsilon_y}{|\varepsilon|} \cdot E$

3 $E_s = \frac{\varepsilon_y}{|\varepsilon|} \cdot E + \frac{E}{SH}\left(1 - \frac{\varepsilon_y}{|\varepsilon|}\right)$

Fig. 4.11 secant moduli of a yielded section

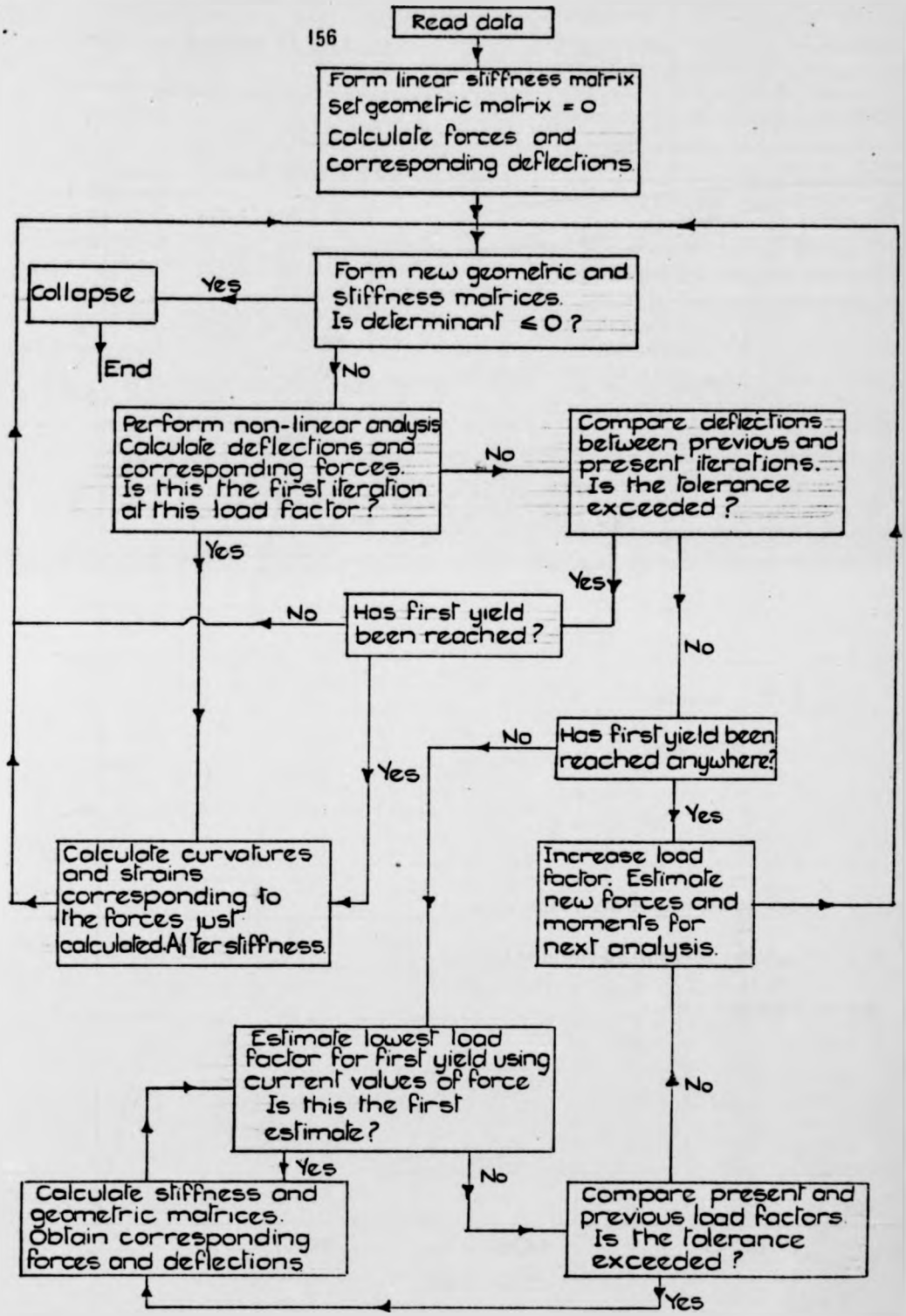

Fig. 4:12 flow diagram for the biaxial elastic-plastic computer analysis

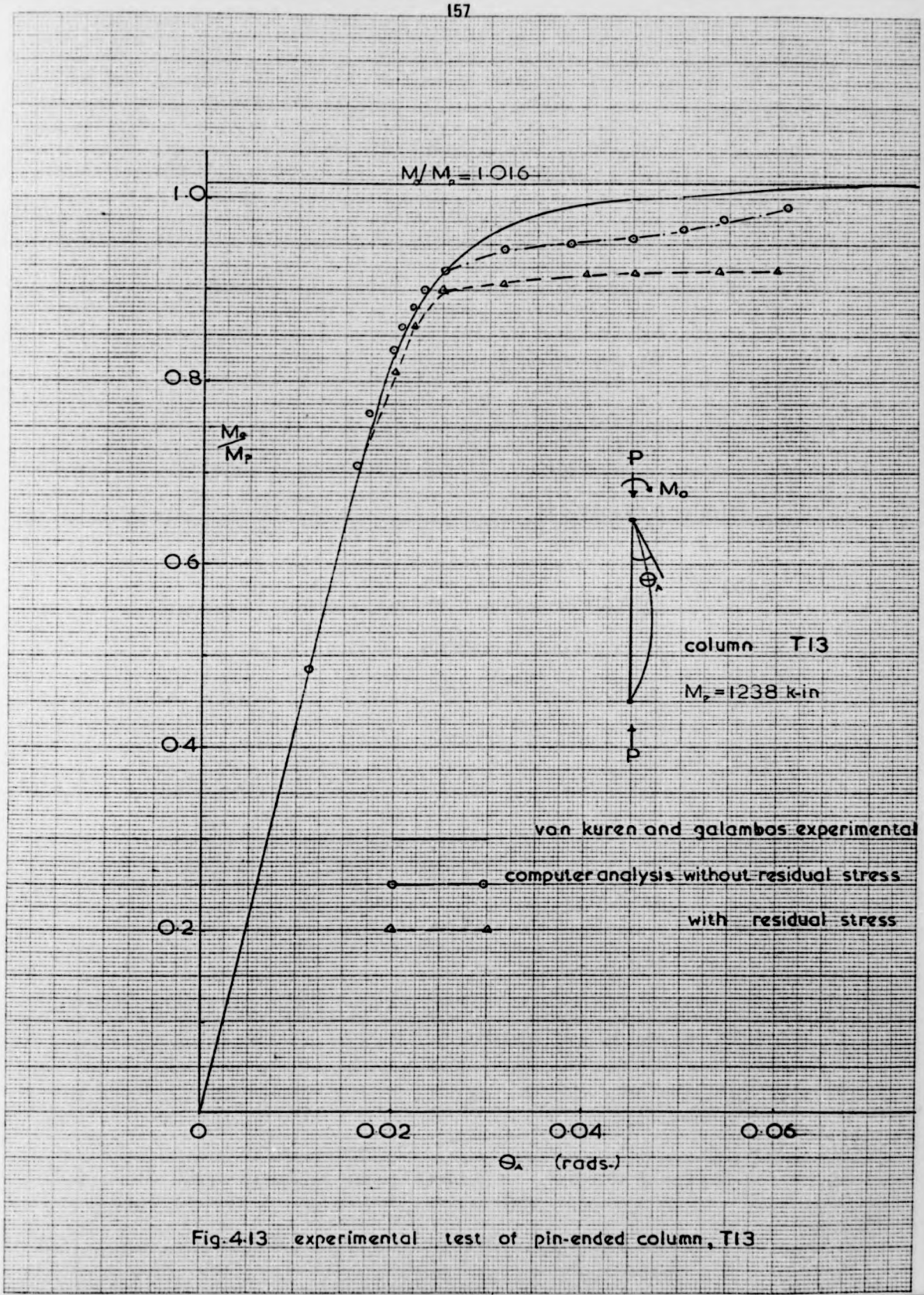

Fig. 4.13 experimental test of pin-ended column, T13

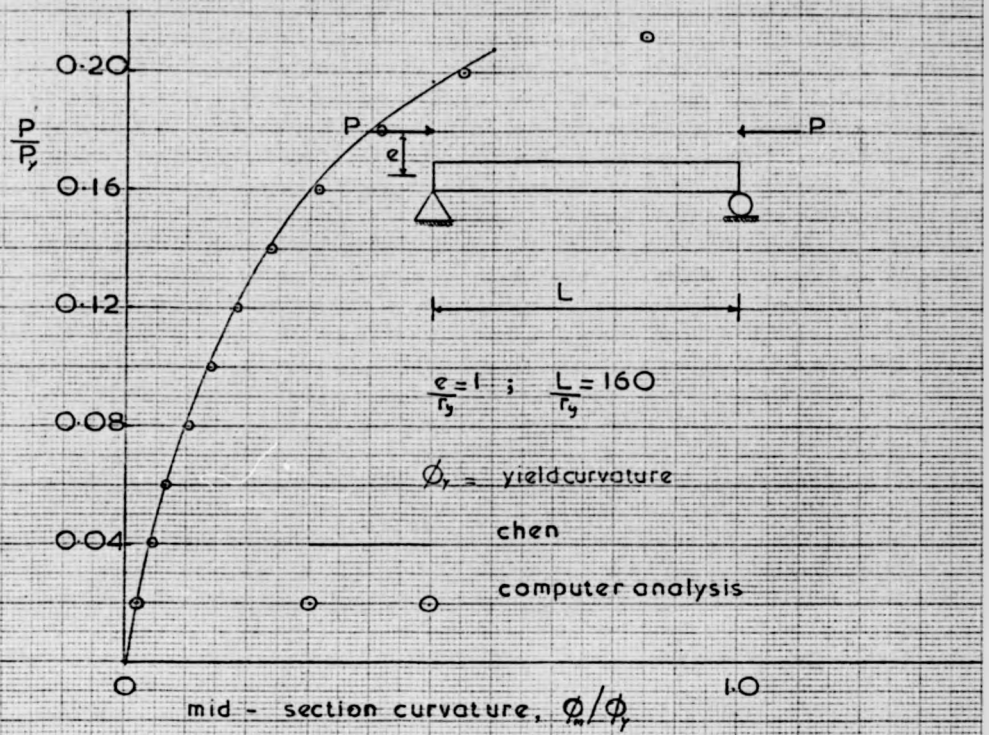

Fig. 4.14 chen's rectangular section curvature curves

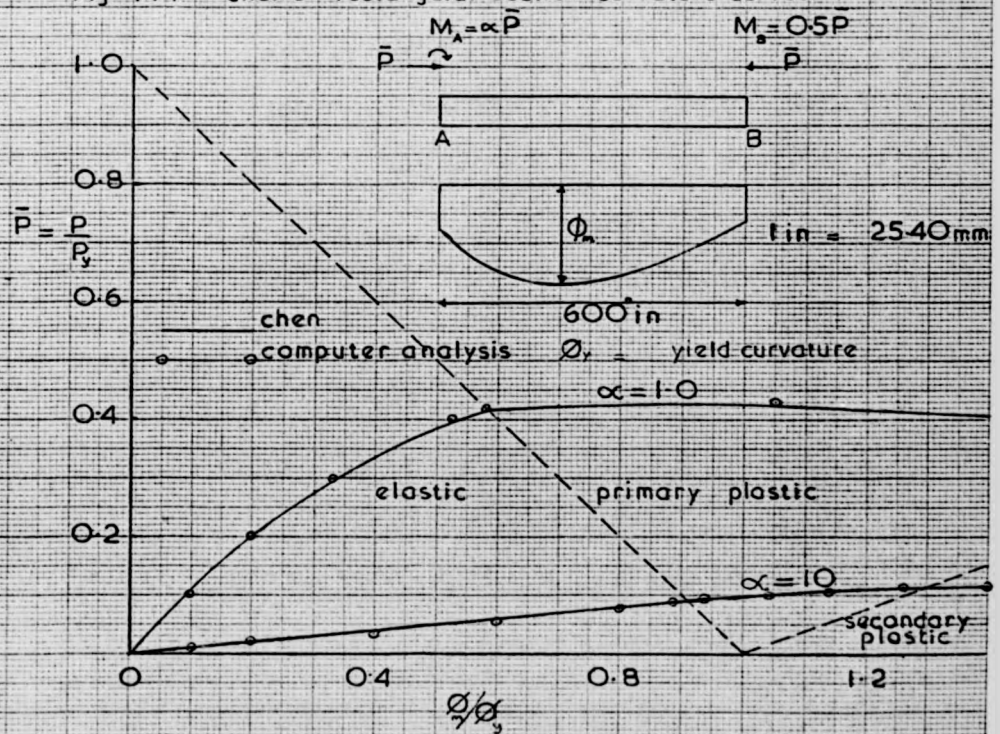

Fig. 4.15 chen's I-section curvature curves

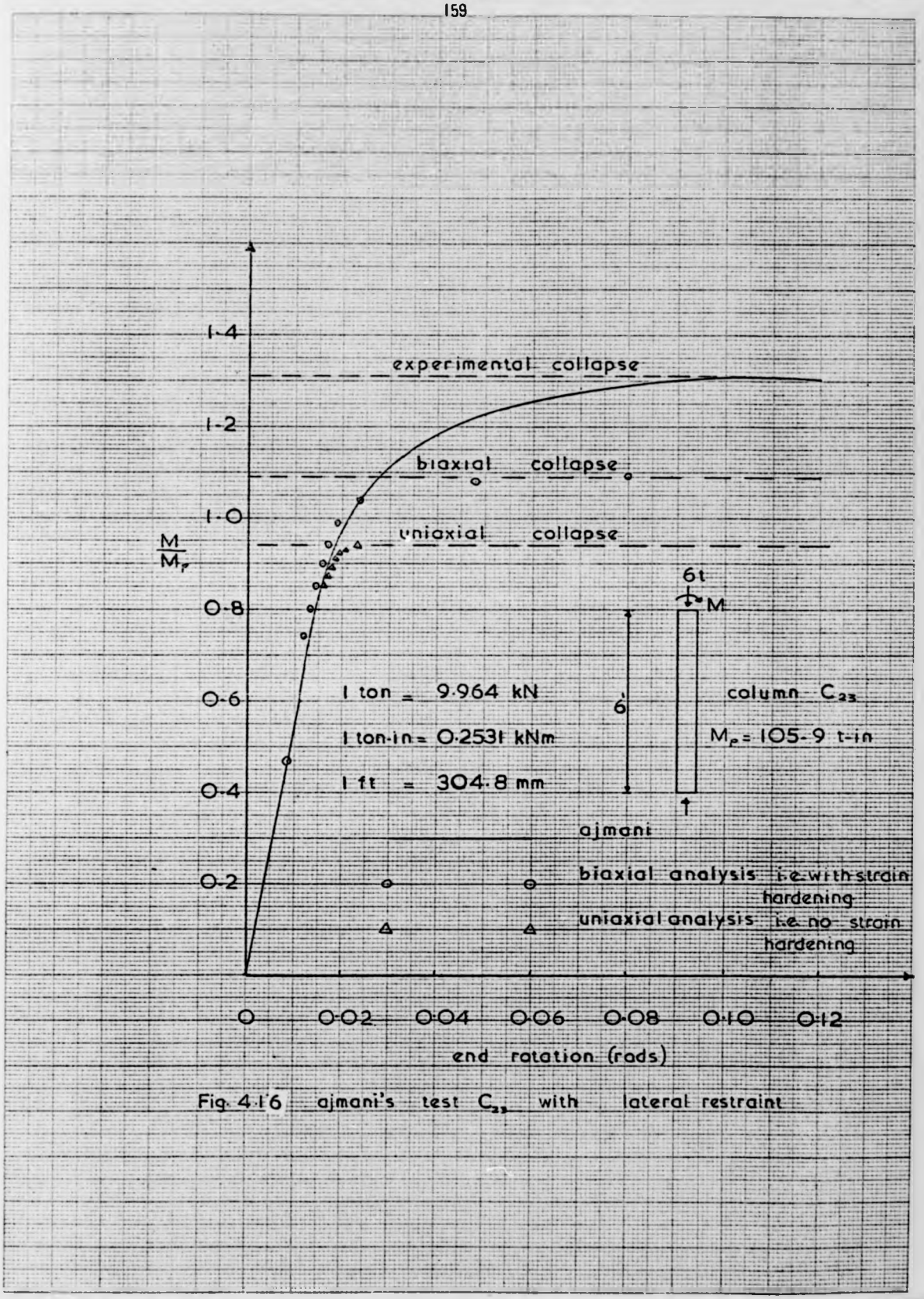

Fig. 4.16 ajmani's test C_{23} with lateral restraint

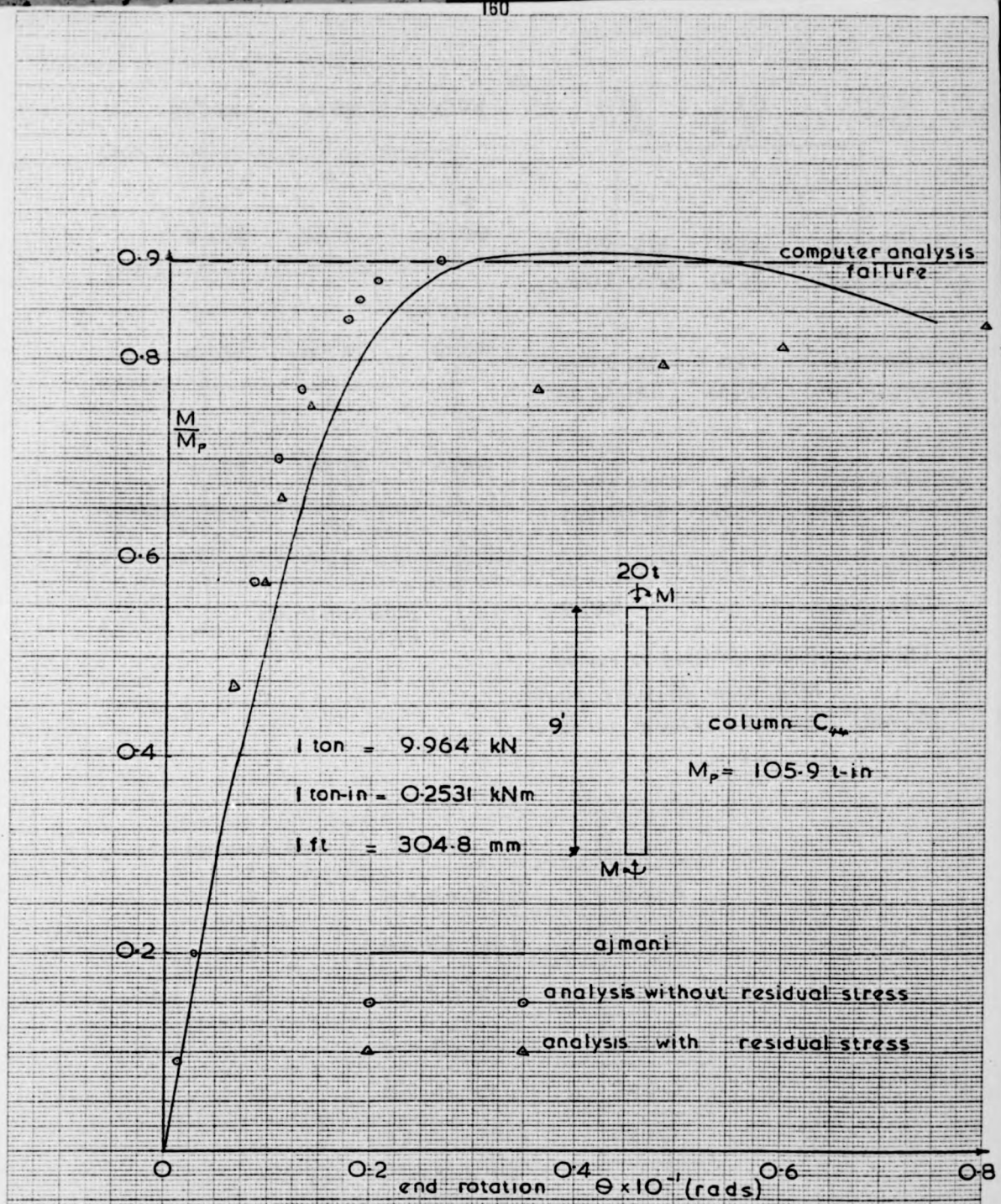

Fig·4·17 ajmani's test C_{44} with lateral restraint

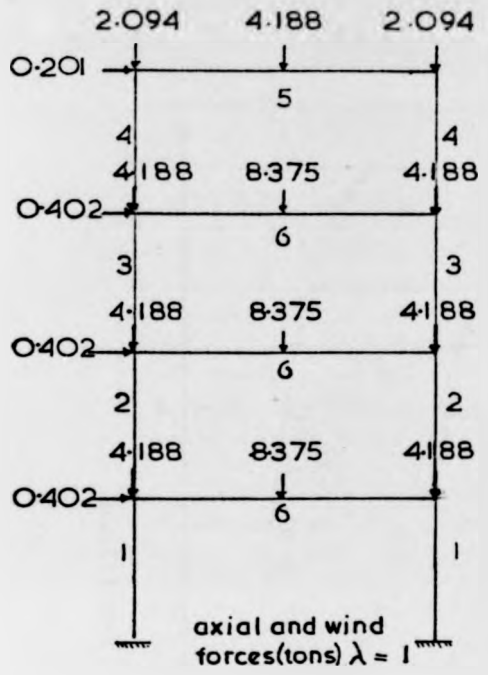

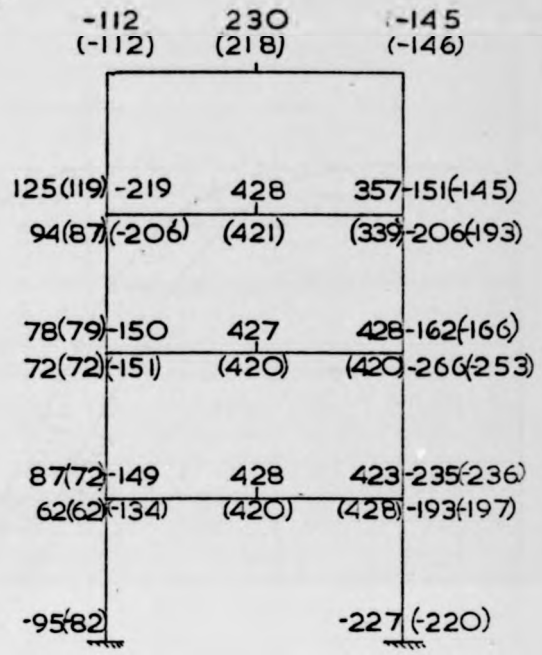

values of bending moment $\lambda = 1.90$
wood s values by each joint
computer results in brackets (ton-in)

member No.	Section	M_p [t-in]
1	8" x 6" x 35 lb	502·3
2	8" x 5" x 28 lb	393·5
3	6" x 5" x 25 lb	259·3
4	6" x 4½" x 20 lb	205·3
5	8" x 4" x 18 lb	244·0
6	10" x 4½" x 25 lb	428·0

1 ton = 9·964 kN
1 ton-in = 0·2531 kNm

Fig. 4·18 wood's 4-storey, 1-bay frame

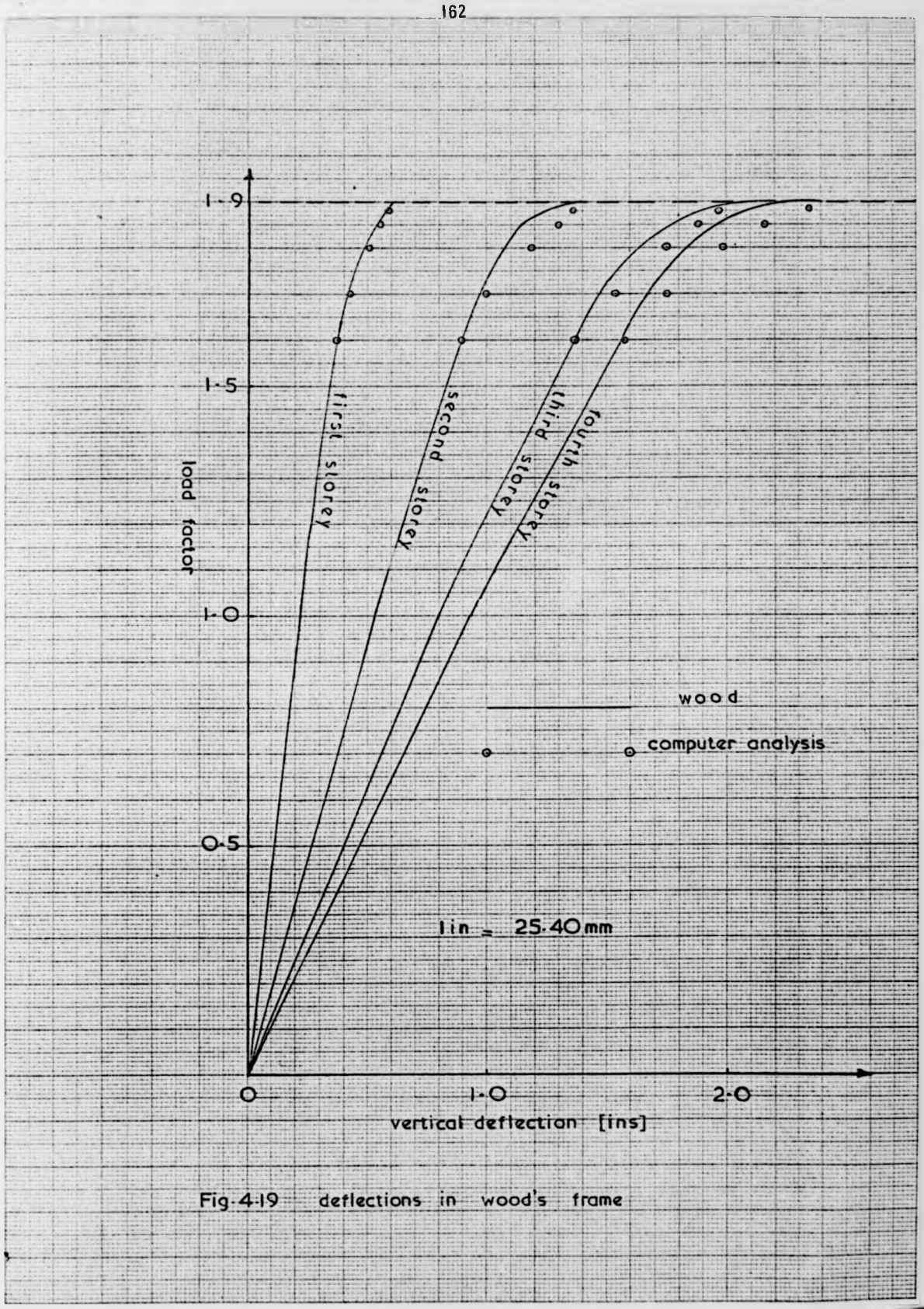

Fig·4·19 deflections in wood's frame

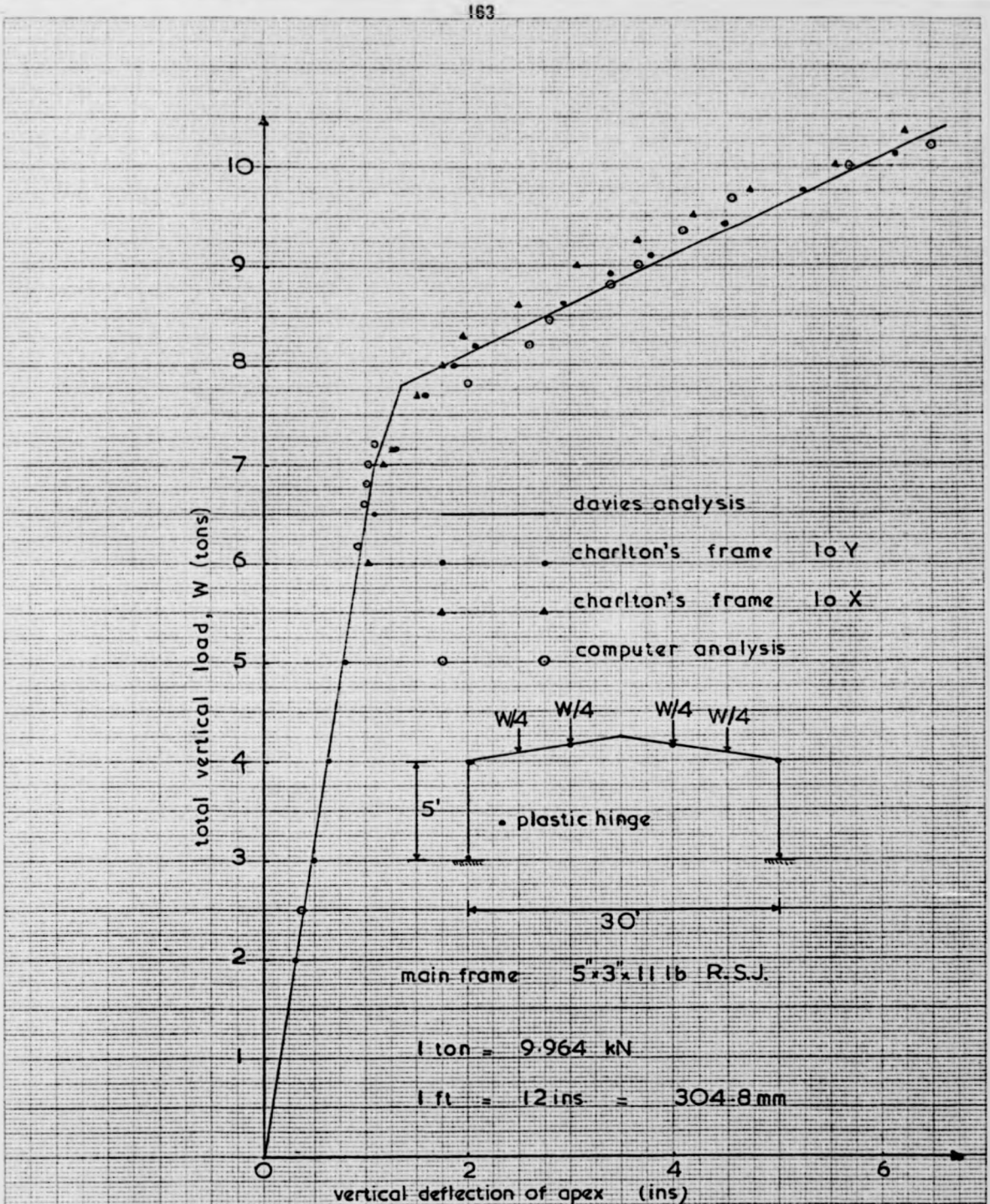

Fig. 4.20 pitched roof portal frame analysis

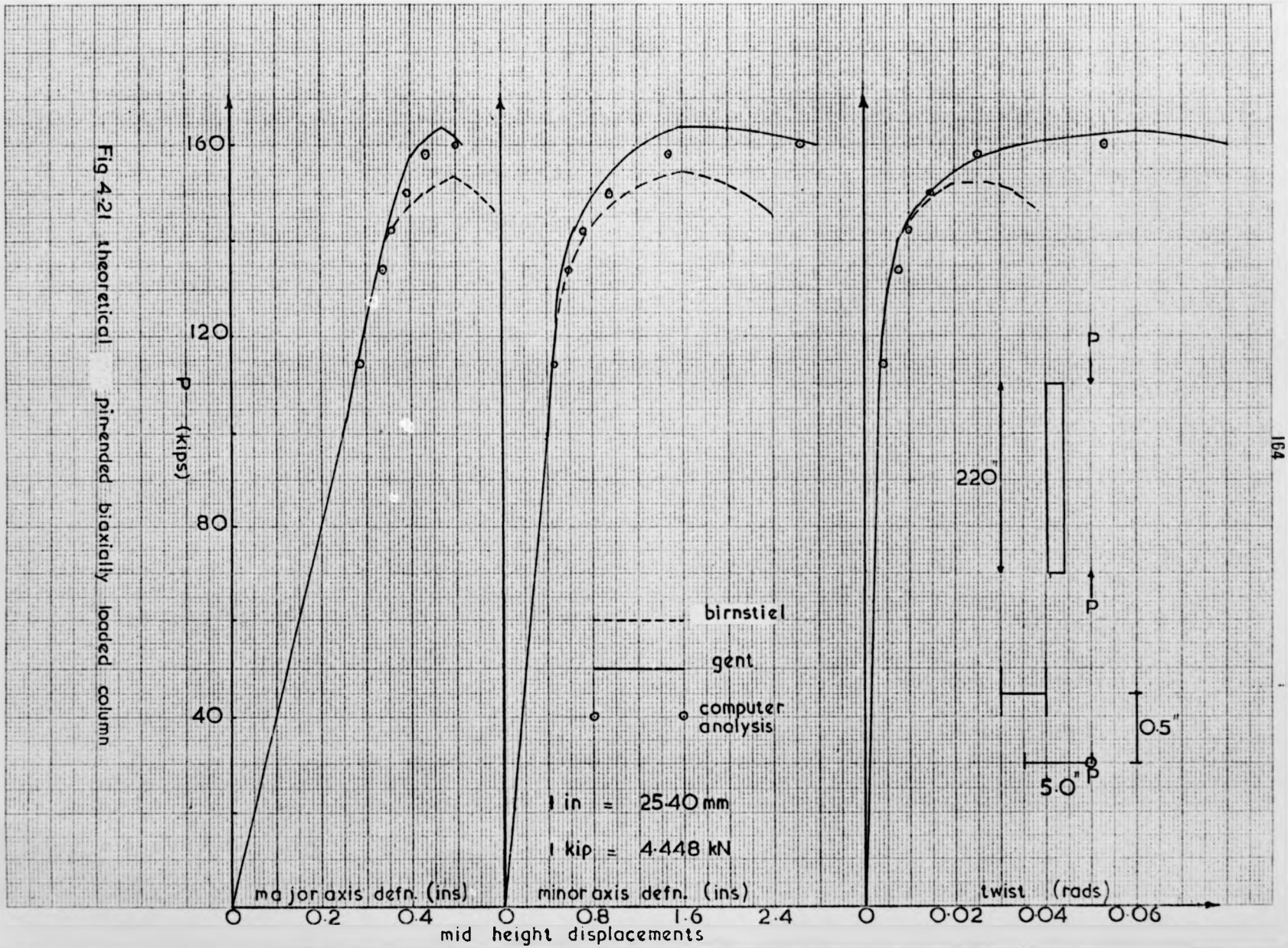

Fig 4.21 theoretical pin-ended biaxially loaded column

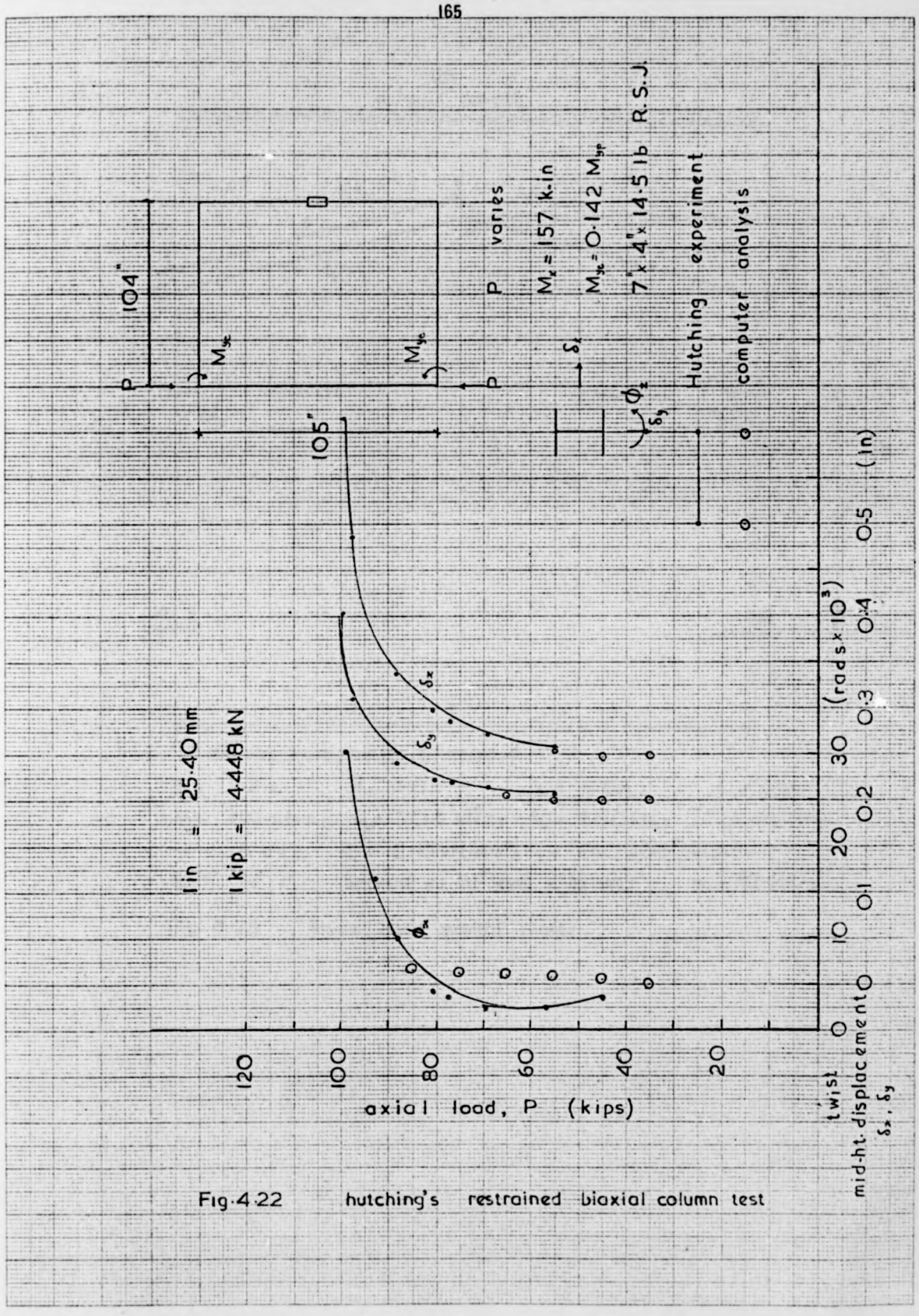

Fig·4·22 hutching's restrained biaxial column test

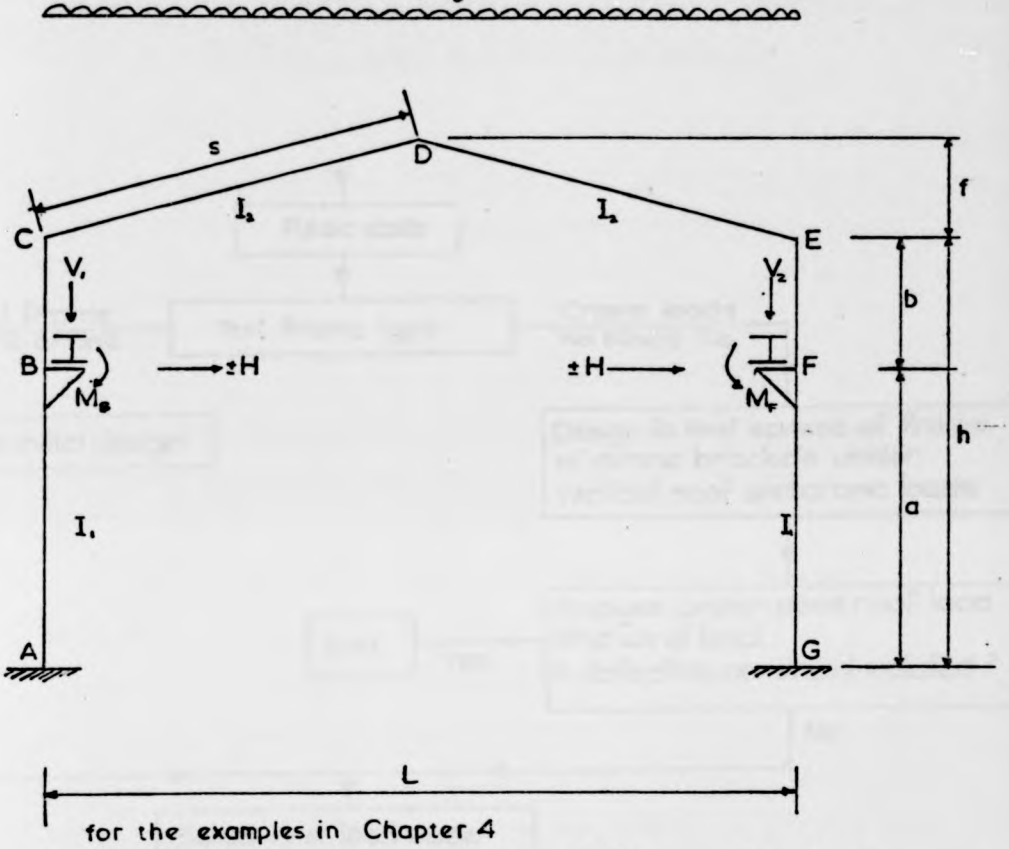

for the examples in Chapter 4

h = 9·2 m ; f = 1·8 m ; a = 6·5 m ; L = 18 m ;

M_B = 192 kNm ; M_F = 704 kNm ; V_1 = 300 kN ; V_2 = 110 kN ;

H = 5 kN ; E = 210 kN/mm² ; F_Y = 250 N/mm² ; PLAT = 11 ;

SH = 32 ; Spread at BF level = 18 mm ; w = 75 kN/m ;

Fig. 4·23 fixed-base portal frame

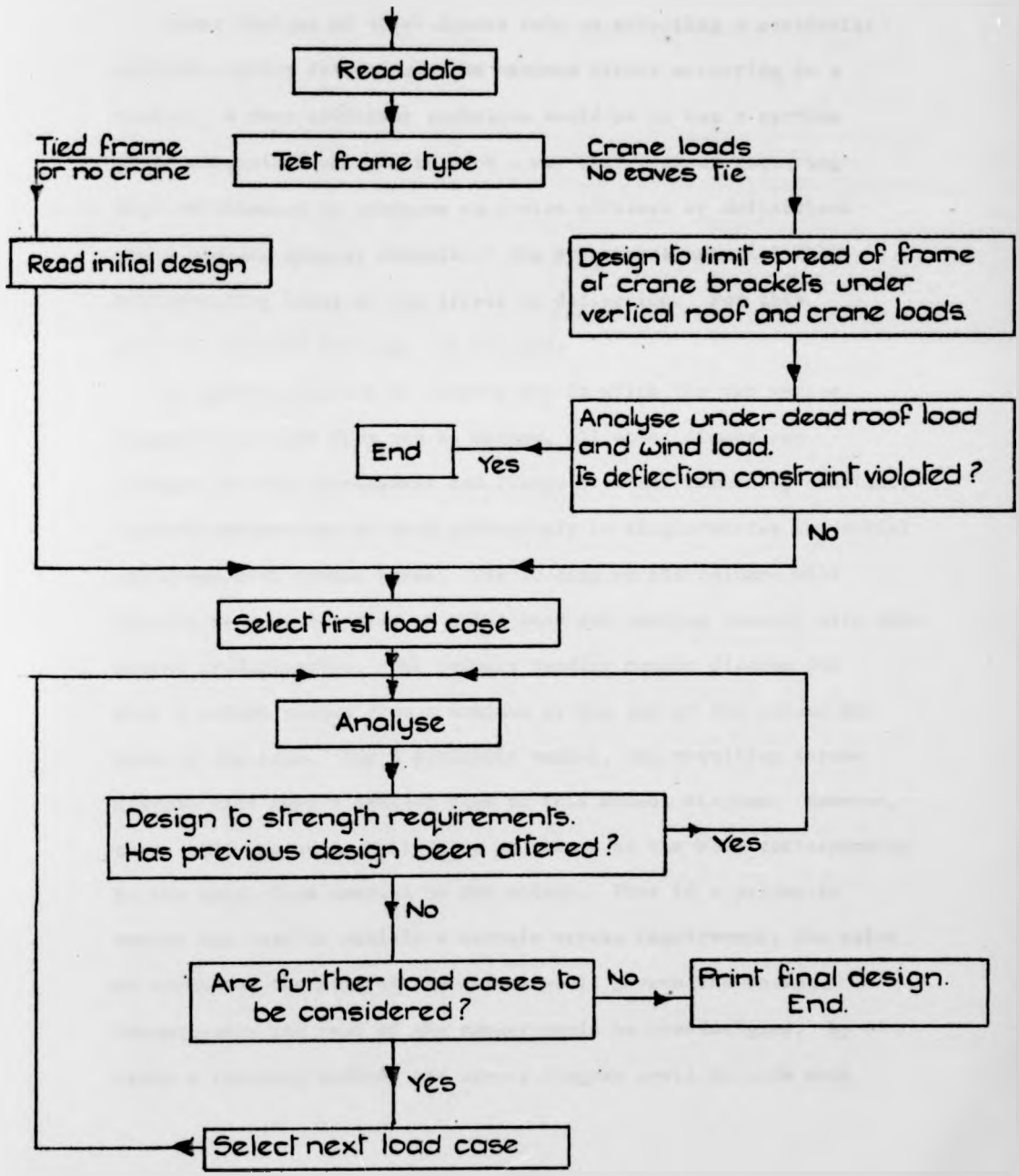

Fig. 4.24 flow diagram for the design of portal frames to satisfy strength and deflection limitations

Chapter 5. Experimental tests on tapered steel columns.

5.1 Introduction.

Most designs of steel frames rely on selecting a particular uniform section to overcome the maximum stress occurring in a member. A more efficient technique would be to use a section whose dimensions changed in such a way that regions requiring high stiffnesses to overcome excessive stresses or deflections would contain greater amounts of the structural material than corresponding areas of low stress or deflection. For this purpose, tapered sections can be used.

A tapered section is usually one in which the web varies linearly in depth from top to bottom, all other dimensions (flange and web thicknesses and flange breadth) remaining constant. Tapered columns can be used effectively in single-storey industrial buildings with pinned bases. The loading on its columns will usually be a combination of axial load and bending moment, with this moment predominating. The primary bending moment diagram for such a column ranges from a maximum at the top of the column to zero at the base. For a prismatic member, the resulting stress diagram will have a similar form to this moment diagram. However, there will now be a small value of stress at the base corresponding to the axial load carried by the column. Thus if a prismatic member was used to satisfy a certain stress requirement, the value of stress at the head of the column would govern the design. Consequently the rest of the member would be overdesigned. By using a tapering member, the stress diagram could be made more

uniform by varying the depth of the column linearly from a maximum at the column head to a minimum value at the base. The degree of taper and depth at the column base will obviously depend on the applied moment from the rafter and the axial load to be carried by the column.

As a result, this will give better utilisation of the material and give a lighter overall structure. However, a lighter structure does not necessarily mean a cheaper structure since the extra fabrication costs of making such sections may offset any material savings. Several manufacturing companies have however developed a system of making such sections which is claimed to be cheaper than conventional prismatic systems. Two rectangular plates forming the flanges and one trapezoidal plate forming the web are connected together using an automatic welding procedure, each flange-web junction being connected by a weld pass on one side only.

Typical sizes of these columns used in practice are:-

1) 3 m in length; depth at the top in the range 375 mm - 750 mm and tapering to a depth of 150 mm or 200 mm at the base.
2) 5.5 m in length; depth at the top in the range 300 mm - 1000 mm and tapering to a depth of 200 mm or 250 mm at the base.

A series of nine tests have subsequently been performed on a selection of tapered columns modelled to approximately half scale of the above sections, and loaded with axial load and major axis being moment.

5.2 Aims of the tests.

An experimental study has been undertaken to investigate the ultimate load capacity of pin-ended tapered steel columns as part of a pinned base portal frame. The test columns have been modelled to approximately half scale to represent typical sizes of actual tapered columns used in practice. They have been fabricated using the same automatic welding process and steel plate as is used in commercial tapered sections.

In the experiments, four parameters have been varied. These are

1) The angle of taper (i.e. the difference in end depths of the column divided by the column length).

In pinned base portal frames, a bending moment occurs at the head of the column due to the loading from the rafter. Hence the designed depth at the top of the column will depend on the value of this moment. Several angles of taper have therefore been used corresponding to typical values used in practice.

One of the problems of using tapered columns in practice is that they often violate maximum allowable depth/thickness ratios at the head of the column for unstiffened webs. Horne[13] has given a maximum value of 53 for the d/t_w ratio (d and t_w are the depth and thickness respectively of the web) in mild steel to permit plastic action to occur in a column. In cases of high primary bending moment, this ratio is often exceeded at the head of the column and for a considerable part of the length also. Values of d/t_w used in the tests have been chosen to violate these limiting conditions.

2) Ratio of the axial load to squash load.

Two major experimental programs have previously been carried out on welded steel tapered sections at Columbia University[55] and New York University[56]. The first series of tests concentrated its interest on the determination of the elastic stability of tapered I-sections. In general, the test members were cantilevered and were subject to axial and transverse loads. The tests were conducted so that several members with the same nominal dimensions were loaded differently, ranging from pure axial load to pure bending. In the second series of tests, interest was directed towards the inelastic lateral stability of tapered beams, the specimens being loading and supported in a similar fashion to gable roof beams. The members were thus subject to high bending stresses coupled with low axial stresses.

The aim of the present tests was to study the ultimate behaviour of tapered steel columns and they are thus subjected to considerable axial as well as bending stresses. The effect of differing values of axial stress on the ultimate moment has thus been examined also

3) Two values of member length have been used in the experimental study corresponding to short and long members in actual use.

4) Provision of lateral restraints.

Tapered columns over 3 m in length are usually provided with a lateral restraint (a girt) on the outer flange at various points along the column. These girts are used to support the

cladding used in the frame.

For the longer columns, therefore, two series of identical tests have been performed on columns with and without lateral restraints. In the restrained tests, one restraint has been provided on the outer flange at the centre of the column.

5.3 Load path.

The loading procedure used in the experimental study was one of initially applying a fixed value of axial load. Subsequently, a bending moment is applied in increments until collapse occurs, whilst keeping the axial load constant.

Horne[90] has argued that the assumed load path of constant axial load and increasing the bending moment to cause failure represents the most likely form of column loading in a building frame. The accumulated axial load on the column due to dead weight and floor loading from above the column remains relatively constant and the live load increases over an isolated floor area within the vicinity of the column, causing collapse due to increase in major axis bending moment.

With reference to Fig. 4.23, the loading in a pinned base portal frame is due to the combination of roof loads and crane loads; these roof loadings cause a combination of axial load and bending moment in the column. However subsequent surging of the crane cause an increase in moment without increasing the axial load.

The load path of applying a fixed axial load and subsequently increasing the bending moment therefore represents a pinned base

portal frame with a fixed amount of roof loading which subsequently fails due to surging of the crane.

5.4 Test rig.

The rig used to test the tapered columns has previously been designed and used as part of a research program to investigate the ultimate behaviour of concrete encased steel columns with end restraint[91]. Subsequently, the rig has been modified to test pin-ended tapered columns with and without lateral restraint at the centre of the column. A schematic drawing showing the rig's essential features together with a general view of the rig are given in Figs. 5.1, 5.15 and 5.16.

5.4.1 Axial load system.

The system is loaded by a 2000 kN hydraulic jack operated by an electric pump through crossed knife edges, contained in a box to which the loading beam and the column under test are bolted. The axial load is measured at the opposite end to the jack at the base of the column after passing through a second set of knife edges by a 2000 kN strain gauged load cell. These crossed knife edges, which convert the load spread over the area of the jack into a point load at the head of the column, provide rotational freedom about both the major and minor axes but prevent any torsional rotation. Both the jack and load cell are reacted against sandwich plates and grillages. The rig is designed to be 'self-reacting', so that reaction to the column loading is taken out within the system rather than to a laboratory strongfloor.

This is achieved by four symmetrically placed 32 mm diameter Lee-McCall prestressing bars connected between the end sets of grillages. One end grillage is bolted to the strong floor (at the base of the column) whilst the other end grillage is allowed to slide on the floor by means of steel rollers. This sliding grillage is only allowed to move along the longitudinal axis of the column, and thus takes up strains within the bars as well as facilitating easy assembly for columns of different lengths.

5.4.2 Beam loading system and shear resistance.

The major axis moment is applied at the top end of the column only by deflecting the attached beam using a threaded rod. This load is measured using a strain-gauged tension-compression load cell. The remote end of this beam rests on a flat plate, between which is a small ballbearing giving complete rotational freedom.

Application of moment at only one end of the column results in quite large shear forces at the ends of the column. These forces are removed from the system by long links placed under the beams, connected at one end close to the box and at the far end to a small frame attached to the strong-floor. These links are capable of resisting axial tension and compression. As a result, the beam at the base of the column is retained to locate the link, even though it has no load applied to it.

5.5 Testing procedure.

The columns were prepared and tested in three batches of three columns. The first and third batches were the columns of the larger length, the second batch being the shorter columns. Before each test, the ends of the specimen were cut in such a way that the longitudinal centre line of the column was perpendicular to the front plate of the end boxes. End plates (25 mm thick) were then symmetrically welded to the ends of the column and a thin layer of brittle plumbers resin was applied to the column web and flanges at regions of expected yield. On subsequent loading of the column, yielding is indicated by the cracking and flaking off of the resin.

For the final batch of columns, a 75 mm wide rectangular plate having the same thickness as the flange was welded to one of the flanges at the mid-point of the column. During the subsequent tests, a rod with "Roseball" joints at each end, giving rotational freedom about the major and minor axes, was attached to this plate and also to a channel section which was bolted to the strong floor of the testing laboratory. This lateral restraint prevents vertical movement of this flange, whilst permitting free axial and bending displacements in the column, and is used to simulate the effect of a girt in pitched roof portal structures (see Fig. 4.17).

Prior to each test also, the surfaces of the flanges at the quarter and mid-points of the column were polished and two resistance strain gauges were positioned 5 mm from the edge of

the flange plate on both the tension and compression faces.

The column was now bolted horizontally into the test rig by connecting the end plates of the column to the bottom plate of the knife edge assembly. Testing columns horizontally enables columns of various length to be used by a simple alteration of the rig, as well as simplifying the design of the accompanying instrumentation.

Before each test, various small combinations of axial load and bending moment were applied to remove any slip from the rig. This small loading was successively added and removed until corresponding deflection and strain readings of similar load stages showed good reproducibility.

5.5.1 Measurement of minor axis initial imperfections.

Before each specimen was prepared for testing, a measure of the minor axis initial imperfections was made. The bare column was placed with its flanges vertical on a Grade B Surface Table with a guaranteed flatness of 0.08 mm. Two screw jacks were placed at the deep end of the column and one screw jack was placed at the small end of the section, between the Surface Table and the web of the specimen.

These three jacks were then levelled so that they gave identical readings on a vernier height gauge (with an accuracy of 0.01 mm). This vernier height gauge was then used to record the minor axis initial imperfections at each eighth point along the column length. At each station, three gauge readings,

corresponding to the centre and edges of the web, were taken to find the average imperfection at that point. This method will probably give an accuracy of 0.05 mm in the readings. The average values of initial imperfection for the nine columns are summarised in Table 5.1.

5.5.2 Measurement of yield stress and strain hardening properties of the steel plate.

Two thicknesses of steel plate (nominally 6.35 mm and 4.76 mm) have been used in the experimental study. It was initially specified that plates of identical thickness were obtained from the same batch at the manufacturing stage. For the first column of each of the batches tested, an unyielded section was cut from the tested specimen. Three coupons (one from each of the flanges and one from the web) were made from this unyielded section in accordance with the specifications of B.S.18.

A characteristic of this steel is that it possesses two distinct yield points (called the static and dynamic yield stresses). The upper value of yield stress (the dynamic yield stress) arises since it takes more stress to initiate a slip plane than to maintain one after initiation. This upper yield stress value is dependent on the rate of straining adopted for the control tests; as the strain rate tends to zero, the dynamic yield stress tends towards the yield stress value. Consequently, the coupons were tested using a slow rate of straining on a Type 'E' Monsanto Tensometer (0.05 mm/min).

Corresponding values of F_y, SH and PLAT (Fig. 4.2) were

obtained from the resulting load deflection plot, and a 50 mm gauge length extensometer placed over the central portion of the coupon. These values are given in Table 5.1.

5.6 Instrumentation.

An instrumentation frame was made from standard 'Dexion' angle sections and was mounted independently of the test specimen. In the event of the supporting test rig moving, this frame was fixed on to the sandwich plates of the supporting rig so that true readings of the deflections relative to the frame could be recorded. The frame was used to support the various electronic gauges recording the displacements of the section.

5.6.1 Resistance strain gauges.

Two resistance strain gauges (of gauge length 10 mm) were placed at the quarter and half span points of the column, 5 mm from the edges of each flange. These gauges, which compensated for any change of temperature occurring during the duration of the test, were used to indicate the onset of yielding, as well as providing a check on the reproducibility of loading during the initial elastic runs prior to each test.

5.6.2 Load Cells.

Two independent load cells (2000 kN and 45 kN capacity) were used to measure respectively the axial load in the column and the transverse load on the beam at the top end of the column. Before each batch of tests, a check on the calibration of these load cells was made using an Amsler tension-compression test rig with a Grade A rating.

5.6.3 Linear voltage displacement transducers and mechanical gauges.

A series of 18 transducers with maximum strokes of 50 mm, 25 mm and 12.5 mm were attached to the instrument frame and located on the column and end boxes as shown in Fig. 5.2. These transducers were used to measure rotations and displacements at various positions along the column.

All these electronic gauges are connected to a Solartron Data Logger and the corresponding voltage changes are immediately converted into values of displacement, rotation, axial force, bending moment and strains by means of Software written for a PDP11 computer.

Separate Digital Voltmeters (DVMs) are connected to each of the load cells to enable a direct value of the load to be known at any load stage. A further DVM is used to monitor any fluctuations in supply voltage to the electronic gauges. These DVMs are also used to ensure that the applied loading is remaining steady prior to a scan of the transducers and strain gauges.

In addition to these electronic gauges, several mechanical gauges are used to align the column and serve as a check on the imminence of collapse. A 50 mm inclinometer is used initially to level the end boxes, and also to record the minor axis rotations of the column during testing. Also, several standard dial gauges are used at the centre of the column to ensure that the column deflections were steady prior to scanning the various electronic gauges.

5.7 Test results.

The behaviour of the specimens under test will now be explained in groups corresponding to the three batches of equal length. Typical

beam load versus end-rotation curves and beam-load versus major axis displacement curves are given in Figs. 5.4 - 5.13.

Series 1 - Columns TC1, TC2 and TC3.

The first column, TC1, was initially subject to a fixed axial load of 100 kN. The beam loading was then applied in increments of 4 kN, until the strain gauges indicated the onset of yielding at $M/M_{PT} = 0.59$ (where M_{PT} is the reduced plastic moment at the head of the column under axial load). The beam load is then increased in increments of 2 kN until collapse occurs.

The efficient nature of the tapered column with respect to carrying major axis bending moments was shown in this test. 91% of the reduced plastic moment at the head of the column was carried before collapse occurred. Considering the situation at the centre of the column, this means that 72% of the reduced plastic moment is being carried here, assuming that the primary bending moment is half the value at the head of the column.

Ultimate failure occurs by lateral torsional buckling (see Fig. 5.14(a)). The failure mode shows that the column flanges remain straight for about 10% of the length at each end of the column, indicating that the boxes give both torsional and warping restraint to the ends of the column. For this test, the onset of failure was quite sudden. Only for the last two load increments did the measured deflections and rotations show any marked non-linearity (see Fig. 5.4(a)). The flaking and cracking of the resin indicated that plasticity was confined to about 10% of the column length, centred about the mid-length of the column.

The second and third columns in this series (TC2 and TC3) were each given an initial axial load of 200 kN, applied in four increments of 50 kN. The beam loading was then applied in 4 kN increments until yielding occurred at respectively M/M_{PT} = 0.42, 0.41 in the two columns. Subsequent beam loading was applied in 2 kN and 1 kN increments until collapse occurred.

The failure mode for both these columns was identical, occurring by lateral buckling (see Fig. 5.14(b) and (c)). The onset of the buckling failure is indicated by a more progressive non-linearity in deflection and rotations than in the first test (see Figs. 5.5 and 5.6(a)).

The ratios M/M_{PT} at failure for these two tests are respectively 0.69 and 0.70, showing that under increased axial load, tapered columns are far less efficient carriers of bending moments. The resulting pattern of fracture in the brittle coating of resin indicates that yielding has extended approximately over the middle two-thirds of the column length.

Series 2 - Columns TC4, TC5 and TC6.

The second series of tests was conducted on the columns of the shorter length (nominally 1900 mm). The first column in the series (TC4) has the smallest end depth and was given a fixed axial load of 200 kN. The beam load was then applied in 2 kN increments until collapse occurred. (Fig. 5.7). Failure occurred due to lateral buckling when the applied moment ratio at the column head, M/M_{PT} was 0.64. The yielded zones at failure are quite extensive with considerable tensile and compressive regions over most of the column

length (see Figs. 5.14(d) and (i)).

The second column in the series (TC5) had the largest top end depth and therefore would be expected to carry the largest applied bending moment. Unfortunately the results proved to be disappointing. The expected load path was again one of a fixed axial load of 200 kN and subsequent increase of bending moment to cause failure.

However, on application of the axial load, an elastic stability failure occurred with the axial load having reached approximately 175 kN, prior to any bending moment being applied. This value represents failure at approximately 56% of the Euler buckling load. The reason for this premature failure is thought to be due to the presence of large imperfections about the minor axis. With reference to Table 5.1, the maximum imperfection in the column is 5.55 mm, or approximately three times the usual tolerance specified in B.S.449 (L/960) for rolled sections. However, the maximum imperfection present in column TC4 (1.45 mm) is well within this tolerance.

The final column in this series (TC6) had a similar initial imperfection pattern to TC5, and was therefore given a fixed axial load of 100 kN. The beam load was then applied in small increments of 1 kN. Failure occurs due to lateral-torsional buckling, in a similar manner to the first column of the last series (TC1) with the moment ratio at the head of the column, $M/M_{PT} = 0.82$. Failure is again quite sudden, with considerable deviation from linearity in the displacements occurring only during application of the last two beam load increments (see Figs. 5.8).

Fig. 5.14(e) shows that the tension flange remains comparatively straight in comparison to the compression flange which has developed a marked curved shape at collapse. This flange has extensive compressive yielding on its top face (indicated by the flaking off of the resin) and small regions of tension yielding on the bottom face (indicated by cracking of the resin on the bottom of the flange).

Series 3 - Columns TC7, TC8 and TC9 (see Figs. 5.9 - 5.11)

The three columns tested in this series were duplicates of tests TC1, TC2 and TC3 with an elastic restraint provided at the centre of the column to prevent lateral movement of one of the flanges.

Columns TC7 and TC8 had this restraint on the tension flange (the flange usually restrained in practice) and were again initially subjected to an axial load of 200 kN. The pattern of initial imperfections for both these columns was similar to their counterpart in the earlier tests (TC2 and TC3).

As the bending moment on the column is increased, the compression flange begins to deflect vertically unhindered (i.e. out of plane), whilst the tension flange is prevented from moving. Collapse finally occurs in a torsional mode due to the relative displacements of the two flanges. Just prior to failure, the restrained tension flange rotates about the web causing a sudden release in strain energy and a corresponding drop off in the applied load, (see Figs. 5.14 (f) and (g) and Fig. 5.17).

The experimental failure moments for both these two columns, however, are not significantly greater than the corresponding ultimate moments for the unrestrained tests. For column TC7, the failure moment ratio, M/M_{PT} is 0.73 (c.f. for TC2, M/M_{PT} = 0.69) and for TC8 this ratio is 0.71 (c.f. 0.70 for TC3)

Since buckling of columns is generally governed by compressive behaviour, the effect of restraining the tension flange is to change the failure from a lateral to a torsional mode (see Figs. 5.9 and 5.10).

Consequently for the final test (TC9), the lateral restraint was placed on the compression rather than the tension flange. This will simulate the provision of knee bracing from the tensile to compressive faces. The effect of this restraint is to resist any initiation of buckling in the compression flange. As a result, the section carries considerably more moment than an unrestrained column. This column is initially subject to an axial load of 200 kN. This value of axial load is greater than the value of 100 kN used in the counterpart test (TC1) since the expected failure moment under this condition may have exceeded the limits of the testing rig. The resulting failure moment ratio at the head of the column, M/M_{PT} is 0.82 as compared to 0.91 for the unrestrained case. This failure moment would however constitute a considerable increase in moment capacity compared to the unrestrained columns with an axial load of 200 kN (columns TC2 and TC3 have ultimate moment ratios of 0.67 and 0.70 respectively).

Subsequently, theoretical analyses using the biaxial computer

analysis were performed on this column assuming a fixed axial load of 200 kN and separately both zero and full lateral restraint at the centre of the column. The results indicated that the analysis assuming full restraint gives a considerably higher failure moment than for the unrestrained column, and also gives the closer approximation to the actual behaviour of the column under test.

The ultimate failure mode is caused by sudden buckling of the restraint giving rise to lateral buckling of the column. The loss of restraint caused a sudden rapid increase in minor axis deflections at the centre of the column and subsequent failure (see Fig. 5.14(h)). It is thought however that actual failure of the column itself was imminent at this stage. The deflections along the column length were becoming markedly non-linear and suggested that failure would probably have occurred in a double curvature type mode, with zero vertical deflection about the central restraint. However the buckling of this restraint gave a sudden change to the lateral buckling modes of earlier tests.

5.8 General observations.

The characteristic failure of the majority of the columns tested is that they have a 'soft' collapse mode; application of further loads causes a steady increase in deflections and rotations rather than a sudden release of stored energy. All the columns tested violate the provisions given by Horne[13] to prevent local buckling in the web. However none of the tests showed any sign of a local buckling failure. It should be noted, nevertheless, that the nature of the end boxes is to restrain part of the column length against this mode

of failure. Also the effect of welding the columns on one side only at the web-flange junction does not appear to be detrimental to the effectiveness of the connection in resisting high shear forces and bending moments.

5.8.1 Summary of conclusions.

1. Tapered columns in pin-ended portal frames are very efficient carriers of primary bending moment. This efficiency reduces under increasing values of axial load.

2. Unrestrained tapered columns with low values of applied axial load ($P/P_E < 0.4$) will ultimately fail on the application of bending moment in a lateral-torsional buckling mode.

3. Unrestrained columns with higher values of axial load ($P/P_E > 0.5$) will ultimately fail in a lateral buckling mode on the application of bending moment.

4. Large minor axis imperfections induced by welding can cause significant reductions in the carrying capacity of tapered columns under axial load.

5. Although Horne's 'D/t' ratios to avoid web buckling will generally be exceeded in tapered columns, local web buckling does not occur.

6. Using weld passes on one side only of a web-flange junction provides adequate continuity between the plates in resisting shear forces and bending moments.

7. Provision of lateral restraints on the tension flange of a tapered

column does not appear to significantly increase the ultimate carrying capacity of the column.

8. The placing of a lateral restraint on the compression flange of a tapered column does appear to give a significant increase in the ultimate carrying capacity of the column.

5.9 Use of the elastic-plastic analysis program in analysing tapered columns.

The elastic-plastic computer program of Chapter 4 has been used to analyse the series of experimentally tested tapered columns. In order to theoretically investigate these columns, several further assumptions are needed in addition to the ones used previously. These are:-

5.9.1 Warping and twisting at the column ends.

The effect of the end plates and the end box system is assumed to give full restraint against warping and twisting at the ends of the column. The experimental tests confirmed that the ends exert considerable restraint to the column at the ends. In the ultimate deformed shapes (see Figs. 5.14), the flanges remain straight for about 10% of the column length, and then adopt the typical curved shape associated with the buckling mode.

5.9.2 Allowance for member taper.

The uniform taper of the column is converted into a series of stepped reductions by splitting the column into 30 element lengths, each element having a uniform depth throughout. The depth of each element is given by the corresponding depth of the actual column at the centre of this element (Fig. 5.2).

5.9.3 Values of yield stress and strain hardening properties.

The coupon tests on the steel specimens show that there is very little variation in the yield stress (F_y) between each coupon. A characteristic of the steel used is that it possesses a very short plateau region after yielding prior to the onset of strain hardening. The values of this plateau length and the strain hardening modulus (PLAT and SH) are found to vary between each set of coupons. For each batch of three tests, therefore, average values of PLAT and SH have been taken from the appropriate coupon results of Table 5.1.

5.9.4 Initial deflections.

The average measured initial imperfections about the minor axis are given in Table 5.1. For the theoretical analysis, initial deflected shapes are obtained about this axis by segmenting the member into small element lengths and estimating their angular rotations corresponding to the measured deflected shape. No allowance, however, has been made in the analysis for any initial twists in the specimens.

5.9.5 Residual stresses.

Although no actual experimental determination on the level of residual stresses present in the column has been made, the pattern suggested by Young and Dwight[92] for welded sections has been used. At each weld, there is a region of 'locked-in' tension. The pattern of this tension region is assumed to be rectangular, the width of which is dependent on the heat input to the weld. Simple statics

can then be used to obtain the balancing stresses (which are mainly compressive) occurring elsewhere in the section. The resultant stress pattern adopted in the analysis for the tapered section is shown in Fig. 5.2.

For such a welded section, the width of the tension block, c^1, is given by:

$$c^1 = \frac{0.12(Q/v^1)}{F_y(t_w + 2 \cdot t_f)} \qquad 5.1$$

where Q/v^1 is the energy input per unit length of weld.
From the fabrication specification for the column tested,

Q = rate of heat input to the arc = 12000 watts.

v^1 = rate of travel of the weld pass = 1/48 m/s.

The stress pattern is then used to obtain average values of initial stress occurring in each of the sub-divided elements of the moment curvature procedure.

5.9.6 Effect of lateral restraints.

The elastic-plastic computer analysis cannot deal with restraints applied to only one flange of the column. Consequently, for each of the three restrained columns, two analyses have been performed. The first analysis assuming zero lateral restraint, and the second full lateral restraint at the centre of the column.

5.10 Discussion of results.

A table of ultimate load values and corresponding major and minor axis rotations and major axis deflections for both the experimental and theoretical analyses are given in Table 5.2 and Figs. 5.4 - 5.13. The assumptions previously cited together with

the initial assumptions of Chapter 4 have been used to obtain ultimate load values for the columns.

Unrestrained Columns - Series 1 and 2.

General ultimate load agreement between the two sets of results is good, with the theoretical analysis usually giving slightly higher ultimate load values than the experimental values. It would perhaps be expected that the opposite should be true with the experimental ultimate load values being the greater. Whilst the column is being loaded up, the stiffness in the knife edge assembly and movement of the loading beam will restrain the column. On the other hand, however, the effect of warping strains on yielding has been neglected in assessing the reduced stiffness properties of the member's elements. At a particular load level, therefore, the extent of yielding is underestimated and a high assessment of ultimate load will result.

The trend of the curves of major axis deflections show that the theoretical analysis usually yields the greater values. The adoption of an assumed level of residual stress can cause significant differences in the theoretical values of these rotations and displacements. In Fig. 5.4(a), two theoretical curves are plotted for the top end rotation of column TC1 with and without residual stresses. It can be seen that the theoretical curve neglecting these stresses underestimates the end rotations whilst predicting an even higher failure load when compared to the analysis including residual stresses. The residual stress pattern used by Young and Dwight[92] will therefore probably overemphasise the level of initial

stresses that are actually present in the section. The analysis which includes residual stresses would therefore be expected to indicate premature yielding in the member, and thus predict a lower failure load. This is found not to be the case. However, slight eccentricity in the loading system may result in a reduced experimental failure load.

It is interesting to note that the experimental end rotations about the minor axis are generally greater than the theoretical values whilst the reverse is true about the major axis. The contrasting effects of a too severe residual stress pattern combined with slight eccentricity in the loading system could account for these discrepancies, whilst still giving a good estimate of failure in the theoretical analysis.

Considering the schematic representation of the end loading system in Fig. 5.3, a cumulation of errors between the ram of the jack and the head of the column can give an eccentricity of loading about both axes.

An assessment of these errors about one axis will now be made.

1. Point A.

The jack and load cell are located centrally on the back plate of the knife edge assembly by means of a location ring which is bolted to this back plate.

Possible error in the central location of the jack and load cell is estimated to be 0.25 mm (e_A).

2. Point B.

The knife edges sit in the curved groove of the middle plate of the knife edge assembly. As the knife edge rotates, it may be

possible for the knife edge to 'ride up' the groove. The estimated movement is 0.50 mm (e_B).

3. Point C.

The end plate of the column is connected to the bottom plate of the knife edge assembly by bolts passing through dowelled holes.

The possible error in alignment of these holes, e_C = 0.25 mm.

4. Point D.

The column is symmetrically welded to its end plate. Possible errors in alignment may occur due to the centre line of the column not coinciding with the centre line of the end plate. The maximum error, e_D is 0.5 mm.

The total possible eccentricity in loading occurring due to misalignment of the axial load through the centre of the column,

$e = e_A + e_B + e_C + e_D = \pm 1.5$ mm.

Clearly, the effect of any eccentricity in the rig will be greater about the minor axis than about the major axis. With reference to Fig. 5.12, however, the effect of any eccentricity is probably masked in column TC6 due to the high level of initial imperfection present. Commencing at low values of applied bending moment, there is a progressive non-linear increase in these rotations until failure occurs. In contrast, columns TC1 and TC3 (both having smaller imperfections) show a much smaller change in the minor axis rotations until failure is imminent.

Restrained columns - Series 3.

The moment versus major axis rotations and major axis deflections

curves for columns TC8 and TC9 are shown in Figs. 5.10 and 5.11, assuming a full lateral restraint at the column centre for the theoretical analysis. The theoretical analysis for column TC8 is found to considerably overestimate the actual failure load, and thus indicates that the tension flange restraint used did not exert much effect. On the other hand, for column TC9 the load and deflection agreement is far better. Although the theoretical analysis again overestimates the failure moment, this is probably due to the sudden buckling of the restraint during the actual test.

A further indication of the benefit of providing a restraint on the compression flange can be seen in Fig. 5.13 where minor axis rotation curves are plotted for columns TC8 and TC9. The minor axis rotations for TC9 show a much less rapid rise than column TC8, showing that minor axis buckling is being restrained.

5.11 Comparison of design methods with the experimental results.

Several current methods of steel column design have been adapted to give an estimate of the failure loads of the tested columns. The methods used are the elastic design procedure of Horne for both laterally restrained and unrestrained columns and the plastic design methods of Wood and Young.

The results are summarised in Table 5.3, together with the corresponding experimental values. Column (3) of this table contains the estimated first yield moments obtained from the strain gauge readings.

5.11.1 Horne's $P_x P_y$ method.

i) unrestrained columns.

Horne's method of elastic design[11] for pin-ended columns prevents the yield stress being exceeded in the extreme fibres anywhere in the column length. Because of the magnification of lateral displacements due to instability effects, the maximum extreme fibre stress may occur away from the ends of the column.

The check on the maximum stress takes the form

$$P/A + N_x \cdot M_x/Z_x + f_o \leq F_y \qquad 5.2$$

where A, Z_x are respectively the area and elastic modulus of the section

N_x is a magnification factor allowing for the excess of stress due to flexure about the minor axis in the presence of the axial load, P.

f_o is the bending stress about the minor axis due to initial imperfections.

M_x is the equivalent uniform moment.

To obtain a value for f_o, an initial imperfection in the form of a sine wave, with maximum amplitude ε, is assumed corresponding to the rolling tolerance of L/960. This value is

$$\varepsilon = 0.0015\ L \cdot r_y/a_y \qquad 5.3$$

where a_y is half the flange breadth

r_y is the minor axis radius of gyration.

The maximum value of stress about the minor axis, f_o, allowing for warping restraint is approximately given by:

$$f_o = \frac{\epsilon\, a_y}{(1-\gamma_y) r_y^2} \left\{ \frac{P}{A} + \frac{M_x^2 / Z_x^2 + \pi^2 E (r_y/L)^2 M_x / Z_x}{\beta} \right\} \quad 5.4$$

where $\beta = T + 2\pi^2 E (r_y/L)^2 - 2 \cdot P/A$

$\gamma_y = P(L/r_y)^2/(\pi^2 EA) + M_x^2 (L/r_y)^2/(\pi^2 \cdot E \cdot Z_x^2 \beta)$

$T = A.G.J.a_x^2/I_x^2$

a_x is half the section depth.

This value of f_o can then be substituted into the inequality of Eqn. 5.2 to give a maximum value of M_x for a given section subject to a fixed axial load.

ii) Laterally restrained columns.

The limiting stress check for the restrained column case has a similar form to Eqn. 5.2. However the value of minor axis stress is altered due to the restraint about one of the flanges. Horne and Ajmani[93] have shown that this stress is given approximately by:-

$$f_o = \frac{30}{\eta} \frac{P/A + 0.65\, M_x/Z_x}{\beta} \quad 5.5$$

where $\beta = 30\,000/(D/t_f)^2 + 200/\eta^2 - P/A - 0.65\, M_x/Z_x$

$\eta = L/(100 \cdot r_y)$

This value of f_o is then substituted into Eqn. 5.2 to obtain a value of M_x.

iii) Application to tapered columns.

For both the restrained and unrestrained cases, Eqn. 5.2 contains terms such as P, M_x and L, and the section properties r_y, Z_x, A, D/t_f and T. For a tapered member, these section properties will

vary along the length of the member. However the tapered columns used in the experimental study are designed to resist primary bending moment at the head, with the base of the column (having zero moment) only resisting axial load. The experiments show that the bending moment carried by the column is dependent on the section at the head of the column. For instance, column TC3 gives an increase of failure moment over column TC2, both columns having the same axial load. Consequently values of Z_x at the head of the column and A at the base of the column have been used in Eqn. 5.2. Also the adoption of a high value of D/t_f and a low value of T will result in a conservative estimate of f_o. Thus values corresponding to the section at the head and base respectively have been used. Finally, the section property, r_y, is found not to change very much in a tapered column since I_{yy} is approximately constant, and the flange areas are constant throughout; hence the value of r_y at the column base has been used.

Substitution of these values into Eqn. 5.2 together with the constant axial load and length of the column will give a polynomial equation for M_x. This polynomial is of degree three for the unrestrained case and of degree two for the restrained case.

These equations are:-

A) Restrained.

$$0{\cdot}65\ f_x^2 + f_x(-\ 0{\cdot}65\ F_y - 0{\cdot}65\ A2 - 0{\cdot}65{\cdot}B2{\cdot}P/A) + (B2\ F_y - A2\ P/A - B2{\cdot}P/A) = 0 \qquad 5.6$$

B) Unrestrained.

$$f_x^3(10^4{\cdot}\eta^2)+f_x^2(10^4{\cdot}\eta^2{\cdot}P/A-3{\cdot}0{\cdot}10^5{\cdot}\eta{\cdot}\delta-10^4{\cdot}\eta^2{\cdot}F_y)+f_x(2{\cdot}10^6{\cdot}A4{\cdot}(1-P{\cdot}\eta^2/(200A)) - 6{\cdot}10^7{\cdot}\delta/\eta)+(2{\cdot}10^6{\cdot}A4(1-P\eta^2/(200{\cdot}A){\cdot}(F_y-P/A)-3{\cdot}10^5{\cdot}\eta{\cdot}\delta{\cdot}A4{\cdot}P/A) = 0 \qquad 5.7$$

where $\eta = L/(100\ r_y)$; $A2 = 30/\eta$; $B2 = 30\ 000/(D/t_f)^2 + 200/\eta^2 - P/A$;

$A4 = A \cdot G \cdot J \cdot D^2/(4 \cdot I_x^2) + 400/\eta^2 - 2P/A$;

δ = ratio of maximum imperfection in the column to the value (L/960) used by Horne.

Solutions of these equations to find the lowest real root will give a value for the equivalent uniform bending stress, f_x, in the column. Multiplication of this stress by the section modulus of the section gives the equivalent uniform moment in the column. The actual moment at the head of the column can then be obtained from Horne's equivalent uniform moment chart.

If m' is the equivalent moment reduction factor, the moment at the head of the column is given by:

$$M_x = f_x Z_x/m' \qquad 5.8$$

The results are summarised in Columns (4), (5), (6) and (7) of Table 5.3. For columns TC1 - TC6, the results are obtained from Eqn. 5.7. Similarly for columns TC7 - TC9, the results are obtained from the above quadratic equation.

Columns (4) and (5) of Table 5.3 have been obtained by assuming that the area and moment of inertia values in the above equations are based on the properties at the bottom and top of the real column respectively. These two sets of values differ however in the value of maximum minor axis imperfection used ; Column (4) corresponds to the actual measured imperfection in the column and Column (5) to the standard value (L/960) adopted by Horne.

A further two series of values (Columns (6) and (7) of Table 5.3)

are presented corresponding to area and inertias at the centre of the column for both sets of initial imperfections.

iv) Discussion of results.

Horne's method of design is based on a limiting stress approach. Consequently comparison between the design method and the actual tests is based on the attainment of first yield in the tests. Column (3) of Table 5.3 is a series of estimated first yield moments obtained from strain gauge readings recorded during testing and by cracking of the brittle lacquer coating.

The effect of assuming section properties at the centre of the column as opposed to top and bottom values is to considerably underestimate the moment capacity of the column (Columns (6) and (7) give considerably lower moment values than Columns (4) and (5) respectively of Table 5.3). In fact, use of 'top and bottom' section properties and the real imperfection values (Column (4)) generally give quite good agreement with the experimental values of Column (3). This indicates that the use of a taper should give a considerable increase in moment capacity.

Comparison of Columns (3) and (4) show that the design method is more conservative as the axial load is increased due to the magnified effect of the minor axis imperfections. Hence the predicted first yield moment for TC1 is higher than the experimental first yield value. For columns TC2 and TC3, however, the design moment is lower than the experimental first yield value. For column TC4, however, the actual imperfection present was smaller than the standard rolling tolerance, and hence the small minor axis stresses cause the predicted first yield value to exceed the experimental value.

It is interesting to note that the design method does not permit a moment to be applied to column TC5, since the high level of imperfection present causes the yield stress to be reached under axial load only.

5.11.2 Wood's plastic design method.

This design method[18] gives an assessment of the reduced stiffness of a column due to the combined effects of plasticity and instability.

The collapse load of the column, P, is defined as

$$P = C\, R_x\, P_E \qquad 5.9$$

where C is the ratio of the critical axial load to the Euler load (P_E)

R_x is a reduction factor allowing for partial plasticity.

The maximum allowable moment, M_{ax}, to prevent excessive plasticity is given by:-

$$M_{ax} = 1.08\, Z_x\, F_y \cdot (1 - F) \qquad 5.10$$

M_{ax} represents the moment causing one flange of the column to become completely plastic

F is the ratio of the axial load to the squash load.

A value of the reduction factor, R_x, is then obtained from:

$$R_x = \left(1 - \frac{M_{max}}{M_{ax}}\,(0.4 - 0.2\,m)\right)(1 - F^2) \qquad 5.11$$

m is the ratio of the top end moment to the bottom end moment

M_{max} is the maximum design moment in the column, and must always be less than, or equal to, M_{ax}.

For a pin-ended column with moment applied at one end only

$$C = 1 \qquad 5.12a$$

$$m = 0 \qquad 5.12b$$

Combination of Eqns. 5.9 - 5.12 together with the known values of P and P_E will give a value of the maximum allowable design moment, M_{max}. In comparison to Horne's method, however, Wood's values of P and M_{max} relate to the ultimate condition of the column at collapse, rather than the attainment of first yield in the column.

The value of squash load used to obtain F is based on the dimension at the base of the column, and the value of Z_x is based on the dimensions at the head of the column as before. In cases where M_{max} exceeds M_{ax}, the value of M_{ax} has been taken as the ultimate moment. In such cases, the design method would have permitted a greater axial load in the column. For the final three restrained columns (TC7 - TC9), two series of ultimate moments have been found; the first assuming zero restraint and the second full restraint at the centre of the column. This second result is obtained by splitting the column into two halves and assuming that $m = -0.5$ is used in Eqn. 5.11 to obtain the ultimate moment corresponding to half the applied moment at the centre of the column.

The ultimate moments (Column (8) of Table 5.3) generally give similar failure moments to Horne's first yield values (Column (5)) using his standard imperfection pattern. Although Wood does not directly specify any initial imperfection, the $1-F^2$ reduction factor of Eqn. 5.11 does give allowance for this. A further effect of this factor is that it gives closer values to the tests than Horne's method at higher values of axial load. However, it predicts a substantial moment for TC5, which due to the high level of residual stresses present

carried zero moment. Hence for cases of high initial imperfections, the $1-F^2$ factor is not adequate.

The effect of splitting the column into two halves is to predict a substantially higher failure moment as compared to the unrestrained case. Indeed, the design moments for the two columns with the tension flange restraint (TC7 and TC8) are unconservative whereas the design moment for the column with the compression flange restraint is conservative when compared to the experimental values. This is a further indication that restraining the compression flange does constitute a full restraint against lateral buckling.

5.11.3 Young's design method.

Young[22] has extended the earlier method of Horne to allow for a region of biaxial plasticity to occur in pin-ended columns. The actual moment capacity of a column is assumed to be reduced below its fully plastic value due to the combined effects of elastic buckling and plasticity.

The moment capacity of a column is assumed to be given by:-

$$M_x = k_x k_T k_y k_H M_{px}$$

where the 'k' values are reduction factors (< 1) allowing for buckling and plasticity

M_{px} is the full plastic moment of the section.

For each of the unrestrained columns, (TC1 - TC6), values of these coefficients are obtained from Young's charts and substituted into Eqn. 5.13, assuming that the full plastic moment (M_{px}) is based on the dimensions at the column head. The corresponding ultimate moments are given in Column (10) of Table 5.3.

For the low values of axial load (TC1 and TC6), Young's method predicts slightly lower failure moments than Wood's method. However, for the higher values of axial load, Young's method predicts higher design moments than for Wood's method, and gives very close (and sometimes unsafe) agreement with the actual failure moments. This method thus allows additional plasticity to occur in the column than Wood's design under these higher axial load values. Young has again adopted the standard rolling mill tolerance of 'L/960' for initial imperfections in obtaining his reduction coefficients.

5.11.4 General discussion of the design methods.

With reference to column (11) of Table 5.3, the reserve of strength beyond the experimental onset of first yield is between 1.53 and 1.79. The exception to this is column TC6 for which this factor is 2.52. However, the large imperfections present in this column would probably cause premature yielding due to initial application of axial load in the tests, whilst subsequent beam loading would probably not worsen the effects of buckling until larger yielded regions are present in the column.

Comparison of the plastic design methods of Wood and Young show that the estimated failure moments are generally in good agreement with the tests. Unfortunately, the exception to this (TC5) is caused by the high level of imperfections which is not allowed for in the design methods.

It is therefore suggested that a modified version of either Wood or Young's method could be used to give a good assessment of

the capacity of the tapered columns.

For instance, a higher order approximation term to account for initial imperfection could be easily incorporated into Eqn. 5.11 by replacing the $(1 - F^2)$ term by a term which would make allowance for the great reduction in stiffness caused by initial deflections under high values of axial load.

column number	flange width	flange thick	web thick	top end depth	bottom depth	length c/c beam
TC1	101.6	6.37	4.73	299.0	128.0	2622
TC2	102.2	6.39	4.67	250.5	124.5	2619
TC3	102.2	6.35	4.74	276.5	126.0	2620
TC4	89.0	4.68	4.71	204.0	102.5	1903
TC5	88.5	4.65	4.67	328.0	102.0	1900
TC6	89.0	4.70	4.70	252.0	102.0	1903
TC7	102.5	6.36	4.70	249.5	124.0	2619
TC8	102.7	6.36	4.67	277.5	126.0	2619
TC9	101.7	6.40	4.72	300.0	125.0	2619

(a)

all dimensions in mm

column number		F_y	PLAT	SH
TC1	top flange	333	4.0	54.4
	bottom flange	318	1.5	39.7
	web	322	3.9	44.0
TC2	top flange	321	1.6	21.0
	bottom flange	306	1.1	22.7
	web	317	1.2	20.0
TC7	top flange	340	2.0	17.0
	bottom flange	326	1.6	20.3
	web	340	2.0	26.0

F_y in N/mm^2

(b)

	imperfections at points along the column (mm)						
column number	1/8	1/4	3/8	1/2	5/8	6/8	7/8
TC1	1.90	2.65	3.45	4.65	4.30	3.25	1.80
TC2	2.30	3.30	4.25	5.30	5.15	3.85	2.15
TC3	1.35	2.10	3.00	3.65	3.70	2.90	1.50
TC4	0.00	-0.75	-0.85	-0.75	0.10	1.05	1.45
TC5	4.05	5.60	5.50	5.55	5.25	4.75	3.45
TC6	4.95	5.60	5.95	6.40	6.70	6.90	5.60
TC7	1.80	3.45	4.90	6.15	5.80	4.65	3.10
TC8	1.50	2.50	3.40	3.80	4.35	3.50	1.80
TC9	1.95	2.80	3.40	4.20	4.05	3.10	1.75

points measured from large end

(c)

values of (a) section properties
(b) yield stress values
(c) initial imperfections - minor axis

Table 5.1

column number	L/r_y	axial load P(kn)	P/P_e	P/P_s	failure moment M (knm)	M/M_{Po}	theoretical failure moments: zero central restraint	theoretical failure moments: full central restraint
TC1	105.3	100	0.29	0.17	82.8	0.91	84.6	
TC2	105.3	200	0.59	0.34	45.6	0.69	53.3	
TC3	105.3	200	0.59	0.34	53.0	0.70	55.2	
TC4	91.2	200	0.64	0.49	22.3	0.64	25.1	
TC5	91.2	175	0.56	0.43		0.0		
TC6	91.2	100	0.32	0.24	44.6	0.82	46.0	
TC7	105.3	200	0.59	0.34	47.4	0.73	46.0	58.8
TC8	105.3	200	0.59	0.34	53.9	0.71	57.6	69.9
TC9	105.3	200	0.59	0.34	71.6	0.82	63.7	77.2

r_y – minor axis slenderness ratio

P_e – euler load

P_s – squash load based on dimensions at column base

M_{Po} – reduced major axis fully plastic moment at column head under axial load

Table 5.2 experimental and theoretical failure loads for the tapered column tests

column	experiment		design methods							
	failure moment	first yield moment	horne's elastic				wood		young	(2)/(3)
(1)	(2)	(3)	(4)	(5)	(6)	(7)	(8)	(9)	(10) xx	(11)
TC1	82.8	54.0	68.3	79.5	36.2	42.6	72.5 x	–	60.9	1.53
TC2	45.6	27.6	16.5	35.1	10.6	21.6	37.5	–	44.5	1.65
TC3	53.0	31.3	27.1	39.5	15.9	22.7	42.2	–	50.9	1.69
TC4	22.3	12.9	15.5	8.4	11.7	6.8	7.7	–	23.7	1.73
TC5	0	–	–	14.8	–	10.0	28.8	–	30.5	–
TC6	44.6	17.7	23.2	40.0	12.7	23.0	38.8 x	–	36.9	2.52
TC7	47.4	29.1	24.1	41.4	11.7	22.9	37.0	48.1 x	–	1.63
TC8	53.9	36.3	33.2	46.8	16.8	25.4	42.7	56.3 x	–	1.48
TC9	71.6	40.1	37.5	51.8	17.6	25.8	47.9	64.2 x	–	1.79

column (4) real imperfections - top and bottom section properties
column (5) horne's imperfections - top and bottom section properties
column (6) real imperfections - centre section properties
column (7) horne's imperfections centre section properties
column (8) unrestrained member
column (9) member split into two halves i.e. full central restraint
x wood's method allows more axial load
xx D/t based on mid-height dimensions

all moments in knm

Table 5.3 comparison of experiment with column design methods

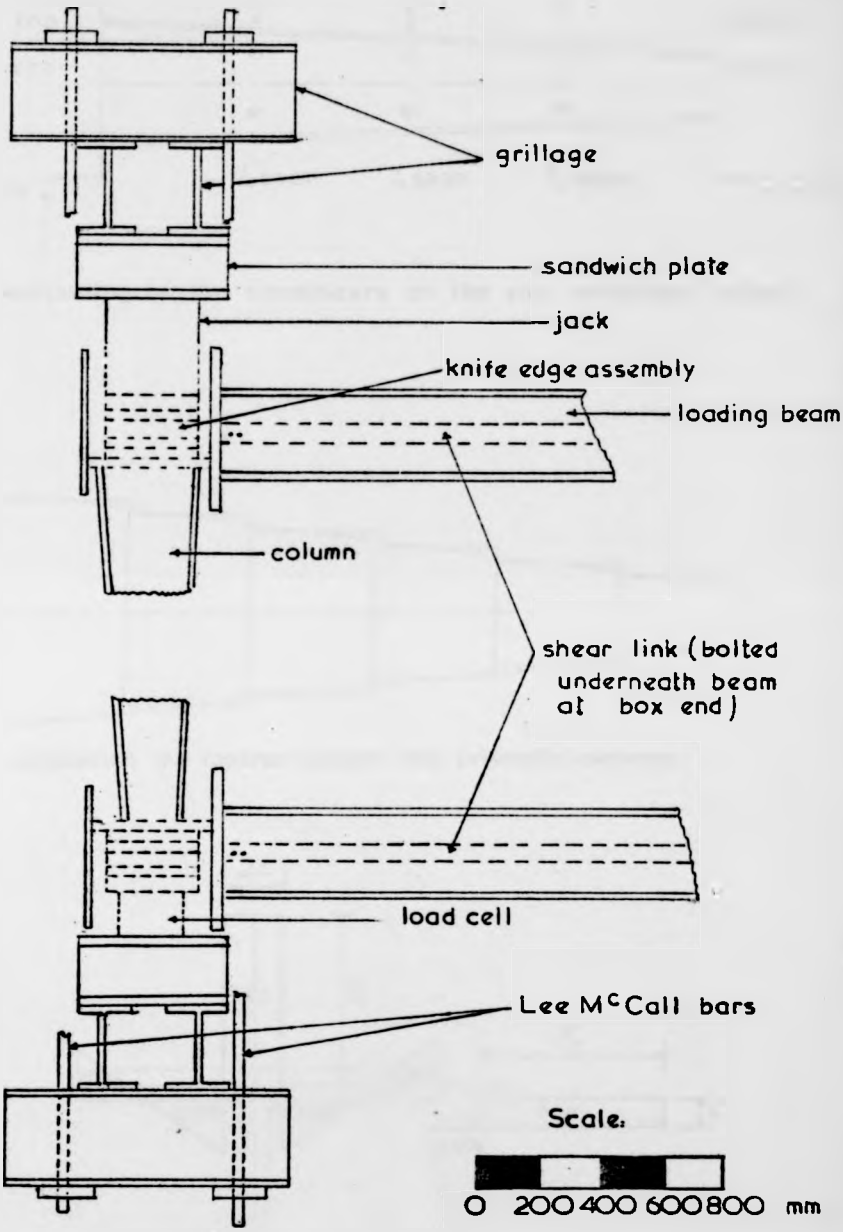

Fig. 5-1 plan of test rig

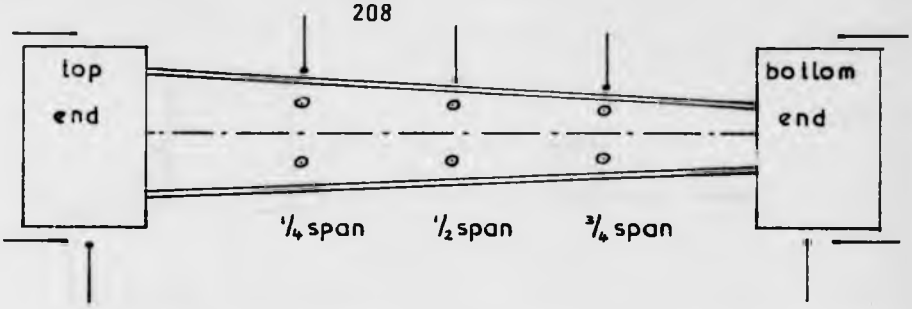

(a) positioning of the transducers on the end boxes and column

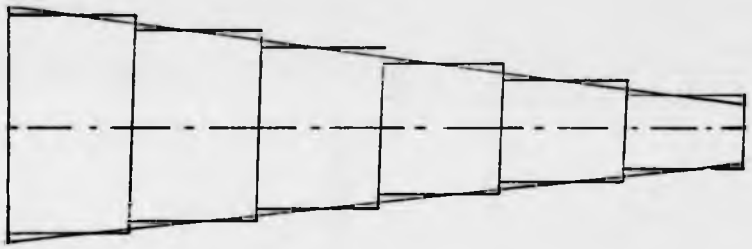

(b) segmenting the tapered column into prismatic elements

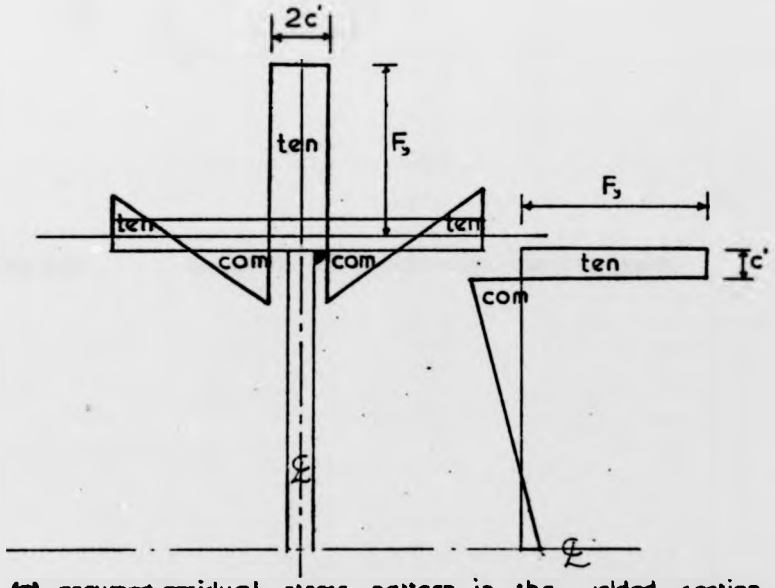

(c) assumed residual stress pattern in the welded section

Fig. 5·2

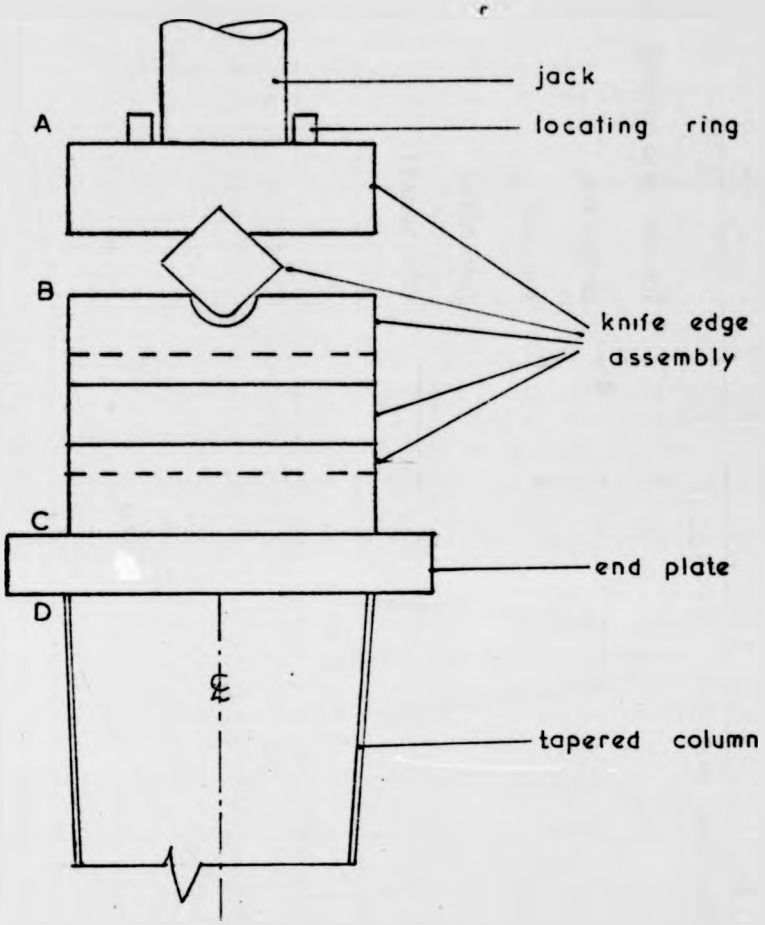

Fig.53 detail of the knife edge arrangement

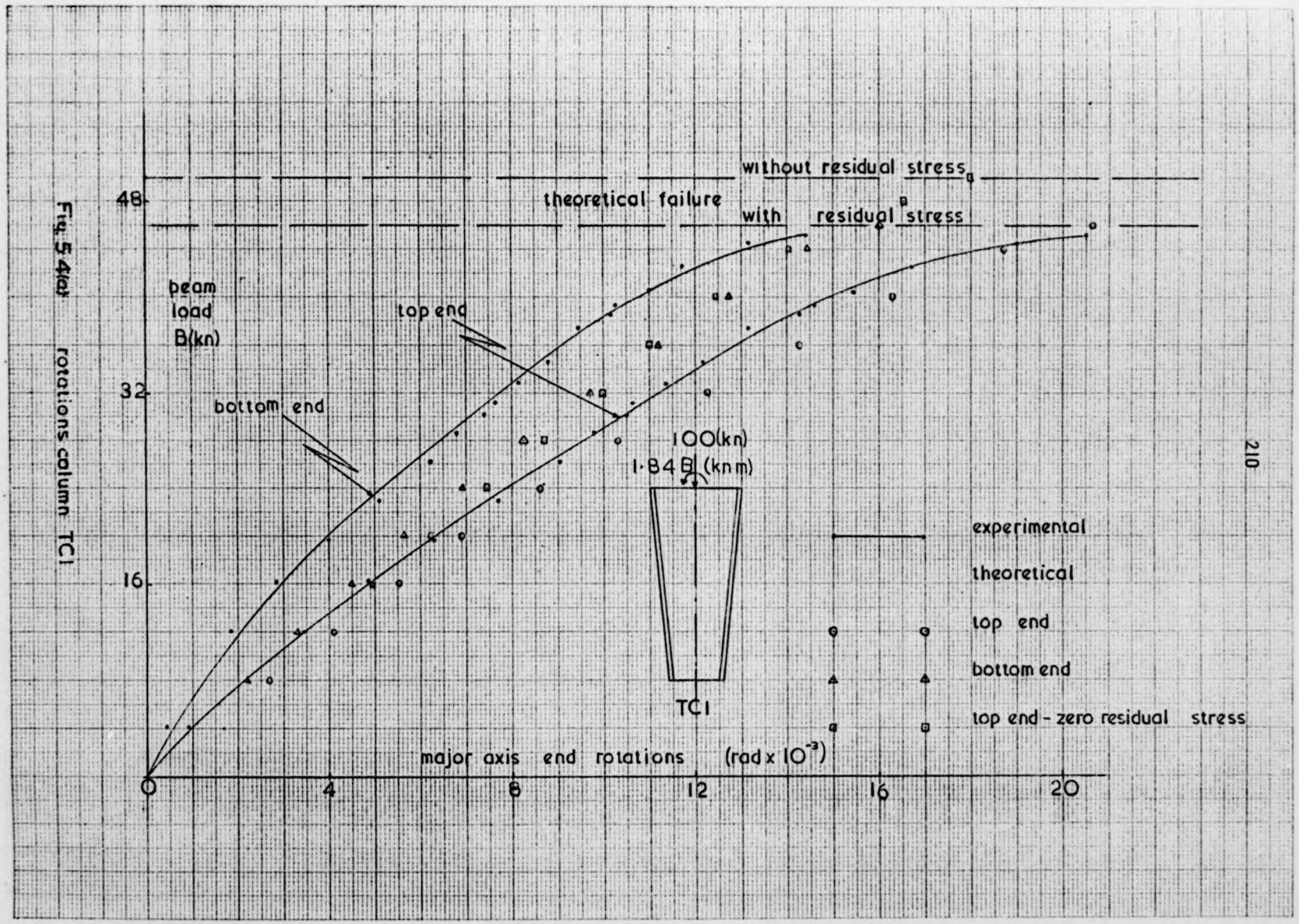

Fig. 5.4(a) rotations column TC1

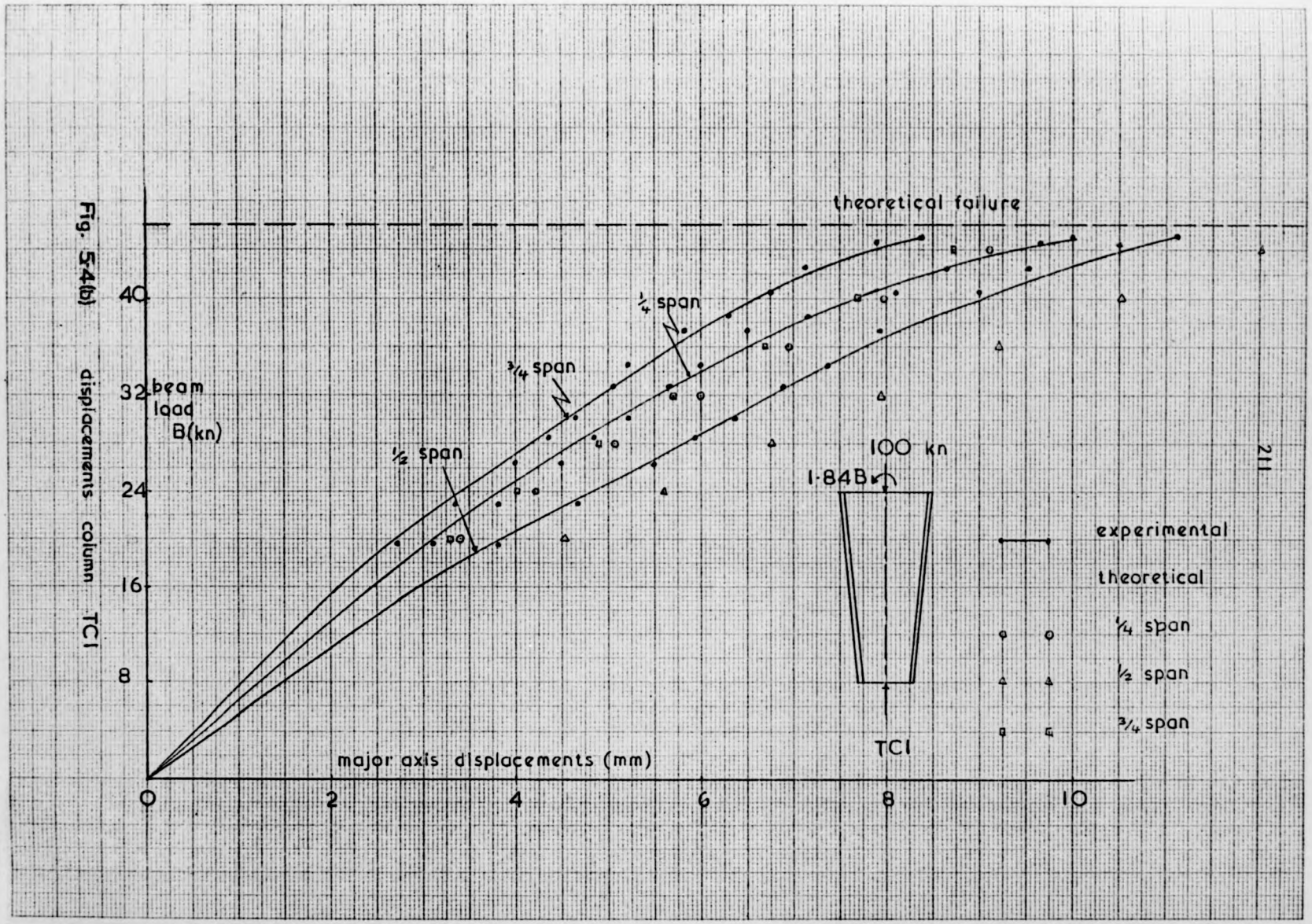

Fig. 5·4(b) displacements column TC1

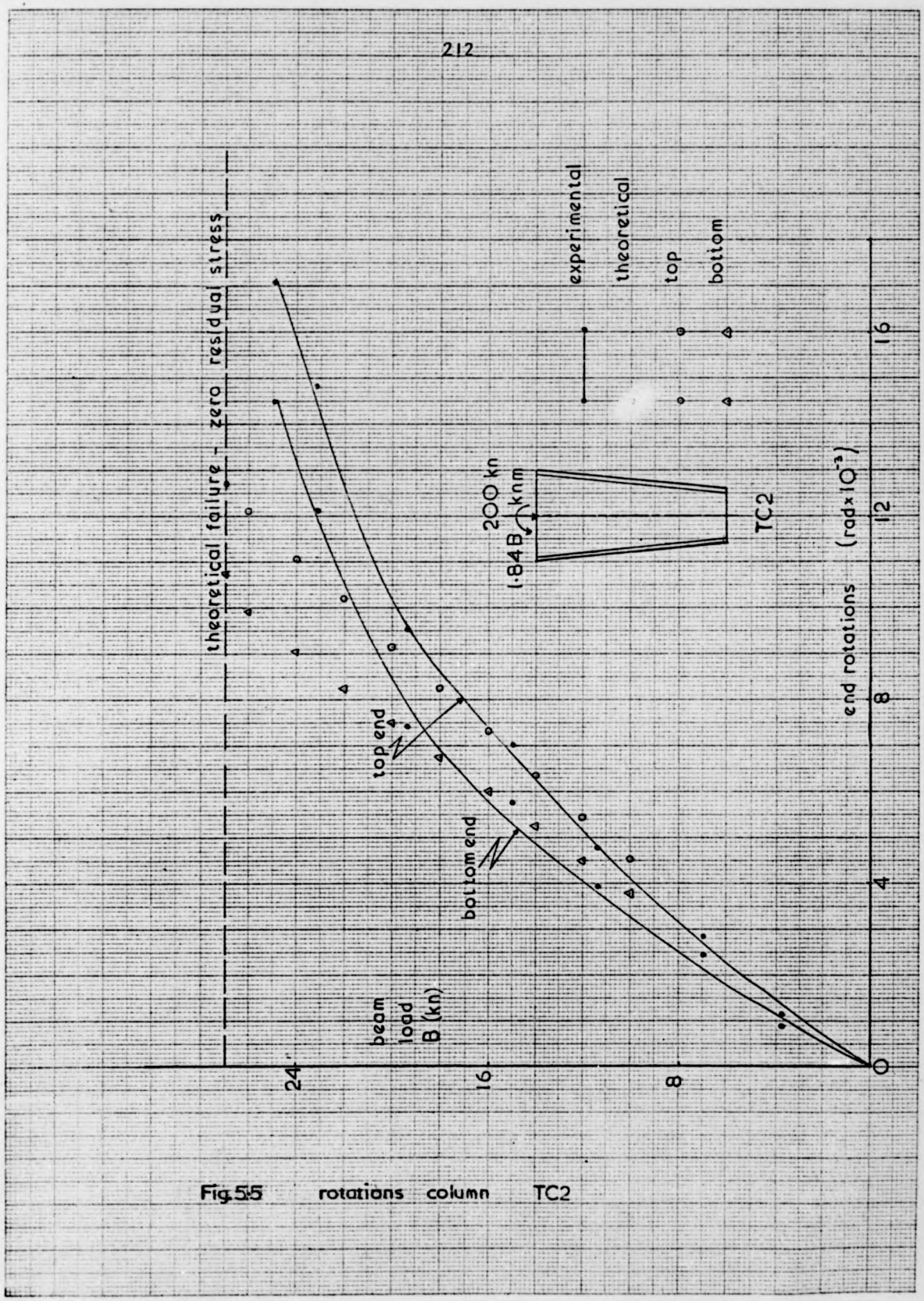

Fig.5.5 rotations column TC2

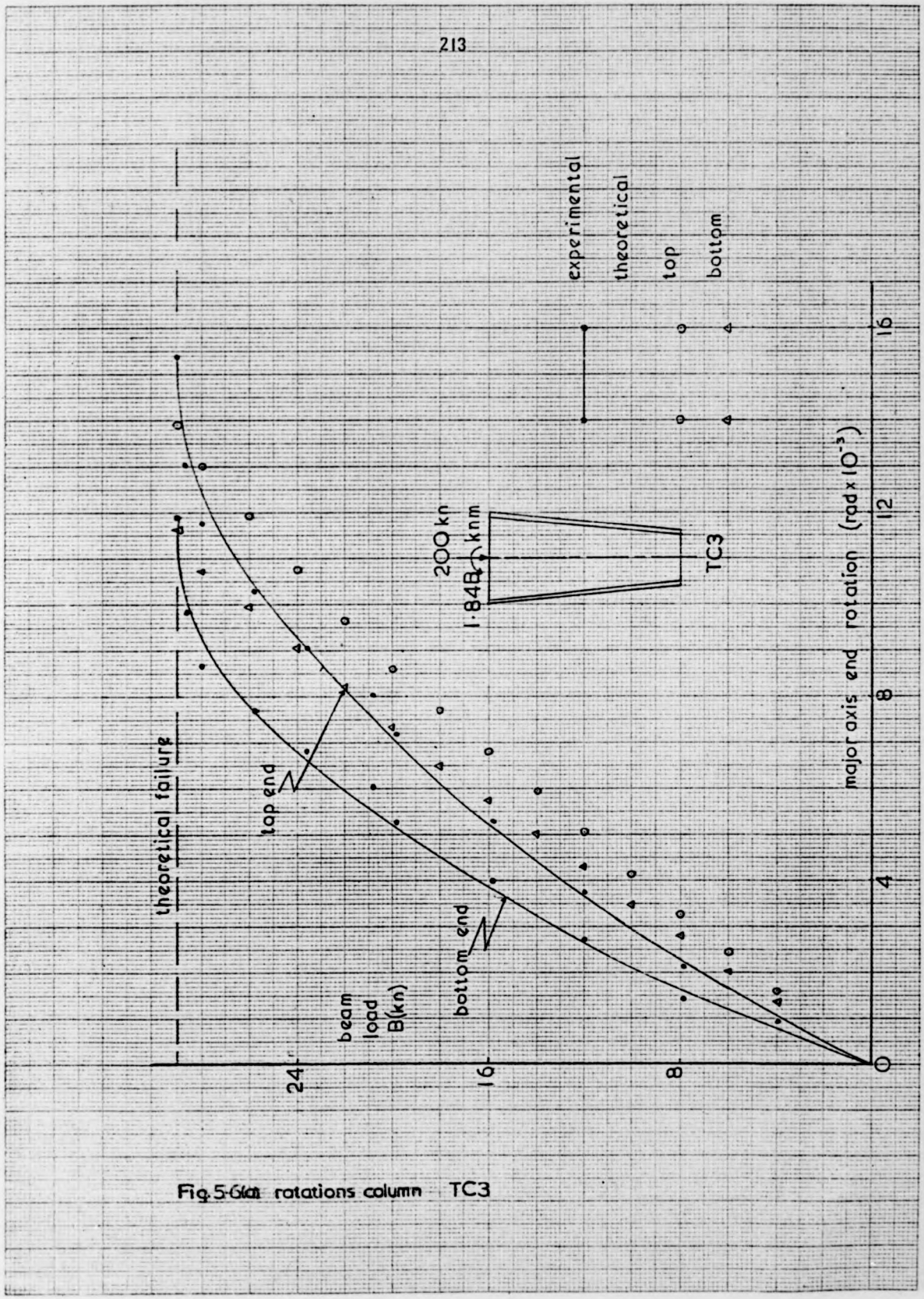

Fig. 5-6(a) rotations column TC3

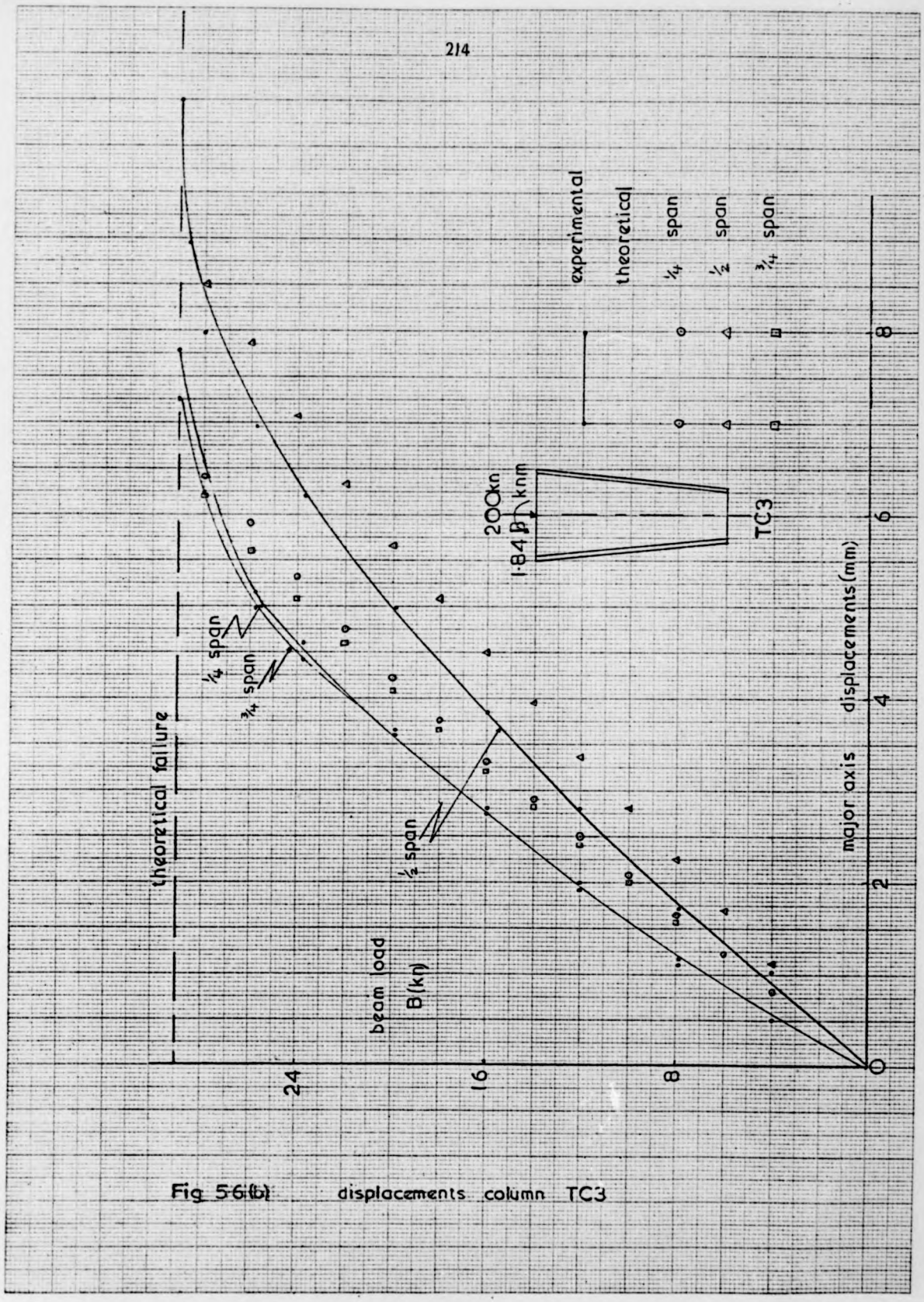

Fig 56(b) displacements column TC3

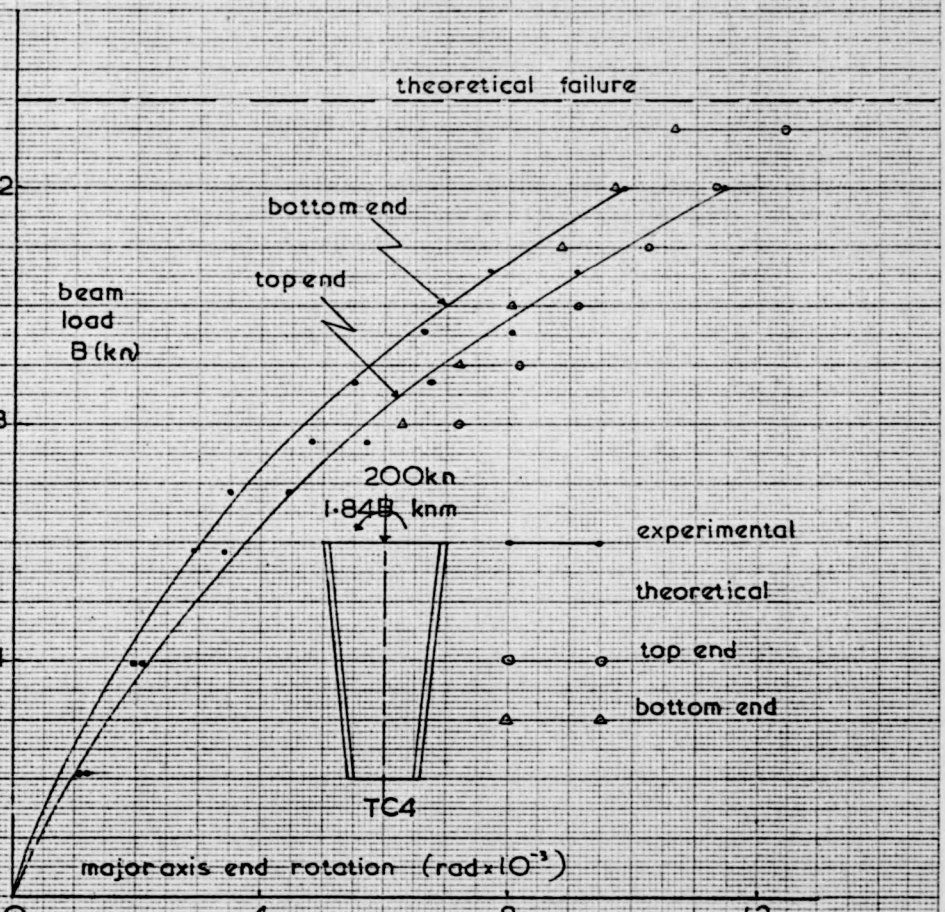

Fig 5·7 rotations column TC4

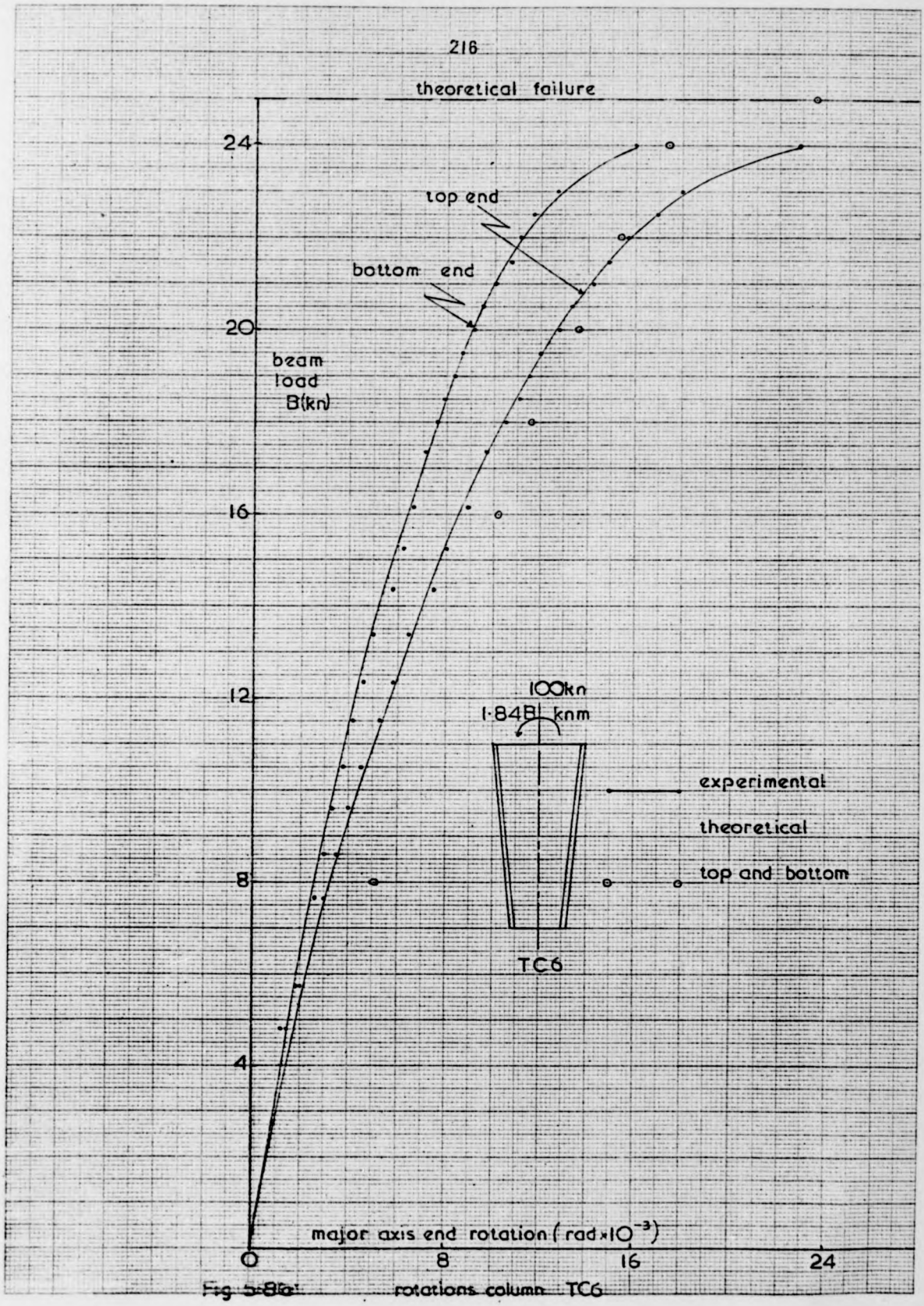

Fig 5·8(a) rotations column TC6

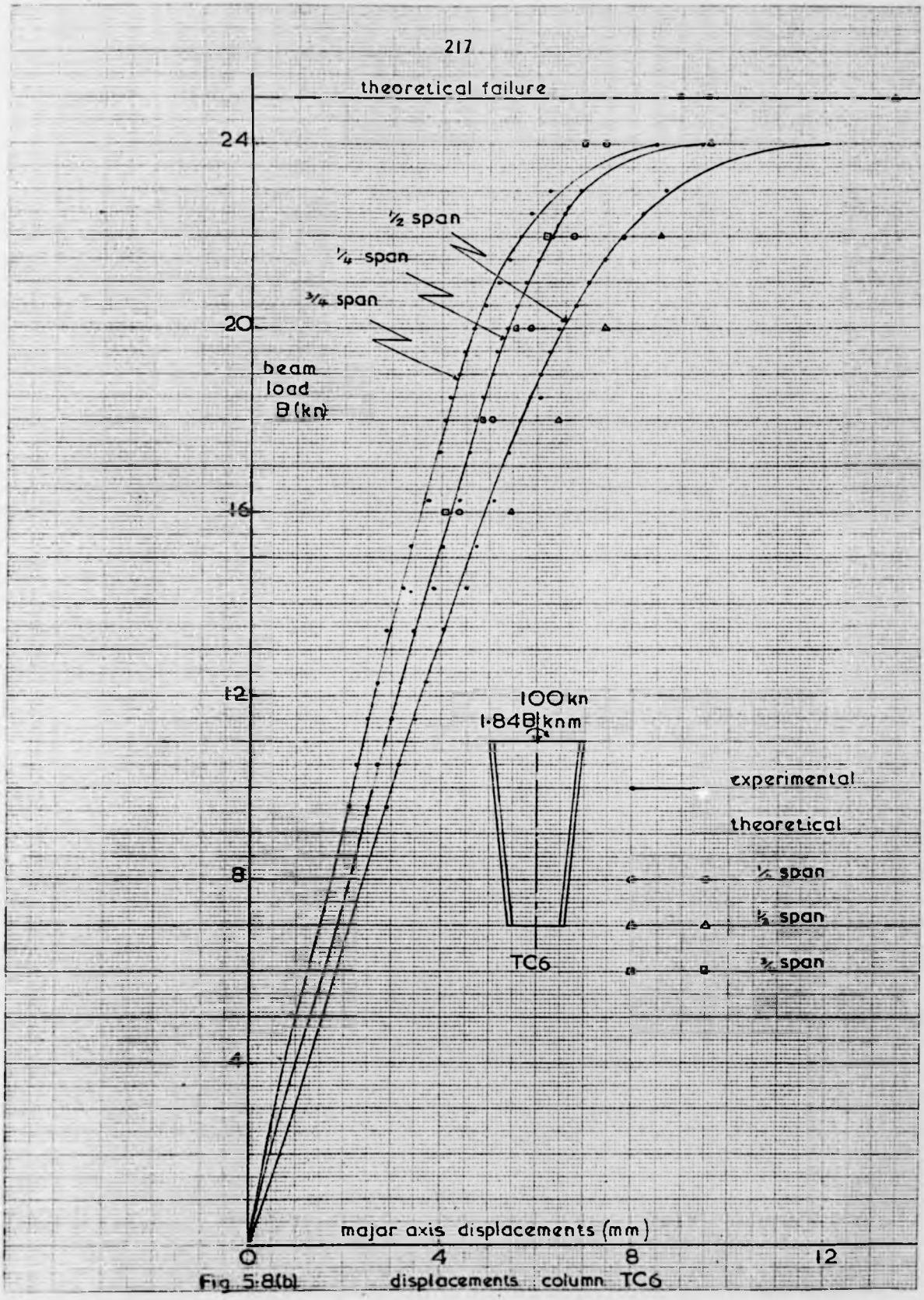

Fig 5:8(b) displacements : column TC6

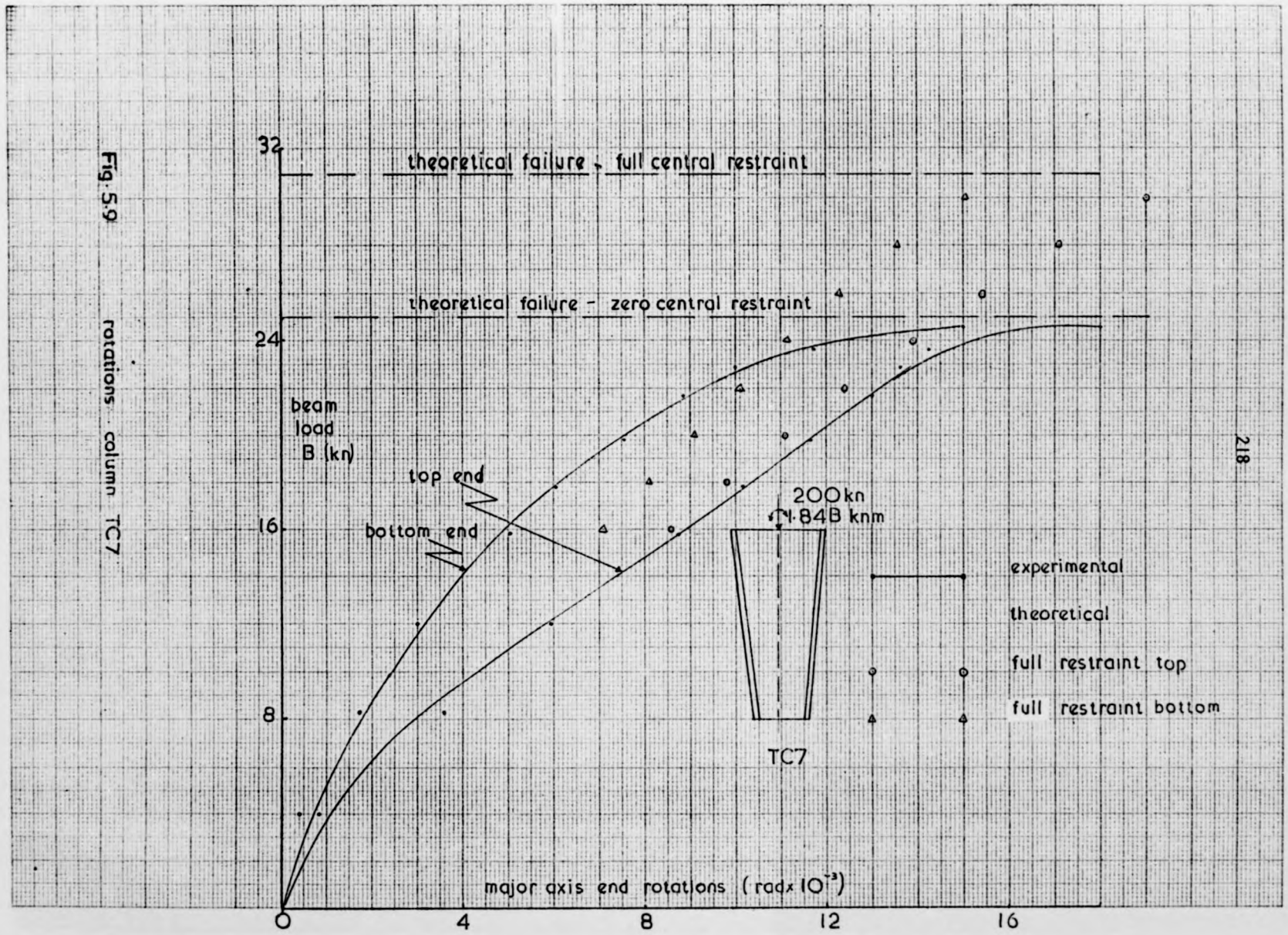

Fig. 5.9 rotations column TC7

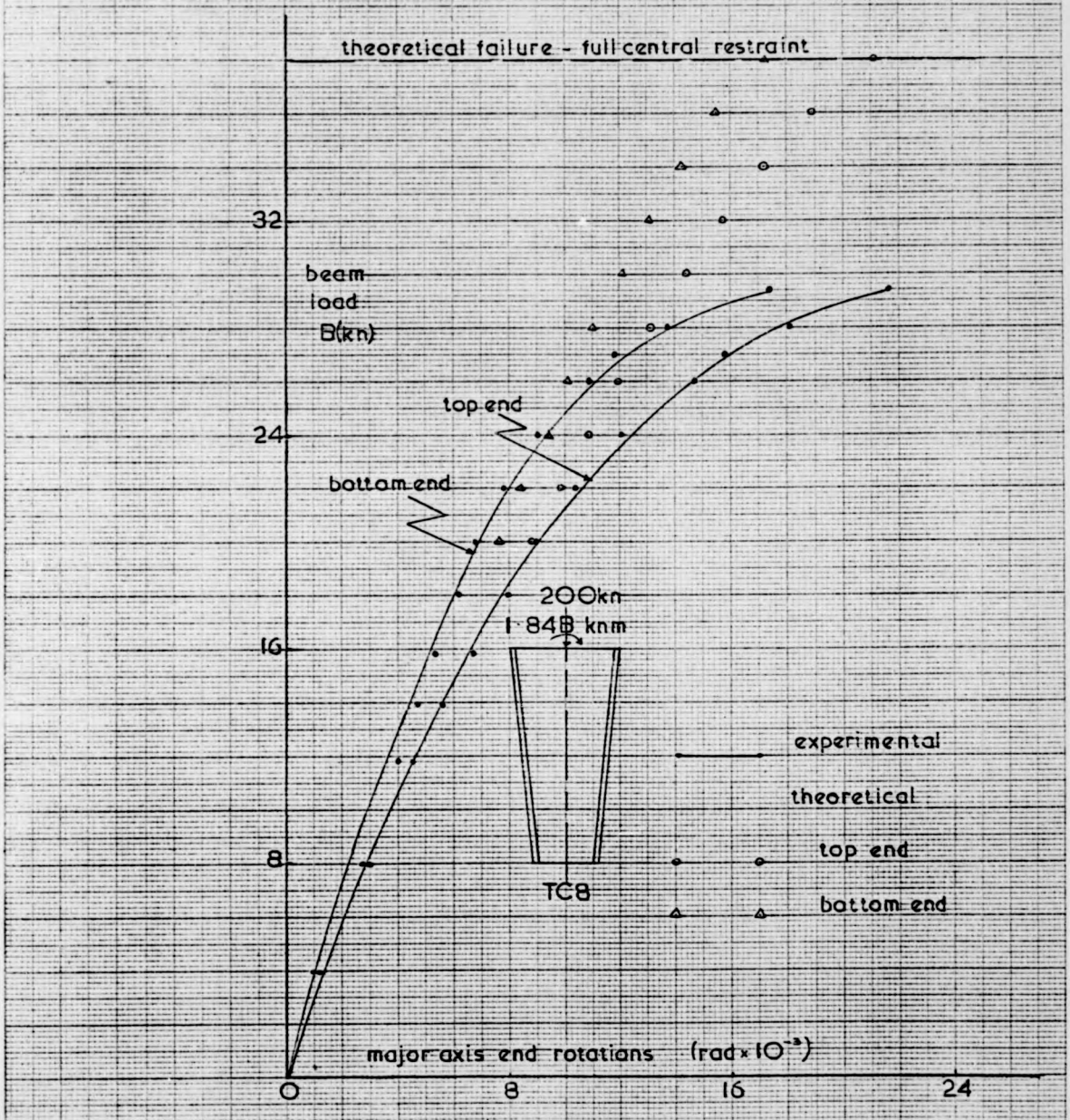

Fig 5.10(a) rotations column TC8

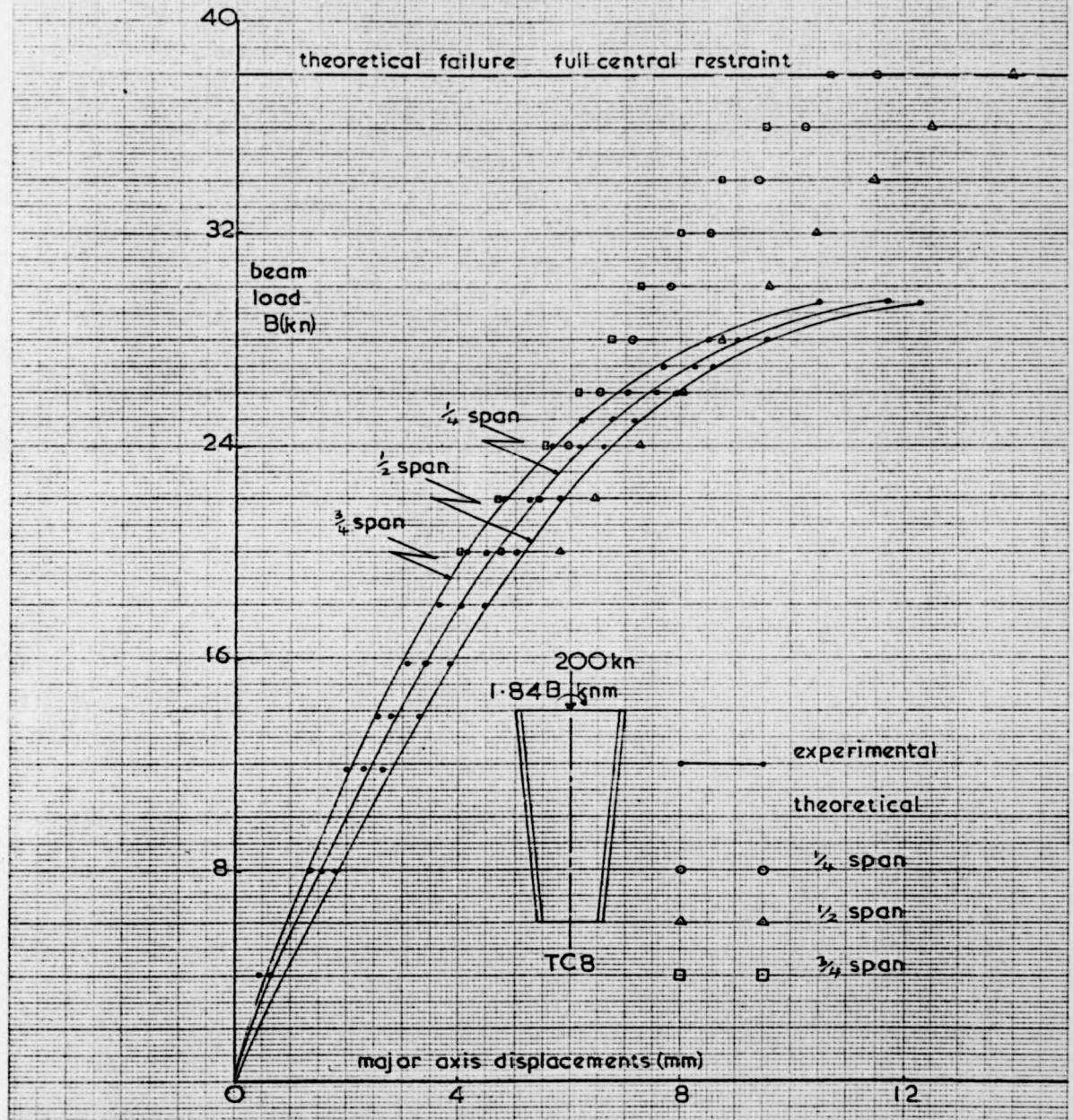

Fig. 5-10(b) displacements column TC8

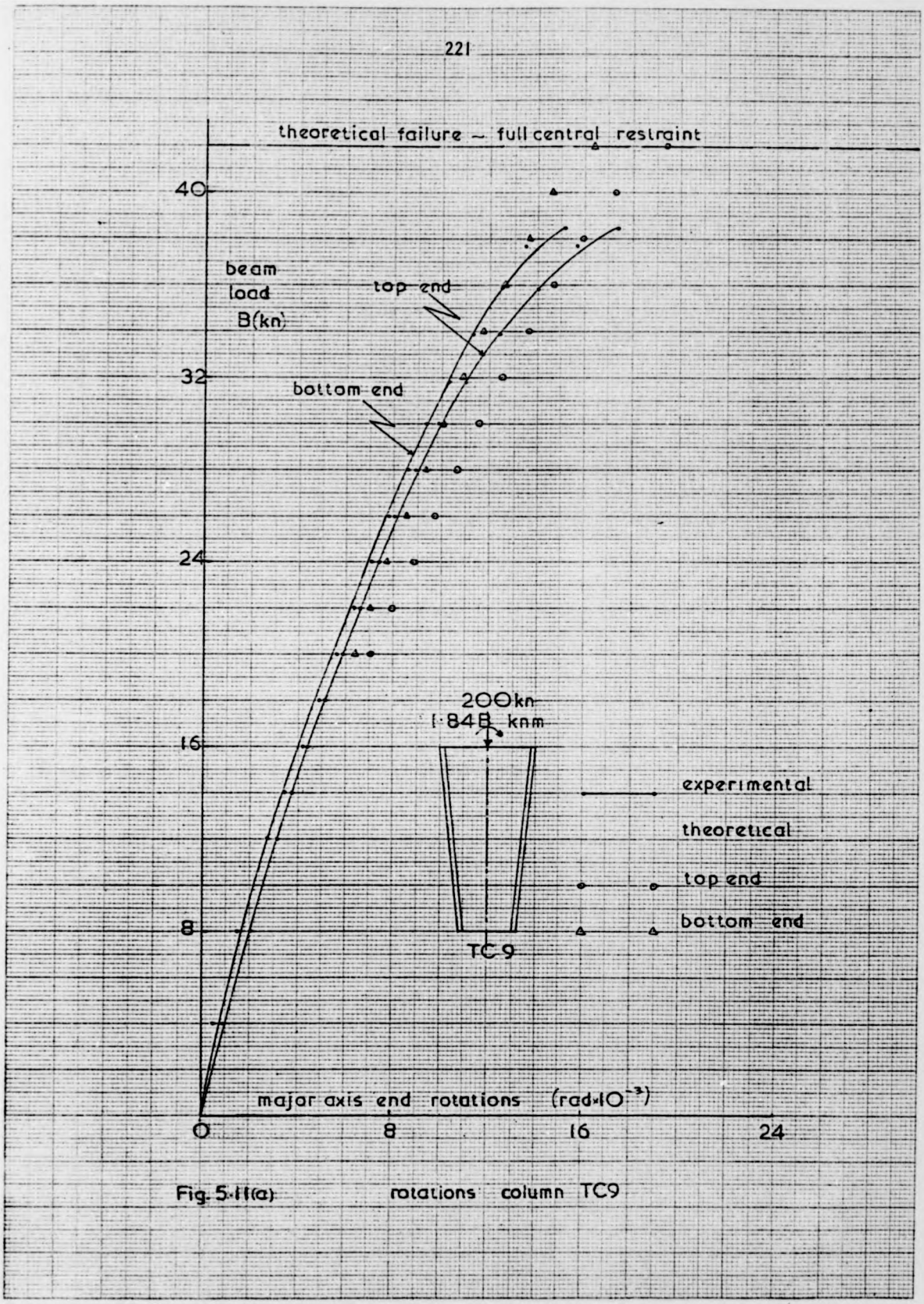

Fig. 5·11(a) rotations column TC9

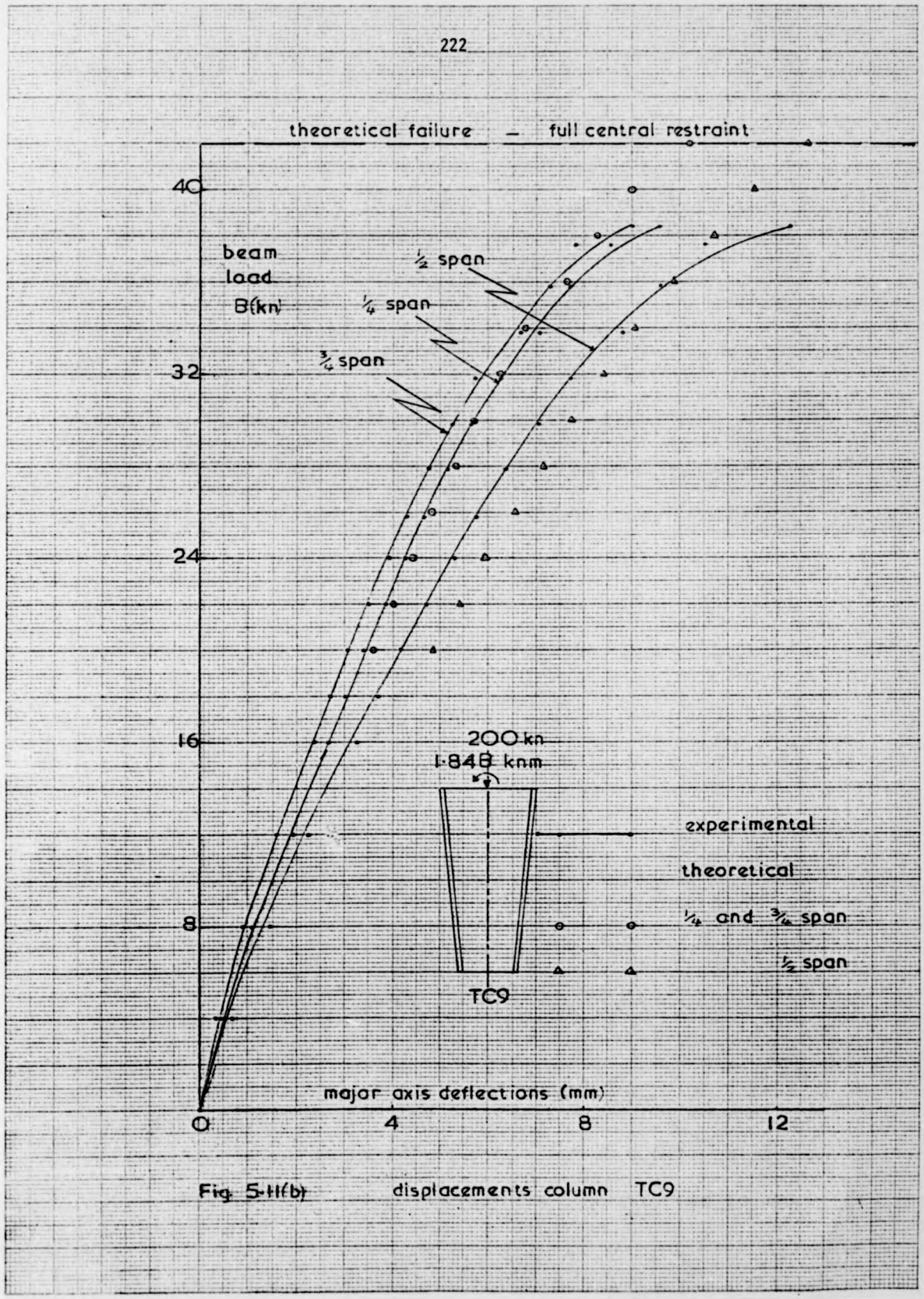

Fig. 5·11(b) displacements column TC9

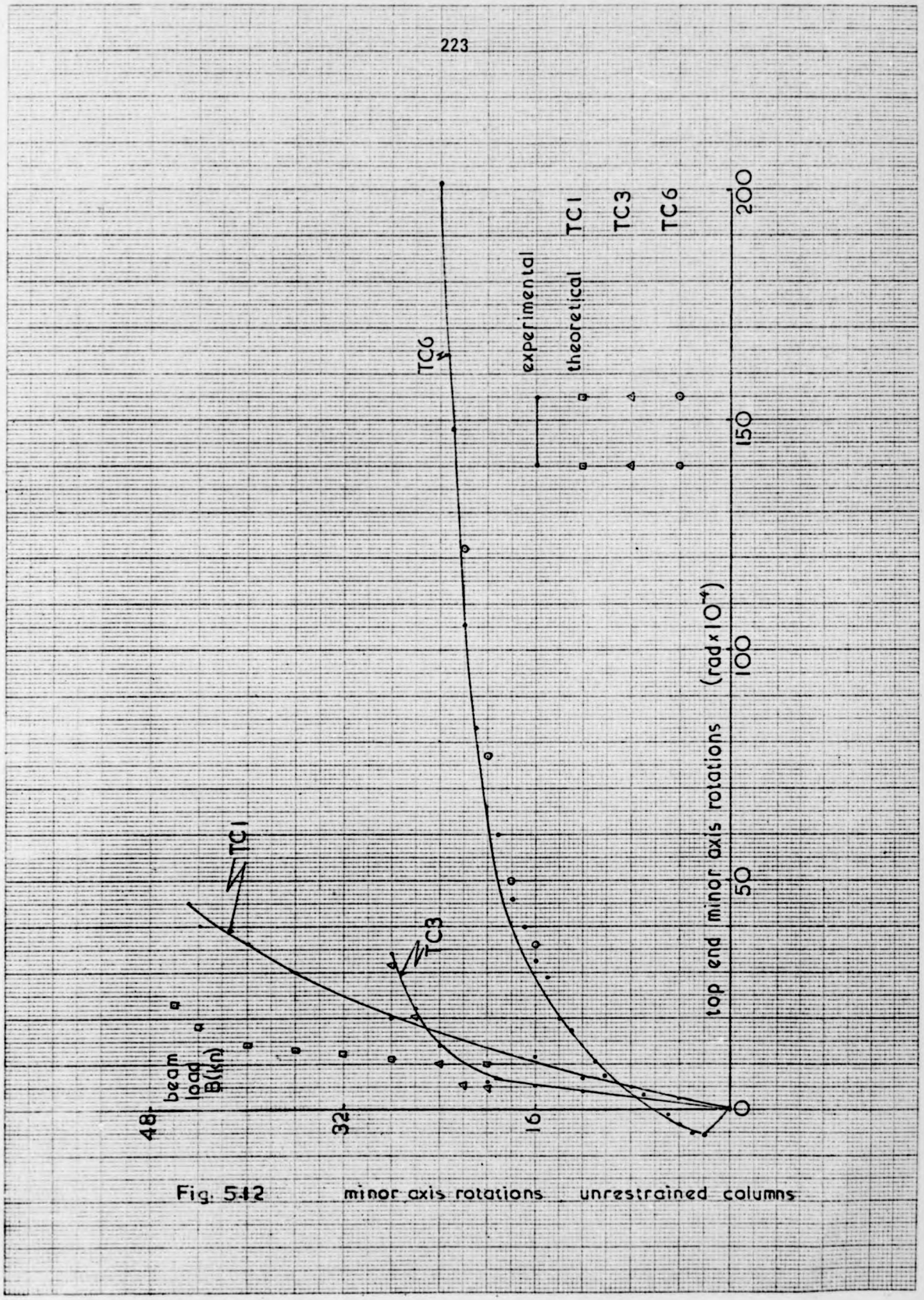

Fig. 5.12 minor axis rotations unrestrained columns

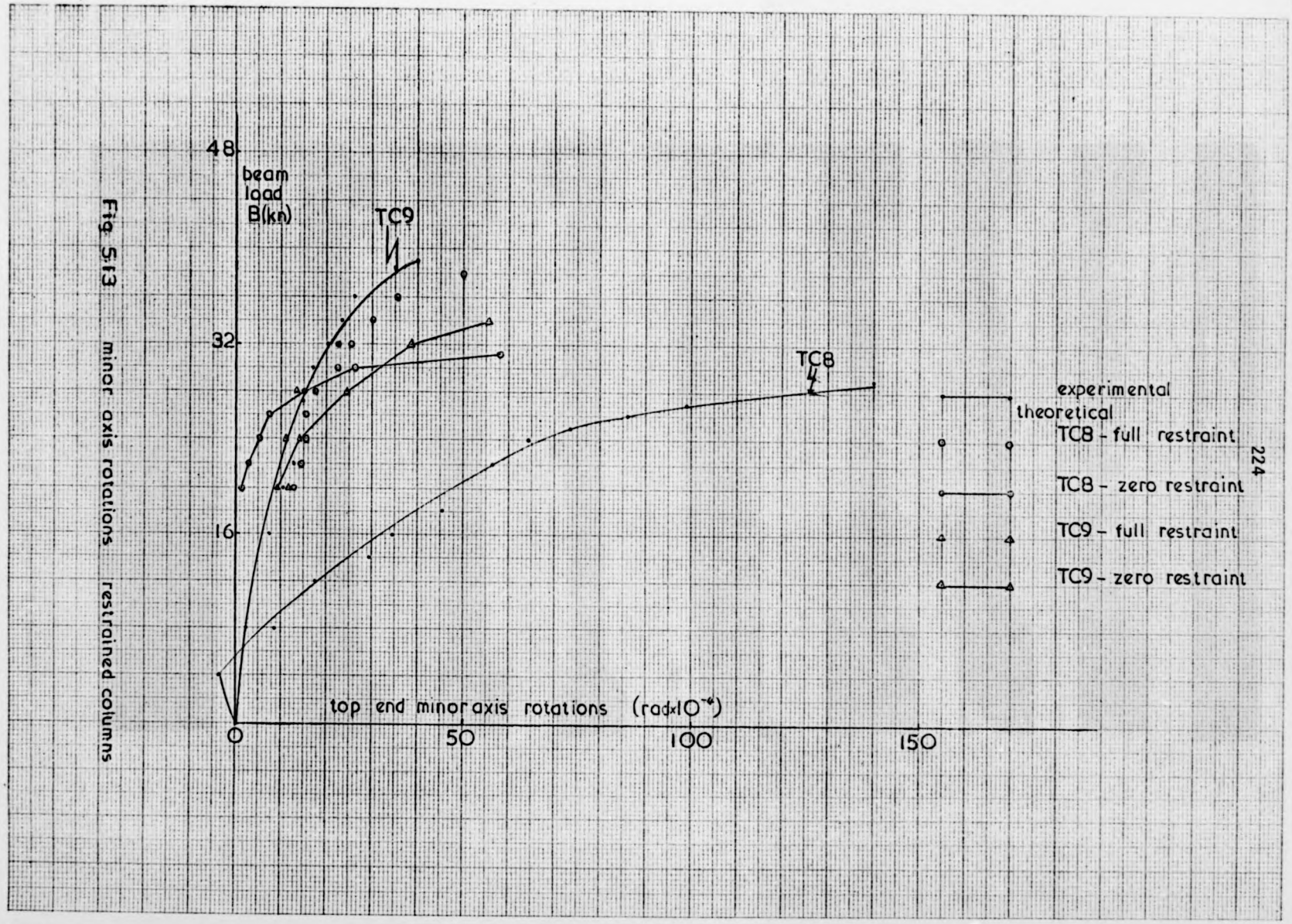

Fig. 5.13 minor axis rotations restrained columns

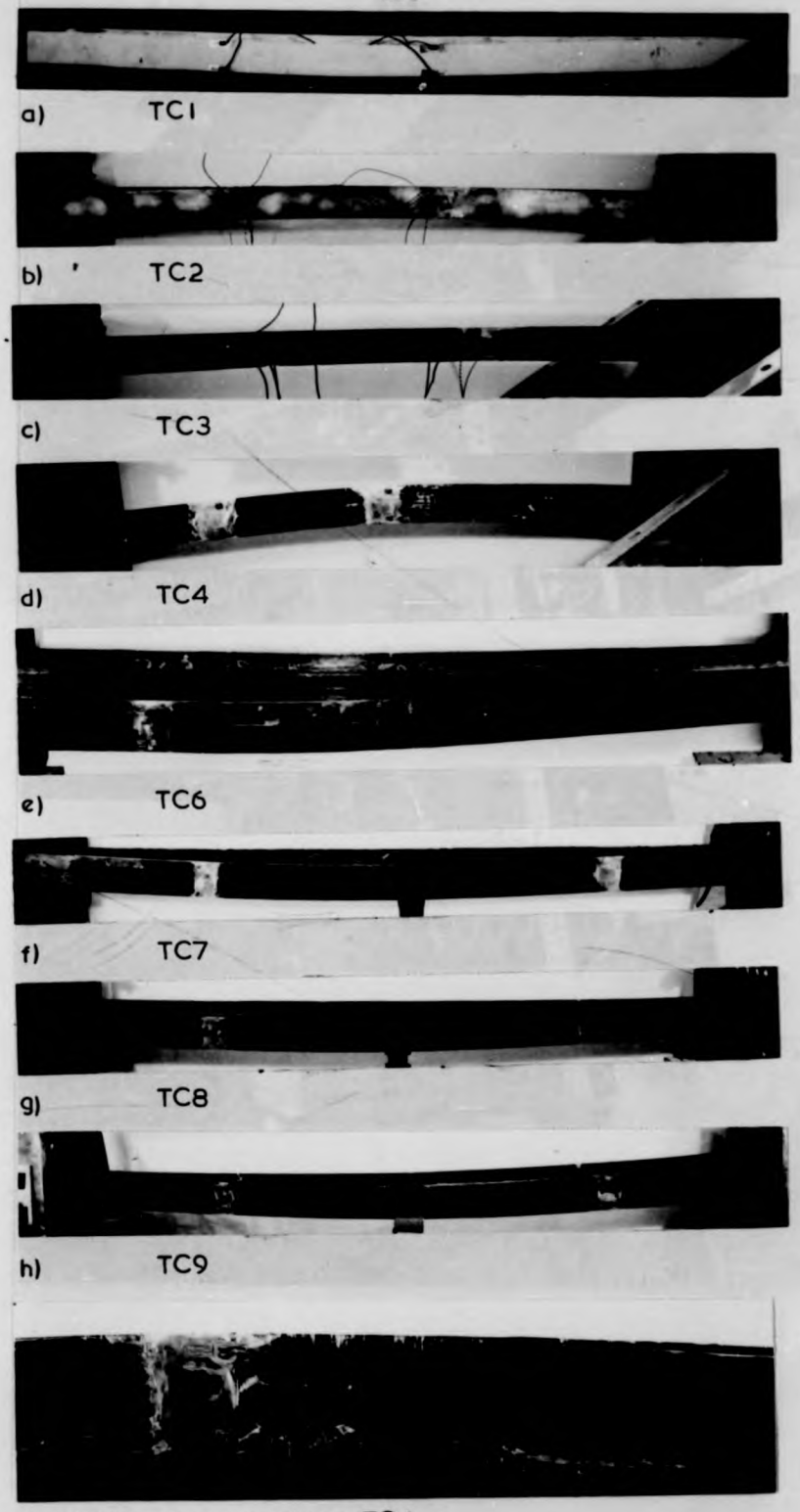

Fig·5·14 failure modes of the tapering columns

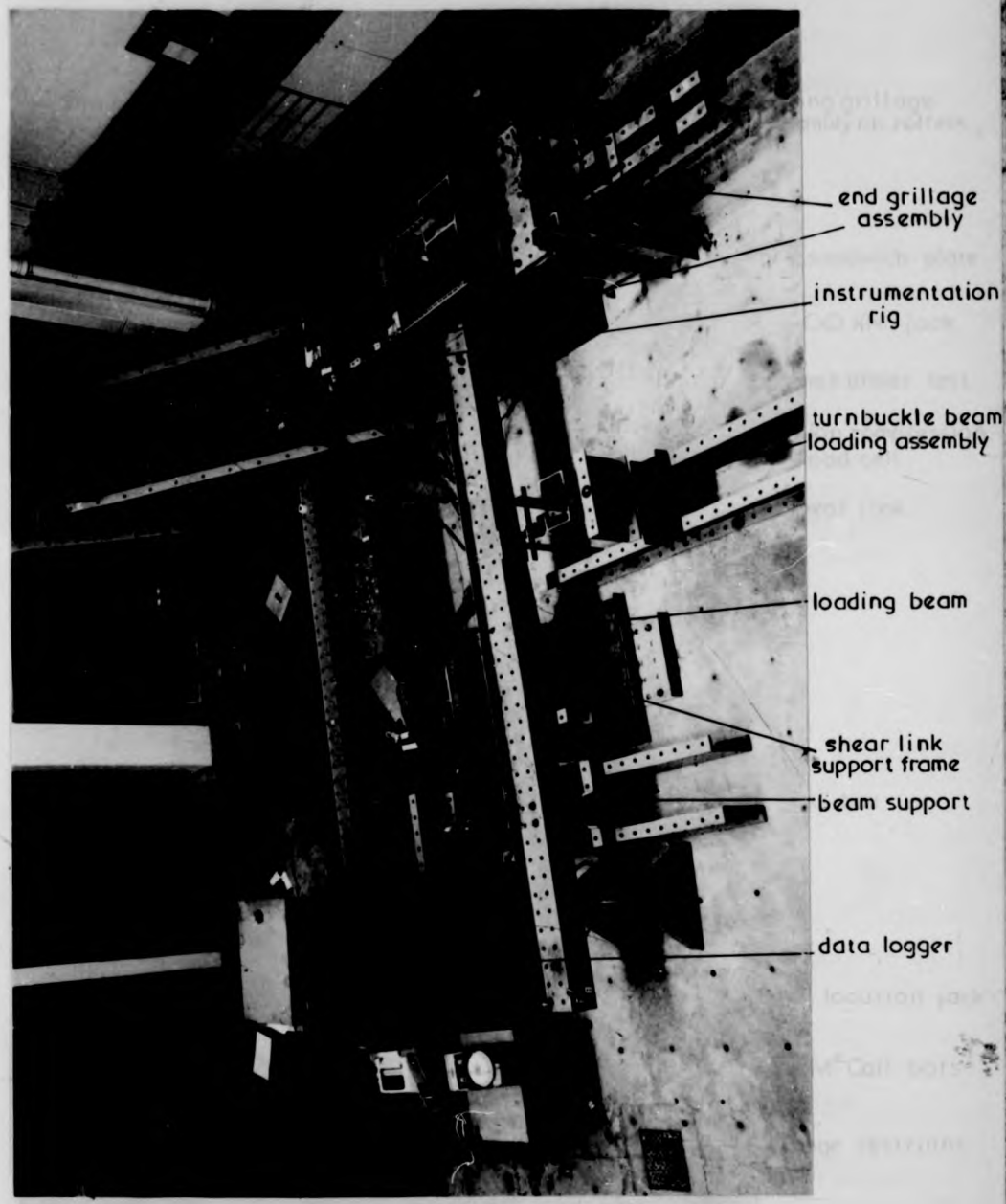

Fig. 5.15 aeriel view of the test rig

Fig 5.16 side view of the test rig

Fig. 5.17 close up view of the flange restraint

Chapter 6. Optimisation of frames to satisfy deflection requirements.

6.1 Introduction.

In a previous chapter, a method of design for portal frames to satisfy both strength and deflection requirements was given. A method for satisfying deflections in an arbitarily shaped frame so that members of the frame are picked in an economic manner will now be given.

The method uses a simple computer based analysis to perform the various steps required during the design process. Initially, a non-linear elastic stiffness analysis is performed on trial sections to obtain the deflections in the structure under the specified loadings. These deflections will usually exceed the permissible values and hence a linear programming technique is employed to determine the most economical changes in section sizes to satisfy these requirements.

6.2 Redesign by linear programming.

Consider the variation of deflection with changing section size; for example Fig. 6.1 shows the variation of the horizontal eaves deflection, x, of a portal frame with increasing column stiffness. For the present, it is assumed that the frame is not haunched. Let a trial analysis be performed with column and rafter moments of inertia I_x' and I_r' respectively. The resulting horizontal eaves deflection is x_1; this deflection is not to exceed a permissible value x_p, where $x_p < x_1$. The design problem is to determine the most economical changes in section sizes that should be made to reduce x to x_p. It is assumed that the cost

of a frame without haunches is directly proportional to the total weight of the frame members, and that deflections due to axial deformations of the members can be neglected. If $\partial x/\partial I$ is the rate of change of deflection with the moment of inertia of a member, then for the portal frame the problem can be stated as:

$$\text{Minimise} \quad W = 2h\,(w_c + \Delta w_c) + 2s\,(w_r + \Delta w_r) \qquad 6.1$$

$$\text{subject to} \quad x_p \geq x_1 + (\partial x/\partial I_c + (\partial x/\partial I_r)\,\Delta I_r \qquad 6.2$$

where W = total weight of the columns and rafters of the frame

w_c and w_r are the weights per unit length for the column section of inertia I_c' and the rafter section of inertia I_r' respectively

ΔI_c and ΔI_r are changes in the column and rafter inertias, respectively which will satisfy the deflection constraint.

Δw_c and Δw_r are changes in the weight per unit length corresponding to inertia changes ΔI_c and ΔI_r.

Constraints on other deflections have a similar form to Eqn. 6.2. Since w_c and w_r are constant, the objective function (Eqn. 6.1) can be written as

$$\text{Minimise} \quad W = 2h\,\Delta w_c + 2s\,\Delta w_r \qquad 6.3$$

In order to solve this problem using linear programming techniques, linear approximations are required for the sensitivity coefficients, $\partial x/\partial I$. An approximation for $\partial x/\partial I_c$ can be obtained by increasing I_c' to a value I_c^2 and reanalysing the frame. Let this analysis correspond to point B in Fig. 6.1.

Hence $\partial x/\partial I_c = (x_2 - x_1)/(I_c^2 - I_c^1)$ 6.4

A value for $\partial x/\partial I_r$ can be similarly obtained by reanalysing the frame with I_r^1 increased to a value I_r^2 whilst keeping I_c constant at its old value of I_c^1.

Within a range of rolled sections, the efficiency of any one section in resisting deflection in a frame can be judged by comparing its major axis moment of inertia with those of other sections of greater weight. Approximate values have been obtained in the form of a trilinear relationship for the correspondence between inertia and mass per unit length for the most economical sections in the Universal Beam and Universal Column ranges.

These relationships cover the complete range of sections can be approximated by:

For Universal Beams

Sections between: 254 × 102 × 22 - 457 × 152 × 60, $\Delta w \propto 1.68\ \Delta I$ 6.5a

457 × 152 × 60 - 610 × 229 × 113, $\Delta w \propto 0.86\ \Delta I$ 6.5b

610 × 229 × 113 - 914 × 419 × 338, $\Delta w \propto 0.42\ \Delta I$ 6.5c

For Universal Columns

Sections between: 152 × 152 × 23 - 203 × 203 × 60, $\Delta w \propto 9.44\ \Delta I$ 6.6a

203 × 203 × 60 - 305 × 305 × 118, $\Delta w \propto 3.70\ \Delta I$ 6.6b

305 × 305 ×118 - 356 × 419 × 634, $\Delta w \propto 2.50\ \Delta I$ 6.6c

The weight function (Eqn. 6.3) may therefore be approximately expressed as:

$$W = 2h\ K_c\ \Delta I_c + 2s\ K_r\ \Delta I_r \qquad 6.7$$

where K_c and K_r are constants dependent on the values of

I_c^1 and I_r^1. It is assumed that K_c and K_r remain constant over the ranges I_c^1 to $I_c^1 + \Delta I_c^1$ and I_r^1 to ΔI_r^1 respectively and are obtained from the constants on the right hand sides of Eqns. 6.5 and 6.6.

6.3 Haunched frames.

Steel portal frame structures usually include eaves haunches which can add considerably to the strength and stiffness of the frame. Such frames can be analysed by treating the haunched length of the rafter as a uniform member whose moment of inertia equals that of the haunched section at the midpoint of its length. This equivalent inertia can now be treated during design in the same way as the unknown section inertias.

The length of the haunched section can also be treated as a design variable in a similar way to the moment of inertia of a section. If the haunch length is initially a_1, then a separate analysis can be performed with a_1 increased to a_2. The variation of displacement with haunch length, $\partial x/\partial a$, can then be found.

For a haunched single bay frame, a typical design constraint becomes.

$$x_p \geq x_1 + (\partial x/\partial I_c)\,\Delta I_c + (\partial x/\partial I_r)\,\Delta I_r + (\partial x/\partial I_h)\,\Delta I_h + (\partial x/\partial a)\Delta a \qquad 6.8$$

where I_h is the equivalent uniform moment of inertia of the haunched section

ΔI_h and Δa are changes in the haunch inertia and length.

The total weight function, W, can now be expressed as:

$$W = 2h\,K_c(I_c^1 + \Delta I_c) + 2(s-a-\Delta a)K_r\,(I_r^1 + \Delta I_r) + 2(a + \Delta a)K_n(I_n^1+\Delta I_h) \qquad 6.9$$

The factor K_h relates the weight of the haunched section to the equivalent uniform inertia; it must also reflect the fact that the cost per unit length of the fabricated haunch will be greater than that of the plain rafter or stanchion. If it is assumed that the cost of the haunch will be 1.5 times that of the plain rafter, then from Eqns. 6.5, the values of K_h are:

Inertia range ($mm^4 \times 10^6$) $28.6 - 254.6$; $K_h = 2.52$ 6.10a

$254.6 - 872.6$; $K_h = 1.29$ 6.10b

$872.6 - 7173.2$; $K_h = 0.63$ 6.10c

From Eqn. 6.9, it can be seen that the weight function is no longer linear in the unknown variables due to the product terms $\Delta a \cdot \Delta I_r$ and $\Delta a \cdot \Delta I_h$. This problem can be overcome by assuming that such terms are small and can be neglected.

Ignoring constant terms, the objective function then becomes

$$\text{Minimise } W = 2h\, K_c\, \Delta I_c + 2(s-a)\, K_r\, \Delta I_r + 2a\, K_h \Delta I_h + 2(K_h I_h^1 - K_r I_r^1)\, \Delta a \quad 6.11$$

The value of 'a' in Eqn. 6.11 should correspond to the optimised value of haunch length. However the value used in this equation is based on the value of haunch length prior to the optimisation. Hence if Δa is non-zero when the optimisation is solved, two solutions should be obtained corresponding to a and $a + \Delta a$ (the correct value) in Eqn. 6.11. Satisfactory convergence is achieved when two consecutive values of Δa are within a specified tolerance.

6.4 Overall design procedure.

This is illustrated by the flow chart in Fig. 6.2. An initial design is supplied by the user, and it is assumed that this is a

lower bound design violating the deflection requirement. Analysis of this design under a particular load case is now made. If necessary, allowance can be made here for the increase in deflections due to compressive axial loads, by using Livesley's stability functions to estimate the reduction in frame stiffness. Members which are to have the same section are grouped together. For each group in turn, the section size is increased and a further analysis is made. From these results, the coefficients $\partial x/\partial I$ are calculated using Eqn. 6.4. The design constraints and the weight function are formulated and solved using a standard method of linear programming (the simplex method[50]).

Using constraints like Eqn. 6.2 will result in non-negative values of ΔI using the simplex method. This is satisfactory for the first iteration as the initial design is a lower bound. The required increases in the moments of inertia of the sections given by the linear programming procedure are added to the initial values, and the analysis is re-entered.

During subsequent iterations provision is not made for the reduction of any section, which has previously been increased. In this way, oscillation between two unsatisfactory designs is eliminated. Instead, the design procedure progresses towards a design to satisfy all the constraints. For such a design to be efficient, it is necessary for the program to execute a number of full iterations before a final design is obtained. This is ensured by the way in which the coefficients $\partial x/\partial I$ are calculated. The incremented inertia I^2 is taken to correspond to either the

next section or the next section but one in the list of preferred sections with an inertia greater than I^1.

In the early stages of the design process, x_1 will be much greater than x_p and large changes in inertia are expected. In such a case, the coefficient $\partial x/\partial I$ will be based on a line such as AB in Fig. 6.1, and the inertia will be underestimated. During later iteration, when the deflection constraint is nearly satisfied, the coefficient may be based on straight lines such as AD of Fig. 6.1, in which case the inertia required to reduce x to x_p will be over-estimated. However, owing to the small values of the inertia increments needed to satisfy the constraints, the use of AD leads to insignificant error in the final design.

Once the deflection constraints are satisfied, the final design inertias must be converted into a series of discrete rolled sections. The simplest way of doing this is to select sections whose moments of inertia are at least equal to the required values. However, if some sections are significantly stiffer than required, it will be more economical to select some sections whose inertias are slightly less than the designed values to counterbalance those that are over stiff. The sensitivity coefficients used at the last iteration will give a guide as to the most efficient way of doing this.

In a haunched frame, it may be convenient to choose both column and rafter sections to have inertias with greater values than those required by the optimisation procedure. In such a case, the inertia and/or length of the haunches could be reduced, and coefficients

$\partial x/\partial I_h$ and $\partial x/\partial a$ can be used to proportion the frame. It is usual practice for the flanges in the haunch to be the same size as those in the adjoining plane rafter. Once the rafter section is chosen, the depth of the web at the mid-length of the haunch can therefore be calculated from the required moment of inertia. This dimension together with the rafter depth and haunch length, then determine the haunch depth at the column face.

As no restriction is placed on the size of the increments, ΔI, the procedure is not an accurate method of non-linear programming, and there is therefore no certainty that a true optimal solution will be converged onto. However, comparisons given below with previous methods of non-linear programming show that designs are likely to be close to the optimum, and in some cases give even better solutions than these more rigorous methods. Unless otherwise stated in the following examples, a linear elastic stiffness analysis has been performed and the 'K' values of Eqns. 6.5, 6.6 and 6.10 have been set to unity.

6.5 Examples using the method.

A) Rectangular portal frame.

The frame analysed is shown in Fig. 6.3; the horizontal deflection of joint B, x, was restricted to 10.16 mm. This frame has previously been designed using the piece-wise linearisation method of linear programming[52].

The various stages of the design procedure using the optimisation procedure are summarised in Table 6.1. Initially the frame was of uniform section throughout, a 127 × 76 R.S.J. ($I = 4.76 \times 10^6$ mm^4),

being adopted. On analysis the deflection, x, was found to be 43.63 mm. The columns and the rafter were in turn increased to a 152 × 89 R.S.J. ($I = 8.81 \times 10^6$ mm^4), resulting in the deflections shown in the second and third rows of Table 6.1. The objective functions and the design constraint therefore became:

$$\text{Miminise} \quad W = 5080\,\Delta I_c + 2540\,\Delta I_r \qquad 6.12$$

subject to

$$10.16 \geq 43.63 - (3.81 \times 10^{-6})\cdot\Delta I_c - (1.36 \times 10^{-6})\cdot\Delta I_r \qquad 6.13$$

The solution to this problem can be readily shown to be $\Delta I_c = 8.78 \times 10^6$ mm^4, $\Delta I_1 = 0$. Hence the revised design becomes $I_c = 13.54 \times 10^6$ mm^4, $I_r = 4.76 \times 10^6$ mm^4. From Table 6.1, it can be seen that the final design is $I_c = 22.59 \times 10^6$ mm^4, $I_r = 16.58 \times 10^6$ mm^4. If the 'weight' of a member is defined as the product of inertia and length, the total weight of the final design is 156.9×10^9 mm^5. This compares favourably with the true optimum design obtained by non-linear programming which gave $I_c = 21.73 \times 10^6$ mm^4, $I_r = 18.01 \times 10^6$ mm^4, and a weight of 156.1×10^9 mm^5.

B) Pitched roof frame.

The frame is Fig. 6.4 has previously been designed by Majid and Elliott[48] using the dynamic search method of non-linear programming. The horizontal movement at the head of each column was not to exceed 1/325 of the height of the column and the vertical displacement of the apex was restricted to 1/360 of the span of the frame.

The initial design for the proposed method was obtained by designing the frame by the rigid-plastic method to a load factor of 1.75 under the vertical roof loading shown in Fig. 6.4. The frame was assumed to be composed of the same section throughout, with steel to Grade 43, and thus a 533 × 210 × 82 U.B. was adopted.

The final design, which was obtained after three cycles of analysis and design was as follows:

$I_c = 1108.1 \times 10^6$ mm^4, $I_r = 797.6 \times 10^6$ mm^4, 'weight' = 38.4×10^{12} mm^5;

The corresponding values of Majid and Elliott were:

$I_c = 1000{\cdot}0 \times 10^6$ mm^4, $I_f = 921{\cdot}1$ mm^4, 'weight' = 39.3×10^{12} mm^5;

Thus it can be seen that the present method has led to a lighter design than that of Majid and Elliott. This shows that in the latter case the non-linear programming technique had located only a local optimum due to the non-linearity of the design problem.

c) Pin-jointed frame.

The optimisation method can also be used to design pin-jointed frames by formulating the problem in terms of the unknown areas of cross-section instead of moments of inertia. For the frame shown in Fig. 6.5, the downward displacements at A and B were restricted to 0.5 mm and 0.25 mm respectively. The cross-sectional areas of the vertical, horizontal and diagonal members are denoted by A_1, A_2 and A_3 respectively. The frame has also been designed by Majid and Elliott[48].

The initial design for the proposed method was obtained by arbitarily choosing all areas to be 645 mm^2.

The final design obtained using the method is:

$A_1 = 3.3 \times 10^3$ mm^2; $A_2 = 32.2 \times 10^3$ mm ; $A_3 = 23.1 \times 10^3$ mm^2;

The corresponding design of Majid and Elliott gave:

$A_1 = 3.0 \times 10^3$ mm^2 ; $A_2 = 32.2 \times 10^3$ mm^2 ; $A_3 = 23.0 \times 10^3$ mm^2;

It can be thus be seen that agreement between the final designs of the two methods is good.

d) Haunched portal frame.

The procedures described above have been applied to the frame shown in Fig. 6.6. The vertical deflection at C and the horizontal deflection at D were to be limited to 1/360 of the span and 1/325 of the column height respectively under both the loading cases (a) and (b) shown. To ensure that the haunches would have realistic dimensions, it was specified that the haunch length, a, should not exceed 2500 mm, and that the depth of the haunched rafter at the face of the column should not be less than 1.5 times the depth of the plain rafter. In the initial design, the haunch length used was arbitarily taken as 250 mm and a constraint of the form below is used (Fig. 6.8).

$$\Delta a \leq 2250 \qquad 6.14$$

A constraint governing the haunch depth was obtained as follows. The equivalent uniform haunch inertia, I_h, corresponds to the middle of the haunch length, and at this point therefore, the depth of the section should therefore be at least 1.25 times the depth of the plain rafter. It was assumed that with constant flange dimensions, the moment of inertia of the cross-section is dependent solely on the contribution to the inertia of the flanges about the centre point of the section. Hence

$$I_h + \Delta I_h \geq (1.25)^2 (I_r + \Delta I_r) \qquad 6.15$$

It was assumed that both rafters and columns would use Universal Beams, and the cost factors of Eqns. 6.5 have thus been adopted. The initial design was arbitarily chosen, and is given in the top row of Table 6.2. The revised designs obtained at the end of each iteration of the design method are also shown, that given in the bottom row being the first design to satisfy all the deflection constraints.

It can be seen that at one stage, increases were made simultaneously in a, I_h and I_r necessitating iteration of the optimisation procedure using Eqn. 6.11. Convergence was achieved in two iterations.

A discrete section design was obtained by selecting a 533 × 165 × 66 U.B. ($I = 350.8 \times 10^6$ mm^4) for the columns, and a 457 × 152 × 60 U.B. ($I = 254.6 \times 10^6$ mm^4) for the rafters. As both these sections provided inertias which were slightly less than those required, the sensitivity coefficients calculated during the final iteration of the design procedure was used to increase I_h so that the deflection constraints would still be satisfied. The resulting depth at the column face of the haunch was 960 mm.

The effect of varying fabricating costs for the haunches has been investigated by increasing the factors, K_h, of Eqns. 6.11 by 33%. In this case, it was found that the haunch length remained at its initial value, although its inertia did rise during subsequent iterations of the optimisation procedure.

e) Latticed portal frame.

The design procedure has also been applied to the latticed portal frame of Fig. 6.7. This frame is assumed to have the same loading as for the haunched portal frame. In such a frame, the lacing members are usually pin-jointed and therefore the area rather than inertia will be the dominant section property for these members. In order to optimise on this area, an extra multiplying factor would be needed in Eqn. 6.7 to convert this area into the equivalent dimensions of inertia so that the comparative effects of increasing its section size to resist deflection can be assessed. Hence for the present analysis, an inertia term has been used in Eqn. 6.7 corresponding to the area of the lacing member. Again, the restrictions on deflection are 1/360 of the span and 1/325 of the column height respectively. The arbitary inertias in Row (1) of Table 6.3 are used for the first analysis. The first optimisation cycle predicts an increase in area and inertia of the lacing member (I_2). On subsequent cycles of optimisation, the effect of increasing this section causes only small reductions in the critical deflections. This represents a change from a line AB in Fig. 6.1 (large reduction in deflection for a small increase in section size) to a line such as BD (small reduction in deflection for a large increase in section size).

The final section sizes which correspond to a design satisfying the initial deflection requirements are given in the bottom row of Table 6.3, each row representing a cycle of the optimisation procedure. A discrete section design is then obtained by using:-

I_1 = 406 × 140 × 39 U.B.

I_2 = 76 × 76 × 10.57 Angle Section

I_3 = 610 × 229 × 113 U.B.

I_4 = 610 × 229 × 101 U.B.

f) Six-storey, two-bay frame.

The pinned-base six-storey two-bay frame of Fig. 6.9 has been designed using the optimisation process. In such a frame, the increase in lateral deflections due to compressive axial loads is usually significant and therefore account of this has been taken in the analysis part of the procedure. It was specified that the lateral deflection at each storey should not exceed 1/250 of the height from the base.

The initial design was obtained by proportioning the beams so that failure by beam-type plastic hinge mechanisms under vertical loading did not occur below a load factor of 1.75. This also governed the size of the external columns. The internal columns were proportioned so that the squash load would not be exceeded at a load factor of 1.75. Grade 43 steel was used throughout, and it was assumed that Universal Beams would be used for the beams and Universal Columns for the stanchions. The moments of inertia of the sections so obtained are shown in the upper row of Table 6.4.

The final design, obtained after five iterations of the optimisation procedure, is given in the lower row of Table 6.4. The beam inertia, I_4, and the internal column, I_{10}, were increased twice and the external column inertia, I , once during the design process.

I_c $mm^4 \times 10^6$	I_r $mm^4 \times 10^6$	x mm	$\delta x/\delta I_c$ $mm^{-3} \times 10^{-6}$	$\delta x/\delta I_r$ $mm^{-3} \times 10^{-6}$	ΔI_c $mm^4 \times 10^6$	ΔI_r $mm^4 \times 10^6$
4.76	4.76	43.63				
8.81	4.76	28.19	-3.81		8.78	0
4.76	8.81	38.13		-1.36		
13.54	4.76	21.15				
22.94	4.76	14.84	-0.67		0	11.82
13.54	8.81	17.38		-0.93		
13.54	16.58	14.72				
22.94	16.58	9.99	-0.50		9.05	0
13.54	28.80	13.18		-0.13		
22.59	16.58	10.14				

Table 6.1 design of rectangular portal frame

I_c	I_b	I_r	a mm
210·4	100·0	50·0	250
210·4	141·4	90·5	2500
210·4	546·1	90·5	2500
210·4	546·1	269·3	2500
352·5	546·1	269·3	2500
352·5	546·1	270·8	2500

inertias in $mm^4 \times 10^6$

Table 6·2 haunched portal frame

I_1	I_2	I_3	I_4
30·0	0·015	80·0	80·0
30·0	0·755	80·0	80·0
30·0	0·755	574·0	80·0
73·7	0·755	574·0	222·9
119·7	0·755	574·0	541·8
119·7	0·755	574·0	803·4
119·7	0·755	777·8	803·4

inertias in $mm^4 \times 10^6$

Table 6·3 latticed portal frame

I_1	I_2	I_3	I_4	I_5	I_6	I_7	I_8	I_9	I_{10}
124·1	213·5	213·5	213·5	52·6	52·6	52·6	17·4	60·9	143·1
124·1	213·5	213·5	493·2	52·6	52·6	314·1	17·4	60·9	1703·0

inertias in $mm^4 \times 10^6$

Table 6·4 six-storey, two-bay frame

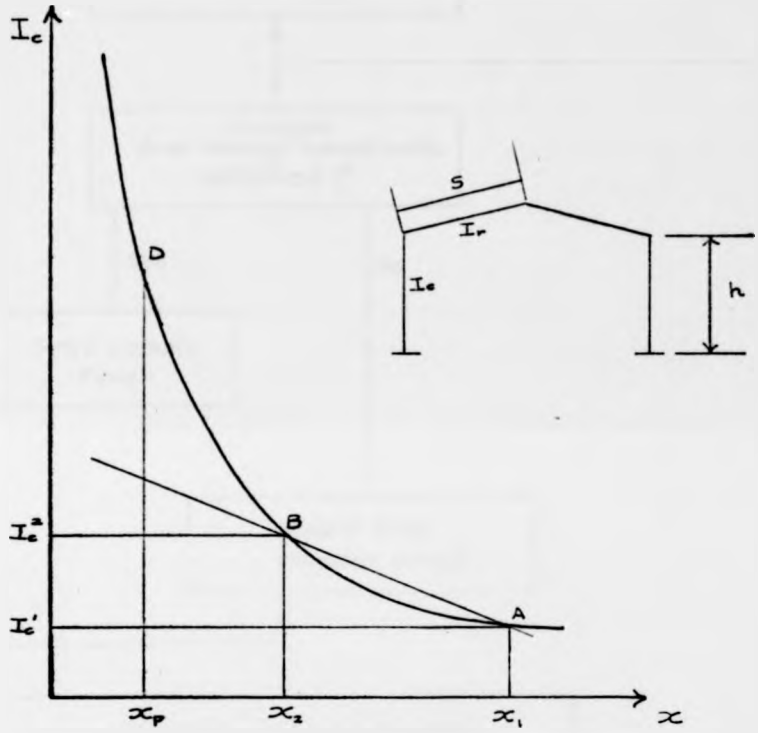

Fig. 6.1 variation of inertia with deflection

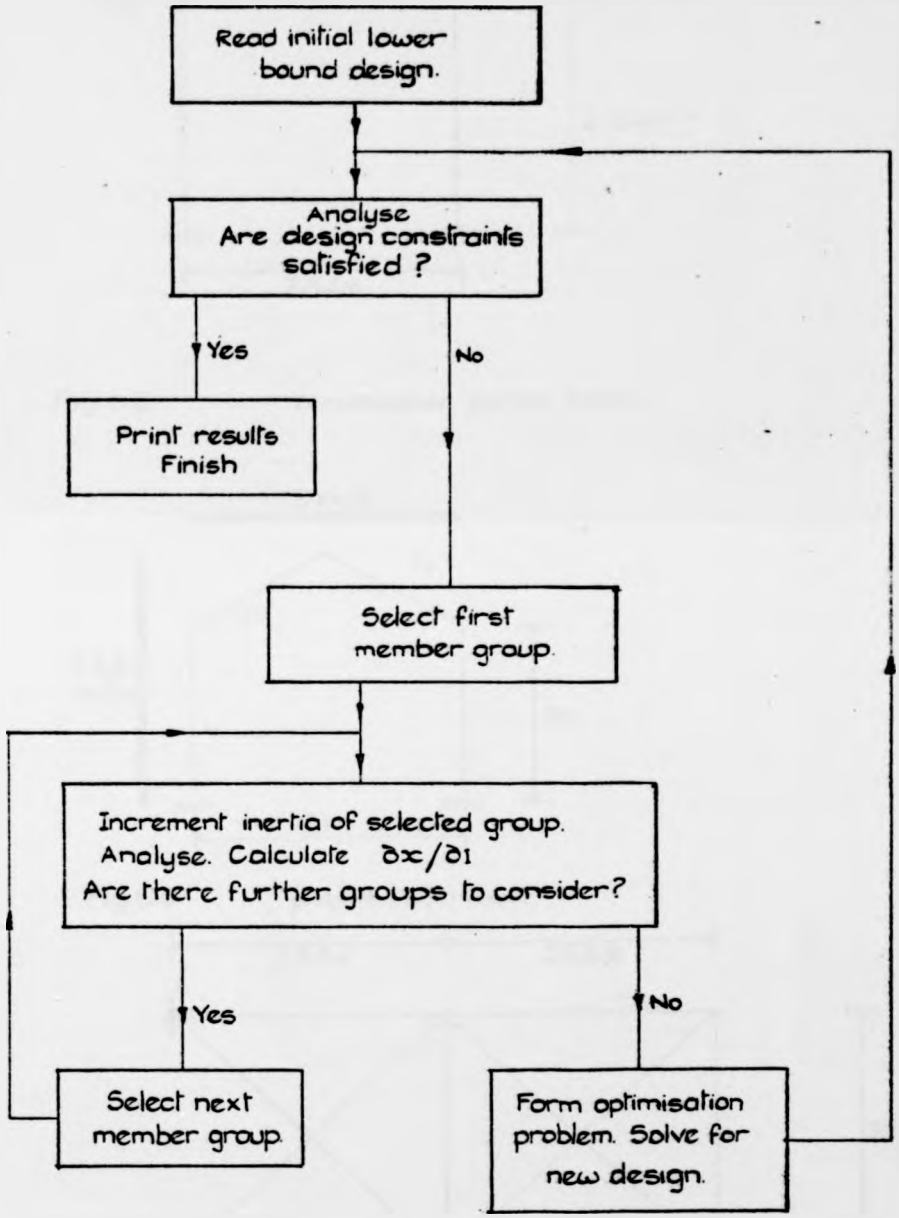

Fig. 6·2 flow diagram for the optimum design of plane frames to satisfy deflection constraints

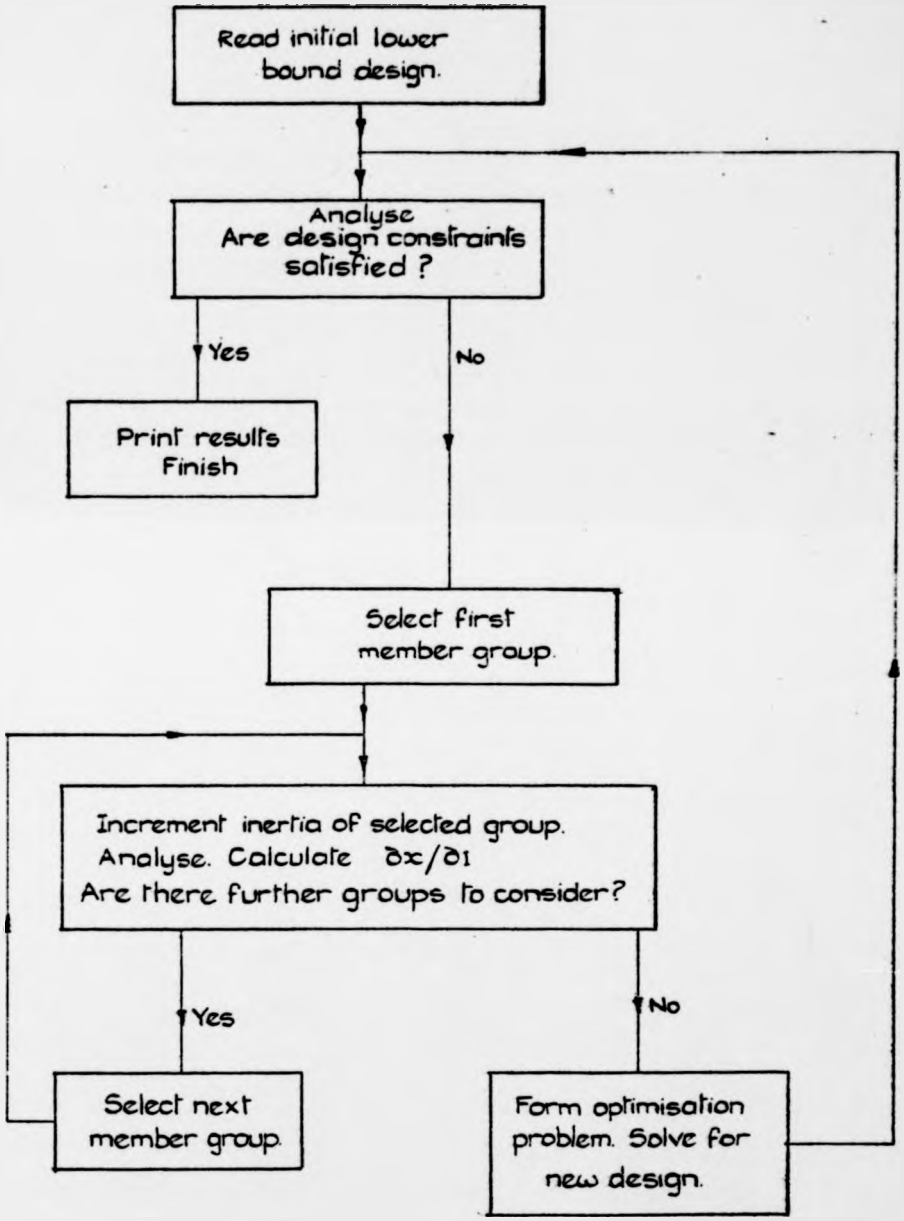

Fig. 6·2 flow diagram for the optimum design of plane frames to satisfy deflection constraints

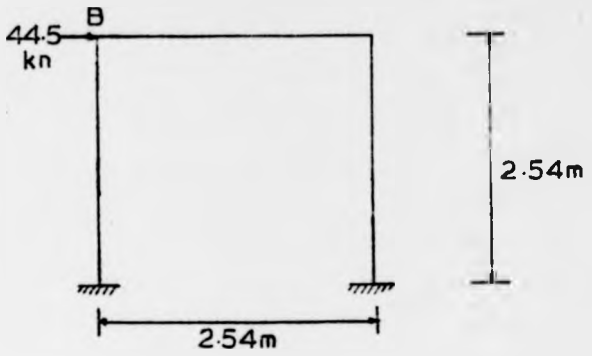

Fig·6·3 rectangular portal frame

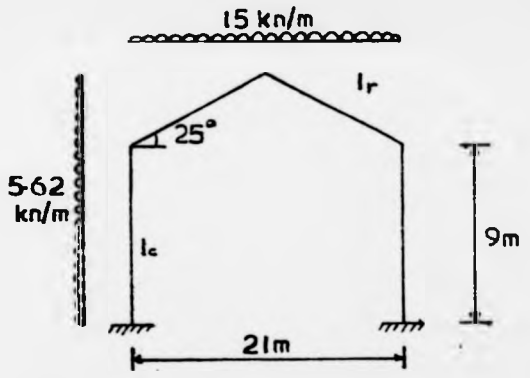

Fig·6·4 pitched roof frame

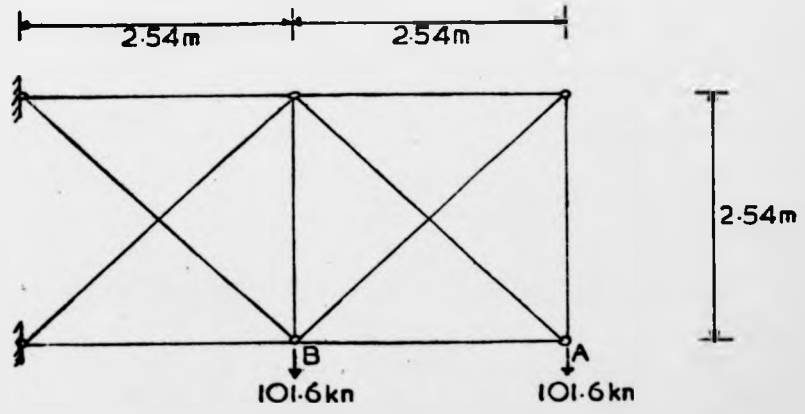

Fig6·5 pin-jointed frame

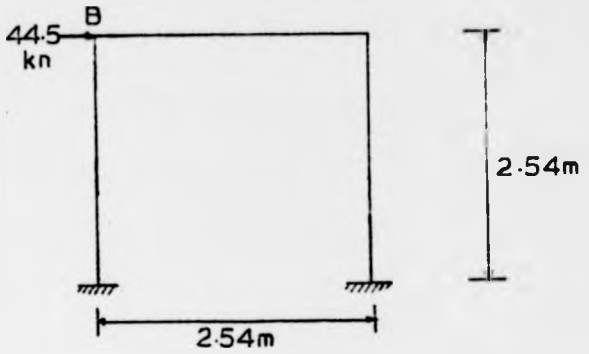

Fig. 6.3 rectangular portal frame

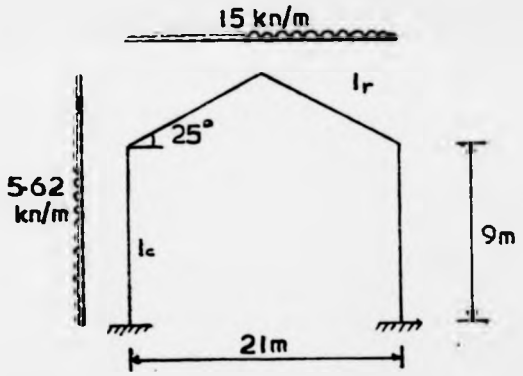

Fig. 6.4 pitched roof frame

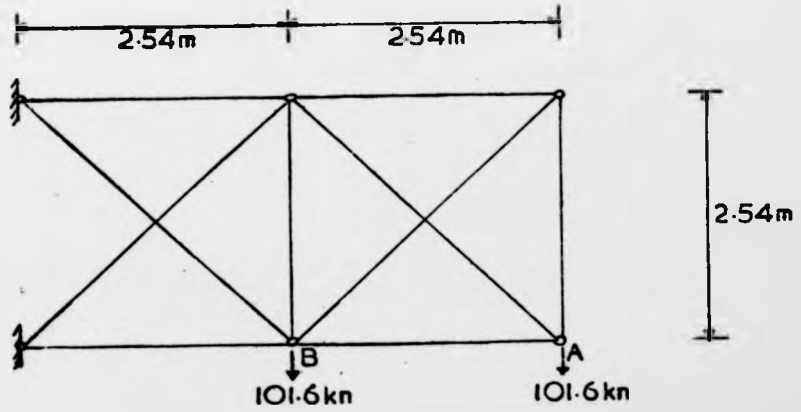

Fig 6.5 pin-jointed frame

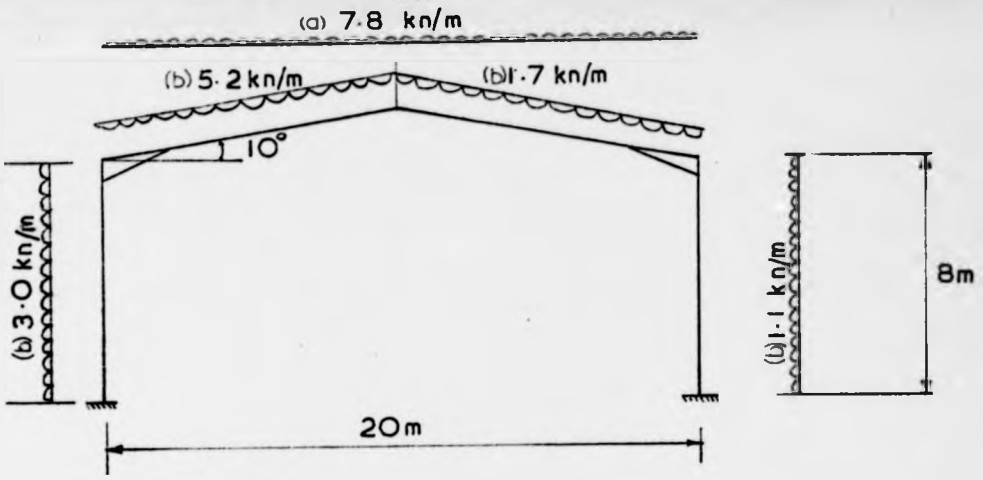

Fig. 6.6 haunched portal frame

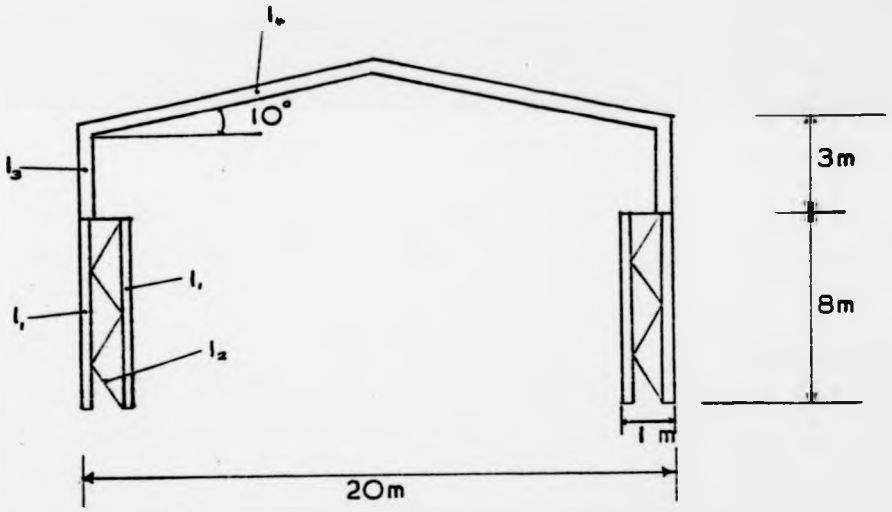

Fig. 6.7 latticed portal frame

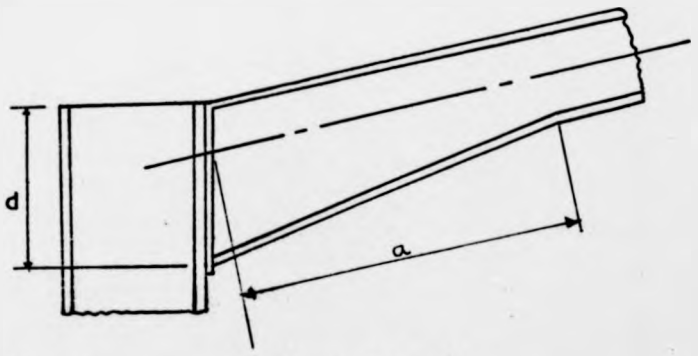

Fig. 6.8 eaves haunch

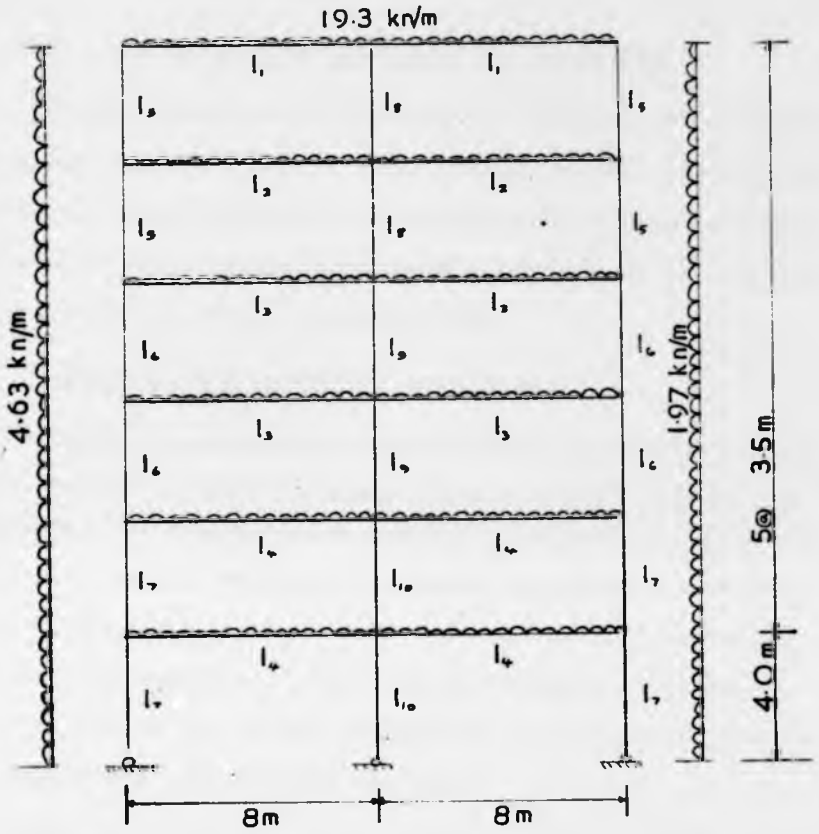

Fig. 69 six-storey two-bay frame

Chapter 7 Conclusions and suggestions for future work.

The work described in this thesis has examined various aspects in the analysis and design of steel building frames. The study can broadly be categorised into three main sections (strength analysis, deflection limitations and experimental testing of tapered columns) which will be separately summarised below.

7.1 Biaxial ultimate analysis of steel frames.

A computer program which analyses complete I-section building frames subject to biaxial bending moments and axial load has been described. The analysis which combined the effects of elastic instability and the development of plasticity enables the ultimate loads of any arbitary shaped frame to be obtained. Most previous ultimate load analyses of steel sections have been concerned with isolated members, or individual members with assumed end conditions or plane frames under uniaxial bending.

The basic method of analysis is to form a complete stiffness matrix for the complete frame. This consists of terms based on the individual members' various stiffnesses, as well as geometric terms dependent on the internal forces present within the frame due to the applied loading. Stiffness equations relating the loads to the unknown joint displacements are stored in a compact manner which leads to a rapid solution of the equations.

As loading is increased on the frame and plasticity develops, an estimation of reduced torsional and flexural stiffnesses is obtained using moment curvature techniques. These reduced stiffnesses are then used in the overall stiffness matrix to obtain

the moments and forces due to the weakened nature of the frame in resisting applied loading.

Unsymmetrical regions of plasticity will generally develop under biaxial bending causing a shift in orientation and position of the principal axes of the section. Unsymmetrical bending theory is then used to allow for the additional torsional effects resulting from this non-symmetry.

There is considerable interaction between the plasticity and instability effects in a steel frame and an iterative method is necessary to obtain an estimation of the ultimate load of the frame under analysis.

The present method has the advantage of being versatile and can be used to analyse a wide range of steel frames with a variety of end support conditions. It is found to give excellent agreement with a wide range of previously quoted analytical and experimental results for both individual members and frames. The program can also be used, if computer storage space and time is available, as a general elastic-plastic analysis for a three-dimensional frame.

The method has also been combined with a procedure for limiting deflections in portal frames to give a plastic design of such frames allowing for strain hardening. This design, which satisfies the deflection limitations by economically proportioning the column and rafter sizes is generally found to give lighter structures than comparative designs given by the rigid-plastic theory due to the beneficial effects of strain-hardening.

7.2 Optimisation of frames to satisfy deflection requirements.

A computer program comprising an existing non-linear stiffness analysis together with a simple linear programming routine has been developed to proportion plane steel frames to satisfy deflection requirements. The stiffness matrix used is a simplified version of the matrix used in the biaxial analysis since it does not include any torsional, warping or minor axis bending degress of freedom.

Procedures which obviate the need for a complete reanalysis when a member's section properties are changed have been presented in the past. However, these techniques depend upon the principle of superposition which is not valid when the reduction of stiffness due to compressive axial loads is to be considered. In the design method sensitivity coefficients, which indicate the suitability of sections to resist deflections in the frame under analysis, are obtained by repeated analysis. As a result, the efficiency of the method and its ability to design large frames depend to a great extent on the capabilities of the analysis program. The present method which stores all the stiffness terms in a very compact manner leads to a rapid solution of the equations and hence uses small amounts of computer time in the analysis part of the design procedure.

Comparisons with methods based on accurate non-linear programming techniques show that the designs obtained by the proposed method are likely to be close to the optimum. Indeed, when a local rather than a global optimum is obtained by non-linear programming, the

method may even generate a more economical design. The absence of any restriction on the size of the increments of moment of inertia or area calculated at each iteration permits the final design to be obtained without a large number of iterations.

Special features of the method include the ability to design haunched and latticed frames, and to allow for the increased deflections resulting from the effects of compressive axial loads on frame stiffness. It is unnecessary to assume that the weight per unit length of a member is linearly proportional to its moment of inertia throughout the entire range of available sections, and frames composed of a mixture of Universal Beams and Universal Columns can be designed. Although a continuous range of sections is assumed during the optimization stages of the design process, the method provides information which assists the designer when discrete sections have to be selected.

7.3 Experimental tests on tapered steel columns.

The main theme of the present work has been to obtain better estimates of the ultimate behaviour of loaded steel frames so that less conservative design methods can be used. Tapered columns can be used in some frames to enable better utilisation of the structural material in resisting stresses to be made.

The efficiency of tapered steel columns in resisting uniaxially applied bending moments and axial load in single storey portal frames has been examined by performing a series of experimental tests on various types of tapering columns. The columns were

subject to a combination of axial load and bending moment which was incrementally increased to cause collapse. They were found to fail either in a lateral-torsional or lateral buckling mode, the mode of failure being dependent on the axial load and degree of minor axis initial imperfection present.

The pattern of yielding just prior to failure showed that the plastic regions were fairly small and localised, occurring where the initial imperfections were a maximum. This indicates that failure of the columns occurred predominantly due to elastic instability rather than excessive plasticity.

The provision of a lateral restraint at the centre of the column has also been examined. Placement of the restraint on the tension flange of the column was found not to give a significant increase in failure load compared to the unrestrained case. However a significant increase in ultimate load was obtained by attaching the restraint to the compression flange.

Several recently proposed ultimate load design methods have been used in an attempt to give an estimate of the failure loads of the column. The results show that the elastic design method of Horne is the most suitable for giving a safe design for the series of columns tested.

Finally estimates of the behaviour of the tapered columns under load have been obtained using the biaxial ultimate load analysis. The column taper is represented by splitting the column into a number of longitudinal elements with varying section depths. Agreement between the two sets of results is found to be fairly good.

7.4 Suggestions for future work.

It is not possible with one particular analysis to solve all the problems associated with steel frame behaviour. However it is hoped that the present work will form the basis of future analyses to enable a more thorough knowledge of the complicated phenomena of inelastic frame instability to be gained. Suggested areas of future work will now be given.

A) Biaxial analyses of steel frames.

A fairly complex biaxial frame analysis has been developed which appears to give good agreement with a wide range of previously quoted results. However the analysis contains several simplifying assumptions which could be modified to give a more rigorous treatment of frames. Suggested modifications are as follows:

i) It is assumed in the moment curvature procedure that yielding is caused by only normal stresses. A further simplification is then made by also neglecting the effect of normal warping stresses on yield. This assumption will tend to overestimate the point at which yielding occurs in a member and thus will subsequently overestimate the member's stiffness. Hence a more complicated yield function should be used in cases where these stresses are not negligible.

ii) Elastic unloading which causes slight increases in frame strength at high strains has also been omitted from the analysis. Gent has indicated that this effect only becomes significant when frames have heavily loaded minor axis restraining beams.

iii) No allowance has been made for any initial twist in the frame members caused by manufacture. Initial imperfections, however, tend to be more significant when considering individual members rather than complete frames. An allowance for initial twists could be made by adding an extra rotation transformation to the member stiffness matrix.

iv) Warping is assumed to be either fully restrained or free at each of the joint positions. In practice, real structural joints probably lie somewhere between these two extremes, and allowance for 'semi-rigid' joints could thus be included in the stiffness analysis.

An analysis based on the present method and containing the above modifications could then be used to conduct a comprehensive parametric study into individual member and steel frame behaviour.

This study could be used to investigate the following effects:-

1. member shape
2. loading combinations (P, M_x and M_y) and end moment ratios about both axes
3. geometrical imperfections, residual stresses and strain hardening
4. restraining beams with rigid and semi-rigid connections.

The present method can only deal with rectangular and I-section steel sections. However the analysis could be altered fairly easily to deal with both reinforced concrete and composite sections as well as other steel section shapes by a suitable modification of the moment curvature procedure.

B) Optimisation of frames to satisfy deflection requirements.

The proposed design has aimed at giving a fairly simple method of assessing the most economical way to apportion a frame to satisfy deflection requirements. However the method requires a computer program to obtain a solution.

The advent of 'table-top' computers capable of performing the analysis part of the overall procedure suggest that the optimisation part of the design could be best presented in chart form for a variety of standard frames. A very rapid optimum design could then be obtained almost immediately.

C) Tapered Column tests.

One of the main difficulties in testing isolated columns is to accurately represent the end conditions that occur in practice. Hence a further series of tests could be performed on portal frames containing tapered columns. These tests could then be used to examine various types of joints, as well as giving information into the circumstances for which failure occurs due to local buckling rather than in an overall buckling mode.

REFERENCES

1. Euler, L. "Sur la force des colonnes", Mem. de l'Acad de Berlin, 1759.
2. Lagrange "Sur la figure des colonnes", Melanges de Phil. et de Math. de la. Soc. Roy. de Turin, 1770-3.
3. Young, T. "A course of lectures on Natural Philosophy and the Mechanical Arts", London, 1807.
4. Ayrton, W. and Perry, J. "On struts", The Engineer, Vol. 62, 1886.
5. Robertson, A. "The strength of struts", Inst. C.E., Selected Engineering Paper No. 28, 1925.
6. B.S.449, "The use of structural steel in building", British Standards Institution, Part 2, 1969.
7. Baker, J., Horne, M., and Heyman, J. "The Steel Skeleton Vol. 2", Cambridge University Press, 1956.
8. Wood, R. "The stability of tall buildings", Proc. I.C.E. Vol. 11, Sept. 1958.
9. Roderick, J. "Tests on stanchions bent in single curvature about both principal axes", British Welding Research Assoc., Report No. FE1/36, 1953.
10. Heyman, J. "Tests on I-section stanchions bent about the major axis", British Welding Research Assoc., Report No. FE1/40A/56, 1957.
11. Horne, M. "The stanchion problem in framed structures designed according to ultimate carrying capacity", Proc. I.C.E., Vol. 5, April 1956.

12. Horne, M. "Safe loads on I-section columns in structures designed by plastic theory", Proc. I.C.E., Vol. 29, Sept. 1964.

13. Horne, M. "The plastic design of columns", B.C.S.A. Publication No. 23, 1964.

14. Wood, R., Lawton, W. and Goodwin, E." Rapid design of multi-storey rigid jointed steel frames: systematic improvements in stanchion design", Building Research Station Note A58, July 1957.

15. Institute of Structural Engineers and Institute of Welding, "Joint Committee's second report on fully-rigid multi storey welded steel frames", I.S.E., London 1971.

16. Wood, R., Needham, F. and Smith, R. "Test of a multi-storey rigid steel frame", The Structural Engineer, April 1968.

17. Smith, R. and Roberts, E. "Test of a fully continuous multi-storey frame of high yield steel", The Structural Engineer, Oct. 1971.

18. Wood, R. "A new approach to column design with special reference to restrained steel stanchions", Building Research Station, 1971.

19. Gent, A. and Milner, H. "The ultimate load capacity of elastically restrained H-columns under biaxial bending", Proc. I.C.E. Vol. 41, Dec. 1968.

20. Stringer, D. "The elastic-plastic behaviour of restrained columns", Ph.D. Thesis, University of Manchester, 1972.

21. Hutchings, R. "The elastic-plastic behaviour of columns under biaxial loading", Ph.D. Thesis, University of Manchester, 1973.

22. Young, B. "Steel column design", The Structural Engineer, Sept. 1973.

23. Galambos, T. and Ketter, R. "Columns under combined bending and thrust", Trans. A.S.C.E., 1961.

24. Basu, A. and Hill, W. "A more exact computation of failure loads of composite columns", Proc. I.C.E. Vol. 40, May 1968.

25. Milner, H. "The elastic plastic stability of stanchions bent about two axes", Ph.D. Thesis, University of London, Dec. 1965.

26. Taylor, D. "The behaviour of continuous columns", Ph.D. Thesis, University of Cambridge, 1971.

27. Johnston, B. "The Column Research Council guide to design criteria for metal compression members" 2nd Ed. John Wiley and Sons, New York, 1966.

28. "Specification for the design, fabrication and erection of structural steel for buildings", American Institute of Steel Construction, 1969.

29. Birnstiel, C. and Michalos, J. "Ultimate load of H-columns under biaxial bending", A.S.C.E. Structural Division, April 1963.

30. Harstead, G., Birnstiel, C. and Leu, K-C. "Inelastic H-columns under biaxial bending", A.S.C.E. Structural Division, Oct. 1968.

31. Birnstiel, C. "Experiments on H-columns under biaxial bending", A.S.C.E., Structural Division, Oct. 1968.

32. Sharma, S. and Gaylord, E. "Strength of steel columns with biaxially eccentric load", A.S.C.E. Structural Division, Dec. 1969.

33. Syal, I. and Sharma, S. "Biaxially loaded beam-column analysis", A.S.C.E. Structural Division, Sept. 1971.

34. Santathadaporn, S. and Chen, W. "Analysis of biaxially loaded H-columns", A.S.C.E. Structural Division, March 1973.

35. Chen, W. and Atsuta, T. "Ultimate strength of biaxially loaded steel H-columns" A.S.C.E. Structural Division, March 1973.

36. Vinnakota, S. and Aoshima, Y. "Inelastic behaviour of rotationally restrained columns under biaxial bending". The Structural Engineer, July 1974.

37. Jennings, A. and Majid, K. "An elastic-plastic analysis by computer for framed structures loaded up to collapse", The Structural Engineer, Dec. 1965.

38. Livesley, R. "The application of computers to problems involving plasticity" Symposium on the use of electronic computers in Structural Engineering, University of Southampton, 1959.

39. Majid, K. and Anderson, D. "The computer analysis of large multi-storey framed structures", The Structural Engineer, Nov. 1968.

40. Davies, J. "Frame instability and strain-hardening in plastic theory", A.S.C.E. Structural Division, June 1966.

41. Chin, M. "The failure loads of high tensile steel structures" Ph.D. Thesis, University of Manchester, 1966.

42. Driscoll, C.Jn. "Plastic design of multi-storey frames", Lecture Notes, Fritz Engineering Lab., Lehigh Univ., 1965.

43. Wood, R. "Effective lengths of columns in multi-storey buildings", Parts 1, 2 and 3, The Structural Engineer, July-September 1974.

44. Livesley, R. "The automatic design of structural frames", Quarterly Journal of Mechanics and Applied Mathematics, Part 3, 1956.

45. Palmer, A. "Optimum structure design by dynamic programming", A.S.C.E. Structural Division, Aug. 1968.

46. Majid, K. and Anderson, D. "Elastic-plastic design of sway frames by computer". Proc. I.C.E., Dec. 1968.

47. Holmes, M. and Sinclair-Jones, H. "Plastic design of multi-storey sway frames". Proc. I.C.E., Sept. 1970.

48. Majid, K. and Elliott, D. "Optimum design of frames with deflexion constraints by non-linear programming". The Structural Engineer, April 1971.

49. Horne, M. and Morris, L. "Optimum design of multi-storey rigid frames". Optimum structural design: theory and applications; Ed. Gallagher R. and Zienkiewicz O., Wiley, London, 1973.

50. Majid, K. "Non-linear structures", Butterworth, London, 1972.

51. Majid, K. and Anderson, D. "Optimum design of hyperstatic structures", International Journal for Numerical Methods in Engineering Vol. 4, 1972.

52. Anderson, D. "Investigations into the design of plane structural frames", Ph.D. Thesis, University of Manchester, 1969.

53. Moy, F. "Control of deflexions in unbraced steel frames", Proc. I.C.E., Dec. 1974.

54. Lee, G., Morrell, M. and Ketter, R. "Design of tapered members", Welding Research Council Bulletin No. 173, June 1972.

55. Butler, D. "Elastic buckling tests on laterally and torsionally braced tapered I-beams", Welding Journal Research Supplement 45, 1966.

56. Prawel, S., Morrell, M. and Lee, G. "Bending and buckling strength of tapered structural members", State University of New York Civil Engineering Report, 1972.

57. Morrell, M. and Lee, G. "Allowable stress for web-tapered beams with lateral restraints", State University of New York Civil Engineering Report, 1973.

58. Livesley, R. and Chandler, D. "Stability functions for structural frameworks", Manchester University Press, 1956.

59. Jennings, A. "A compact storage scheme for the solution of symmetric linear simultaneous equations". The Computer Journal, Vol. 9, Nov. 1966.

60. Chen, W. and Atsuta, T. "Column curvature curve method for analysis of beam-columns", The Structural Engineer, June 1972.

61. Ajmani, J. "Collapse loads of columns with intermediate supports", Ph.D. Thesis University of Manchester, May 1968.

62. Powell, G. and Klinger, R. "Elastic lateral buckling of steel beams", A.S.C.E. Structural Division, Sept. 1970.

63. Barsoum, R. and Gallagher, R. "Finite element analysis of torsional and torsional-flexural stability problems", International Journal for Numerical Methods in Engineering Vol. 2, 1970.

64. Timoshenko, S. and Gere, J. "Theory of elastic stability", McGraw-Hill, New York, 1952.

65. Bleich, F. "Buckling strength of metal structures", McGraw-Hill, New York, 1952.

66. Coates, R., Coutie, M. and Kong, F. "Structural analysis" Nelson, London, 1972.

67. Nethercot, D. "Buckling stability of partially plastic beams", Proc. I.C.E., Sept. 1972.

68. Trahair, N. "Elastic stability of continuous beams", A.S.C.E. Structural Division, June 1969.

69. Vacharajittiphan, P. and Trahair, N. "Elastic lateral buckling of portal frames", A.S.C.E. Structural Division, May 1973.

70. Culver, C. "Exact solution of the biaxial bending equations", A.S.C.E. Structural Division, April 1966.

71. Young, B. "Moment-curvature properties of certain hot-rolled and welded structural sections", Cambridge University Engineering Department Technical Report 10, 1971.

72. Galambos, T. "Inelastic lateral buckling of beams", A.S.C.E. Structural Division, Oct. 1963.

73. Trahair, N. and Kitipornchai, S. "Buckling of inelastic I-beams under uniform moment", A.S.C.E. Structural Division, Nov. 1972.

74. Fukomoto, Y. and Galambos, T. "Inelastic lateral-torsional buckling of beam columns", A.S.C.E. Structural Division, April 1966.

75. Santathadaporn, S. and Chen, W. "Tangent stiffness method for biaxial bending", A.S.C.E. Structural Division, Jan. 1972.

76. Neal, B. "The lateral instability of yielded mild-steel beams of rectangular cross-section", Philosophical Transactions, Royal Society, Jan. 1950.

77. Haaijer, G. "Plate buckling in the strain-hardening range", A.S.C.E. Mechanics Division, April 1957.

78. Massey, C. "The torsional rigidity of steel I-beams already yielded under uniform bending moment", Civil Engineering and Public Works Review, Mar. 1963 and April 1963.

79. Ely, J. and Zienkiewicz, O. "Torsion of compound bars - a relaxation solution", International Journal of Mechanical Sciences Vol. 1, 1960.

80. Booker, J. and Kitipornchai, S. "Torsion of multilayered rectangular sections", A.S.C.E. Mechanics Division, Oct. 1971.

81. Closure on "Torsion of multilayered rectangular sections", A.S.C.E. Mechanics Division, June 1973.

82. Megson, T. "Linear analysis of thin walled elastic structures", Wiley and Sons, New York, 1974.

83. Anderson, J. and Trahair, N. "Stability of monosymmetric beams and cantilevers", A.S.C.E. Structural Division, Jan. 1972.

84. Van Kuren, R. and Galambos, T. "Beam-column experiments", A.S.C.E. Structural Division, April 1964.

85. Charlton, T. "A test on a pitched roof portal structure with short stanchions", British Welding Journal Vol. 7, 1960.

86. Gent, A. Discussion on "Inelastic H-columns under biaxial bending" (Reference 30) A.S.C.E. Structural Division, Aug. 1969.

87. Anderson, D. and Salter, J. "The design of portal frames by computer to strength and deflection requirements", International Conference on Computers in Engineering and Building Design, CAD 1974, Imperial College, London, Sept. 1974.

88. Allwood, B., et al. "Steel designers manual", Crosby-Lockwood, London, 1966.

89. Burnett, N., et al. "Plastic design", B.C.S.A. Publication No. 28, 1965.

90. Horne, M. "Failure loads of biaxially loaded I-section columns restrained about the minor axis", Engineering Plasticity, Edited by J. Heyman and R. Leckie,Cambridge University Press, 1968.

91. May, I. "The test rig", Interim Report No. 10, University of Warwick, Department of Engineering, Dec. 1975.

92. Young, B. and Dwight, J. "Residual stresses due to longitudinal welds and flame-cutting", Cambridge University Engineering Department, Technical Report 9, 1971.

93. Horne, M. and Ajmani, J. "Design of columns restrained by side-rails", The Structural Engineer, Aug. 1971.

MISSED AT START

OF FILM

RETAIN AND INSERT

ON COMPLETION.